Robust Modelling of Heat and Mass Transfer in Processing of Solid Foods

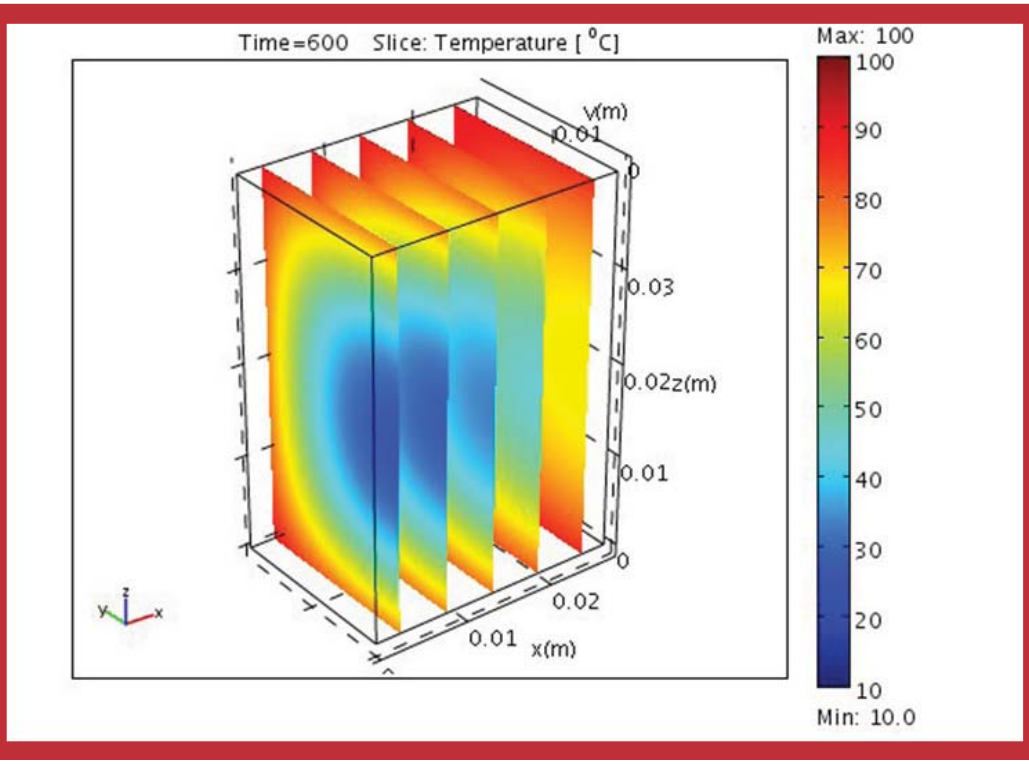

$$c_{p,p}\rho_p \frac{\partial T}{\partial t} = \nabla(k_p \nabla T) - \rho_w c_{p,w} u_w \nabla T - Q_{evp}$$

Aberham Hailu Feyissa

PhD Thesis

2011

DTU Food

National Food Institute

Robust Modelling of Heat and Mass Transfer in Processing of Solid Foods

Ph.D Thesis

Aberham Hailu Feyissa

National Food Institute, Food Production Engineering

Technical University of Denmark

February 2011

Supervisors:

Professor, dr.techn. Jens Adler-Nissen, National Food Institute, Food Production Engineering, Technical University of Denmark
Associate Professor, Krist V. Gernaey, Department of Chemical Engineering, Technical University of Denmark

Preface

This Ph.D thesis was carried out at the Food Production Engineering, National Food Institute in collaboration the Department of Chemical and Biochemical Engineering, at the Technical University of Denmark. The Ph.D thesis was carried out in the period from February 1st 2008 to February 28th 2011 with the supervision of Professor, dr.techn. Jens Adler-Nissen and Associate Professor, Krist V. Gernaey.

The financial support from the Technical University of Denmark is gratefully acknowledged.

First all, I would like to express my deepest gratitude to my principal supervisor Professor, dr.techn. Jens Adler-Nissen and my co-supervisor Associate Professor, Krist V. Gernaey for their guidance, advice, countless ideas with fruitful discussions, and encouragement throughout the whole research work. It has been a great experience working with both of you in this project. Without your advice and unique support this thesis would have never become a reality.

I would like thank Jette Høj for her great help to make linguistic corrections for my thesis. I would like also to thank Department of Chemical and Biochemical Engineering, DTU for allowing me to modify and use some of the MATLAB scripts (m-files).

My gratitude goes to all my colleagues at Food Production Engineering, National Food Institute, for providing such a good working atmosphere and for being very supportive.

I would like to express my gratitude for all my family for their care and inseparable prayer. Last but not the least, thanks to God for my life, may your name be exalted, Amen!

Lyngby, February 2011

Aberham Hailu Feyissa

Summary

The study is focused on combined heat and mass transfer during processing of solid foods such as baking and frying processes. Modelling of heat and mass transfer during baking and frying is a significant scientific challenge. During baking and frying, the food undergoes several changes in microstructure and other physical properties of the food matrix. The heat and water transport inside the food is coupled in a complex way, which for some food systems it is not yet fully understood. A typical example of the latter is roasting of meat in convection oven, where the mechanism of water transport is unclear. Establishing the robust mathematical models describing the main mechanisms reliably is of great concern. A quantitative description of the heat and mass transfer during the solid food processing, in the form of mathematical equations, implementation of the solution techniques, and the value of the input parameters involves uncertainty.

The objective of this thesis is to develop robust models of heat and mass transfer during processing of solid foods. The study consists of formulating the mechanistic models, solving the models by the Finite Element method (FEM), calibrating and validating the models by experimental data, evaluating the models by an uncertainty and sensitivity analysis. In the study, contact baking and roasting of meat in convection oven were chosen as representative case studies. For both representative cases, the experiments were performed and the relevant data such as product temperature, mass loss, and other process conditions were obtained.

For roasting of meat in convection oven, the mechanism of water transport during roasting was studied; a theoretical assessment was made on the change in structure, water holding capacity and shrinkage. The mechanism of water transport was tested by measuring the local water content. For the roasting process, 3D and 2D mechanistic quantitative models describing the coupled heat and mass transfer were developed. The governing model equations are based on the conservation of energy and mass. Further, Darcy's equation was used to describe the pressure driven transport of water in meat during roasting. The change in elastic modulus, evaporation, and moving boundary were incorporated into the model equations. The arbitrary Lagrangian–

Eulerian (ALE) method was implemented to capture the moving boundary during the roasting process. The model equations for coupled heat and mass transfer were solved using the FEM (COMSOL).

For the contact baking process, a 1D mathematical model of the coupled heat and mass transfer was developed. The model developed for the contact baking process considered the heat transfer, local evaporation, and multiphase water transport (liquid and vapour). The model equations were implemented in the COMSOL-MATLAB computing environment with the following features: parameter estimations, model validations and uncertainty and sensitivity analysis. The unknown parameters in the model were estimated by comparing the measured and simulated data – using the least square method by comparing the measured temperature against the simulated temperature. Further, the model was validated using the experimental data and a reasonably agreement between the simulated and experimental data were obtained.

The uncertainty and global sensitivity analysis method were incorporated for the model of coupled heat and mass transfer. The uncertainty of model predictions due to the uncertainty in input parameters such as thermo-physical properties, heat and mass transfer coefficients, phase change initial and boundary conditions parameters were studied. A Monte Carlo based method of the uncertainty and global sensitivity analysis was used. The sensitivity analysis was performed to determine the relative effect of the different parameters on the model prediction. The relative effects of parameters on the model prediction were indentified, and their relative impact on each model output was ranked.

Generally, the developed mathematical models of heat and mass transfer provide better insights about the processes. The proposed robust modelling approach was found to be a useful tool in the model building that help to cope up with different challenges in modelling of heat and mass transfer during processing of solid foods and the potential of using the approach is particularly great for frying and baking operations.

Resume

I dette ph.d. studium er der fokuseret på samspillet mellem energi- og massetransport ved tilberedning af faste fødevareprodukter såsom bage- og stegeprocesser. Modellering af energi- og massetransport er en væsentlig videnskabelig udfordring. Under bagning og stegning ændres fødevarens mikrostrukturelle og fysiske egenskaber. Energi- og vandtransport i fødevaren er komplekst koblet, og for nogle fødevarer endnu ikke fuldt beskrevet. Et typisk eksempel på dette er stegning af kød i en konvektionsovn, hvor mekanismen for transport af vand er uklar. Etablering af robuste matematiske modeller der troværdigt beskrivelser de grundlæggende mekanismer vil være af stor betydning. En kvantitativ beskrivelse af energi- og massetransport under tilberedning af faste fødevareprodukter, i form af matematiske ligninger, implementering af løsningsteknikkerne, samt værdien af input parametrene involverer usikkerheder.

Målet med denne afhandling har været at udvikle robust modeller til beskrivelse af energi- og massetransport i faste fødevareprodukter. Studiet består i formulering af de mekanistiske modeller, løsning af modellerne vha. en Finite Element (FEM) metode, kalibrering og validering af modellerne med eksperimentel data, samt evaluering af modellerne ved en usikkerhed- og sensitivitetsanalyse. I studiet er kontaktbagning og stegning af kød i en konvektionsovn udvalgt som repræsentative eksempler. For begge eksempler, er fysiske eksperimenter udført og relevant data opsamlet, såsom produkttemperatur, vægttab og procesindstillinger.

Vandtransportmekasnismerne i kød under stegning i en konvektionsovn, blev undersøgt. En teoretisk afdækning blev udført for ændringen i struktur, vandbindingsevne og skrumpning. Mekanismerne bag vandtransport blev testet ved måling af lokale vandindhold. For stegeprocessen, blev 2D og 3D mekanistiske kvantitative modeller udviklet til beskrivelse af energi- og massetransport. De grundlæggende ligninger er baseret på princippet om energi- og massebevarelse. Ydermere er Darcys ligning brugt til beskrivelse af trykdrevet transport af vand under stegning af kød. Ændringer af det elastiske modul, fordampning og bevægelige

grænseflader blev inkorporeret i de anvendte modelligninger. Den arbitrære Lagrangian-Eulerian (ALE) metode blev brugt til at udtrykke de bevægelige grænser under stegeprocessen. Ligningerne for koblet energi- og massetransport blev løst ved brug af FEM (COMSOL).

For kontaktbagning blev en 1D matematisk model udviklet til beskrivelse af energi- og massetransport. Den udviklede model medtager energitransport, lokal fordampning og multifase vandtransport (væske og damp). Ligningerne blev implementeret i et COMSOL-MATLAB miljø med de følgende funktioner: parameterestimering modelvalidering samt usikkerheds- og sensitivitetsanalyse. De ukendte parametre i modellen blev estimeret ved sammenligning mellem målte og simulerede temperaturdata, ved brug af mindste kvadraters metode. Ydermere blev modellen valideret ved brug af eksperimentelt data. En rimelig overensstemmelse imellem de målte og simulerede data blev opnået.

Usikkerheds- og global sensitivitetsanalyse blev indarbejdet i modellen til beskrivelse af koblet energi- og massetransport. Modellens usikkerhed, grundet usikkerheder i input parametre såsom termo-fysiske egenskaber, varme- og masseovergangstal, faseovergang, samt start- og grænsebetingelser blev undersøgt. Der blev anvendt en Monte Carlo baseret metode til usikkerheds- og global sensitivitetsanalyse. Sensitivitetsanalysen blev udført for at bestemme den relative effekt af de undersøgte parametre på modellens prædiktion. Parametrenes relative effekt på modellens output blev identificerede og deres indflydelse rangordnet for hvert at modellens output.

Generelt giver den udviklede matematiske model til beskrivelse af energi- og massetransport bedre indsigt i de undersøgte processer. Den anvendte indgangsvinkel i form af robust modellering, har vist sig at være et brugbart værktøj til modelopbygning og til at håndtere forskellige udfordringer ved modellering af energi- og massetransport under tilberedning af faste fødevareprodukter. Potentialet for at bruge netop denne indgangsvinkel er især stort for stege- og bageprocesser.

Contents

Preface i

Summary iii

Resume v

List of publications xi

Symbols and Abbreviations xiii

1 Introduction 1

1.1 Representative cases 2

1.2 Physical-based model 4

1.3 Uncertainty 5

1.4 Objective 7

1.5 Overview 7

2 Robust modelling approach 11

2.1 Introduction 11

2.2 Robust modelling approach 11

2.2.1 Mechanistic model formulation (component 1) 12

2.2.2 Building a FEM model of solid food process (component 2) 14

2.2.3 Model calibration and model validation (component 3) 14

2.2.4 Uncertainty and sensitivity analysis (component 4) 15

3 Literature, heat and mass transfer in solid foods 17

3.1 Introduction 17

3.2 Heat transfer (to/within) solid foods 17

3.3 Mass transfer mechanism - water transport 20

3.3.1 Water transport mechanisms during roasting of meat in convection-oven 21
3.4 Thermo physical properties 29
3.5 Summery 30
4 Experimental work and mechanism interpretation 31
4.1 Introduction 31
4.2 Sample and sample preparation 31
4.3 Contact baking process 32
4.3.1 Local temperature profile 33
4.3.2 Mass loss 36
4.4 Roasting process 37
4.4.1 Roasting oven and set-up 37
4.4.2 Heat transfer coefficient 38
4.4.3 Product temperature and mass loss profile 40
4.4.4 Local water content and mechanism of water transport 41
4.5 Shrinkage 43
4.6 Change in the microstructure during the roasting of meat 44
4.7 Summary 48
5 Model formulation 49
5.1 General governing equations 49
5.1.1 Heat transfer 49
5.1.2 Mass transfer 50
5.2 Roasting process (case study 1) 51
5.2.1 Problem formulation and assumptions 51
5.2.2 Governing equations 52

5.2.3 Pressure driven transport of water inside meat 53
5.2.4 Boundary condition 54
Heat transfer 54
5.2.5 Moving boundary 55
5.2.6 Thermo-physical proprieties 56
5.3 Contact baking process (case study 2) 56
5.3.1 Problem formulation and assumptions 56
5.3.2 Governing equations 58
5.3.3 Boundary conditions 59
5.3.4 Evaporation rate 60
6 Finite Element Modeling – Implementation and Solution 63
6.1 Numerical solution 63
6.1.1 Finite Element method 64
6.1.2 COMSOL Multiphyics software 65
6.2 3D model of coupled heat and mass transfer during roasting of meat in the convection oven 67
6.3 2D model of coupled heat and mass transfer with moving boundary 70
6.4 Summary 76
6.4.1 COMSOL-MATLAB 77
7 Model calibration and validation 79
7.1 Parameter estimation 79
7.1.1 Result of parameter estimations (contact baking process) 82
7.2 Model validation (contact baking) 82
7.3 Model validation (roasting process) 85

7.4 Summary 86
8 Uncertainty and sensitivity analysis 87
8.1 Introduction 87
8.2 Contact baking process 88
8.2.1 Model equations 88
8.2.2 Model output variables 88
8.2.3 Input parameters 89
8.3 Monte Carlo method 89
8.4 Uncertainty in the model prediction 92
8.5 Sensitivity analysis 94
8.6 Parameter ranking 96
8.7 Conclusion 100
9 Conclusion and general perspective 101
9.1 Conclusion 101
9.2 Perspective 103
References 106
Appendix 115
Paper I-V 121

List of publications

I. Feyissa A.H., Adler-Nissen J., & Gernaey K.V. (2009). Mechanism of water transport in meat during the roasting process. In *Proceedings 55th ICOMST, International Congress of Meat Science and Technology, Meat - Muscle, Manufacturing and Meals, 2009, (pp.425-429),* Copenhagen, Denmark.

II. Feyissa A.H., Adler-Nissen J., & Gernaey K.V. (2009). Model of Heat and Mass Transfer with Moving Boundary during Roasting of Meat in Convection-Oven. In *Proceedings of the COMSOL Conference, 2009, (pp.1-8), October 14-16,* Milan, Italy.

III. Feyissa A.H., Gernaey K.V., Ashokkumar S., & Adler-Nissen J., (2011). Modelling of Coupled Heat and Mass Transfer during a Contact Baking Process, *Journal of Food Engineering, doi:10.1016/j.jfoodeng.2011.05.014 (in press, accepted manuscript, published online)*

IV. Feyissa A.H., Gernaey K.V., & Adler-Nissen J., (2011). Uncertainty and Sensitivity Analysis: Mathematical Model of Coupled Heat and Mass Transfer for a Contact Baking Process, *Journal of Food Engineering, (to be submitted early March,2011)*

V. Feyissa A.H., Gernaey K.V., & Adler-Nissen J., (2011). 3D Modelling of Coupled Mass and Heat Transfer of a Convection-Oven Roasting Process, *Journal of Food Engineering, (to be submitted early March,2011)*

Other publications related to Ph.D project

Adler-Nissen J., **Feyissa A.H.,** & Gernaey K.V., (2010), Approaches to Robust Modelling of Frying Processes *Proceedings of Dansk Kemiingeniørkonference* (DK2-2010), (pp.114-115), 16-17 June, Lyngby, Denmark

Feyissa A.H., Gernaey K.V., & Adler-Nissen J., (2010) Uncertainty and Sensitivity Analysis of Heat and Mass Transfer in Food Processing, *5th International Conference on the Food Factory for the Future, Smart process control and automation*, June 30th to July 2nd, 2010, Gothenburg, Sweden.

Symbols and Abbreviations

h	:	Heat transfer coefficient	$W \cdot m^{-2} \cdot K^{-1}$
k_m	:	Thermal conductivity of meat	$W \cdot m^{-1} \cdot K^{-1}$
μ_w	:	Viscosity of water	$kg \cdot m^{-1} \cdot s^{-1}$
C	:	Moisture content (wet basis), kg of water/kg of sample	$kg \cdot kg^{-1}$
C_{eq}	:	Water holding capacity at equilibrium	$kg \cdot kg^{-1}$
$c_{p,m}$	:	Specific heat of meat	$J \cdot kg^{-1} \cdot K^{-1}$
$c_{pp,\ and}$ $c_{pAl,}$	:	Specific heat capacity of product, and aluminium, respectively	$J \cdot kg^{-1} \cdot K^{-1}$
D	:	Diffusion coefficient	$m^2 \cdot s^{-1}$
D_l *and* D_v	:	Liquid and vapour diffusion coefficient respectively	$m^2 \cdot s^{-1}$
E	:	Elastic modulus	$N \cdot m^{-2}$
E_a	:	Activation energy	$kJ \cdot mol^{-1}$
$e_{i,m}$	:	Error of regression model	
f	:	Fraction of energy used for evaporation	
h_{bot}	:	Overall heat transfer coefficient at the bottom boundary of the baking disc (rig)	$W \cdot m^{-2} \cdot K^{-1}$
H_{evp}	:	Latent heat of evaporation	$J \cdot kg^{-1}$
h_{top}	:	Heat transfer coefficients at the top surface (at air-product interface)	$W \cdot m^{-2} \cdot K^{-1}$
K	:	Permeability	m^2
k_{evp}	:	Evaporation rate constant at the evaporation temperature	s^{-1}
k_l *and* k_v	:	Liquid and vapour mass transfer coefficient respectively	$m \cdot s^{-1}$
k_p, k_{Al}, *and* k_{air}	:	Thermal conductivity of product, aluminium, and air, respectively	$W \cdot m^{-1} \cdot K^{-1}$
m	:	Mass	kg
M_w	:	The molecular weight of water	$kg \cdot mol^{-1}$
P	:	Pressure	Pa

q	:	Heat flux	$W \cdot m^{-2}$
R	:	Radius	m
R_{evp}	:	Evaporation rate (local)	$kg \cdot kg^{-1} \cdot s^{-1}$
R_g	:	The gas constant	$J \cdot K^{-1} \cdot mol^{-1}$
T	:	Temperature	K
t		Time	s
T_{air}	:	Surrounding air temperature	K
T_{evp}	:	Evaporation temperature	K
T_{set}		Temperature set point	K
$T\sigma$	:	Sigmoidal temperature	^{o}C
X_l *and* X_v	:	Liquid and vapour water content (dry basis), respectively	$kg\ kg^{-1}$
Y	:	Output variable [*TA, TB,…], vector*	
y_i	:	The mass fraction of each component (water, protein, carbohydrate and fat)	
z	:	The variation along the z direction	m
β_{im}	:	Normalized regression coefficient	
β	:	Shrinkage coefficient	
ε	:	Porosity	
ρ_m *and* ρ_w	:	Density of meat and water, respectively	$kg \cdot m^{-3}$
ρ_p, ρ_{Al} *and* ρ_{air}	:	Density of product, aluminium, and air, respectively	$kg \cdot m^{-3}$
θ	:	Uncertain input parameters [$k_{evp}\ k_v\ k\ D_v$ …], vector	
∇	:	Del operator	m^{-1}
PDE	:	Partial differential equation	
FEM	:	Finite Element method	
ALE	:	Arbitrary Lagrangian–Eulerian	
SRC		The standardized regression coefficient	
		Subscripts	
o	:	Initial value	

air	:	Air
Al	:	Aluminium
av	:	Average
c	:	Carbohydrate
d	:	Solid
eq	:	Equilibrium
evp	:	*evaporation*
f	:	Fat
i	:	Index of Monte Carlo simulations (a vector)
i	:	Component
j	:	Index of parameter vector
l and v	:	Liquid and vapour
m	:	Index of output vector
m	:	Meat
oven	:	Oven
p	:	Product (pancake batter)
p	:	Protein
s	:	Surface
w	:	Water

1 Introduction

Heat treatment is a common and important step in the manufacturing of many solid foods such as baked products, meat, canned foods, dried and fried products. Heat transfer (without mass transfer) is a classical form of heat transfer that takes place in several important thermal processing of foods for example as in canning – heating in a closed container, where there is no evaporation loss. In many solid food processes heat transfer is also accompanied by mass transfer mainly in the form of water transport. Such a process is called a coupled heat and mass transfer. The coupled heat and mass transfer is governing many common solid food processes such as baking, drying and frying.

The heat and mass transfer play an important role in baking (Mondal and Datta, 2008, Sumnu and Sahin, 2008), frying (Skjöldebrand and Hallstroem, 1980) and drying (Srikiatden and Roberts, 2007). There is a strong coupling between temperature and moisture content. When a solid food is heated, the water inside the food migrates either in the form of liquid water or in the form of liquid water and water vapour (Thorvaldsson and Janestad, 1999). The temperature and water content inside a solid food are varying in space and time during a heat treatment. Their entire history and their spatial distribution influence the quality and the safety of the processed foods. For example the acrylamide formation during bread baking (Ahrne et al., 2007) and production of the breakfast cereal (Jensen et al., 2008) depend upon the temperature and the heating time. Further, a quantitative understanding of heat and mass transfer in food process is also an essential role for scale up to industry. Generally, there is a great need for a quantitative understanding of heat and mass transfer to optimize and control the final product quality. Developing mathematical models of solid food processes such as baking and frying require physical as well as mathematical insight into a food material and the processes (Halder, et al., 2011).

A solid food system undergoes several changes during heat treatment. It undergoes phase changes for example evaporation of water (Datta, 2007b; Adler-Nissen, 2007), changes in

microstructure such as pore formation in bread baking (Lee, et al., 1996), shrinkage during roasting of meat (Tornberg, 2005), and shrinkage and pore formation during drying processes (Talla, et al., 2004, Yang, et al., 2001). It undergoes expansion of volume for example as in bread baking (Purlis and Salvadori, 2009). It develops a crust (Jefferson, et al., 2006) and colour change for example as browning in bread (Purlis, 2010). These changes may influence the heat and mass transfer, either the mechanisms directly (e.g., phase change, formation of porous media) or through the heat and mass transfer properties such as thermal conductivity, diffusivity and permeability. These processes are complex and in some cases, their coupling mechanisms have not yet been fully understood. As result, a complete quantitative knowledge of their physical processes is still lacking (Datta, 2008).We will illustrate these situations by two representative cases: roasting of meat in a convection-oven, and a contact baking process.

1.1 Representative cases

Roasting in a convection oven is a common way of frying a whole piece of meat in households, in professional kitchens and in the ready-meal industry. We have chosen the roasting of meat in a convection process because of its importance in the supply of professionally prepared meals and because the process includes a number of physical processes of general significance in most cooking processes. These include non-stationary heat transfer, internal transport of liquid water, evaporation of water at the surface, and change in geometry – here in the form of shrinkage of the meat matrix with the onset of denaturation of the different meat proteins (Tornberg, 2005). Several researchers have formulated different hypotheses to model mass transfer during roasting, mostly from the perspective of diffusion (Chen, et al., 1999, Huang and Mittal, 1995, Ngadi, et al., 1997) while disagreements are often seen with regard to other types of water transport mechanisms (Godsalve, et al., 1977, Thorvaldsson and Skjöldebrand, 1996, Wählby and Skjöldebrand, 2001). The pure diffusion based models do not adequately describe the moisture transport phenomena during meat cooking (Godsalve, et al., 1977, Thorvaldsson and Skjöldebrand, 1996, Wählby and Skjöldebrand, 2001), because the effects of water binding capacity and shrinkage phenomena are not considered.

Recently, Van der Sman (2007) considered a pressure-driven water transport in meat during cooking and his model predicted a large increase in water content in the centre of the meat. Nevertheless, this prediction does not agree with the observations made by Wählby and Skjöldebrand (2001). One probable reason is that Van der Sman (2007) did not consider the dynamic change in the meat microstructure during cooking. The change of the meat microstructure during processing is evident from the reviewed paper by (Tornberg, 2005). Besides, most of the published works on the modelling of heat and mass transfer during meat roasting do not at all consider shrinkage in the form of moving boundary. Nevertheless, a considerable shrinkage of meat was observed e.g., 7-19 % on area basis (Tornberg, 2005), and 11-20.3 % on diameter basis (Kovácsné Oroszvári, et al., 2006) and plays a key role in the water transport during the roasting process. It is important to know, how this effect influences the prediction of state variables (e.g., temperature, T and water content, C).

Contact baking is a widely applied process in for example baking of crisp bread, tortillas, pizzas, chapatti, pancakes, pita breads etc. We have chosen the contact baking of pancake, first of all because it includes a number of important processes for example non-stationary heat transfer, local evaporation, multiphase transport in the form of liquid water and water vapour, further most heating of solid foods involves contact heating. Secondly, the pancake is a good model food – that means several different food products can be modelled by changing the composition of its ingredients. Thirdly, a controlled experimental heating rig for contact baking has been developed in our research group during another PhD project - which was used for experimentation (Ashokkumar and Adler-Nissen, 2010). There are only a few publications on modelling of contact baking (Gupta, 2001) and the related contact frying process (Pan, et al., 2000, Pan and Singh, 2002, Wichchukit, et al., 2001). Gupta (2001) studied stationery heat transfer during contact baking of Indian chapatti, whereas the others such as (Pan et al (2000), Pan and Singh (2002) and Wichchukit et al (2001) studied contact frying of beef burgers. The contact baking involves complex heat and mass transfer – a multiphase water transport (liquid and vapour) and evaporation. These physical processes are coupled and interact with each other during the baking process.

To understand heat and mass transfer during roasting and contact baking processes, it is important to study the physical processes altogether. We have chosen a mechanistic model as the framework to represent available knowledge on heat and mass transfer in the contact baking process and the roasting of meat in the convection-oven.

1.2 Physical-based model

A physical-based model (mechanistic model) of heat and mass transfer is derived from fundamental physical laws such as conservation of mass, conservation of energy and supplemented with empirical (but fairly universal law) rate (Datta, 2008). In general, there is a great need of physics-based models in food processing. This is evident in a recent reviewed paper "*status of the physics-based models in the design of food products, processes, and equipment*" (Datta, 2008). The review clearly stated the needs and the challenges of the physical based model. A physical-based model can find applications in many situations. In food production, the model may find use in predicting the state variables for example for a given centre temperature for a given piece of food or to estimate the average product properties as a function of the process conditions. This means, it benefits the food production system by providing predictive capability - a way of performing 'what if scenario for example by varying the process conditions'. For baking and roasting the detailed physical-based models are not yet available (Datta, 2008). The model equations of coupled heat and mass transfer for baking and roasting are often a system of coupled partial differential equations (PDEs). They cannot be solved by analytical methods. Heat and mass transfer equations were solved analytical for only simple situations – for example geometry and boundary condition. For the classical heat transfer, the analytical solution for sterilization of foods goes back to at least the pioneering work of Balls and Olsen (1957) and until the late 1980s, the work was mostly analytical, as confirmed by Datta (2008). When attempting to get the analytical solutions to heat and mass transfer, there is always a tendency to oversimplify the problem in order to make mathematical models sufficiently simple to obtain an analytical solution. It comes as no surprise that moving boundary, nonlinearity such as the temperature dependence or changes in other physical properties are seldom considered.

Nowadays, the growing computing power allows the use of numerical solution such as the Finite Element Method (FEM) (Moens and Vandepitte, 2005, Mohamed, 2010, Wang and Sun, 2003). The FEM is widely used to solve coupled partial differential equations in many science and engineering applications - ranging from medical to aerospace engineering, including food engineering. The use of the FEM is a powerful tool in research and in evaluating the physical-based models and allowing the phenomena to be visualized. For complex systems, the FEM is too time consuming and computationally intensive to allow such models to be employed as models for general daily use in for example a production environment. Nevertheless, the FEM solution of physical-based models can assist in a better understanding in evaluating the effect of deviations from ideal conditions, in assessing the consequence of e.g. evaporation and shrinkage. It can be a great help in taking decisions on whether the effects can be ignored or considered. Besides, a combination of experimental work and theoretical considerations of the transport mechanism can lead to crucial simplifications. Deviations from the ideal situation can be handled by including appropriate correction factors or functions, in the best engineering tradition. The experimental work also assists the physical-based model in obtaining the missing parameters and in the validation of the model.

1.3 Uncertainty

The model uncertainty is a combination of model formulations (lack of knowledge or simplification) and parameter uncertainty. The first type of uncertainty can to some extent be reduced by developing the model from the fundamental laws (as discussed above), with appropriate assumptions. The parameter uncertainty is a major problem in the physical-based model (Datta, 2008). Some physical properties of the food product can be estimated with reasonable accuracy (e.g., density and heat capacity of the composition), whereas the coefficients of heat and mass transfer, evaporation rate and other parameters often only can be estimated with considerable uncertainty. In complex systems as baking and roasting, the physical-based model contains several variables and parameters, their number increases as more details are taken into account. Besides, the food system, as a biological material, has a natural variability, which is not avoidable. It is therefore important to evaluate the reliability of the model predictions in relation to uncertainty in the parameters.

Two general methods of sensitivity analysis are used in the literature (Dimov and Georgieva), namely the local and global methods. In the local sensitivity analysis method, also called one factor at a time method, small variations of input around a given value are introduced one at a time, and the resulting change of the value of the output is quantified. The local sensitivity analysis is used frequently, due to its relatively low computational burden. Global sensitivity analysis methods take into account all the variation in the values of the input on the prediction of the output variables (Sin, et al., 2009). In other words, global methods will cover the whole parameter space. Only few researchers have considered local sensitivity analysis during the modelling in the context of food engineering (Halder, et al., 2007b, Nicolai and DeBaerdemaeker, 1996, Zhang and Datta, 2006). An uncertainty and global sensitivity analysis was not incorporated in the modelling coupled heat and mass transfer during solid food processing.

Uncertainty and global sensitivity analysis have been used in several other fields for the evaluation of models. Some examples of applications are: environmental models (Campolongo and Saltelli, 1997), quality assessment of composite indicators (Saisana, et al., 2005), ecological models (Cariboni, et al., 2007), a blood flow and blood pressure model (Ellwein, et al., 2008), a hydrology model (Ratto, et al., 2007), chemical models (Saltelli, et al., 2005), a fermentation model (Sin, et al., 2009) and food risk models (Frey and Patil, 2002). An uncertainty analysis is used to map input uncertainty to output uncertainty, while a sensitivity analysis is applied to decompose input uncertainty, i.e. to identify the parameters that are most influential on the model output (Saltelli et al., 2008).

In relation to the above challenges, an uncertainty and global sensitivity analysis assist the physical-based model, if the important aspects of the state variables (e.g. average water content or a final temperature in the centre of a piece of food) can be shown to be insensitive with respect to variations in the values of input parameters, it is important that the models reflect this. Alternatively, if the global sensitivity analysis dictates that the prediction is indeed sensitive towards a poorly assessed parameter, then the model can identify this situation and serve as a platform for generating a better theoretical or experimental assessment of the particular parameter value. The physical-based model can also evaluate the effect of fluctuations in the

process conditions. This way of building models will make the model robust with respect to variations in values in such parameters. A robust modelling is, "by definition, a model that takes these uncertainties into account"[1], see also (Saltelli et al., 2008). The current work will therefore pursue this approach which will be expounded in chapter 2.

1.4 Objective

The goal of this project is to develop robust models of coupled heat and mass transfer during processing of solid foods. The model is based on the two representative cases – roasting of meat in a convection oven and a contact baking process. The specific objectives of the work were to: (1) develop the mechanistic mathematical model for two representative cases - identify the crucial equations and the parameters governing the transfer of heat and mass transfer (2) indentify and investigate the mechanisms of heat and mass transfer (water transport) and associated phenomena, (3) identify numerical solution strategies for PDEs of coupled heat and mass transfer using the FEM (COMSOL Multiphyics) for the two representative cases, (4) evaluate the models, verify them theoretically, and validate the models (assisted by experiments), and (5) to develop stochastic modelling to study the uncertainty and the sensitivity of the models with respect to uncertain parameters.

1.5 Overview

The PhD dissertation is organized in the 9 chapters: introduction (Chapter 1), a robust modelling approach (Chapter 2), the theory on heat and mass transfer (Chapter 3), the experimental work (Chapter 4), mathematical model formulation (Chapter 5), numerical solution and model implementation (Chapter 6), parameter estimation and model validation (Chapter 7), uncertainty and sensitivity analysis (Chapter 8) and conclusion and the general perspective (Chapter 9).

Chapter 2 describes the main components of the robust modelling approach. It is the roadmap for the current work (Figure 2-1) as well as the basis for the remaining chapters. In general, the robust modelling approach has four components. Each of the four components are briefly discussed.

[1] http://scmsa.pagespro-orange.fr/RMM/robust1.htm

Chapter 3 brings a review on the mechanisms of heat and mass transfer, and also includes an overview of the major heat induced associated physicochemical processes during frying and baking. The review on heat and mass transfer includes the mechanisms of heat transfer and the mechanisms of mass transfer. The evaporation of water is also discussed, where both local evaporation and surface evaporation (sharp boundary condition) are discussed. The overview of the major heat induced phenomena includes microstructure changes such as pore formation, reduction in water holding and shrinkage. The microstructure change and the effect of this change on the transport properties (e.g., permeability) are discussed. In addition, the thermophysical properties and heat transfer coefficient are briefly presented.

In Chapter 4 experimental works, both quantitative and qualitative measurements are presented. The measured variables together with suitable measuring techniques are briefly presented: product temperature, mass loss, local water content, the process conditions, and images of microstructure. Illustrative examples of experimental data are presented; subsequently, mechanistic interpretations of the observations are made. The obtained experimental and the observed data are used in later chapters for model building, model calibration and validation.

In Chapter 5, the heat and mass transfer processes are *formulated into mathematical equations*. The chapter presents the problem formulation of the governing equations of heat and mass transfer, and all the constitutive equations. The governing equations are based on the conservation of mass and energy. The problem formulation and the model assumptions for the two representative case studies: roasting of meat in a convection oven and the contact baking of pancake are presented. On the basis of the assumptions made on the physics of the system, model equations are established for the two representative cases. For both representative cases constitutive equations are also presented. The constitutive equations include the formulations of boundary equations, moving boundary and evaporation.

The sixth chapter deals with the numerical methods and the implementation of the mathematical model on the computer to *solve the model equations* formulated in chapter 5. The chapter starts with a short introduction to numerical methods. Then, the Finite Element Method, within the framework of COMSOL Multiphysics® version 3.5, is discussed in more detail. The solutions to

the model equations using the software and the implementations of the equations are illustrated: creation of geometry, meshing, implementation of physics, boundary conditions, and other rate equations, implementation of moving boundary. Some of the FEM simulations and results will be demonstrated with a model of the meat roasting process: 1) 3D model and 2) 2D (with moving boundary) model. The chapter ends with a summary and a brief introduction to COMSOL-MATLAB® computing environment for parameters estimation and uncertainty and sensitivity analysis.

Chapter 7 focuses on model evaluation: *(1) model calibration and (2) model validation*. Initially, a brief introduction of the parameter estimation and validation is given. The simulated data are compared to the experimental data. In the model calibration section, the technique and the algorithm for parameter estimations are discussed: implementation of the least square method, setting the objective functions and criteria, computing the correlation coefficients and the confidence interval of the estimations, the optimization algorithm itself. In the next section the model validation is validated with independent data. Some of the results are presented in the form of figures: the comparison of the predictive vs. the measured data is provided.

Chapter 8 deals with methods for the *uncertainty analysis and sensitivity analysis*. The chapter begins with a brief introduction on uncertainty and sensitivity analysis methods. Especially the Monte Carlo method is discussed in more detail. An uncertainty analysis consists of different steps: (1) Determination of the uncertain input, their range and distribution; (2) sampling the uncertain input parameters, (3) propagating input uncertainty to the output (FEM simulations); and (4) representation of output uncertainty. With respect to sensitivity analysis, the implementation of the standardized regression coefficient method and the Monte Carlo simulation are discussed. The rankings of input parameters for the different output are illustrated. The chapter ends with a summary of the uncertainty and sensitivity results.

In the last chapter - Chapter 9, the overall method/approach and the results obtained are summarized. A general conclusion and remarks on the developed physical model of heat and mass transfer are made. Last but not least, the perspective of the developed physical models towards industrial baking and frying operations in the food industry is discussed.

2 Robust modelling approach

2.1 Introduction

To successfully describe the coupled heat and mass transfer during heating of the solid foods and to evaluate the reliability of the model predictions (i.e., to deal with the uncertainty), the modelling strategy has to be formulated. Here, this strategy is called the robust modelling methodology. The robust modelling methodology (or approach) consists of systematic efforts to cope with the uncertainty (lack of knowledge, variations, assumptions or changes in the circumstance). These efforts are founded on an awareness of uncertainty which can be applied in all stages of modelling procedures. This definition is partially derived from the definition used in robust design (Arvidsson and Gremyr, 2008)[2]. The propose of the approach was aimed to describe the heat and mass transfer on the basis of the mechanistic mathematical model so that the model has broad applicability, and the model also takes uncertainty into account. This is precisely what will be discussed here.

2.2 Robust modelling approach

In this work, the robust modelling approach has four main core components Figure 2-1: (1) mechanistic mathematical model formulations, (2) solution of model equations using a FEM solution, (3) model calibration and validation, (4) uncertainty and sensitivity analysis and refinement of the model/ (e.g., propose simplification or reduction). These four components of model building are the roadmap of the thesis.

[2] *"A robust design methodology means systematic efforts to achieve insensitivity to noise factors. These efforts are founded on an awareness of variation and can be applied in all stages of product design* (Arvidsson and Gremyr, 2008)*"*.

2.2.1 Mechanistic model formulation (component 1)

The model formulation begins with the selection of a limited number of representative case studies for developing a model (as discussed in chapter 1), followed by identification of all the necessary mechanisms (e.g., heat transfer, mass transfer, evaporation and other transport associated processes), governing equations and constitutive equations. The ambition is to establish a general model that can accommodate many situations, which has broad applicability. Therefore, the formulations of the governing equations are based on the known laws (i.e., conservations of mass and energy) and the corresponding mechanism for each process.

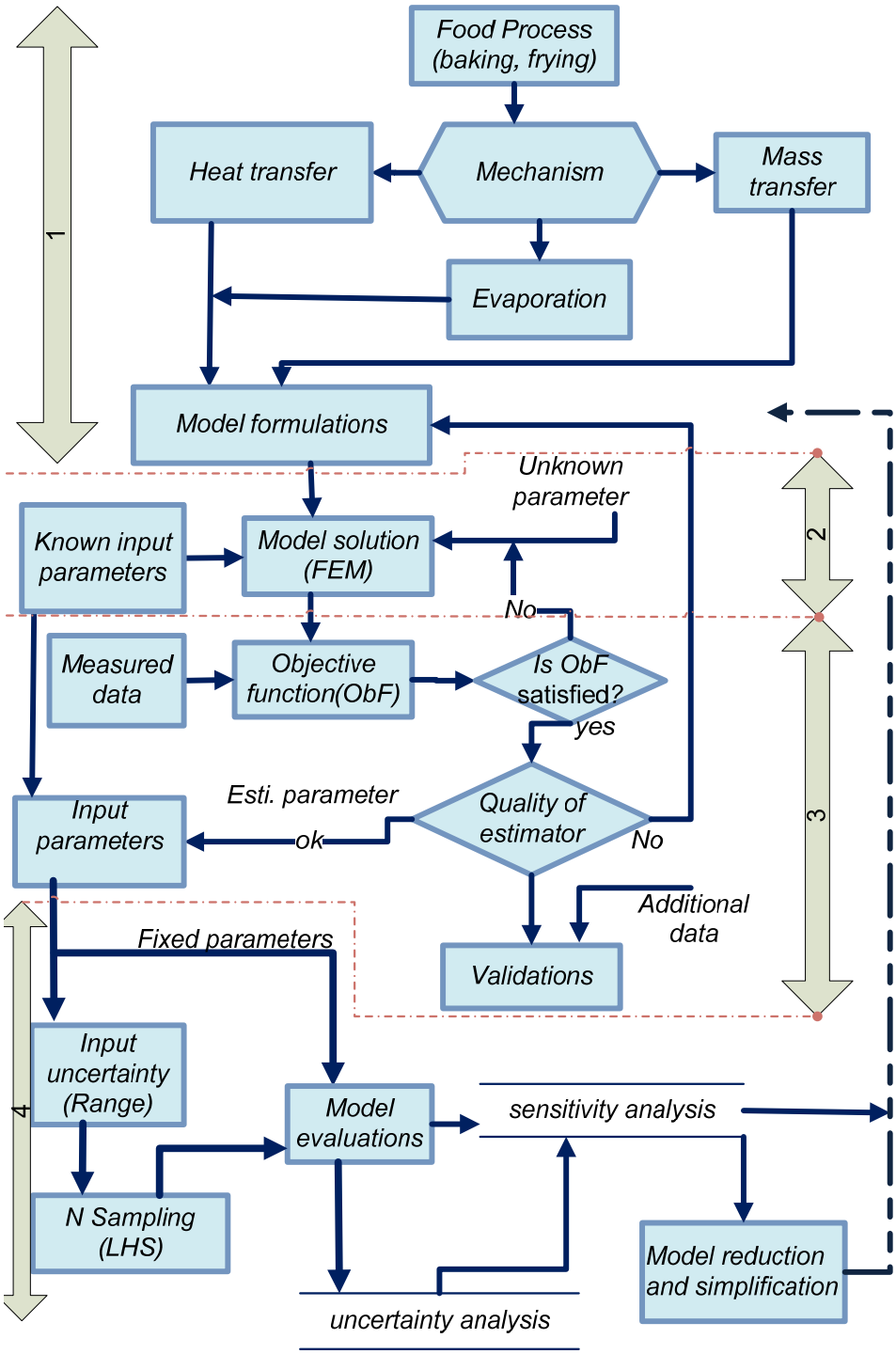

Figure 2-1 Robust modelling approach for coupled heat and mass transfer during processing of solid foods

In the model formulation, an adequate mechanistic understanding of the process (here the representative cases) is necessary in order to derive the physical-based model from general universal conservation laws that can be tractable in terms of mathematical treatment. Ideally, the model should include all the essential processes to obtain a high reliability of predictions; however, it should also include only the essential processes and no other ones in order to limit model complexity. This required a number of experimental studies to validate or to falsify some of the different mechanisms proposed in the literature. For example, the heating of meat in the convection oven drives the transformation of the raw meat into a palatable steak. To describe the roasting process, the first step is to develop the mechanistic understanding of the roasting of meat into a model that incorporates the essential physical processes (for detail see chapter 4 and 5).

In the meat roasting process, the mechanism of liquid water transport inside the meat was the subject of dispute in the literature, and the lack of a full understanding of this phenomenon has led to unrealistic predictions (paper I). The disagreement between theory and experimental data is probably due to the missing right mechanisms in the developed equations. In the current work, we have shown that the transport of water is driven by the over-pressure generated in the elastic meat matrix because of the gradual shrinkage of the meat fibres (paper I).

2.2.2 Building a FEM model of solid food process (component 2)

The second component of the model building is to solve the coupled heat and mass transfer model which is usually described by the coupled partial differential equations. Further, to interpret the mechanistic model into a set of physically meaningful and realistic boundary conditions (see chapter 6). When the model is solved, the solution or the predictions provide insight into the process by visualization (e.g., 3D and 2D temperature and water content distributions in meat). For example using the FEM, the effect of shrinkage as the moving boundary can be modelled (see chapter 6) and better understanding can be obtained for example whether to include the moving boundary or not. This means, the knowledge obtained from the FEM simulations can also be used in the reformulation of the heat and mass transfer model.

2.2.3 Model calibration and model validation (component 3)

The third main (Figure 2-1, no 3) component of the robust model approach has two main steps: calibration and validations. The developed model is tested by experimental data, in order to validate and refine the model. In the model calibration step, the missing parameters or parameters with unknown values are found by comparing the experimental data with the predictions. The unknown parameters are obtained by the parameter estimation method using the least square method (Hangos and Cameron, 2001). Once, all the parameters are known, the model is validated by comparing the validation data with the prediction (see for detail in Chapter 7).

2.2.4 Uncertainty and sensitivity analysis (component 4)

The fourth component of the robust modelling approach is dealing with parameter uncertainty. There are number of reasons why an uncertainty and global sensitivity analysis should be a part of model building procedures (Saltelli et al., 2008). The uncertainty and sensitivity analysis is important in identifying the impact of the parameter uncertainty on the predictions, and also to indentify the parameters with large impact from those with less impact on the model predictions. The sensitivity analysis is also the key ingredient in the model building to indentify the lack of fit, and then to refine it (Saltelli and Scott, 1997; Saltelli et al., 2000; Sin et al., 2009).

The uncertainty analysis allows mapping or propagation of the input uncertainty to output uncertainty (Saltelli et al., 2008). This means, the uncertainty analysis provides a range of uncertainty on the prediction. We used a Monte Carlo procedure in propagating the input uncertainty to output uncertainty (Helton and Davis, 2003, Sin, et al., 2009). After the uncertainty analysis, a global sensitivity analysis based on the Monte Carlo simulations with standardized regression coefficient is performed to identify the relative effect of the different parameters on the model predictions (chapter 8). In this way, the uncertainty in the input parameters and their relative effects on the model predictions are assessed and ranked. For example, the uncertainty analysis is used to quantify uncertainty in the model prediction (e.g., local temperature and water concentration) due to parameter uncertainties such as coefficients of heat and mass transfer, evaporation rate and other parameters. Such results can be used to distinguish between parameters that are robust to model prediction and those that need further

treatment to capture the behaviour of the system. This means that the sensitivity analysis serves as a guide to identify the key parameters and to further refine the model. Then, the model established above serves as a reference against which simpler and more practice-oriented models may be tested.

In the robust modelling approach, a robust model can be achieved by tackling different challenges at different stages (Figure 2-1) of the modelling building for example at component 1, 2 and 3 to test different assumptions and at component 4 to deal with parameter uncertainty. In chapter 3, mechanisms of heat and mass transfer are briefly reviewed. Then, the robust modelling approach will be exemplified by results from the representative cases.

3 Literature, heat and mass transfer in solid foods

3.1 Introduction

In this chapter, the main theories related to mechanisms of heat transfer and mass transfer, and other heat induced associated phenomena during roasting/frying and baking processes, are briefly presented. The latter heat induced phenomena include phenomena such as shrinkage, change in water binding capacity, phase changes mainly in the form of evaporation, and pore formation. The literature on heat processing of foods is evidently vast and scattered – a large number of studies have been done, but looking at different specific problems. The focus of the chapter is to discuss the previous work and provide background knowledge on heat and mass transfer during solid food processing.

3.2 Heat transfer (to/within) solid foods

Heating of solid foods involves an external (to the solid food) and an internal (within the solid food) heat transfer (Therdthai and Zhou, 2003). The former takes place between the heating medium (fluid or solid) and the solid food, whereas the latter takes place within the solid food itself. A solid food and a heating media exchanges heat at their boundaries by conduction, convection or radiation, or by a combination of those mechanisms (Gupta, 2001; Therdthai and Zhou, 2003). The contribution by different mechanisms/modes varies with different processes. For example, (Gupta, 2001) studied the contribution of heat transfer by individual heat transfer modes during the baking of Indian chapatti and he found that the contribution: by conduction (67%), by combined radiation (25%), and by free convection (8%). The external heat transfer mostly takes place on the boundary of a solid surface i.e., between the solid food and the heating media and it is often considered as the boundary conditions for governing heat transfer (Bird et al., 2001).

Convective heat transfer is a common form of heat transfer in many processes such as roasting of meat, baking of bread and cookies in a convection oven, where the food is heated with hot air

(Carvalho and Martins, 1992; Chen et al., 1999; Skjöldebrand and Hallstroem, 1980). In such a process, the convective heat flux at the boundary of the food is described by Newton's law ($q_{conv} = h(T_{oven} - T_{sur})$), where h is the heat transfer coefficient ($W \cdot m^{-2} \cdot K^{-1}$), T_{oven} is the temperature of the surrounding fluid (K), and T_{sur} is the product surface temperature (K) (Incropera and De Witt, 1985). The surface heat transfer coefficient (*h*) is one of the important parameters in the model of heat transfer and its value is obtained by several methods: dimensionless correlations, the lumped capacity method, the heat flux method and an inverse method (or time–temperature matching method) (Sakin et al., 2009).

Many heat transfer text books provide the dimensionless correlations to calculate the heat transfer coefficient for the free convection (Nu = f(Re, Gr))[3] and forced convection (Nu = f(Re, Pr)[4] with different geometric configurations (Bird et al., 2001; Brodkey and Hershey, 1988; Cengel, 2007; Gebhart, 1993; Incropera and De Witt, 1985). The dimensionless correlation method is only applicable for convective boundary conditions, if the properties of the fluid such as density, viscosity and the flow conditions (e.g., velocity, geometry) are known. In the heat flux method, the heat transfer coefficient is obtained from the heat flux measured at the surface by the heat flux sensor (Sakin et al., 2009). The lumped method is based on assumptions of the spatially uniform temperature, i.e., the Biot number must be checked (Bi < 0.1) for the validity of the method (Cengel, 2007; Incropera and De Witt, 1985). In the context of food processing, the lumped method was used to determine the heat transfer coefficient (Erdogdu et al., 2005; NITIN and KARWE, 2001). Nitin and Karwe (2001) used aluminium disks instead of model food products to determine the heat transfer coefficient of cookie shaped objects, and (Erdogdu et al., 2005) determined a spatial variation of the heat transfer coefficient value over a disk shaped copper surface during cooling under impinged air conditions. In the inverse method (an iterative technique), the temperature history at a fixed position of the model system is measured and the heat transfer coefficient is estimated using analytical or numerical solutions of heat transfer, alternatively (Anderson and Singh, 2006). Contrary to the lumped method, the inverse method

[3] Nu is Nusselt number(*Nu=hD/k),Re is Reynolds number, Gr is Grashof number*

[4] *Pr is Prandtl number*

requires a model system of a well-defined geometry and known thermo-physical properties (Sakin et al., 2009).

The energy emitted by radiation depends on the temperature of the surface and the radiation properties (emissivity) of the food material and the radiation heat transfer is described by the Stefan–Boltzmann equation (Incropera and De Witt, 1985).

On the basis of the assumptions, several models have been developed to describe the heat transfer inside the solid food, from the relatively simple 1D pure conduction heat transfer problem to the very complex multidimensional heat transfer with phase changes. The complexity of the model increases with increase in the number of spatial dimensions, phase changes (e.g., evaporation), heterogeneity for example change of thermal properties during processing.

Heat transfer inside the solid food takes place mainly by conduction or sometimes combined with internal convection and evaporation-condensation (Therdthai and Zhou, 2003). The conduction heat transfer in solid foods is usually described by Fourier's (second law) equation of heat conduction (Sakin et al., 2007). The solution of Fourier's equation of heat conduction gives the temperature profile inside the food. If one of the dimensions of the food is very small compared to the remaining other (two) dimensions. The 1D governing equation of unsteady state heat transfer is solved by an analytical method by assuming that the food is an infinite plate or infinite cylinder (Erdoğdu and Turhan, 2006). This method is extended for the finite body, i.e., for the multi-dimensional heat transfer problem, by using the geometric factor (e.g., the equivalent heat transfer dimensionality, EHTD), where the solution of the multi-dimensional heat transfer problem is expressed as the product of the one-dimensional solution of each of the dimensions of the finite body (Hossain et al., 1992). For example, the solution of the finite 2D cylindrical problem is approximated as the product of an infinite cylinder and infinite plate (Fasina and Fleming, 2001). In such classical approach the physical properties of food are assumed to be constant, and the approach is restricted to regular shapes which is often not the case. This limitation is due to the difficulty in mathematical treatment in solving the heat transfer with varying physical properties of food and irregular shapes (Erdogdu et al., 1998).

The heat conduction equation or Fourier's equation can be solved by numerical methods, and in the context of food engineering detailed methods and examples can be found (Floury et al., 2008; Jefferson et al., 2007; Martins et al., 2008; Ngadi et al., 1997b; Puri and Anantheswaran, 1993; Sandeep et al., 2008) and also further discussed in Chapter 6.

3.3 Mass transfer mechanism - water transport

Baking and frying processes are characterized by mass loss which is mainly in the form of water (Mondal and Datta, 2008; Skjöldebrand and Hallstroem, 1980; Sumnu and Sahin, 2008). The transport of water is driven by the gradients in the water concentration. Water migrates during the heating of solid foods by different mechanisms: molecular diffusion, pressure driven flow, capillary diffusion, thermo-diffusions (Srikiatden and Roberts, 2007). For example, during bread baking inside the dough, the diffusion and evaporation-condensation has been assumed to be the mechanism for water transport (Therdthai and Zhou, 2003).

The Fick's equation of diffusion is widely used as a model for water transport in food processes. The transient diffusion equation for water transport is solved using experimentally determined effective diffusivity (Dincer, 1996; Dincer et al., 2002; Kondjoyan et al., 2006; Shilton et al., 2002; Wang and Singh, 2004). In these models, all modes of water transport together are lumped as diffusion transport. This cannot always be justified for example when other phenomena such as pressure-driven flow due to intensive heating become important. A typical example is roasting of meat in a convection oven, where the water transport in the meat due to the shrinking of the meat induces pressure driven water transport (see section 3.3.1). Also, the use of effective diffusivity does not yield insight into the prevalent transport mechanisms (Halder et al., 2011).

Heating of solid food such as baking and frying of foods, are often accompanied by the evaporation of water, which can be interface evaporation or distributed evaporation (Datta, 2007). In the case of interface evaporation, the evaporation front can be a fixed interface (i.e., at the surface of the food) or a moving interface. The fixed interface is assumed when the crust or the dry region is thin and does not prevent the water transport; in other words, when there is no drying out from the surface. If evaporation only occurs at the surface, the product temperature near the surface stays below or at wet bulb temperature (Van Der Sman, 2007). Adler-Nissen

(2002) observed that the average temperature of vegetables in the quasi-stationary condition during frying in continuous wok stays below 80 °C, while the average surface temperature rises above 90 °C.

The moving interface (i.e., moving front) is presumed, when two distinct separate regions are formed as the heating progresses, for example a dry and a wet region as in the deep-fat frying process (Farid and Chen, 1998; Farkas et al., 1996), or a crust and a crumb region as in a bread baking process (Purlis and Salvadori, 2009). Contrary to the interface evaporation, a distributed evaporation occurs over a zone rather than at an interface (Halder et al., 2007; Ni and Datta, 1999; Yamsaengsung and Moreira, 2002). Water evaporates entirely in inside the food, which is also called local evaporation, during intensive heating of solid foods (Datta, 2007). This occurs when the food is vigorously heated at higher temperature. In the case of the latter, the consideration of local evaporation requires significant reformulation of the model, and it is much debated in many of the scientific literature, among them (Datta, 2007; Huang et al., 2007). One of the challenges is the determination of the evaporation rate, and the other is its implementation or incorporation into the model of heat and mass transfer (Huang et al., 2007; Peters et al., 2002). The evaporation rate is an important variable that determines the heat loss and the rate of water that is evaporated during heating of solid foods at higher temperatures.

Besides, other phase changes processes may occur during heating for example melting of fat or ice. In this study, they were not considered. Because, it is assumed that the food product of concern (e.g., roasting of meat and baking of pancake batter) have low fat content for example in the case of meat it is only 3 % of the total meat weight (Tornberg, 2005). Secondly, these products are heated from the unfrozen state, i.e., the initial temperature is around room temperature, implying there is no ice in the raw food to be melted.

3.3.1 Water transport mechanisms during roasting of meat in convection-oven

Water is a major (e.g., lean muscle contains approximately 75%) component of the whole meat muscle and the remaining 25 % consists of protein (20%), fat (3%) and soluble non-protein substances (2%) (Huff-Lonergan and Lonergan, 2005; Tornberg, 2005). Most of the water in

muscles is held within the cell structures (which is mainly protein); inside myofibrils and intermyofibrillar spaces, between myofibrils and cell membranes, between muscle cells and between bundles of muscle cells (Kołczak et al., 2007).

The water in meat muscles exists in three forms: bound, entrapped and as free water. Bound water is tightly bound to the proteins, has very low mobility and is very resistant to being driven off by conventional heating (Huff-Lonergan and Lonergan, 2005). This fraction of water is very small in muscle cells (less than 10% of the total water) (Huff-Lonergan and Lonergan, 2005) and (Tornberg, 2005). Entrapped (immobilized) water is held within the structure of the muscle, and does not bind to protein. The entrapped water does not flow freely from the tissue, yet it can be removed by heating (e.g., by frying or drying processes). This water escapes from the meat during heating. This is because the heat changes the muscle cell structure that leads the water to escape (Huff-Lonergan and Lonergan, 2005). Free water is not seen in pre-rigor meat, but can develop as conditions change, which allows the entrapped water to move from the structures, for example it easily escapes during heating (Huff-Lonergan and Lonergan, 2005).

When the food is heated, its constituent migrates, the physiochemical changes, and these changes are reflected in the microstructure (Aguilera, 2005). Heating induces structural changes, which decreases the water-holding capacity of the meat (Godsalve et al., 1977). The unbalanced pressure is generating a contracting stress that removes more water from the meat structure, leading to meat shrinkage. Tornberg (2005) reviewed the structural changes and its effect during the meat cooking. The study revealed that meat samples being cooked would shrink in a multi-direction (transverse and longitudinal) which leads to a final product with large irregularities in shape. There were some controversial observations on meat shrinkages among early studies. For the transversal shrinkage, Davey and Gilbert found that there was no change in the cross-sectional area on cooking of the neck muscle as confirmed by Tornberg (2005). On the contrary, Bendall and Restall (1983) found that the transverse shrinkage of both fibres and fibre bundles starts at about 40 °C (Bendall and Restall, 1983). In relation to longitudinal shrinkage, Bendall and Restall (1983) observed that fibres do not shorten until 60 °C. On the other hand, Hostetler and Landman (1968) reported that both sarcomere and fibre shortening usually begin at temperatures of 40–50 °C (Hostetler and Landmann, 1968).

According to Tornberg (2005) the shrinkage of meat can be summarized as: (1) the transverse shrinkage of the fibre starts at 35–40 °C, it occurs mainly at 40–60°C and it widens the gap between the fibres and their surrounding endomysium, (2) the shrinkage of the connective tissue starts at 60 °C, and at 60–70 °C the connective tissue network and the muscle fibres co-operatively shrink longitudinally. Shrinking of the connective tissue exerts a pressure that drives water into the extracellular void space Figure 3-1. The extent of shrinkage increases with the increase in temperature and causes large water loss during cooking (Tornberg, 2005).

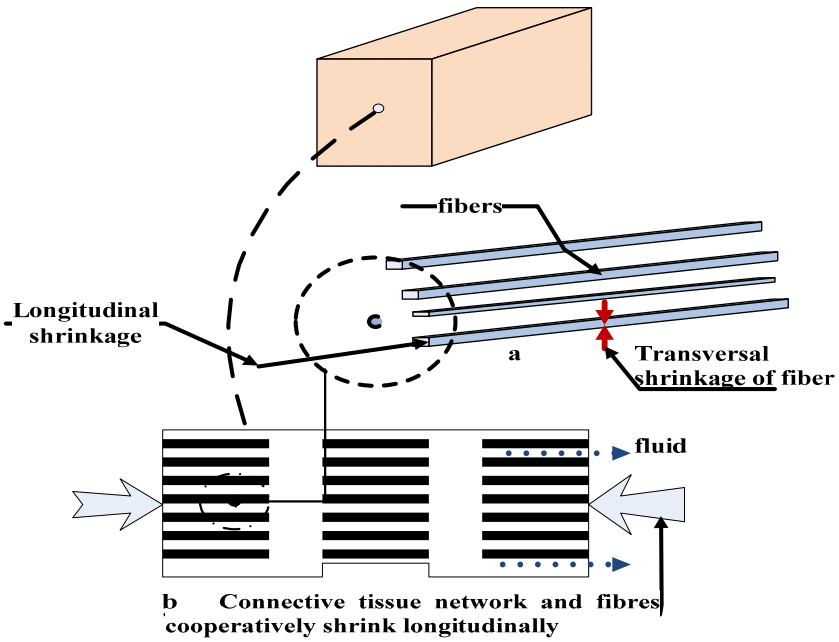

Figure 3-1 Schematic diagram of shrinkage of meat structures

Modelling of meat frying processes is largely concerned with contact frying of meat patties or deep-fat frying of (battered) meat products, reflecting the wide-spread industrial interest in these types of products (Dincer, 1996; Ikediala et al., 1996; Ou and Mittal, 2006; Pan et al., 2000). There are some earlier modelling studies of the oven roasting process, which all emphasize the crucial effect on the energy transfer from water evaporating from the meat (Bengtsson et al., 1976; Chang et al., 1998; Singh et al., 1984; Skjoldebrand and Hallstrom, 1980). As shown already in the classical study (Skjoldebrand and Hallstrom, 1980), the transport of water inside

the meat is also coupled to the heat transfer in a complex and yet not fully understood way. Some of the models of heat and mass transfer of meat cooking processes are totally lumped and do not include any important physics (Bengtsson et al., 1976; Fowler and Bejan, 1991; Ikediala et al., 1996). Such models are based entirely on empirical data, are only suited for a specified processing condition.

Several researchers have formulated different hypotheses to model mass transfer during roasting, mostly from the perspective of diffusion (Chen et al., 1999; Huang and Mittal, 1995; Ngadi et al., 1997a) while disagreements are often seen with regard to other types of water transport mechanisms (Godsalve et al., 1977; Thorvaldsson and Skjöldebrand, 1996; Wählby and Skjöldebrand, 2001). Purely diffusion based models do not adequately describe the moisture transport phenomena during meat cooking because the effects of the water holding capacity and the shrinkage phenomena are not considered. These are, however, the main driving mechanisms for the exudation of water during the cooking or roasting of meat, and some of the early studies on this topic agree with this fact (Godsalve et al., 1977; Tornberg, 2005; Wählby and Skjöldebrand, 2001). Roasting of meat causes the muscle protein to denature, resulting in a decrease in water holding capacity and leading to shrinkage of the protein network. Shrinkage of the network ultimately induces a pressure gradient inside the meat muscle.

Outside the field of meat science, similar physics occur during syneresis of curd (Barriere and Leibler, 2003) and polymer gels (Tijskens and De Baerdemaeker, 2004; Wu et al., 2004). The curd and polymer gels during heating can be regarded as a “self-squeezing sponge” (Kaasschieter and Frijns, 2003) and the model of such a system can be described by the poroelastic theory. A similar approach was also applied in meat science for the first time by Van der Sman (2007) who studied water transport inside meat during cooking (van der Sman, 2007). Nevertheless, the pressure driven water transport is not new in meat science, the drip loss in meat was observed before the work of Vand der Sman (2007). For example, the shrinkage induced drip loss was observed during the rigor process – the water moves out of the meat structure by creating a drip channel as the overall volume of the cell is contracted (Huff-Lonergan and Lonergan, 2005; Offer and Cousins, 1992).

Vand der Sman (2007) applied the Flory–Rehner theory to quantitatively describe the pressure that drives water transport. The Flory–Rehner theory has been used to describe water transport in food gels, biological tissues, and artificial muscles (Eichler et al., 2002; Mizrahi et al., 2001). In these studies, the pressure is called matrix or swelling pressure. According to the Flory–Rehner theory, the swelling pressure is the sum of the mixing pressure (or osmotic pressure) and the network pressure due to elastic deformation of the cross-linked polymer gel (π_{el})(Mizrahi et al., 2001). On the basis of the Flory–Rehner theory, Van der Sman (2007) derived the swelling pressure (P) in meat in terms of the moisture content (C), equilibrium water holding capacity (C_{eq}(T)) and modulus of elasticity (E) as:

$$P = E\left(C - Ceq\,(T)\right) \tag{3.1}$$

The gradient in the pressure drives the liquid water flow.

During heating, water can be released into the pore space and then transported through the porous media[5] or the food matrix. The water flow inside the meat is described by Darcy's law of porous media (for laminar flow) as a function of the pressure gradient (Datta, 2006). The pressure driven water transport is formulated using Darcy's law with the physical properties such as permeability, elastic module and viscosity of the fluid.

Van der Sman (2007) predicted a quite large increase in the moisture content at the centre of the whole meat, which is in disagreement with the observations of Wahlby and Skjöldebrand (Wählby and Skjöldebrand, 2001). Van der Sman (2007) did not consider the change in meat properties (e.g., elastic model and permeability) during the cooking. Although, Skjöldebrand and Thorvaldsson in their earlier (Thorvaldsson and Skjöldebrand, 1996) study on pre-cooked meat observed a slight increase in water content at the centre of the sample, they did not observe any increase in water content in their later study on the roasting of *raw* whole meat (Wählby and Skjöldebrand, 2001). The reason for the disagreement between theory and observation can be ascribed to differences in the microstructures of raw and pre-cooked samples. The dynamic

[5] A solid food is considered as porous media, when its void (pore) space is filled with fluid (gas or liquid)(Datta, 2007)[5]. In the vast majority of food systems, proteins or carbohydrates form a porous skeleton, which contains fluid (water and fat) physically or chemically bound to it (Halder et al., 2011).

change of the microstructure of meat during the heating process plays a great role in water transport. This is often neglected, however, and this leads to ambiguity in the description and modelling of the water transport (see paper I).

Permeability is the most important physical property of a porous medium; it measures the ability of a porous matrix to conduct fluid flow (Datta, 2006). The permeability of food materials changes during heating due to changes in its microstructure for example pore formations or opening of channels. However, there are very few studies on permeability in solid food and the obtained data quite varies (Datta, 2006; Kovácsné Oroszvári et al., 2006). Datta (2006) measured the permeability of raw potato and raw whole beef tissues and the obtained the values of water permeability was in between 10^{-19} m^2 and 10^{-17} m^2, where the values for potato being slightly lower than for the meat. In the same study, the influence of porosity on the intrinsic and relative permeability was studied and the water permeability increases with porosity. Kovácsné Oroszvári, et al. (2006) studied the intrinsic permeability of the heat-treated beef burgers for temperatures ranging from 50 °C to 80 °C. They found an intrinsic permeability of water in the range of 6.8×10^{-18} m^2 to 1.6×10^{-16} m^2, where the highest water permeability value was obtained for the beef burger made of the lean meat and cooked at 60 °C. Using a light microscope, they also observed the most open structure of the beef burger at the same temperature. However, the results obtained by both studies on the permeability of meat do not agree with each other – there is a significant difference and there is also large variation in the permeability values. Moreover, the data on the spatial and time dependency of permeability are not available.

Elastic modulus is a material property and for meat it varies with the cooking temperature (Tornberg, 2005). This was already observed during cooking of whole meat and beef burger, which is illustrated by Figure 3-2. The storage modulus increases steeply with the temperature from 50 to 65 °C for the whole and the minced meat, where it levels off to values for the modulus of 80 and 70 kPa for the whole and minced meat, respectively (Tornberg, 2005). The change of the modulus elasticity was not considered in the model equations of Van der Sman (2007), therefore in our case the elastic modulus, E is described as a function of temperature, which can be derived from Figure 3-2.

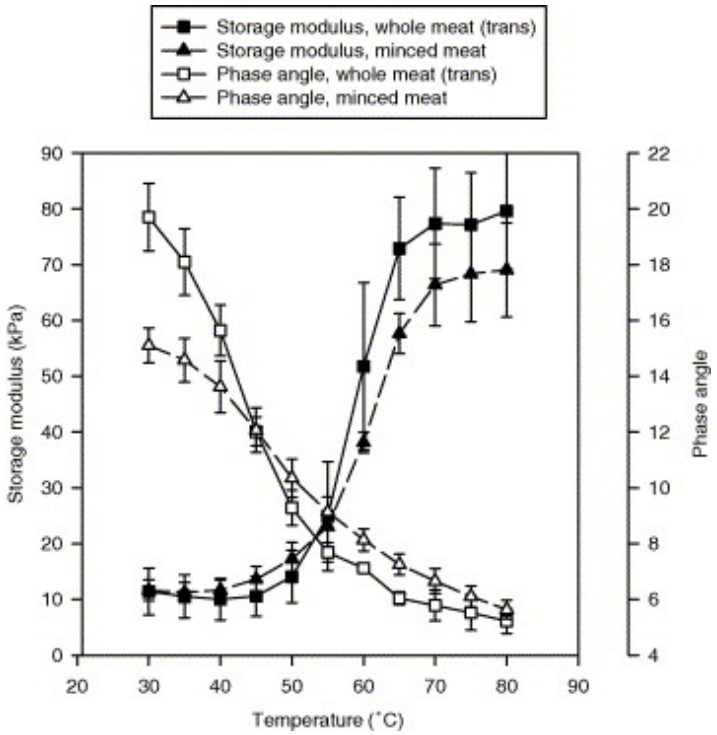

Figure 3-2 Storage modulus (kPa) and phase angle (degrees) for whole meat (■, □) and for minced meat (Δ, Δ), respectively, made out of beef M. biceps femoris, as a function of cooking temperature. The bars give the standard deviation. Adopted from (Tornberg, 2005).

Transport of water in solid food materials can be complex, as water is removed: the space may be replaced by air, i.e., pore formation (Kassama and Ngadi, 2005; McDonald and Sun, 2001) or it may be compensated by shrinkage. Shrinkage is undesired, because it has a negative consequence on the quality of the final product – changes in shape, loss of volume and increased hardness.

The methods used to consider material shrinkage differ greatly throughout the literature (Katekawa and Silva, 2006). Nevertheless, it is often considered that the change of dimensions is proportional to the volume of liquid water removed (Katekawa and Silva, 2006). For meat cooking, Cheng-Jin Du and Da-Wen Sun (2005) found a good correlation between the shrinkage (volume based dimension changes) and cooking loss (Cheng-Jin Du and Da-Wen Sun, 2005). Cheng-Jin Du and Da-Wen Sun (2005) confirmed that a higher shrinkage leads to more cooking loss, and vice versa. However, neither Cheng-Jin Du and Da-Wen Sun (2005) incorporated

shrinkage into the model of heat and mass transfer, nor did all the above mentioned models of heat and mass transfer including the recent study, Van der Sman (2007), did not consider the change of volume (overall shrinkage) during meat cooking. This means that the governing model equations were solved on fixed boundary, where the material boundary remains the same for the entire roasting period.

The action of roasting causes denaturation of meat proteins. This leads to dehydration and shrinkage of the meat, and the simultaneous formation of air-filled and water-filled pores (Kovacsne Oroszvari et al., 2006). The water-filled pores are formed due to the reduction of water binding capacity and shrinkage that release water into the intercellular space, whereas as the air-filled pores are due to the water loss mainly by evaporation. The pore formations and structural changes during heat treatment of beef burger made from rib meat were studied using the light microscope at different pan temperatures (50°C, 60°C, 70°C and 80°C) (Kovácsné Oroszvári et al., 2006). The authors found that the water-filled porosity varies with pan temperature: for beef burger made of rib meat the highest water-filled porosity was 32% when it was cooked at the temperature of 60 °C and no significant differences were found in the water-filled porosity at 50 °C, 70 °C or 80°C. However, in the case of whole meat, there is no corresponding data.

Our description of these changes, which are expounded in (paper I) is as follows: The structure of raw meat is intact at the start of the cooking process, and water transport is hindered by low permeability. However, during the roasting of the raw meat, dramatic changes in the microstructure (such as pore formation, change of elastic modulus) are induced, which affect the water transport. Spatial variation in temperature creates a spatial difference in permeability and elastic modulus, where parts of the meat sample closer to the surface have larger permeability and elastic modulus than the parts closer to the centre. There is therefore a much larger resistance to water flux towards the centre than towards the surface of the meat piece. Since water moves in the direction of least resistance, the water will preferentially flow towards the surface against the temperature gradient and form exudates. It is therefore crucial that the models consider these phenomena for better understanding and prediction of the roasting process.

3.4 Thermo physical properties

The thermal properties such as specific heat, thermal conductivity, and density of foods are important parameters in describing heat transfer during the heating of solid foods (Rao et al., 2005). Their values can be obtained from published literature, by measuring (Baik et al., 2001; Fasina and Fleming, 2001; Ghazala et al., 1995), by estimating from the thermal properties of each composition (Davey and Pham, 1997; Rao et al., 2005) or using the inverse approach (i.e., using the solution of heat transfer models and experimental temperature profiles) (Mohamed, 2010; Schmalko et al., 1997). Baik et al., (2001) made a critical review on the thermal proprieties of bakery products. The reported data on the thermal properties of foods varies with product type, composition and origin, process condition, and structure of the foods. The thermal properties of some foods (e.g., bakery products) are very limited compared to other types of foods (Baik et al., 2001). Generally, for most solid foods, data at various temperatures and moisture levels are not readily available. Some text books give only background information of limited general data (Rao et al., 2005). On the other hand, some journal articles giving the comprehensive data set of the thermal property values for groups of food products at certain temperature and water content, e.g., for bakery products can be found in (Baik et al., 2001; Zanoni et al., 1995) and several different types of equations, even for the same product. Some of these semi-empirical equations are not accurate beyond the particular range of process conditions (Datta, 2007). The temperature and composition based calculation of the thermal properties is relatively more generic (Baik et al., 2001). The main compositions of foods usually are water, protein, carbohydrate, fat, fibre, and other (salt and ash are very small), their temperature dependent thermal properties can be found in the literature (Rao et al., 2005). The composition based estimation of the thermal properties for density (ρ_p), specific heat capacity (cp_p) and thermal conductivity (k_p) are given as:

Density: $$\rho = 1 \Big/ \sum_i \frac{y_i}{\rho_i} \tag{3.2}$$

Specific heat capacity: $c_p = \sum c_{p_i} y_i$ (3.3) $c_{p_i} = c_o + c_1 T - c_2 T^2$ (3.4)[6]

Thermal conductivity: Parallel model: $k = \sum_i \frac{\upsilon_i}{k_i}$ (3.5

Perpendicular model: $\frac{1}{k} = \sum_i \frac{\upsilon_i}{k_i}$ (3.6)

where υ_i and y_i are the volume and mass fraction of each component *i* (water, protein, carbohydrate and fat) respectively. These models have been applied successfully for different food materials, and the models of specific heat and density are also valid in porous foods, including bakery products (Baik et al., 2001; Rao et al., 2005). Parallel and perpendicular models have been found to provide the upper and lower limits of thermal conductivity, respectively (Rao et al., 2005). However, applications of such models to some foods (e.g., bakery products) have been limited (Sumnu and Sahin, 2008). The thermal conductivity of foods decreases with decreasing water content (Maroulis et al., 2002).The pore formation (air-filled pore) in food during processing further decreases the conductivity. In that case, an effective thermal conductivity is calculated from the porosity and the water content (Baik et al., 2001; Rao et al., 2005). One of the limitations to the latter approach is that the porosity of most foods is not readily available.

3.5 Summery

An overview of literature reviews related to the mechanisms of heat and mass transfer during processing of solid foods was presented. It is evident that heating of solid foods such as baking and roasting processes involves combined complex processes – heat, mass transfer, evaporation and heat induced associated processes, as illustrated by the roasting of meat in convection-oven. As the result of the complexity, the physics of heat and mass transfer are less understood.

[6] The values of the constants were obtained from (Rao et al., 2005) and here, the temperature is in ^oC

4 Experimental work and mechanism interpretation

4.1 Introduction

In this chapter, the experimental work of two representative case studies, i.e. roasting of meat in a convection oven and a contact baking process are presented. The overall aim of the experimental work was to obtain experimental data that could be used in the model building (e.g., input parameters[g], to test the mechanisms for example in the case of local water transport and to obtain data to be used in the model calibration and validation). The detailed experimental method, the procedure and the results were described in the attached papers: the contact baking process in (paper III) and the roasting process in (paper I and V). The reported results and the discussion in the upcoming sections were therefore mainly extracted from these papers.

4.2 Sample and sample preparation

A sample preparation includes all the procedures prior to the actual heating of the sample – in this case the meat sample in the convection oven (paper I and II) or the pancake batter in a contact heating process (paper III). Before processing the sample or heating it under the given process conditions, (convection-oven or contact heating), the sample was prepared into the required geometry, size and composition. In the case of roasting of meat in the convection oven, the meat (Longissimus dorsi) was cut in the form of: (1) a rectangular (54mm×40 mm×40 mm), and (2) a cylinder (54mm×40 mm, length and diameter respectively). In the case of pancake batter baking, the pancake batter was prepared from its ingredients (50 g egg white, 30 g egg yolk, 150 g of milk, 125 g of wheat flour and 20 g of sugar) and (paper III, section 3). Before the sample was heated the initial conditions such as water content, temperature and the size of each sample were measured.

[g] Input parameters includes such as process temperature, initial condition of state variables, heat transfer coefficient, and others.

4.3 Contact baking process

The pancake batter was baked using the contact baking experimental set-up (heating rig, data logger with temperature sensors and computer) as shown in Figure 4-1.

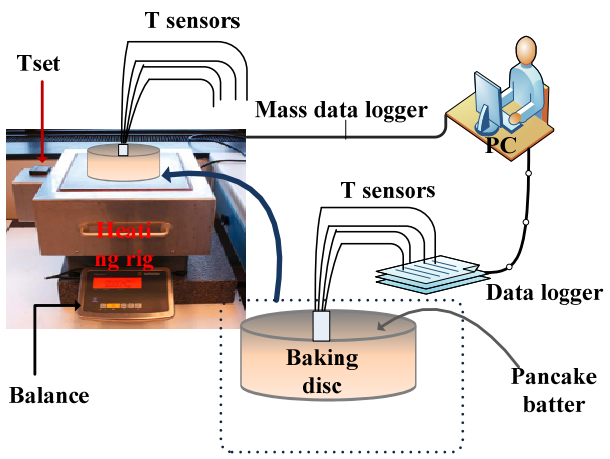

Figure 4-1 Schematic of controlled experimental set-up during the contact baking process

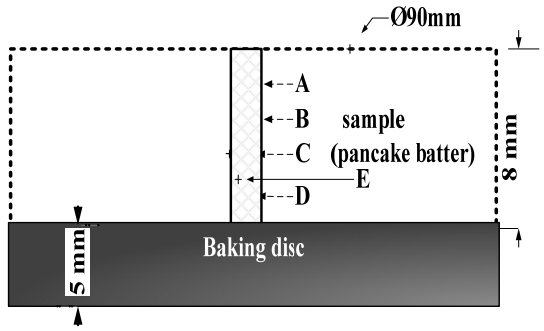

Figure 4-2 Temperature sensor position within dough (A = 6.4 mm, B = 4.8 mm, C = 3.2 mm, and D = 1.6 mm from the bottom surface, E = the sensor holder)

A circular baking disc with a diameter of 90 mm and a thickness of 5 mm was used for the pancake baking experiments. The baking disc is made of 5754-aluminum (paper III). To fix the temperature sensors at a given position within the pancake batter, a temperature sensor holder (E) was constructed at the centre of the baking disc, as shown in Figure 4-2. Four holes were made through the sensor-holder (E), which is made of Teflon. In each hole, temperature sensors (T-type thermocouples) were placed at four different positions (A, B, C and D) and thermocouples were connected to the PC (computer) through a data logger (Tc-08 Pico Technology, Cambridgeshire, UK). Once, the thermocouples were placed at different positions

within the sample, the pancake batter was baked using the heating-rig[h] for 20 min and the temperatures were recorded at every second during the pancake baking. The pancake batter was baked at three different temperature set points (160, 200 and 240 ºC) (section 3.2 in paper III). The local temperature measurements were repeated four times for each temperature set point and the average local temperatures were computed. The corresponding mass loss was measured online using the balance, connected to the computer via the data logger (using setup Figure 4-1). From the mass loss data, the average water content of the product was calculated (Appendix B.1). Besides, the surrounding air temperature above the pancake batter was measured and its value was in between 35 ^{o}C to 46 ^{o}C (at the temperature set point of 160 ^{o}C). During the experimentation, other qualitative observations effects on the product such as burned surface at the bottom of the product, water bubble and the expansion of the pancake were made.

4.3.1 Local temperature profile

Figure 4-3 shows the measured temperature profiles at the four positions (Figure 4-2) inside the pancake during baking at 160 ^{o}C. Generally, two major distinct periods can be distinguished in the temperature profiles: the heating period (sensible heat dominant zone) and the evaporation period (latent heat dominant zone). In the heating period, most of the supplied heat energy from the heating rig is used to increase the temperature of the pancake batter. The heating period is short compared to the evaporation period, particularly for the position in the product that is closest to the bottom surface (e.g. at position D, about 200 s, Figure 4-4).

During the evaporation period, where the temperature curves only increase slowly, nearly all of the supplied heat to the product is used for evaporating the water. In the evaporation period, with a temperature set point of 160 ^{o}C, the temperature at position C is more or less stable around the boiling point of water (attains $T = 100\ ^{o}C$ *at* $t = 600\ s$), while towards the end of the baking process, there is a slight temperature rise ($t = 1200\ s,\ T = 103\ ^{o}C$). For the same temperature set point of 160 ^{o}C, however, the temperatures at the positions A and B remain below 100 ^{o}C for the entire period of baking. They remain almost constant (*approximately at* $T_A = 89\ ^{o}C$ *and* $T_B = 95$

[h] The heating rig was constructed with a 300 x 300 x 25 mm aluminium slab cast of the alloy AA-6082 (AlMgSi1) which entirely rests on the balance, for detail see paper III.

^{o}C, respectively) for most of the heating time. The length of the period, in which this constant temperature level is observed, is getting shorter as the temperature sensor position moves from the top to the bottom surface.

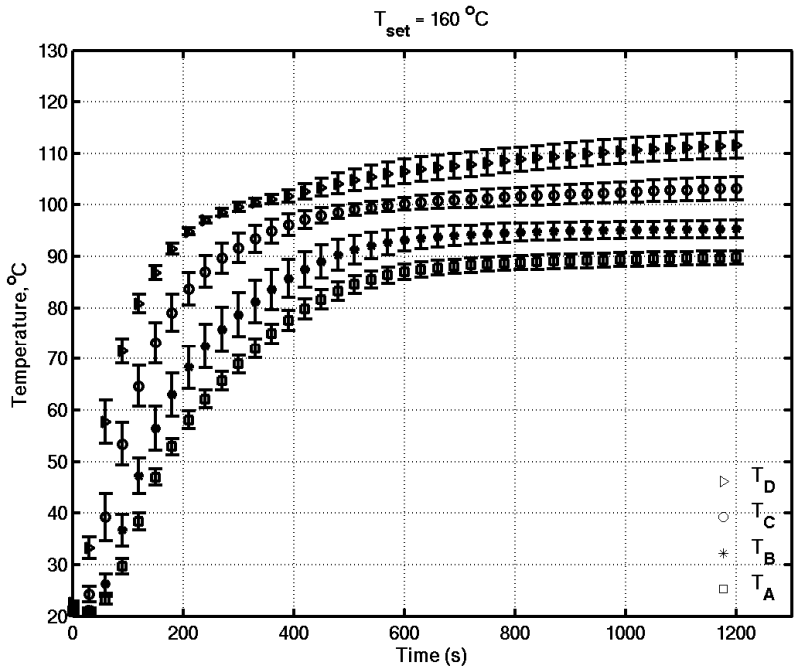

Figure 4-3 Temperature profiles inside the pancake batter at different positions (position A, B, C and D) with temperature set point of 160 ^{o}C. The data are only shown with a sampling interval of 30 seconds, for clarity. The bars show the standard deviation.

At position D, in the evaporation period, an early increase of the temperature above 100 ^{o}C was observed. The early increase in temperature above the boiling point of water is explained by the drying-out effect at the bottom surface due to vigorous evaporation. This means that, as the liquid water content diminishes near the bottom surface: (1) an insulating layer is formed at the bottom surface, which reduces the thermal conductivity, and in turn the thermal diffusivity; and (2) less and less energy is consumed by evaporation at the bottom surface layer, compared to earlier times where the concentration of water was higher. This effect is more pronounced with higher temperature set points, especially at position D (Figure 4-4).

In the heating period, the temperature profiles with the three temperature set points follow each other and there is only a slight difference in temperature profile between each temperature set point (Figure 4-4). However, in the evaporation period, the three temperature set points have resulted in different product temperature profiles. This is particularly the case at position D (Figure 4-4, top-left). The increase in the temperature set point leads to a higher evaporation rate, and as a consequence a faster drying out, which in turn induces a temperature rise. Towards the end of the baking process (*t = 1200 s*), the product temperature at position D attains a temperature of 112 ^{o}C , 127 ^{o}C and 148 ^{o}C, with temperature set points of 160 ^{o}C, 200 ^{o}C and

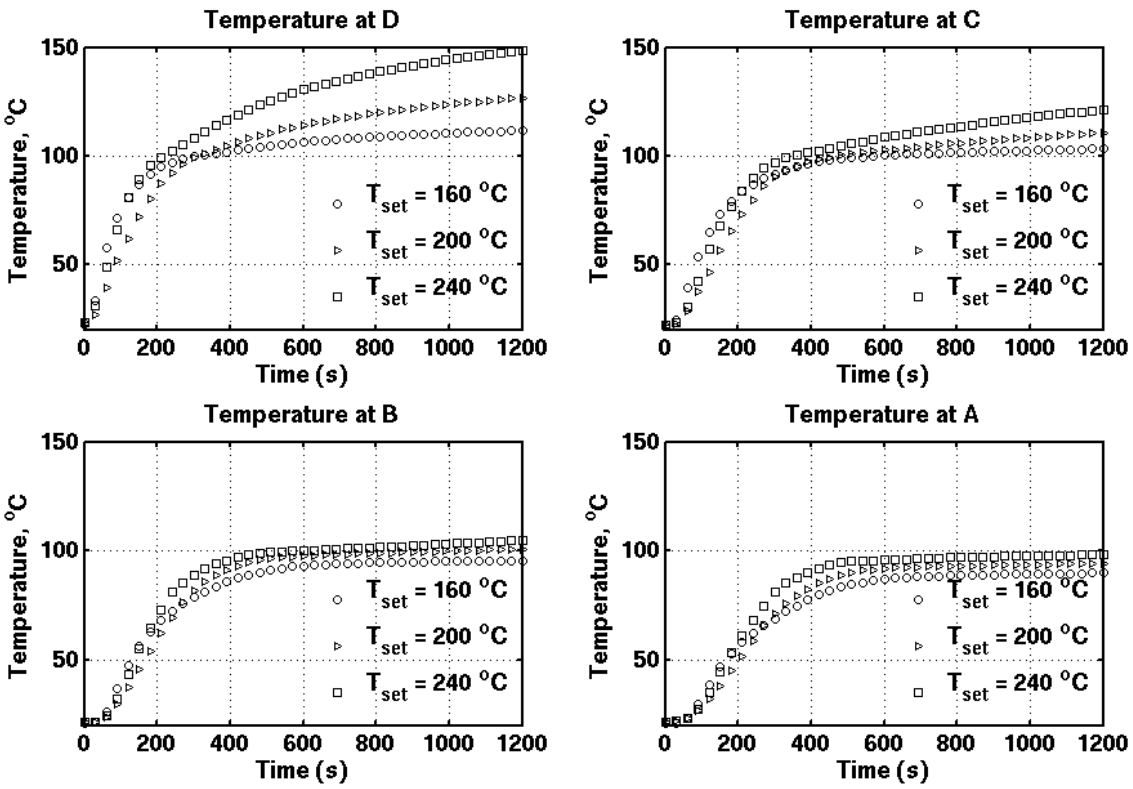

Figure 4-4 Temperature profiles at different positions (position A, B, C and D) with temperature set points of 160 ^{o}C, 200 ^{o}C, and 240 ^{o}C. The data are only shown with a sampling interval of 30 seconds, for clarity.

240 ^{o}C, respectively. The temperature profile of the product closer to the bottom surface is very sensitive to the temperature set point, while this sensitivity decreases as the position of the

temperature sensor is further away from the bottom surface (Figure 4-4, compare at four positions, D to A) (further see chapter 8). The effect of the temperature set point on the product temperature profile at position A is quite small compared to the effects observed at position D. Besides, the spatial variation of temperature (temperature gradient) in the pancake batter is relatively smaller with lower temperature set points compared to higher temperature set points. This implies that the quality of the end product related to temperature is more uniform when baked at a lower temperature set point compared to a higher temperature set point.

4.3.2 Mass loss

Figure 4-5 shows the obtained average water content of the product when baked at the three temperature set points (160 ^{o}C, 200 ^{o}C, and 240 ^{o}C). The average water content of the pancake batter decreases as a function of time. In the early stages of the experiment (t < 200 s), the rate of decrease is relatively low, and visually there is no difference between the three average water content profiles. The turning point for the rate of decrease is around t = 200 s, when the bottom region of the product has reached the evaporation temperature (Figure 4-4, at position D). After that time, $t = 200\ s$, the average water content of the product decreases rapidly, and the rate is different for the three temperature set points (Figure 4-5). The rate of evaporation, and thus the rate of weight loss, increases with increasing temperature set point. The latter is convincingly illustrated by the average slopes of the water content profiles: (-1.4, -2.3 and -3.8)$\cdot 10^{-4}$ kg/kg/s, for a temperature set point of 160 ^{o}C, 200 ^{o}C, and 240 ^{o}C, respectively.

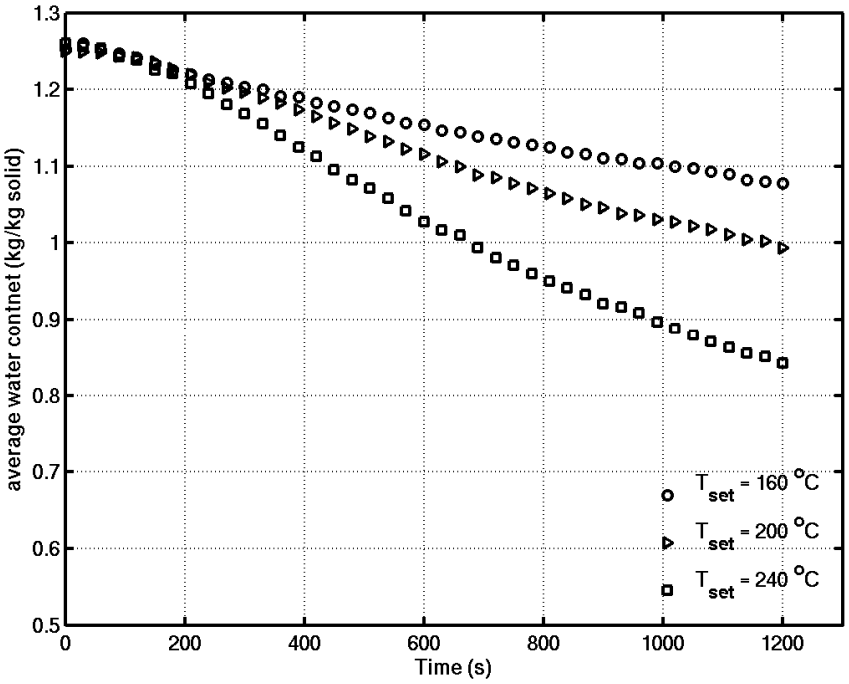

Figure 4-5 Average water content (kg of water / kg of solid) during baking of the pancake batter at three different temperature set points (160 °C, 200 °C, and 240 °C, respectively). The data are only shown with a sampling interval of 30 seconds, for clarity.

4.4 Roasting process

4.4.1 Roasting oven and set-up

A professional oven, Rational Combi-steamer ccc (with an oven space of 0.83 m x 0.645 m x 0.495 m) was used for the frying of meat. Dry hot air is circulated inside the oven by means of a fan, which reverses its direction of rotation every 1-2 min to ensure a more uniform heat transfer from the hot air to the product. The temperature of the hot air is controlled by the oven thermostat (stable around the set point with a standard deviation of ± 3°C). The oven was set to dry air (no humidification), 50% of the maximum fan speed and an oven temperature of 175 °C. The oven was heated until a constant temperature of 175°C was reached. This means, the oven was initially heated to 175°C before placing the sample in it. This was monitored by measuring the oven air temperature at different positions. The preheating of the oven avoids non-stationary

conditions at the beginning of the process and as such reduces uncertainty. Once, the oven temperature reached the temperature set point, a sample was placed centrally in the oven, the sample itself was placed on a stainless steel baking tray. The heat transfer coefficient and oven temperature are required to determine the heat flux from the hot air to the food, these process variables were measured (paper V).

4.4.2 Heat transfer coefficient

The convective heat transfer coefficient was determined using the Lumped heat transfer method (Eq. 4.1). The Lumped heat transfer method is valid, if the Biot number is less than 0.1 (Incropera and De Witt, 1985, page 215 and 216). A rectangular and a cylindrical aluminium (Al) block of the same size as the food samples were constructed to determine the convective heat transfer coefficient (Nitin and Karwe, 2001). The Biot number for these Al blocks is very low (Bi = 0.004[i], which is <<0.1, see paper I). The temperatures at the geometric centres of the aluminium cylinder and rectangle were recorded every 10 seconds (for total time = 1400s).

$$\ln\left(\frac{T_{oven} - T_{Al}}{T_{oven} - T_0}\right) = -bt \qquad (4.1) \qquad\qquad b = \frac{h\,A_s}{V_{Al}\,\rho_{Al}\,c_{p,Al}} \qquad (4.2)$$

where b is the slope and T_{Al} and T_0 are the temperatures of the aluminium block at time t and at the start *(t = 0),* respectively, A_s is the surface area of the Al block (m^2), $c_{p,Al}$, V_{Al} and ρ_{Al} are heat capacity (J/(kg·°C)), volume (m^3) and density (kg/m^3) of Al, respectively. A plot of equation (4.1) gives a straight line with a slope of b (illustrated as Figure 4-6). The value of the average heat transfer coefficient, h was determined from the slope of the line. The results were summarized in Table 4-1.

[i] The corresponding biot number was calculated from l_{Al} = 0.02m, k_{Al} = 168W/ (m·K), h = 33w/m^2K

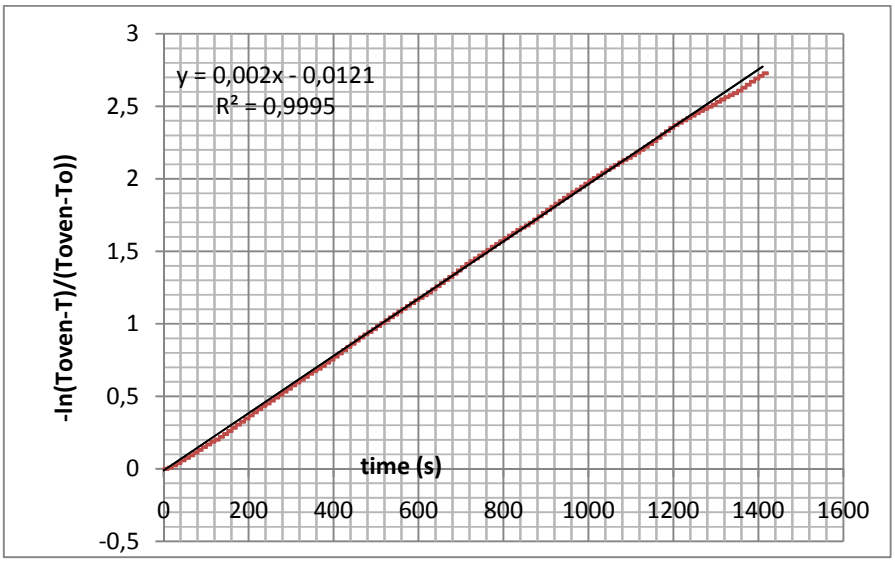

Figure 4-6 Illustration of the average heat transfer coefficient determination for a rectangular aluminium block using the lumped heat transfer method (red = equation (4.1) with measured), and (black = fitted)

Table 4-1 Heat transfer coefficients for rectangular and cylindrical shapes at half and full fan-speed

	Rectangular[j]	*Cylindrical*[k]
Half fan-speed*	33.9±1.8	33.5 ±1.3
Half fan-speed**	32.2±1.3	32.7±0.9
Full fan-speed*	47.5±2.5	47±1.4
Half fan-speed* and coated with spray-maling (black)	35.2 (the effect of radiation, 3%)	37.2 (the effect of radiation is 10 %)

mean± std, cp_{Al} = 903kJ/(kg.K) and ρ_{Al} = 2702 kg/m3. * and ** are indicating the aluminium cylinder and the rectangle were placed vertically and horizontally in the oven, respectively.

The heat transfer coefficient was determined at half fan-speed (50% of the maximum fan-speed) and at full fan-speed (100% of the maximum fan speed). One of the interesting observations is that the obtained heat transfer coefficient increases by a factor 1.4 when the velocity is doubled.

[j] Dimensions (*L*=40mm,*W*=40mm, *H*=50mm), V_{Al} = 8.64 $^{x}10^{-5}$ m^3, A_{Al}= 11.84 $^{x}10^{-3}$ m^2

[k] Dimensions (*D*=40mm, *and H*=54 mm), V_{Al} = 7.54 ^{x} 10^{-5} m^3, A_{Al} = 10.05 $^{x}10^{-5}$ m^2

This fits well with the theoretical correlation of the dimensionless Nusselt number (Nu[l]), which is briefly illustrated as follows. The Nusselt number is a function of the Reynolds number[m] (Re) and Prandtl number[n] (Pr). The average Nusselt number for flow over the flat surface is given by Eq (4.3) (Cengel, 2007):

$$Nu = hD/k_{air} = 0.664Re^{0.5}\,Pr^{1/3}\ (\text{for } Re < 5x10^5) \qquad (4.3)$$

In the concerned experiment set-up only the velocity was changed, the other process parameters (e.g., air temperature) remain the same for both set-ups (i.e., at half fan-speed and full fan-speed). Therefore, using the dimensionless correlations (Nu and Re), the ratio of the heat transfer coefficient, i.e., at full fan-speed (h_{full}) to at half fan-speed (h_{half})) can be derived. For the rectangular sample, the ratio is $\left[\frac{h_{full}}{h_{half}} = \frac{Nu_{full}}{Nu_{half}} = \left(\frac{v_{air,full}}{v_{air,half}}\right)^{\frac{1}{2}} = \sqrt{2} = 1.4\right]$. Thus, the ratio of the obtained heat transfer coefficient (h_{full}/h_{half} = 47.5/33.9 = 1.4, Table 4-1) from the measurement well agrees with the theoretical results obtained by dimensionless correlation. The average velocity was calculated from the measured heat transfer coefficient using the using the dimension correlation for example for rectangular geometry using Eq. 4.3.The calculated average air velocity is around 3.8 m/s at full fan-speed (or 1.9 m/s at the half fan-speed).

4.4.3 Product temperature and mass loss profile

The temperature was measured at different positions within the meat as a function of time during the roasting process. For the cylindrical meat, the temperature was measured at 3mm (near the top surface), 10 mm, 20 mm (centre), 30 mm, 38 mm (near the bottom surface) from the top surface. For the rectangular meat piece, the temperatures were measured at 3mm (near the top surface) and at the centre (for detail see paper V). The measured temperatures were used for the

---

[l] $Nu=hD/k_{air}$

[m] $Re = \rho v D/\mu$

[n] $Pr = cp_{air}\mu/k_{air}$ where D is the characteristic length (m), ρ, v, and μ are the density ($kg \cdot m^{-3}$), the velocity ($m \cdot s^{-1}$), and viscosity ($kg \cdot m^{-1} \cdot s^{-1}$) of the fluid (air), respectively and the thermal conductivity of the air, calculated at film temperature.

validation of the heat and mass transfer model (see, Chapter 7). The mass loss was also measured (paper V and Appendix A, Figure A.3).

4.4.4 Local water content and mechanism of water transport

A local water content was measured at different positions and times (Figure 4-7, Box 4.1), in order to investigative the mechanisms of water transport (e.g., weather there is an increase in water content at the centre or not).

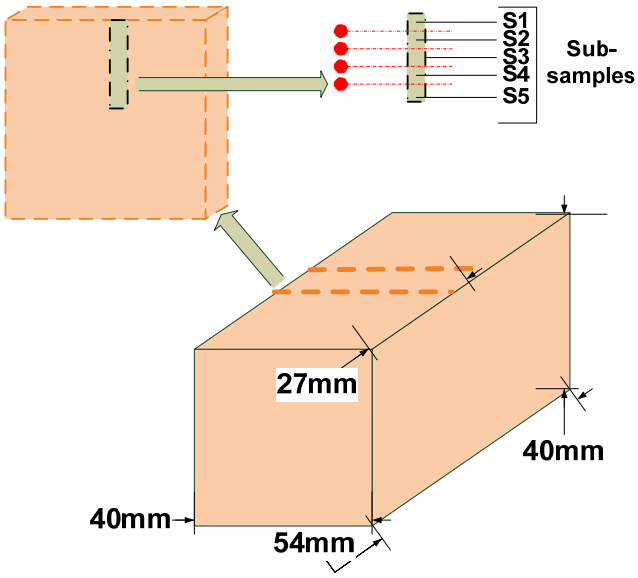

Figure 4-7 Local sampling, positions and procedures

Box 4.1

Rectangular meat samples (40mm x40 x 54mm) were roasted in the convection oven for a specified period of time of 8, 11, 15, 20, 25, 30 and 35 min, respectively. Each sample was instantaneously taken from the convection oven and immersed in liquid nitrogen for approximately 30 s to stop water migration by freezing, and then they were placed in a freezer for 2-4 hours. Then the sample was sliced with a meat slicer and a knife into small sub-samples of approximately 4×4×4 mm^3 (for detail see paper I).

The obtained initial water content is around 0.746 (kg of water/kg of sample), which also agrees with the result reported in (Huff-Lonergan and Lonergan, 2005, Tornberg, 2005). The local increase in water content towards the centre (s_5 = 16 to 20 mm from the surface, Figure 4-7) was not observed (Table 4-2). This result agrees well with the work of Skjöldebrand (2001). Generally, the local water content decreases with an increase in distance from the centre and decreases with increasing roasting time (with few exceptions). The local water content at position (s_1) decreases steadily for the initial stage up to t = 20 min (to 0.646 kg of water/kg of sample). Then at t = 25 min it increases (to 0.705 kg of water/kg of sample) and then later on it

decreases again. The increased water content near the surface at t = 25 min, is probably due to the large outward water flux directing water from the centre of the meat piece to the surface. A rapid drop in water holding capacity (chapter 3), a large pressure gradient at the centre, and larger permeability in the outer part (s_1) than in the inside part (s_5) cause the water to move faster towards the surface. When the internal water flux is larger than the water flux away from the surface of meat, water is accumulated near the surface (s_1), and consequently the local water content increases. Later on the internal flux decreases and the local water content continues to drop for the remaining time of the roasting experiment.

Table 4-2 Local water content (kg of H2O per kg of sample)

Time(in min)	Position(mm) from surface to centre					Surface				centre
	s_1(0-4) *Surface*	s_2(4-8)	s_3(8-12)	s_4 (12-16)	s_5(16-20) *center*	↓	s_1..s_2	s_3	s_4	s_5 ↓
0	Mean = 0.746, Std.dev = 0.0034									
8	0.720	0.730	0.740	0.730	0.740	**X**	**-**	**-**	**-**	**-**
11	0.701	0.716	0.727	0.737	0.745	**X**	**X**	**-**	**-**	**-**
15	0.690	0.720	0.730	0.730	0.740	**X**	**X**	**-**	**-**	**-**
20	0.646	0.727	0.744	0.741	0.736	**X**	**-**	**-**	**-**	**-**
25	0.705	0.706	0.727	0.732	0.736	**X**	**X**	**-**	**-**	**-**
30	0.693	0.712	0.719	0.716	0.734	**X**	**X**	**X**	**X**	**-**
35	0.659	0.618	0.665	0.667	0.681	**X**	**X**	**X**	**X**	**X**

Position is distance from surface in mm, 0 and 20 are surface and centre respectively, see also the position in Figure 4-7. (X) = significant change, (-) = insignificant change in water content, The initial water content was considered as reference point to evaluate the change of water content during roasting.

In later work not reported here, we occasionally observed a slight moisture rise (up to 0.03 kg water/kg of sample) near the centre after 15 and 20 min of roasting in the convection oven. Still, that level of increase of the moisture content is far below Van der Sman's (2007) predicted (0.1 kg of water/kg of sample, 10% rise). The slight increase of the local water content is not necessarily observed at the centre of the meat piece; this minor local increase can be anywhere within the sample, depending on the magnitude of the pressure gradients and the permeability of the medium. Our hypothesis is that the onset of heat denaturation and shrinking may give rise to occasional crevices in the meat because the shrinking causes uneven stresses in the meat piece.

4.5 Shrinkage

Rectangular meat samples, the same size as section 4.4.4, were prepared and roasted in the convection oven. The size (length, L, width, W, and height, H) and mass, M of the samples were measured both before and after the roasting. The relative dimensions (L/Lo, W/Wo and H/Ho) and the relative mass (M/Mo) as function of time were determined the detailed procedure and results were presented in paper I. The obtained results will be discussed as follows: meat samples shrink in the length and width direction, with larger shrinkage in the length direction.

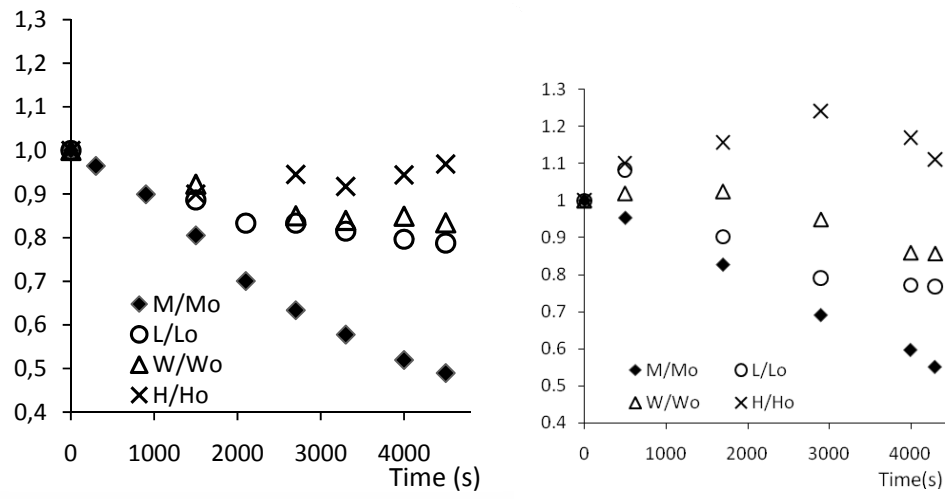

a) b)

Figure 4-8 Shrinkage and mass loss as function of time: a) meat sample shrinking in 3 directions; b) meat sample shrinking in x and y-direction and expanding in the z direction (height). M is mass (g), L, W and H are length width and height (mm), respectively. Subscript 'o' refers to initial state.

The rate of shrinkage is large from t = 900 to t = 2100 s, (Figure 4-8a), and from t = 500 to t = 2900 s, (Figure 4-8b) and the corresponding mass loss rate is also large in the same range, the relative mass decreases from 90 to 70% and 90 to 69%, respectively. This verifies that shrinkage is the basis for larger water loss which agrees with the hypothesis of Godsalve (Godsalve, et al., 1977). However, later on, after 2700 s (Figure 4-8a) the rate of shrinkage is considerably reduced, a change of 4% in the length and 2% in the width from t = 2700 to t = 4500 s. The most probable reason for such reduced shrinkage rate is that the elastic modulus of the meat increases drastically when the meat is heated above 65°C (Tornberg, 2005).

Another interesting observation was that mass loss is larger if the sample is shrinking in all directions (Figure 4-8a) compared to a situation where it is expanding in one of its directions (Figure 4-8a). This can be explained by the fact that the stress is larger when the meat shrinks in all directions than when it expands in one of its directions. Larger stress causes a greater squeezing pressure, which means more water is squeezed to the surface (larger mass loss). The exact cause for the differences in shrinking behaviour between the meat samples is not identified, but must be related to the fact that the biological variation between the same muscles but from different animals is considerable (Tornberg, 2005).

Meat with low fat content was used for our study to avoid complications from fat transport. To test the validity of this assumption, 16 meat samples were roasted (under the same condition as above) and their initial (M_o) and final mass were measured. A sample was taken from the oven and the dry matter lost with the exudate left on the tray was collected after the water had been evaporated in the oven. The solid residual was removed from the tray with a knife and its mass was determined. The percentage of DSL (= dry solid loss) was estimated as 1.33±0.18% of the total weight loss. Thus, it is quite a small fraction of the total loss (1.33 g per 100 g of total loss) and it substantiates the hypothesis of mass transfer based on water transport alone (paper I). Besides, other qualitative observations were made during the experimentations, this includes: the thin crust where the meat was cut and seen through the cross-section, the expulsion of water from the meat during roasting, and the colour change (see appendix A.2).

4.6 Change in the microstructure during the roasting of meat

The structure of the raw meat is intact at the start of the cooking process, and water transport is hindered by low permeability. During the roasting of the raw meat, dramatic changes in the microstructure (such as pore formation) are induced, which affect the water transport. To examine this, images of the microstructure of the meat were taken at different positions (Box 4.2, Figure 4-9) and at different times. Figure 4-10 illustrates meat microstructures (a binary image at t = 5 min and 10 min and different positions). The white area corresponds to pores (water-filled + air-filed) and the black corresponds to solid structure. Visually, the meat microstructure changes during the roasting of meat (larger pores in size and become more interconnected, when

comparing after t = 5 min with after t = 10 min). The changes (pore formations) vary with position. The spatial variation in temperature creates a spatial difference in structure change, where parts of the meat sample closer to the surface have larger pores than the parts closer to the centre. Therefore the permeability of the meat also changes with position and time. A permeability to water flux: (1) is probably much larger at the end of the process (with open pore structure) than at the beginning of the process when it is raw and (2) is larger towards the surface than towards the centre of the meat piece. This method can further be proceeded in future with quantification pores size and distribution.

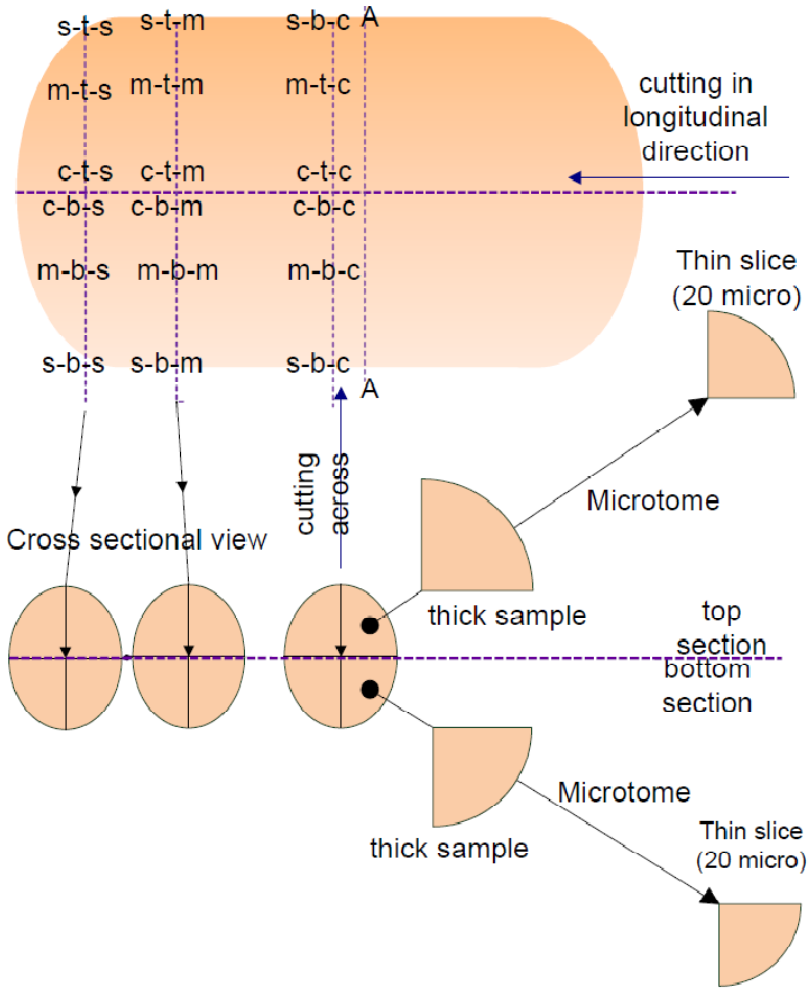

Figure 4-9 the position of the sample and the cutting direction and the procedure

Box 4.2: The procedure for the analysis of the change in microstructure during roasting

The cylindrical (d = 40mm, and length, L = *54 mm*) pork meat samples (*Longissimus-dorsi*) were roasted in the convection oven (the same setting as section 0) for a specified period of time of 5 min, 10 min, 15 min, and 20 min, respectively. Each roasted meat sample was instantaneously taken from the convection oven and wrapped with plastic foil and stored at 0 ^{o}C (in the refrigerator). The meat sample was cut into two parts at the middle (see, Figure 4-9, across A-A), and they were used for two experimental set-ups (cutting across the fibre and cutting along the fibre (Figure 4-9). The first part (e.g., the one to the left) was cut across the fibre and the second part was cut along the fibre.

Sample blocks (thick sample in Figure 4-9) were taken from the heat-treated pork meat, and the samples were cryo-sectioned using a Frigocut N, Cryostat 2800E (REICHERT-JUNG, Denmark). The temperature of the cryostat chamber was maintained at −19 °C, and the samples were equilibrated in the chamber for about two hours. The meat sample (thick sample) was sliced to obtain thin slices of 20 µm (thickness without destroying the structure) (Figure 4-9). The thin sections, 20 µm thick, were mounted on object glasses. The samples were stained with orange G for 5 min, followed by rinsing in distilled water for 1 min, they were subsequently stained with methyl blue for 5 min followed by rinsing in the distilled water for 5 min. Finally, the samples were rinsed with distilled water for extra 5 min, were subsequently covered (with cover glasses) and stored at 0 ^{o}C. The slices (thin) were examined by a light microscope, Nickon ECLIPSE 80i (DFA instrument, Denmark) and images were photographed at different positions using an integrated camera (within the light microscope). For the identification of the microstructures (pore and solid structure), the raw images were converted to binarized images (in MATLAB® software). Image analysis was performed using the image processing algorithms written in the MATLAB®7.2 software (The MathWorks Inc., USA). From the images the area of the white regions in relation to the total picture area [%] was quantified (Mendoza and Aguilera, 2004). The porosity (water-filled+air-filled porosity, together) of the meat was determined based on the binarized images and calculated as a percentage of the total area.

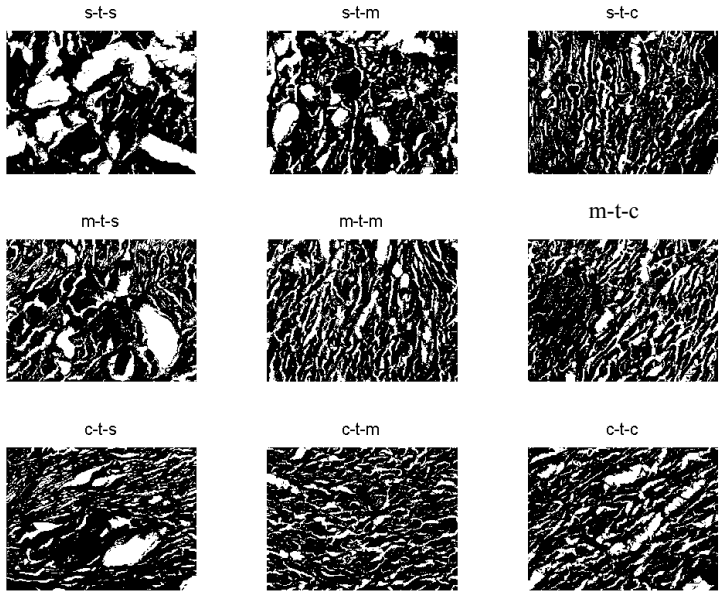

After 5 min (across)

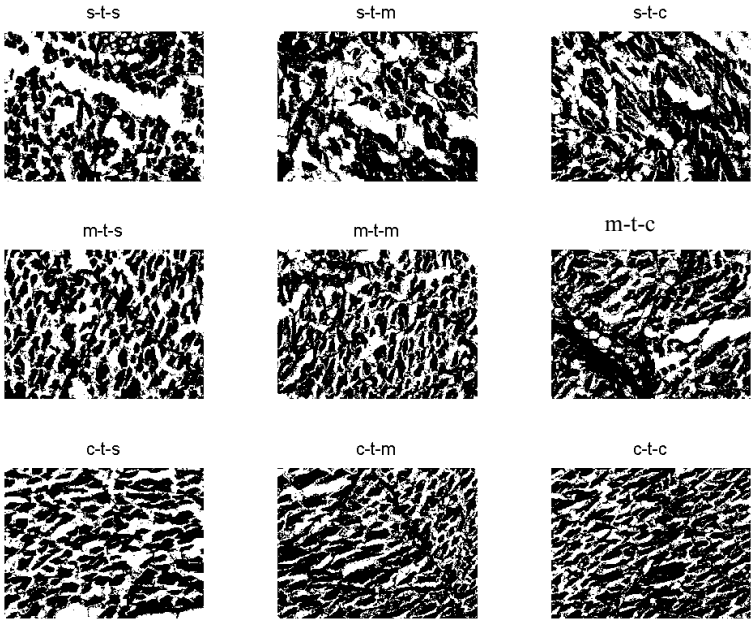

After 10 min (across)

Figure 4-10 Illustration of binarized image of meat microstructure (at different positions)

4.7 Summary

In this chapter, a pertinent experimental for the concerned representative cases: contact baking and roasting of meat in convection oven data were obtained. In relation to contact baking, the initial conditions (e.g., temperature and composition), local temperature at different positions and mass loss were measured. The temperature and mass profiles were discussed and their mechanism interpretations were made. In relation to the roasting of meat, process condition (e.g., heat transfer coefficient), local temperature, and mass loss were measured. The local water content, shrinkage and change in microstructure (image), together with their mechanisms were presented. One of them, for example, the spatial distribution of the local moisture content in the meat was studied, and a large increase of the water content was not observed in the centre of the meat. The knowledge and the data obtained in this chapter are useful for model building (model formulations and validations).

5 Model formulation

5.1 General governing equations

In this chapter, the physical-based models of heat and mass transfer are formulated. Fundamental physical laws, conservation of energy and conservation of mass are the basis for the formulation of the governing equations of heat and mass transfer (Bird, et al., 2001). The physical-based models of heat and mass transfer is derived from the fundamental laws using the continuum approach, such an approach is extensively applied in the chemical engineering field (Brodkey and Hershey, 1988, Gebhart, 1993). As discussed in Chapter 3, the processing of solid foods involves complex heat and mass transfer, choosing the most appropriate formulation and simplifications among the many available approaches is often challenging. In the coming subsections, the general model equations of heat and mass transfer for solid foods are presented. Then, the general model equations are applied to the representative cases: roasting of meat in convection-oven and the contact baking process.

5.1.1 Heat transfer

On the basis of the conservation of energy, the governing mathematical equation of heat transfer is given by Eq. (5.1) (Bird, et al., 2001):

$$\underbrace{c_{p,p}\rho_p \frac{\partial T}{\partial t}}_{I} = \overbrace{\nabla(k_p \nabla T)}^{II} - \underbrace{\rho_w c_{p_w} u_w \nabla T}_{III} - \overbrace{Q_{evp}}^{IV} \tag{5.1}$$

where ρ_p and ρ_w are the density of a product and a fluid (water) ($kg \cdot m^{-3}$), respectively, k_p is the thermal conductivity of the product ($W \cdot m^{-1} \cdot K^{-1}$), $c_{p,p}$ and $c_{p,w}$ are the heat capacity of the product and water ($J \cdot kg^{-1} \cdot K^{-1}$)), respectively, u_w is the fluid velocity ($m \cdot s^{-1}$), T is the temperature (K), and t is the time (s). In Eq. (5.1) the first term (I) is the accumulation term (time dependent part of the governing equation); the second term (II) is the heat transfer by conduction; the third term (III) is the heat transfer by convection; the fourth term (IV) is the generation or disappearance of the energy – the heat that dissipates in evaporating the water, Q_{evp}. In this study, Equation (5.1) is

used as the reference equation for heat transfer in solid foods, and on the basis of the mechanisms and assumptions; Eq. (5.1) will be applied to the two representative cases (see Table 5-1 and Table 5-2).

5.1.2 Mass transfer

The governing mass transfer equation based on the conservation mass is given by Eq. (5.2) (Bird, et al., 2001)

$$\frac{\partial C}{\partial t} = \nabla\left(D \nabla C\right) - u_w \nabla C \pm R_{evp} \tag{5.2}$$

where C is the concentration of water (kg of water/kg of sample), and D is the diffusion coefficient (m^2/s). In Eq. (5.2): the first term is an accumulation of mass (time dependent); the second term is the mass transfer by diffusion; the third term is the mass transfer by convection (pressure driven); the fourth term can be the generation or disappearance of mass (local water evaporation). In case of a one component mass transfer, Eq. (5.2) is applied. In case of a multi-component transport when two or more components are considered, two or more governing equations are applied to descibe the mass transfer. In case of transport of two components, for example the liquid water and the water vapour transport, the govering equations are given by Eq. (5.3) and Eq. (5.4), respectively.

Liquid water transport:

$$\frac{\partial C_l}{\partial t} = \nabla\left(D \nabla C_l\right) - u_w \nabla (C_l) - R_{evp} \tag{5.3}$$

And water vapour transport:

$$\frac{\partial C_v}{\partial t} = \nabla\left(D_v \nabla C_v\right) - u_v \nabla (C_v) + R_{evp} \tag{5.4}$$

where C_l and C_v are the liquid and the water vapour concentration (kg of water/kg of sample), respectively. The equations (5.3 and 5.4) are applied to describe the water transport in solid food

(see section 5.3).

5.2 Roasting process (case study 1)

The majority of the discussions in this section are extracted from paper II and IV.

5.2.1 Problem formulation and assumptions

As dicussed earlier (Chapter 1 and 3), roasting in a convection oven is a common way of frying a whole piece of meat in households, in professional kitchens and in the ready-meal industry. During roasting processes, the heat is transfered from the hot air to the product by convection and inside the product mainly by conduction. As the meat is heated, the water migrates within the product by diffusion and convection mechanisms, where the later transport of water is pressure driven as the result of the denaturation of proteins and a reduction in water binding capacity. The liquid water at the surface of the meat is lost by evaporation and drip. The main process during the roasting of meat in an convection oven is illustrated in Figure 5-1.

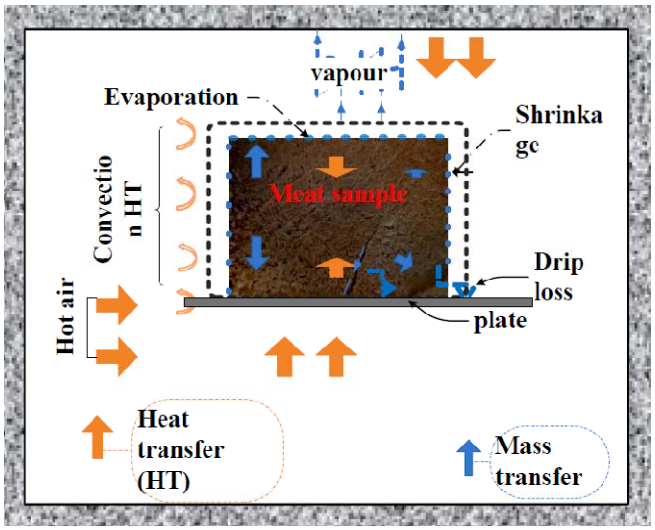

Figure 5-1 Heat and mass transfer during roasting of meat in convection-oven roasting, orange arrow: the direction of heat transfer; blue arrow: the direction of water transport

To formulate the governing equations of mass and heat transfer the following assumptions are

made:

a) Fat transport is negligible, this because lean meat is considered having less than 2% fat
b) The crust is thin – this is observed when inspecting a cut through the cooked meat) and does not hinder the transport of water to the surface (paper II), moreover, the meat has low air-filled porosity, (Kovácsné Oroszvári, et al., 2006)). Evaporation therefore takes place at the surface. This means that the internal evaporation, the IV term in Eq. (5.2) can be neglected.
c) There is no internal heat generation (in the Eq.5.1) IV term = 0)
d) Dissolved matter lost with water can be neglected in the material and energy balance (paper I).
e) The initial distributions of the water content ($C_{(x,y,z,0)} = Co$) and temperature ($T_{(x,y,z,0)} = T_o$) are uniform.

5.2.2 Governing equations

On the basis of the aforementioned assumptions, the governing equations of heat and water transport inside the meat during roasting are summarized in Table 5-1. For example, the governing equations (5.1) and (5.3) are simplified based on the assumption item b) and c) to (5.5) and (5.6), respectively.

Table 5-1 the governing model equations of heat and mass transfer during the roasting of meat in the convection-oven

Reference	Eq.	I	II	III	IV	Governing equations of roasting of meat
HT	(5.1)	√	√	√	0	I = II + III $c_{p,m}\rho_m \frac{\partial T}{\partial t} = \nabla(k_m \nabla T) - \rho_w c_{p_w} u_w \nabla T$ (5.5)
MT	(5.2)	√	√	√	0	I = II + III $\frac{\partial C}{\partial t} = \nabla(D\nabla C) - \nabla(C u_w)$ (5.6)

HT = heat transfer, MT = Mass transfer (I, II, III and IV are the first, second, third and fourth term of equation 5.1 and 5.2), when it is counted from the left to right.

The detailed formulations can be found in paper (II and V). The pressure driven transport that occurs during the roasting of the meat is discussed in section 5.2.3.

5.2.3 Pressure driven transport of water inside meat

The relationship between the velocity and the pressure gradient that drives the moisture transport inside the meat can be expressed using Darcy's law of porous media Eq.(5.7) (Datta, 2006) and Equation (5.7) can be rewritten in terms of velocity as (Eq. 5.8).

$$Q_w = \frac{-A\,K}{\mu_w}\nabla P \qquad (5.7)$$

$$u_w = \frac{-K}{\mu_w}\nabla P \qquad (5.8)$$

where Q_w is the flow rate (discharge, m^3/s), K is the permeability of the medium or meat (m^2), A is the flow area (m^2), and ∇P is the pressure gradient vector ($pa \cdot m^{-1}$), μ_w is the dynamic viscosity of the fluid ($pa \cdot s$), u_w is the velocity of the fluid (m/s). The pressure is proportional to the excess moisture concentration within the meat (Barriere and Leibler, 2003, van der Sman, 2007) as discussed in Chapter 3. The expression for the swelling pressure P is given as with Eq. (3.1). Substituting P with Eq. (3.1) into (5.8) gives the expression of velocity, u_w

$$u_w = -\frac{K\,E}{\mu_w}\nabla(C - Ceq(T)) \qquad (5.9)$$

where, $Ceq(T)$ is the equilibrium water holding capacity as a function of temperature (T) and E is the modulus of elasticity (N/m^2). The water holding capacity decreases with an increase in temperature (Bengtsson, et al., 1976). The expression for the water holding capacity is given by an empirical relation (Bengtsson, et al., 1976, van der Sman, 2007):

$$C_{eq(T)} = a_1 - \frac{a_2}{(1 + a_3 \exp(-a_4(T - T\sigma)))} \qquad (5.10)$$

where T_σ =52 ^oC is the centre of a logistic curve (water holding capacity vs. temperature), a_1 = 0.745, a_3 = 0.345, a_3 = 30, a_4 = 0.25 (van der Sman, 2007)

The elastic modulus of meat changes with an increase in temperature during the cooking (as discussed in chapter 3), thus E should be given a function of the temperature. However, there is no expression for E(T) that can be readily incorporated into the model. A dramatic change of elastic modulus occurs between T = 50 and T = 80 ^{o}C (Tornberg, 2005). On the basis of this experimental observation, a logistic function with a slight modification is proposed to describe the E(T) functionality as shown in (5.11).

$$E_{(T)} = E_o + \frac{E_m}{(1 + \exp(-E_n(T - E_D))} \tag{5.11}$$

where E_o is the minimum value (at the initial state with raw meat before heating) of the elastic modulus, E_0 = 12 kpa, E_m is the maximum value, E_m = 83 kpa at T = 80 ^{o}C; E_n and E_D are the parameters of Eq. (5.11), respectively. The values of E_o and E_m were obtained from the experimental data in (Tornberg, 2005). And, the E_n and E_D were obtained by fitting Eq. (5.11) with the experimental data. For the whole meat, E_n = 0.3, and E_D = 60 were obtained from the curve fitting. The experimental data were taken from (Tornberg, 2005), also see Chapter 3.

5.2.4 Boundary condition

Heat transfer

For meat subjected to convection roasting (see Fig.5.1) at the surface, the heat flux into the meat is equal to the difference between the convective heat transfer and the heat of evaporation. Thus, the boundary condition at the surface (air-meat interface) is given by equation (5.12):

$$-n.(k_m \nabla T + u_w c_{pw} \rho_w T)_{surface} = h(T_{oven} - T_s) - q_{evp} \tag{5.12}$$

where the term on the left-hand side of equation (5.12) refers to heat transferred by conduction and convection from the outer surface to the inside of the meat sample, the first term on the right-hand side is heat penetrating from the oven (hot air) to the product by means of convection (see chapter 3), and the second term on the right-hand side denotes heat dissipation for evaporation of the water at the air-meat interface (paper II).

Mass Transfer

For the product subjected to convection roasting, the governing mass transfer equation (5.6) is solved using the boundary condition given by Eq. (5.13), (see for detail paper II)

$$n.\left(-D\nabla C + u_w C\right) = \frac{q_{evp}}{H_{evp}\rho}\left(C - C_{eq}\right) \tag{5.13}$$

5.2.5 Moving boundary

The change of dimensions (shrinkage) is proportional to the volume of liquid water removed (see Chapter 3). By assuming that the relationship between the removed volume of water and the shrinkage holds for roasting of cylindrical meat, with an additional consideration for the effect of air-filled pore formation, the following theoretical expressions are formulated. The volume of a cylindrical meat sample at any given time is expressed in terms of the initial volume (V_o) and the volume of water lost ($V_{w,l}$) as :

$$V = V_0 - \beta V_{w,l} = V_0\left(1 - \frac{\beta V_{w,l}}{V_0}\right) \tag{5.14}$$

The coefficient β is used to describe the effect of air-filled pore formation during a roasting process. For shrinkage, the value of β varies between 0 and 1. If β is 1, there is no air-filled pore formation i.e. the volume of water removed is equal to the volume deformation. Contrary, if β is 0, then there is no shrinkage i.e. the volume water lost is entirely replaced by the air and no deformation occurs. The fraction (1-β) is the fraction of the volume of water removed from the meat during roasting that is replaced by the air-filled pore space. For minced meat, this value is roughly estimated. For example, for the mass loss of 15%, the corresponding air-filled pore formation is 3% (Kovácsné Oroszvári, et al., 2006). In this case, the β value is around 0.8 (or 1-β = 0.2). For isotropic shrinkage (Trujillo, et al., 2007), the Eq. (5.14) can be re-written in terms of length of cylinder (Z) and the radius of cylinder (R) as:

$$V = \pi R_0^2\left(1 - \frac{\beta V_{w,l}}{V_0}\right)^{2/3} Z_0\left(1 - \frac{\beta V_{w,l}}{V_0}\right)^{1/3} = \pi R^2 Z \tag{5.15}$$

After derivation (see the full derivation in paper II), the interface velocity components (v_r and v_z, r-component and z-component, respectively) are given as:

$$v_z = \frac{dZ}{dt} = -\frac{Z_0\beta}{3V_0}\left(1-\frac{\beta V_{w,l}}{V_0}\right)^{-2/3}\frac{d}{dt}(V_{w,l}) \quad (5.16) \qquad v_r = \frac{dR}{dt} = -\frac{R_0\beta}{3V_0}\left(1-\frac{\beta V_{w,l}}{V_0}\right)^{-2/3}\frac{d}{dt}(V_{w,l}) \quad (5.17)$$

$V_{w,l}$ is a function of water content, and which given by Eq. (5.18) :

$$V_{w,l} = \frac{m_d(X_0 - X)}{\rho_w} = \frac{\rho_0 V_0(1-C_0)}{\rho_w}\left(\frac{C_0}{1-C_0} - \frac{C_{av}}{1-C_{av}}\right) \quad (5.18)$$

and the rate change of $V_{w,l}$ is given by (5.19) :

$$\frac{dV_{w,l}}{dt} = -\frac{\rho_0 V_0(1-C_0)}{\rho_w}\left(\frac{1}{1-C_{av}}\right)^2\frac{dC_{av}}{dt} \quad (5.19)$$

where C_{av} is the average water content (kg of water/kg of sample). For this case, we used the measured mass loss to determine the C_{av} as function of time.

5.2.6 Thermo-physical proprieties

The density and heat capacity of meat are estimated from the composition of the meat using Eq. (3.2 to 3.4, Chapter 3) (Rao, et al., 2005).

5.3 Contact baking process (case study 2)

The majority of the discussions in this section are extracted from paper III.

5.3.1 Problem formulation and assumptions

Contact baking is a thermal process, where the product is heated at high temperature (140 ^oC to 300 ^oC) by contact with a hot surface. As discussed in chapter 4, the product (pancake batter) is heated on a horizontal heating rig, where heat is transferred by conduction through several layers of materials. These layers of materials include: (1) the heating rig (paper III, section 3.2), (2) the thermal conducting paste, and (3) the bottom surface of the baking disc, which is made of aluminium (Al), as shown in Figure 5-2a . For the remaining part of this thesis, the term ‘heating rig’ will be used when referring to the rig and the thermal conducting paste together (1 and 2, in

Figure 5-2 a). The heat transfer causes a rapid raise of the temperature within the pancake batter, which induces water migration by diffusion and evaporation. Heat and mass transfer interact via evaporation (Huang, et al., 2007). The most important phenomena influencing the key process variables (temperature, concentration of liquid water and concentration of water vapour) within the pancake batter are described in Figure 5-2b.

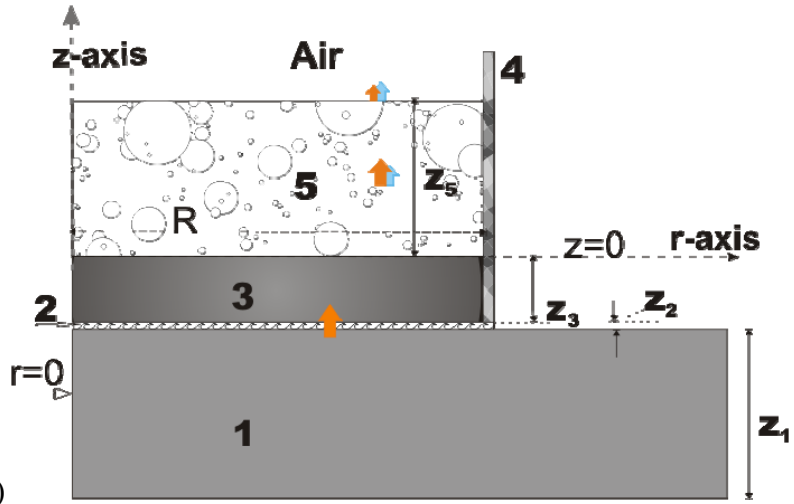

a)

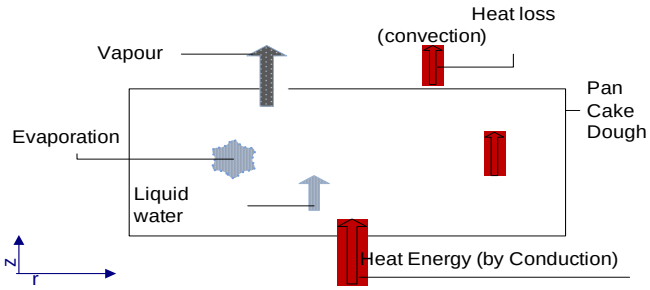

(b)

Figure 5-2 (a): Part of the heating rig used for studying the contact baking process; domain 1 is the rig (aluminium block), domain 2 is the thermal conducting paste (copper paste), domain 3 is the aluminium plate (bottom part of the baking disc), domain 4 is the wall of the baking disc (stainless steel), and domain 5 is the product (pancake batter); (b) Schematic representation of the main phenomena during the contact baking process (within the pancake batter)

The following assumptions were made when developing the model: a) heat is transferred within the pancake batter by conduction in the beginning (later, evaporation and partial condensation also contribute to heat transfer, see item c and e); this is reasonable, because the pancake batter is rather viscous and its thickness is relatively low (no natural convection); b) heat is lost from the product to the surrounding air via convection: rough calculations indicate that the radiation can be neglected because the surface temperature of the product is below 100 ^{o}C, (the measured temperature at position A, 6.4 mm from the bottom only 1.6 mm from the top surface, is well below 100 ^{o}C); c) the liquid water is transferred by diffusion within the pancake batter and simultaneously local evaporation takes place; d) liquid water and water vapour transport through the product are considered separately as multi-phase transports; e) the water vapour is generated within the pancake batter, then it migrates to the top surface (water-air interface, at $z = z_5$, Figure 5-2a) and subsequently diffuses to the external environment (air); f) a transient one dimensional model (only heat and mass transfer in the z direction) is considered. This assumption is valid, because the diameter (2R = 90 mm) of the pancake batter is very large compared to the height (z_5 = 8 mm), and the effect of heat flux from the sides (in x and y directions) is small compared to the effect of heat flux from the bottom.

5.3.2 Governing equations

On the basis of aforementioned assumptions and considerations (section 5.3.1), the governing equation of heat, liquid water and water vapour transport during the contact baking of a pancake batter are given in Eq,5.21, 5.22, and 5.23, which are derived from the general governing equations (5.3) and (5.4) (see Table 5.2). In the contact baking formulations, the X (dry basis, kg of water/kg of the solid) is used instead of C (wet basis, kg of the water/ kg of sample). The detailed formulations can be found in paper III.

Heat transfer through baking disc

During the contact baking process, the pancake batter is poured into the baking disc (Chapter 4, see Figure 4-1), and placed on the heating rig for baking. The heat transfer through the bottom surface of the baking disc (domain 3 in the Figure 5-2 a, made of aluminium) is given by Eq.

(5.20), where ρ_{Al}, $c_{p,Al}$ and k_{Al} are the density, the specific heat capacity, and the thermal conductivity of the Al, respectively. In domain 3, there is no mass transfer.

Table 5-2 the governing equations of 1D coupled heat and mass transfer during roasting of meat in the contact baking process

Reference	Eq.	I	II	III	IV	Governing equations for contact baking	
HT	(5.1)	√	√	0	0	I=II (baking disc, no evaporation) $\rho_{Al} c_{p,Al} \frac{\partial T}{\partial t} = \frac{\partial}{\partial z}\left(k_{Al} \frac{\partial T}{\partial z}\right)$	(5.20)
HT	(5.1)	√	√	0	√	I=II+IV (pancake batter) $c_{p,p}\rho_p \frac{\partial T}{\partial t} = \frac{\partial}{\partial z}\left(k_p \frac{\partial T}{\partial z}\right) - Q_{evp}$	(5.21)
MT						(within pancake batter)	
L	(5.3)	√	√	0	√	I=II+IV $\frac{\partial X_l}{\partial t} = \frac{\partial}{\partial z}\left(D_l \frac{\partial X_l}{\partial z}\right) - R_{evp}$	(5.22)
V	(5.4)	√	√	0	√	I=II+IV $\frac{\partial X_v}{\partial t} = \frac{\partial}{\partial z}\left(D_v \frac{\partial X_v}{\partial z}\right) + R_{evp}$	(5.23)

HT = heat transfer, MT = Mass transfer (L=liquid, V=vapour) (I, II, III and IV are first, second, third and fourth term of equation 5.1), when it is counted from the left to the right. The last column to the left is the reduced form of reference equation on the basis of the assumptions for contact baking.

5.3.3 Boundary conditions

The following boundary conditions apply for heat transfer:

The heat flux from the heating rig is equal to the heat flux conducting through the baking disc and at z = -z_3) is given by Eq. (5.24):

$$-k_{Al} \left.\frac{\partial T}{\partial z}\right|_{z=-z_3} = h_{bot}\left(T_{set} - T\right) \tag{5.24}$$

At the bottom of the pancake batter surface (z = 0, pancake batter-baking disc interface), the net heat flux at the interface is equal to the heat of evaporation at the interface:

$$q_3\big|_{z=0} - q_5\big|_{z=0} = q_{evp}\big|_{z=0} \tag{5.25}$$

At the top surface of the pancake batter (z = z_5, pancake-air interface), heat is exchanged with the surrounding air by convective heat transfer:

$$-k_p \frac{\partial T}{\partial z}\bigg|_{z=z_5} = h_{top}\left(T - T_{air}\right) \tag{2.26}$$

where T_{air} and T_{set} are the surrounding air temperature and the frying rig's temperature set point, respectively, h_{top} is the heat transfer coefficient at the top surface (W/(m^2·K)), i.e. at the air-product interface and h_{bot} is the contact heat transfer coefficient at the bottom boundary (at the heating rig-baking disc interface), q_3, q_5 and q_{evp} are the heat flux at z = 0, from domain 3, to domain 5 and through evaporation at the interface, respectively.

The following boundary conditions apply for mass transfer:

At the bottom surface of the pancake batter (z = 0), the rate of liquid water lost by evaporation, the rate of water vapour generation and the rate of evaporation are equal, Eq. (5.27).

$$-D_l \frac{\partial X_l}{\partial z}\bigg|_{z=0} = D_v \frac{\partial X_v}{\partial z}\bigg|_{z=0} = -\frac{q_{evp}}{H_{evp}\rho_s}\bigg|_{z=0} \tag{5.27}$$

At the top surface (z = z_5): the boundary conditions for liquid water and vapour are given by Eq. (5.28) and (5.29), respectively

$$-D_l \frac{\partial X_l}{\partial z}\bigg|_{z=z_5} = k_l\left(X_l - X_{l.air}\right) \tag{5.28}$$

$$-D_v \frac{\partial X_v}{\partial z}\bigg|_{z=z_5} = k_v\left(X_v - X_{v,air}\right) \tag{5.29}$$

where k_l and k_v are the liquid and vapour mass transfer coefficient (m/s), respectively.

Initial conditions

The initial distributions of the water content (liquid water, $X_{l(z,0)} = X_{l,o}$ and water vapour, $X_{v(z,0)} = X_{v,o}$) and temperature ($T_{(z,0)} = T_o$) are uniform.

5.3.4 Evaporation rate

A phase change from liquid water to water vapour is considered as a heterogeneous reaction with first order kinetics (Peters, et al., 2002), where the evaporation rate is based on the Arrhenius equation. The basic Arrhenius equation for the rate of evaporation incorporates varying water

content and temperature dependence. However, the limitation to the basic Arrhenius type equation when used for the evaporation rate is that it induces evaporation of water at low temperature in the model (temperature far below the evaporation temperature), which is not the case in practice. Here a modified rate equation has been adopted by considering the fact that the evaporation takes place around the evaporation temperature. The modified rate equation which mathematically takes the same form as the Clausius–Clapeyron equation, the evaporation rate near the evaporation temperature, T_{evp}, is given by:

$$R_{evp} = k_{evp} X_l \underbrace{\exp\left(-\frac{E_a}{R_g}\left(\frac{1}{T} - \frac{1}{T_{evp}}\right)\right)}_{f_{phase}} \tag{5.30}$$

where k_{evp} is the evaporation rate constant at the evaporation temperature (1/s), R_g is the gas constant (J/(K·mol)), E_a is the activation energy (J/mol). Evaporation of water utilizes evaporation enthalpy, and then $E_a = H_{evp} M_w$ and M_w is the molecular weight of the water (kg/mol), T_{evp} is the evaporation temperature (K) (reference temperature), and f_{phase} is a function that describes the phase change coefficient.

Equation (5.30) can describe the evaporation rate, because 1) at lower temperatures (far below T_{evp}), the value of f_{phase} is close to 0, and thus the rate of evaporation is close to zero. On the contrary, when T is close to T_{evp}, the value of f_{phase} is close to 1, and the rate is close to the rate at T_{evp}, 2) when equation (5.30) is combined with the above governing model equations (5.21), (5.22), and (5.23), the resulting set of equations describes the heat and mass transfer during the contact baking process for the entire heating period (heating and evaporation phase), without any discontinuity. Thus it eliminates numerical problems as well. In this study, the value of the parameter k_{evp} (rate constant of evaporation) is estimated together with the other unknown parameters by comparing the numerical results of the current model with measured experimental data (see Chapter 7).

The mathematical equations formulated in this chapter require a numerical method. In the next chapter, the model equations of coupled heat and mass transfer are solved with the FEM.

6 Finite Element Modelling – Implementation and Solution

The solution of the heat and mass transfer model equations (formulated in chapter 5) provides the predictions of state variables (e.g., temperature, water concentration) in space and time. The solutions of coupled partial differential equations (PDE) require the numerical method. The FEM, was used to solve the model equations of heat and mass transfer. The FEM solution provides a quantitative understanding of heat and mass transfer. Therefore, the aim of this chapter is to briefly introduce the method and to discuss some of the results.

6.1 Numerical solution

In the past few years the growth of powerful computers with greater computational capabilities has facilitated the formulation of sophisticated numerical methods that mimic and simulate the real physical systems by solving complex mathematical models (Moens and Vandepitte, 2005, Mohamed, 2010, Wang and Sun, 2003). In the literature, there are different numerical methods which include differential methods (e.g., Finite difference method, FDM), integral methods (variation and weighted residuals, e.g.., FEM), and stochastic methods (e.g. Monte Carlo method) (Sandeep, et al., 2008). In food engineering applications, the FDM and the FEM[15] are the commonly employed numerical techniques (Puri and Anantheswaran, 1993). The former is a less complex and computationally inexpensive method compared to the latter (Wang and Sun, 2003). However, the former has limitations in modelling for example non-heterogeneous foods (Martins, et al., 2008). Overall, the latter has several advantages compared to the former - the FEM is more flexible in handling the spatial variation of material properties (e.g., food compositions), irregular shape and regions, nonlinear problem, mixed boundary and initial conditions (Martins, et al., 2008, Puri and Anantheswaran, 1993). These situations are

[15] Some of the examples (where FEM modelling was employed in food application) are: modelling the mechanisms of dough puffing during vacuum microwave drying (Ressing, et al., 2007), modelling moisture transfer in chicken drum during deep-fat frying (Ngadi, et al., 1997), modelling conventional cooling processes of cooked meat (Wang and Sun, 2002), and modelling of heat transfer in meat patties during single-sided pan-frying (Ikediala, et al., 1996). A review on the FEM applications in food processing can be found" (Puri and Anantheswaran, 1993).

particularly the case here (for heating of solids), where heat and mass transfer take place with large complexity such as change in the boundary condition, geometry, spatial variations, and others. Therefore, FEM within the framework of *COMSOL Multiphysics®3.5* software *(COMSOL A/S, Kgs. Lyngby, Denmark)* was chosen to solve the mathematical model of coupled heat and mass transfer during solid food processing.

6.1.1 Finite Element method

The finite element discretization divides the problem domain of interest (e.g., irregular or regular food piece) into a finite number of elements, and each element is connected to each other at points called nodes (Sandeep, et al., 2008). The collection of the elements and nodes is called the Finite Element mesh (Figure 6-1a). The nodes typically lie on the element boundary where adjacent elements are connected. The nodal values of the field variable and the interpolating functions for the elements define the behavior of the field variable within the elements. The nodal points depict the field variable or the unknown, defined in terms of approximating or interpolating functions within each element. A detailed discussion of the FEM and techniques can be found in many books, in the context of food engineering relevant literature can be found in for example (Martins, et al., 2008, Puri and Anantheswaran, 1993).

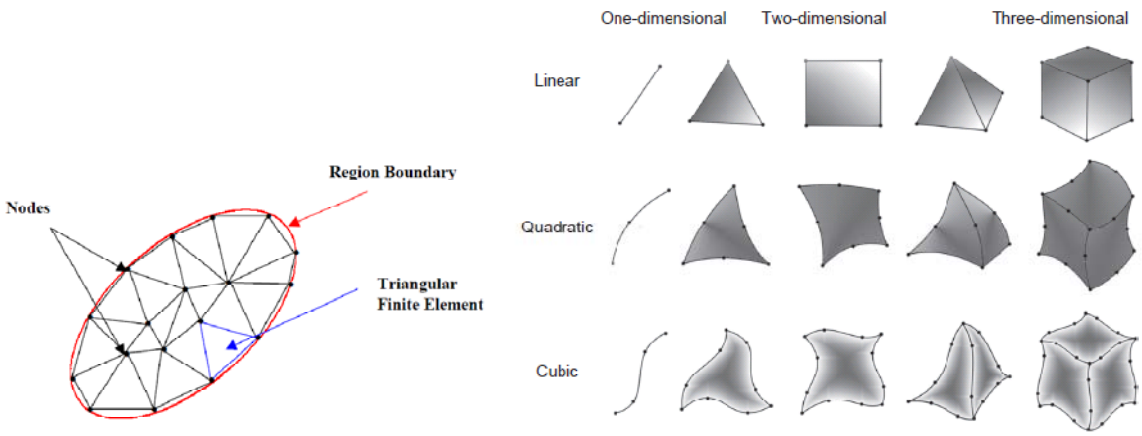

a) b)

Figure 6-1 a) two-dimensional Finite Element mesh, b) Finite elements and shape function order (adopted from (Martins, et al., 2008)

6.1.2 COMSOL Multiphyics software

The COMSOL Multiphyics® is powerful and widely used FEM based software for solving coupled partial differential equations. Its applications range from the medical field to aerospace engineering, mechanical, chemical, electrical engineering, and others[16]. It has several advantages, among them, it has an integrated environment that allows implementation and solution of the Multiphyics problem[17] (e.g., in our case, Darcy's transport, heat transfer and mass transfer); and it provides modelling with several domains and complex geometry. Moreover, COMSOL can accommodate the implementation of different boundary conditions (e.g., Dirichlet boundary condition[18], Neumann boundary condition[19], and the overall mixed boundary condition[20]).

The FEM modelling in the framework of the COMSOL has several steps. The main steps are briefly summarized as (Box 5.1).

[16] http://www.comsol.com/
[17] Multiphysics models are models with more than one type of physics (e.g., here, heat and mass transfer).
[18] If the value of the dependent variable is given along the boundary
[19] If the derivative of the dependent variable is given along the boundary
[20] If the BC along a part of the boundary is of the Dirichlet type, and another part is of the Neumann type

Box 5.1: The main steps in FEM (COMSOL) modelling

Step 1 (*Geometric modelling*): The first step is to build a geometric model for the simulation domain. This includes identifying the type of geometry to use (e.g., 1D or 2D or 3D) and simplifying the geometry, if possible (e.g., symmetry, axial symmetry, e.g. see section 6.2, Figure 6-2 and 6.3) and to generate the geometry in COMSOL.

Step 2 (*mesh generation*): the solid domain (model geometry step 1) is divided into many small, finite elements (also referred to as grids, elements) section 6.1.1.This is an important step because the accuracy of the Finite Element solution depends on the mesh size (Sandeep, et al., 2008).

Step 3 (Mathematical modelling): This step includes problem specification (chapter 5) and the implementations of model equations such as governing equations, boundary equations, initial conditions, material properties and other input parameters in the COMSOL.

Step 4 (Solution): the governing equations, constitutive equation together with boundary and initial condition are solved to obtain the desired state variables (e.g., T (x,y,z,t) and C(x,y,z,t)).

Step 5 (Post-processing): the results are visualized in the form surface plot, colour contours, XY plots, cross-section, etc.), see section 6.2 and 6.3.

Step 6 (Validation): the results are compared to available data, making sure that they are reasonable and acceptable.

Some of the FEM simulations and results will be demonstrated with a model of the meat roasting process in the following sections: (1) 3D model (paper V) and (2) 2D (with moving boundary) model (paper II). The first aims to obtain a 3D understanding of the meat roasting process (e.g. the prediction of the temperature profile), whereas the second aims to consider the effect of moving the boundary during the roasting processes.

6.2 3D model of coupled heat and mass transfer during roasting of meat in the convection oven

A 3D rectangular geometry of dimensions (20mm x 20mm x 27mm, corresponding to only one-fourth of the original dimensions of the sample) was built in COMSOL for numerical simulations (Figure 6-2b). The geometry (one-fourth of the original dimensions) was chosen on the basis of the symmetry in the x and y directions (no symmetry in the z direction because of the baking plate). As a consequence, the computational burden during the simulations was significantly reduced. The geometry was meshed (Figure 6-2c) and the mesh quality was checked using a technique called mesh sensitivity analysis (Ilhan and Ashwini, 2006). A series of simulations were done with increasingly finer mesh until the change in mesh density no longer had an impact on the solution. The generated mesh was refined (e.g., at the boundaries where there is high gradient) to improve the accuracy of the numerical results. In this way unnecessary computation burden can be avoided.

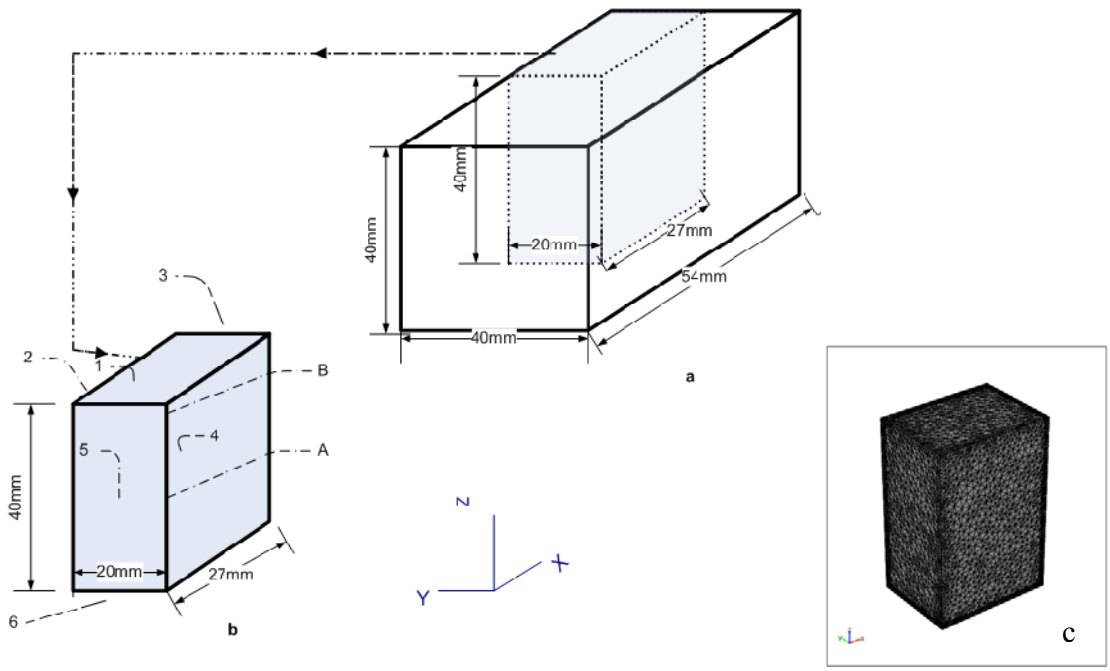

Figure 6-2 3D: schematic view of rectangular shaped meat sample showing a domain, boundaries (1-6) and dimensions. a) original sample b) selected sample for the FEM modelling and point A and B are corresponding to the centre (0, 0, 20mm) and a point close to the surface (0, 0, 38mm), respectively. c) 3D FEM mesh

The governing mathematical model, Eq. (5.5) and Eq. (5.6), the constitutive equations together with the boundary conditions and initial conditions (Chapter 5), all describing the coupled heat and mass transfer during the roasting process, were implemented in COMSOL Multiphyics®version 3.5 and solved. The state variables temperature and moisture concentration (water content) were predicted in space and time. The illustration, Figure 6-3 shows the temperature profile at t = 600s, t=1000s and t = 1500 s during meat roasting in a convection oven. At t = 600 s, the surface temperature of the meat sample is at much higher temperature than the inside part (e.g., it is raw near the centre). This means there is a large temperature gradient (at t = 600s). At the same time, a large moisture gradient is created between the inside part and the outside part (paper V). The meat is losing water due to the higher temperature that causes denaturation of the meat protein on the surface, which leads to a reduction in water binding capacity, whereas at the central part of the meat sample, the water transport is not affected at this time of the roasting because the temperature has not reached the temperature of denaturation.

To illustrate the effect of permeability, the model was simulated with two different values of K, ($K = 10^{-16}$ m^2 and $K = 10^{-17}$ m^2), the latter is corresponding to raw meat (Datta, 2006) and the moisture profile was plotted for the cases (paper V). The simulation indicated that there is a slight rise in water content at the centre with larger permeability ($K = 10^{-16}$ m^2). However, with lower permeability ($K = 10^{-17}$ m^2), which is also a more realistic value for raw meat; there is no rise in water content at the centre. The latter agrees with the experimental result obtained on local water content in chapter 4. The measured and simulated temperature was compared at point A (centre) and B (near surface). Both curves show a similar trend, but with a slight offset between both curves. The deviation at the centre is probable due to the uncertainty in the thermal properties of the meat.

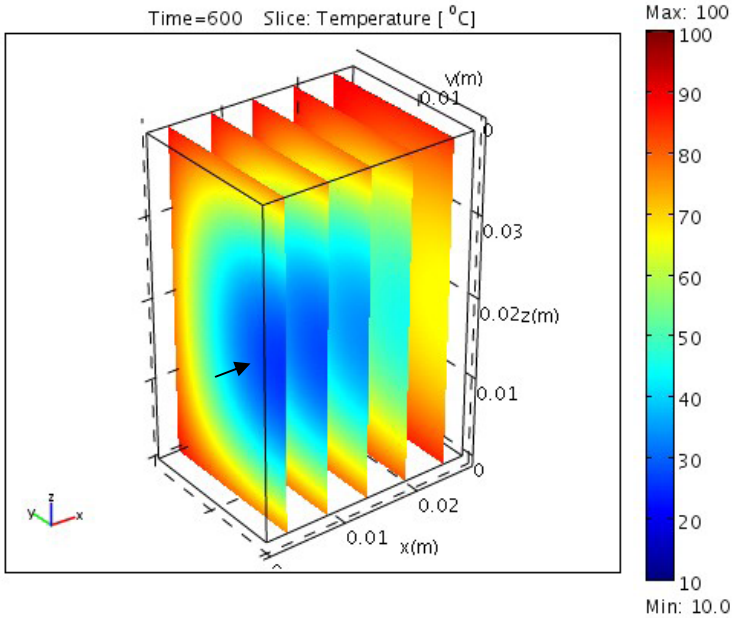
Time=600 Slice: Temperature [°C]
Max: 100
100
90
80
70
60
50
40
30
20
10
Min: 10.0
y(m)
0.01
0
0.03
0.02 z(m)
0.01
0
0.02
0.01 x(m)

a)

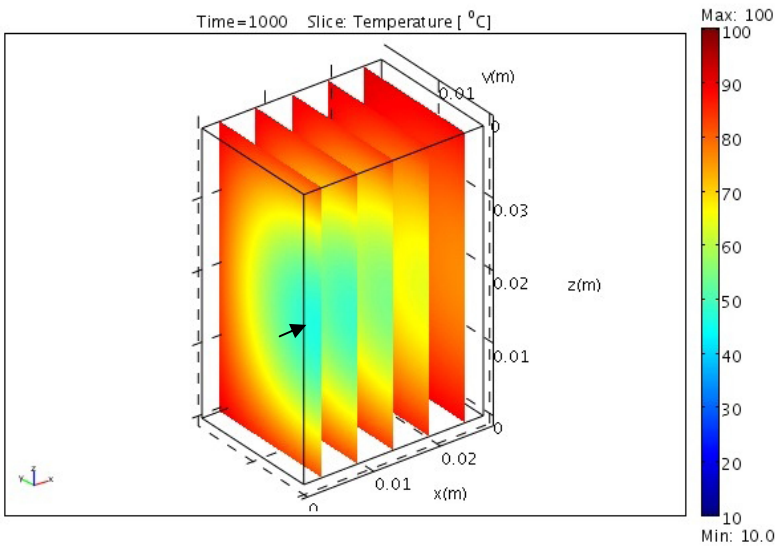
Time=1000 Slice: Temperature [°C]
Max: 100
100
90
80
70
60
50
40
30
20
10
Min: 10.0
y(m)
0.01
0
0.03
0.02 z(m)
0.01
0
0.02
0.01 x(m)

b)

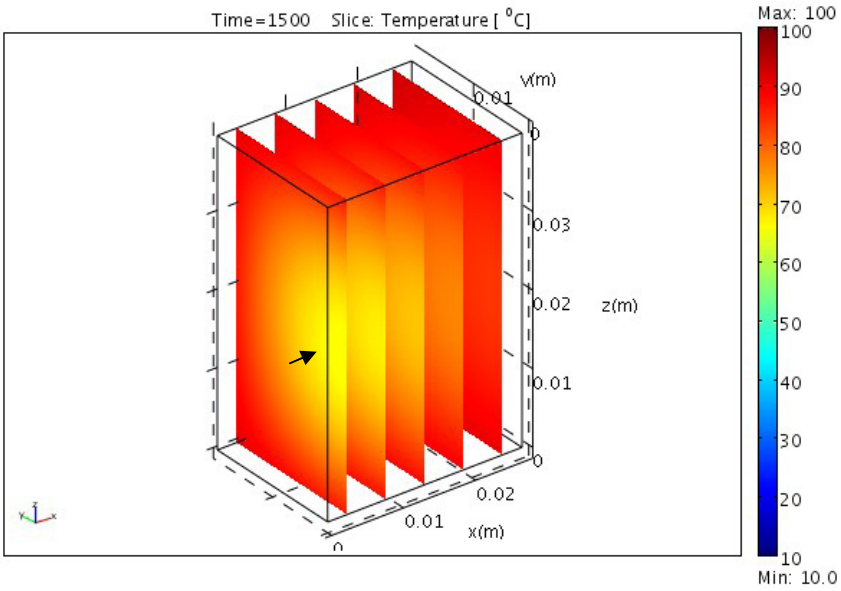

c)

Figure 6-3 Simulated temperature distribution within meat a) t=600s, b) t=1000s and c) t=1500s. The arrows are pointing to centre of meat piece.

6.3 2D model of coupled heat and mass transfer with moving boundary

As we previously discussed, roasting of meat involves shrinkage which leads to change in the overall dimensions (Chapter 3). This means that the boundary of the meat sample is moving during roasting (Figure 6-4). In order to consider this moving boundary and its effect on the prediction of state variables (e.g., temperature and water content), a 2D cylindrical geometry of meat with moving boundary was developed. The 2D cylindrical geometry of dimensions (radius of 20 mm and length of 54 mm) was built in COMSOL for numerical simulations (Figure 6-3). Here, the cylindrical geometry was chosen because of its axial symmetry. A 2D geometry (Figure 6-3) was simulated instead of a 3D geometry, which significantly reduced the computation burden and complexity.

The coupled PDEs for heat and mass transfer along with the boundary conditions were implemented using the *Chemical Engineering module* (transient heat transfer and transient mass transfer) and the *moving mesh module (*arbitrary Lagrangian–Eulerian, *ALE)*. The ALE uses two

sets of reference systems; the Eulerian reference system to track the moving water and the Lagrangian reference system to handle the deforming meat surface. In the ALE method, the computational system is not a prior fixed in space (as Eulerian) or attached to material (as Lagrangian). In the ALE the computational mesh inside the domains can move arbitrarily to optimize the shapes of the elements, while the mesh on the boundaries and interfaces of the domains can move along with the materials to precisely track the boundaries and interfaces of a material system, the detailed discussion can be found in (Anahid and Khoei, 2010, Benson, 1992, Donea, et al., 2004;Hirt, et al., 1974, Hirt, et al., 1997, Khoei, et al., 2008, Taciroglu, et al., 2009).

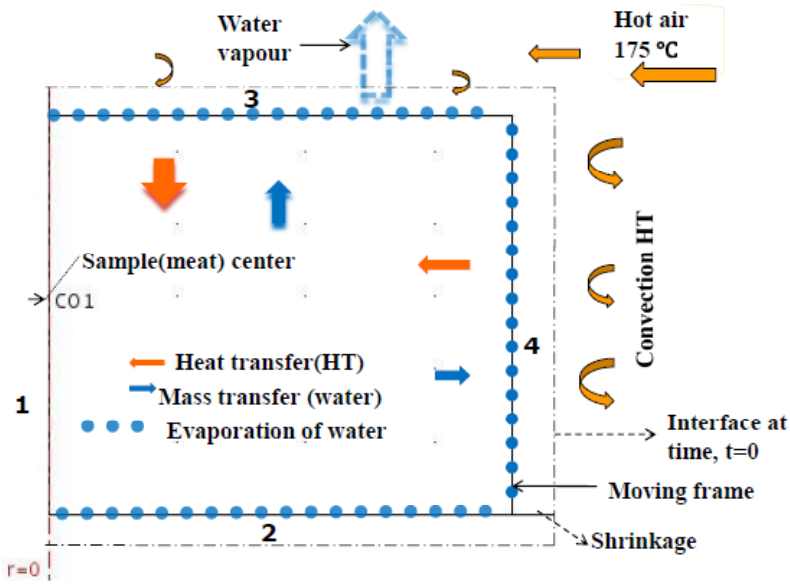

Figure 6-4 A schematic representation of coupled heat and mass transfer accompanied by shrinkage and evaporation processes.

For our purpose, the ALE method was implemented to capture the moving boundary (product-air interface) during the roasting of the meat in the convection oven. The incorporation of ALE gives the ability to track the position of the product-air interface (with the interface velocity, v_r and v_z that were derived in Chapter 5). The meat-air interface (boundary 2, 3, and 4, Figure 6-4) are moving with the interface velocity (v_r and v_z are r and z component, respectively), whereas the boundary 1 (the centre line, at r = 0) is fixed in the r-direction (i.e., $v_r = 0$, and $v_z = v_z\,(z/z_o)$). The z component of the velocity is assumed to move with z-component velocity (v_z), in such a

way that the corner (or end) of boundary 1 is moving as others boundaries are moving, while the boundary 1 has $v_z = 0$ at $z = 0$. The input parameter values and the algebraic expressions in the model are given in paper II.

The governing model equations (Eq. (5.5) and Eq. (5.6), see Chapter 5) describing the coupled heat and mass transfer in convection roasting of meat were solved using the Finite Element method (COMSOL Multiphyics®version3.5). Figure 6-5 a and b show the simulated spatial temperature and moisture distributions, respectively, for a 2D cylindrical meat sample at different times of the roasting process (t = 0, 500, 1000, 1500, 2000, 2500, 3000, and 3500 s).

Generally, the temperature increases with an increase in time, whereas the water content and the dimensions decrease with the increase in time. From these figures a change of dimensions - a moving boundary - can be noticed. Figure 6-5 a, illustrates the progress of the temperature distribution during roasting of meat in a convection oven. Initially, there is a sharp increase in the surface temperature because of the large temperature difference between hot air (175 ^{o}C) and the meat (13°C). At t = 500 s, the surface of the meat is at a much higher temperature than the inside part of the meat sample, and a large temperature gradient is developed in the region close to the surface (Figure 6-5 a and Figure 6-6a). As the roasting process proceeds, this large temperature gradient shifts gradually from near the surface to the inside of the meat.

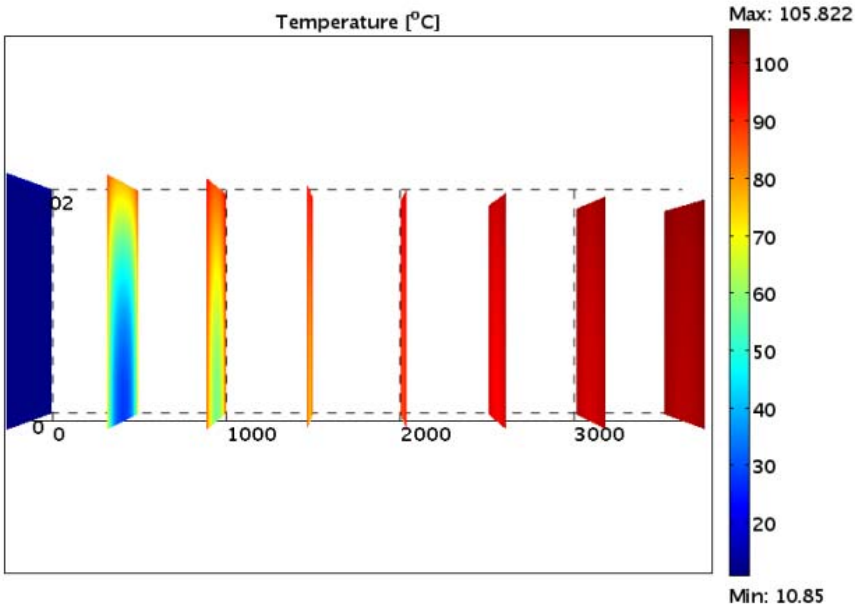

a)

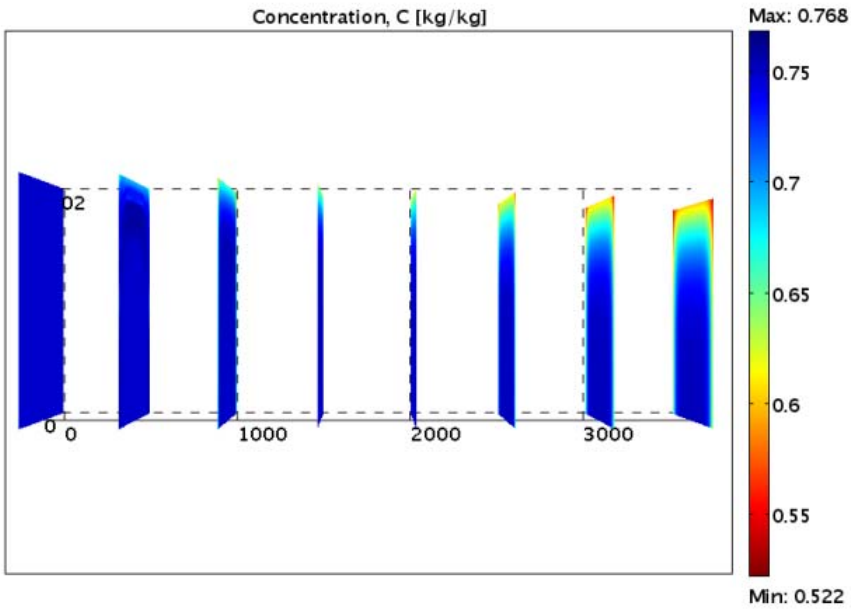

b)

Figure 6-5 a) Temperature distribution, and b) water content distribution at (t = 0, 500, 1000, 1500, 2500, 2000, 3000, and 3500 s)

Moreover, its magnitude decreases as a function of time, as the heat energy is slowly penetrating into the centre of the product, thereby raising its temperature (Figure 6-6a). In the final period of this roasting experiment, at time t = 3000 s, the temperature of the meat is almost uniform.

Figure 6-5 b, illustrates the progress of the water content distribution within the meat product during the roasting process. The water content distribution changes from being uniform (= initial condition) to a non-uniform profile. The increase in temperature (to the denaturation temperature zone) causes the meat to reduce its water holding capacity and induces shrinkage. The reduction of the water holding capacity and the shrinkage of the meat protein network cause the meat to exudate water to the surface, which is lost by evaporation at the surface. As a result, the water content gradient is developed within the meat, as shown by iso-concentration lines at t = 500 s (Figure 6-6 b). A large water concentration gradient is observed near the surface and the gradient gradually shifts towards the interior of the product (Figure 6-5 b).

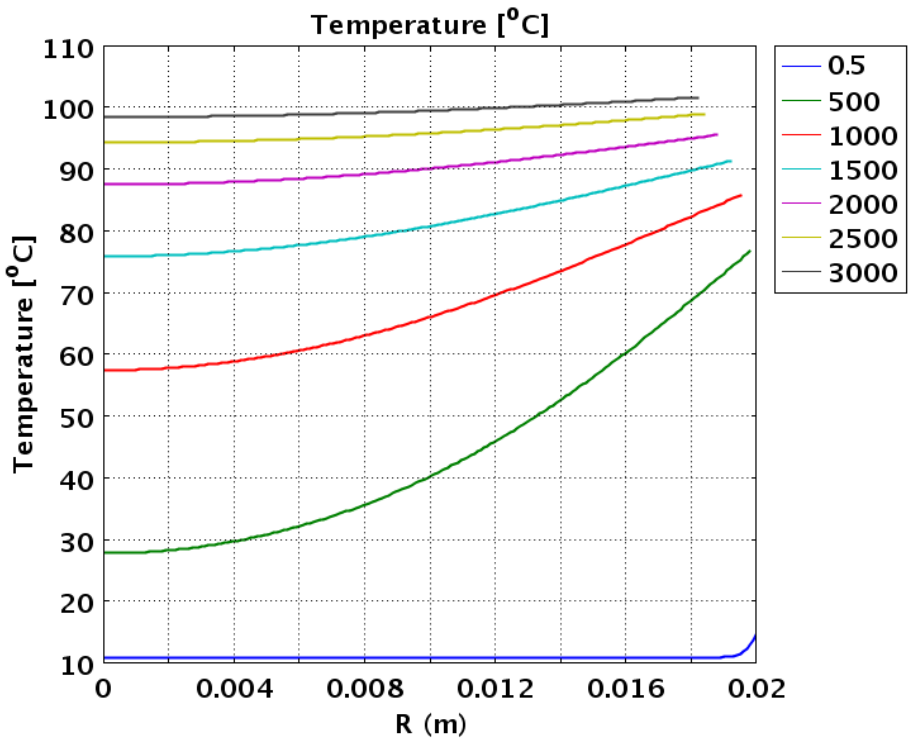

a)

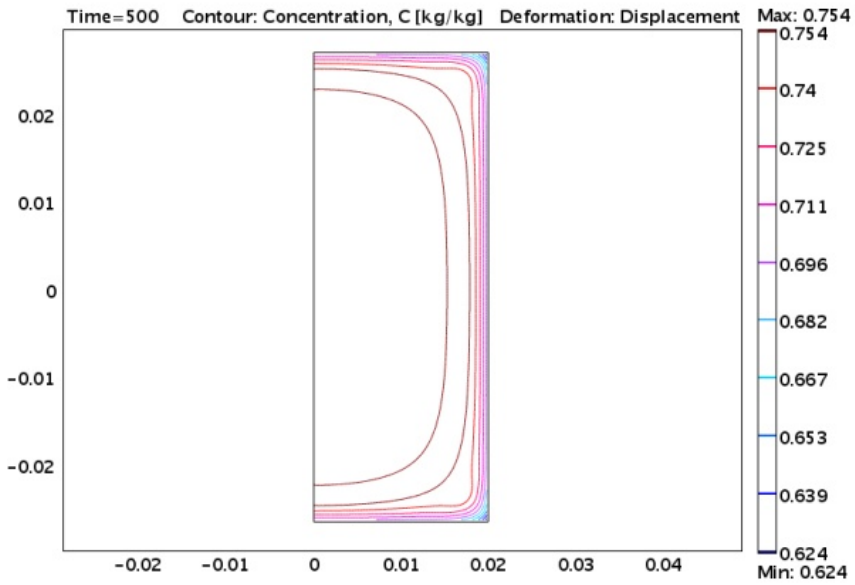

b)

Figure 6-6 Temperature profile across cylindrical sample (Z = 0), b) Iso-concentration, C (kg/kg) at t = 500 s

The temperature profiles with moving boundary (MB) and fixed boundary (FB) are compared (paper II). The centre and the surface temperature values predicted by both methods coincide well at the beginning of the process (t = 0 to t = 1000 s). But later on, (t > 1000 s), the two predictions start deviating from each other. The FB predicts lower centre temperature than the MB. However, the FB predicts higher water content than MB (see for detail paper II). In the same study (paper II), the relative dimensional change (radius), R/R_o, in the r-direction was obtained. During the first part of the roasting process (until t = 300 s), there is no shrinkage. The meat starts shrinking slowly from t = 300 s to 500 s. In the period (between t = 500 s to t = 2000 s), the relative change of dimension is large (steep profile was observed). In this zone (for t = 500 s to t = 2000), a major part of the meat is in the denaturation zone, where a reduction of water holding capacity and shrinkage of protein network take place, (as discussed in chapter 3). In the last period, after t = 2000 s, the relative change of deformations (shrinkage rate) is reducing and particularly, after t = 3500 s, the rate of change of the relative dimension has clearly diminished. The probable reasons for the latter situation are; 1) the mechanical properties of the meat have changed (e.g. elastic modulus increase, (Tornberg, 2005)) and 2) there is a reduction of the water content near the surface, which makes the product more rigid and less susceptible to deformations.

6.4 Summary

The coupled mathematical models of heat and mass transfer during roasting of meat in a convection oven (3D and 2D with/without moving boundary) were developed and solved using the COMSOL Multiphyics. Heat and mass transfer with moving boundary during the roasting of meat were modelled and the effects on the prediction of state variables (temperature and water content) were evaluated. Overall, the FEM solution of the physics-based model of heat and mass transfer during roasting of meat in convection oven provided the state variables as function of position and time. The model provided a better insight i.e., in understanding the physics of meat during the roasting process.

6.4.1 COMSOL-MATLAB

Further analysis, such as parameter estimation, model validation and uncertainty and sensitivity analysis are needed to evaluate the reliability of the model predictions. For unsteady state coupled heat and mass transfer, the COMSOL Multi-physics is not well suited for such purpose (e.g., to set the optimization problem in parameter estimation). The parameters were estimated manually by tuning the values of parameters until the prediction matched with the experimental data. Alternatively, the parameter estimation was performed in a COMSOL-MATALB computing environment. The COMSOL model developed (in this Chapter) was converted into the MATLAB (m-files) and the model was modified within MATLAB by adding more features such as parameters estimation, model validations, uncertainty and sensitivity analysis and other post processing options. In the MATLAB computing environment, parameter estimation (Chapter 7), uncertainty and sensitivity analysis (Chapter 8) were incorporated (Figure 6-7).

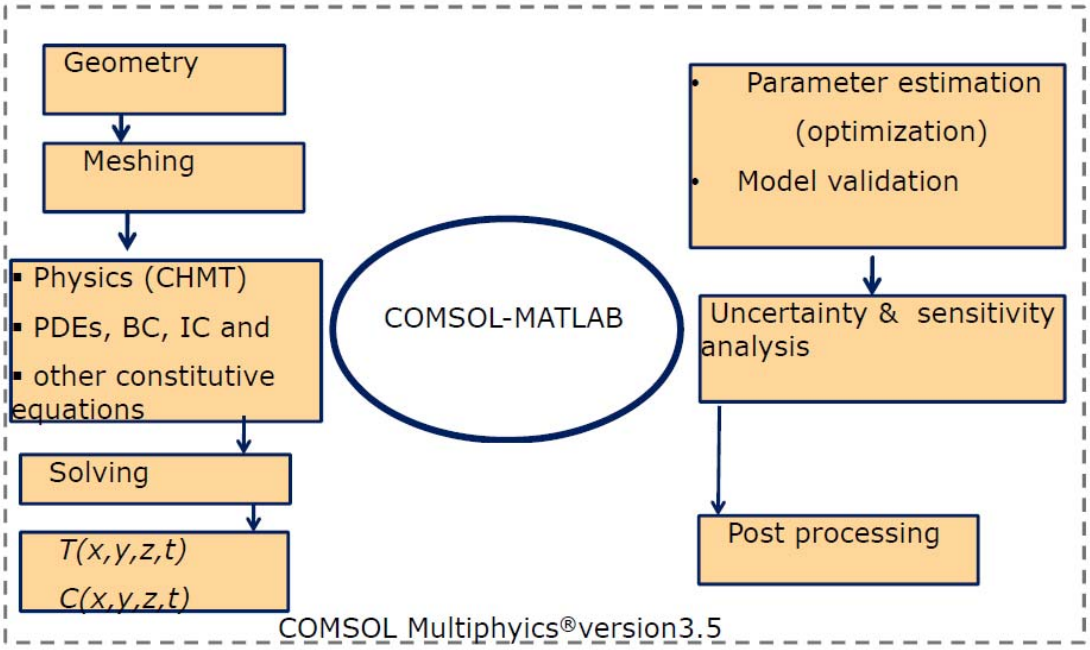

Figure 6-7 COMSOL-MATLAB: the left column what was done using COMSOL and both columns (the left and right) were incorporated in COMSOL-MATLAB, CHMT=coupled heat and mass transfer, BC=boundary condition and IC = initial condition

7 Model calibration and validation

To provide a credible basis for prediction, the ability of the model to represent real physical processes should be demonstrated through a process of model calibration and validation (Hangos and Cameron, 2001). The heat and mass transfer model developed in Chapter 5 for the contact baking process contains parameters with unknown values or non-measurable parameters (e.g. k_{evp}). One way of obtaining the values of these parameters is by the parameter estimation method – the procedure is called model calibration (Hangos and Cameron, 2001). In the model calibration, the model equations (in Chapter 5) and the measured data (in Chapter 4) were used to find the values of unknown parameters, by matching the prediction and experimental data. After the model was calibrated, i.e., when the values of the parameters were estimated with a maximum accuracy, the model was validated with additional experimental data (independent data) by comparing the model prediction and experimental data. The model calibration and validation for contact baking processes were presented in paper III. The reported results and the discussion in the upcoming sections are therefore mainly extracted from this paper.

7.1 Parameter estimation

The formulated model of coupled heat and mass transfer (in Chapter 5) for the contact baking process contains some parameters with unknown values (evaporation rate parameter, k_{evp}, heat transfer coefficient at the bottom surface, h_{bot}). The remaining parameters of the model were obtained from the measurements and literature data, given in Table 7-1.

The unknown parameters ($\omega = [k_{evp}, h_{bot}]$) in the model were estimated using the least square method by comparing the simulated and experimental temperature profiles. The resulting solution of the parameter estimation problem is a set of model parameters which minimizes the value of the objective function ($J(T_{exp}, \omega)$) (Omlin and Reichert, 1999). The objective function is the sum of the squared differences between the simulated temperature (T_{sim}) and the measured temperature profile (T_{exp}) (Hangos and Cameron, 2001). For contact baking, the measured temperature profile at position A (see, chapter 4) was used for parameter estimation.

Table 7-1 Input parameter values

parameter	*value*	*parameter*	*value*	*parameter*	*value*
$y_{p,o}{}^{b}$	0.07 kg/kg	$\rho_f{}^{d}$	920 kg/m^3	$D_v{}^{e}$	$8 \cdot 10^{-7}$ m^2/s
$y_{c,o}{}^{b}$	0.33 kg/kg	$\rho_p{}^{d}$	1320 kg/m^3	$D_l{}^{g}$	$1 \cdot 10^{-9}$ m^2/s
$y_{f,o}{}^{b}$	0.03 kg/kg	$\rho_c{}^{d}$	1600 kg/m^3	k^{d}	0.65 W/(m·K)
$X_{lo}{}^{a}$	1.25 kg/kg	$\rho_w{}^{d}$	1000 kg/m^3	$X_{l,air}{}^{c}$	0 kg/kg
$T_o{}^{a}$	293.15 K	$\rho_s{}^{b}$	1467 kg/m^3	$k_{air}{}^{d}$	0.023 W /(m·K)
$z_5{}^{a}$	0.008 m	$\rho_{Al}{}^{f}$	2660 kg/m^3	$k_l{}^{e}$	$2.3 \cdot 10^{-11}$ m/s
$z_3{}^{a}$	0.005 m	$c_{pAl}{}^{f}$	960 J/(kg·K)	$T_{set}{}^{c}$	433.15 K (160 ^{o}C)
R_g	8.314 J/(K·mol)	$k_{Al}{}^{f}$	150 W/(m·K)	$T_{air}{}^{a}$	308.15 K (35 ^{o}C)
M_w	0.018 kg/mole	$X_{v,air}$	0.0062 kg/kg	$T_{evp}{}^{c}$	373.15 K
H_{evp}	$2.3 \cdot 10^{-6}$ J/kg	$k_v{}^{e}$	$9.6 \cdot 10^{-5}$ m/s	$h_{top}{}^{b}$	8 W/(m^2·s)

Superscripts**: **a: measured, ***b***: calculated or estimated, ***c***: set (assumed), ***d***: (Rao, et al., 2005) , ***e***: Obtained from (Thorvaldsson and Janestad, 1999), ***f***: Obtained from (Martienssen and Warlimont, 2005) , and ***g***: (Toledo,1991)
Subscripts: *p: protein, c: carbohydrate, f: fat and w: water*

The measured and simulated temperature values were taken at 10 seconds sampling intervals. For the minimization of the objective function, the Trust-Region Methods numerical algorithm (within the Matlab® environment), suited for nonlinear estimation problems, was used. Afterwards, the estimated parameters (ω_{est}) were found at the minimum value of the objective function, J_{min} and the confidence interval and the correlation coefficients were computed. The covariance matrix of the estimations (ω_{est}) was computed using a linear approximation method where the sensitivity functions were evaluated at the minimum objective function (J_{min}), Eq. (7.1) (Omlin and Reichert, 1999). Then, the confidence intervals (95% or 1-α = 0.05) for each estimate (ω_{est}) were computed using Eq. 7.2. And, the correlation coefficients between two estimations were also computed using Eq. 7.3. The correlation coefficients, the confidence interval, and the

plot of predictive temperature and the measured temperature were used to evaluate the quality of the estimation. The model solution and calibration were implemented in the *COMSOL-Matlab®* ***version 3.5*** interface environment suited for nonlinear estimation problems. The parameter estimation routine is summarized in Fig. 7.1.

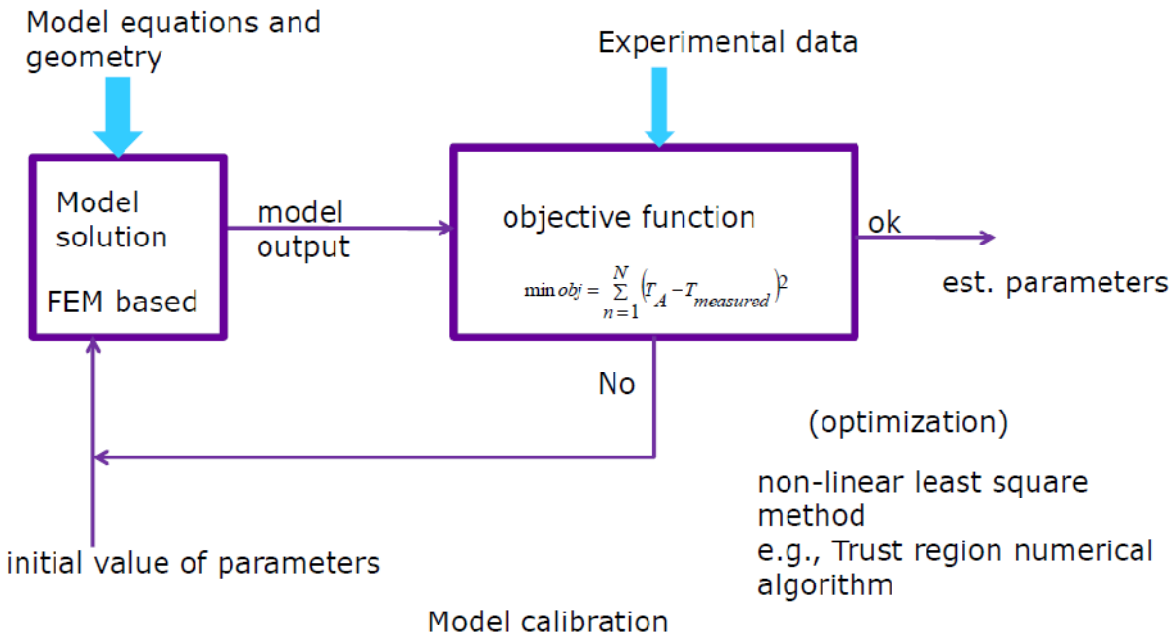

Figure 7-1 Schematic representation of the operation of the parameter estimation routine

Table 7-2 Equation for confidence interval and correlation coefficient

The covariance matrix of estimations, COV (ω)	$\mathrm{cov}(\omega_{est}) = \frac{J_{\min}(T_{\exp}, \omega_{est})}{N - m_{est}} \left(\frac{\partial T_{sim}^T}{\partial \omega} \frac{1}{\sigma^2} \frac{\partial T_{sim}}{\partial \omega} \right)^{-1}$	(7.1)
The (1-α) confidence interval of the estimations:	$(\omega_{est})_{1-\alpha} = \omega_{est} \pm \sqrt{diag(\mathrm{cov}(\omega_{est}))} t(N - m_{est}, \alpha/2)$	(7.2)
The correlation coefficients between two estimations:	$R_{ij} = \frac{\mathrm{cov}((\omega_{est})_i, (\omega_{est})_j)}{\sqrt{\sigma_{\omega,i}^2 \sigma_{\omega,j}^2}}$	(7.3)

where (N-m_{est}, α/2) is the upper α/2 quintile of the *t*-distribution with N-m_{est} degrees of freedom, COV is covariance matrix; *diag* is diagonal elements of COV **(ω_{est})**

7.1.1 Result of parameter estimations (contact baking process)

The model equations of heat and mass transfer developed for the contact baking process in chapter 5 were solved and the unknown parameters of the model were estimated. The parameters (k_{evp} and h_{bot}) were estimated by fitting the simulated temperature profile to the data available for position A (T_{set} = 160 ^{o}C). The estimation results, presented as nominal value ± confidence interval of the parameter, are: $k_{evp} = (11.4 \pm 0.2) \cdot 10^{-5}$ and $h_{bot} = 360.7 \pm 12.8$. The model fit is shown in Fig. 7-2.

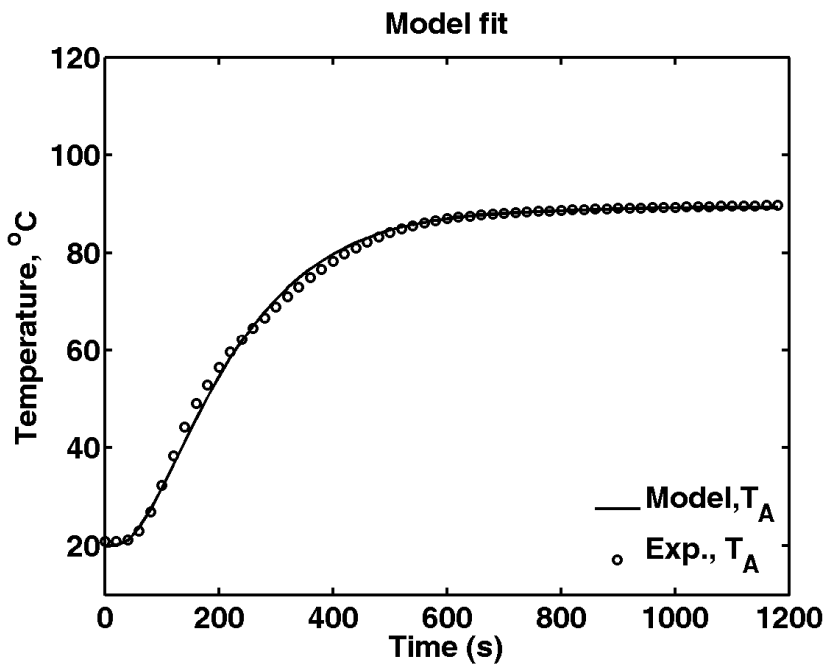

Figure 7-2 Model fit: comparison between the measured (o) and simulated (-) temperature profiles at position A (T_{set} = 160 ^{O}C).

7.2 Model validation (contact baking)

The model was validated by comparing the simulated and measured temperature profiles at three other positions (B, C, and D), using the parameters estimated on the basis of the data collected at position A. The results of these validations are presented in Fig. 7-3 (T_{set} = 160 ^{o}C) and show a good agreement between the simulated and measured temperature profiles at the positions B and

C. At position D, the simulated and measured temperature profiles show a good agreement for the heating period, but there is a clear deviation between the simulated and measured temperature profiles in the evaporation period (Fig. 7-3, at position D). This deviation is assumed to be due to: (1) the burning and crust formation at the bottom surface, which is not well-described in the model; (2) uncertainty on the sensor position - the sensor at position D is less stable compared to the temperature sensors at other positions. Indeed, around t = 200 s the sensor position (D) might move slightly upward as a result of vigorous water vapour generation which can create upward pressure.

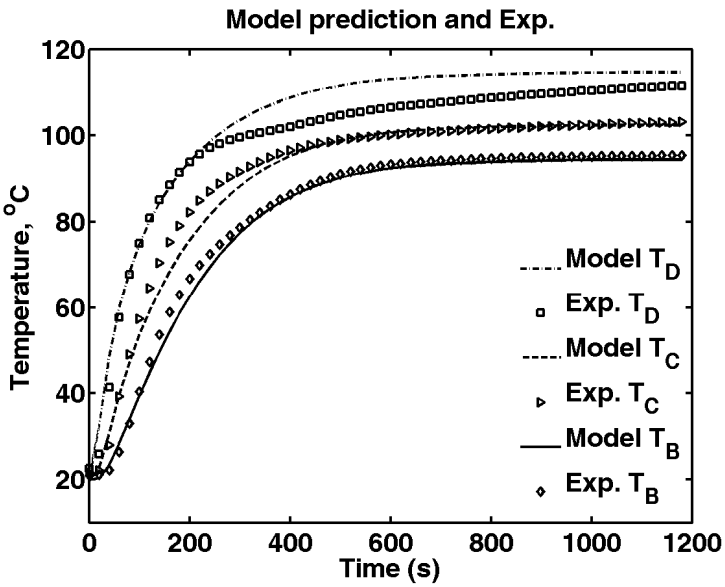

Figure 7-3 Model validation: Simulated and measured temperature profiles compared at different positions (B , C and D) for a temperature set point of 160 ^{O}C .

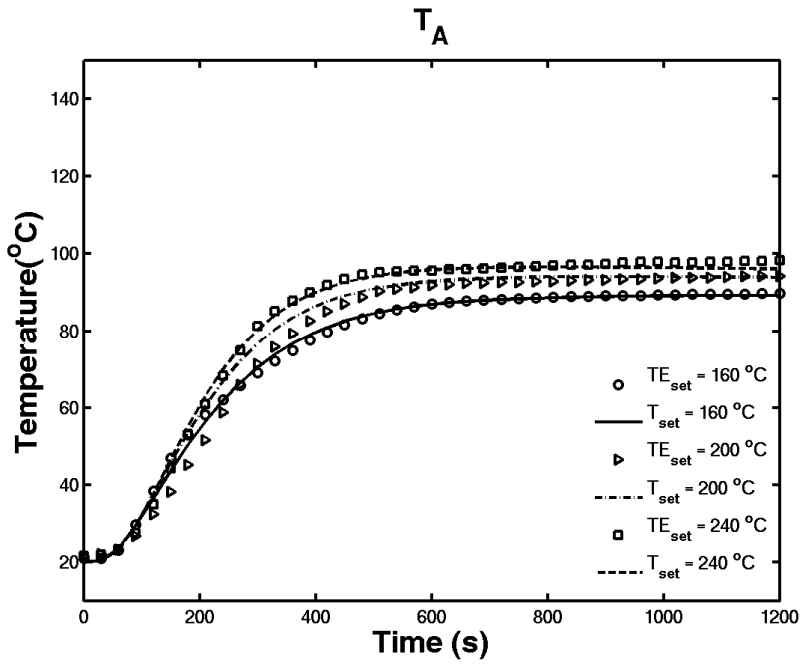

Figure 7-4 Comparison of simulated and measured temperature profiles at position A with different temperature set points (160 °C, 200 °C, and 240 °C). The data are only shown with a sampling interval of 30 seconds, for clarity.

Moreover, the model was validated by comparing the simulated and measured temperature profiles at other temperature set points (200 ^{0}C and 240 ^{0}C) at position A (Figure 7-4) and at position B (paper III).

The simulated results in Figure 7-4 were obtained on the basis of the model for the three temperature set points with all the same settings (as above, obtained in the model calibration, T_{set} = 160 °C), except that the thermal conductivity for the set points 200 ^{0}C and 240 ^{0}C is reduced by 10% compared to the value at the set point of 160 °C. The reduced value of the thermal conductivity for higher temperature set points is motivated by the increased insulation effect at the bottom surface. This insulation effect, due to drying out and crust formation, is compensated in the model by reducing the thermal conductivity value. The higher temperature set point creates a thicker insulating layer at the bottom surface of the product, which means higher resistance, or lower thermal conductivity in the case of a higher temperature set point.

7.3 Model validation (roasting process)

Similarly, model of coupled heat and mass transfer during roasting of meat in convection oven was also validated by comparing the measured and the simulated temperature profiles. The obtained results are given by Figure 7-5 and Figure 7-6. There is a reasonably agreement between the measured and the simulated temperature profiles. Further, the Figures illustrate the effect of mass transfer (evaporation and convection) on temperature profile.

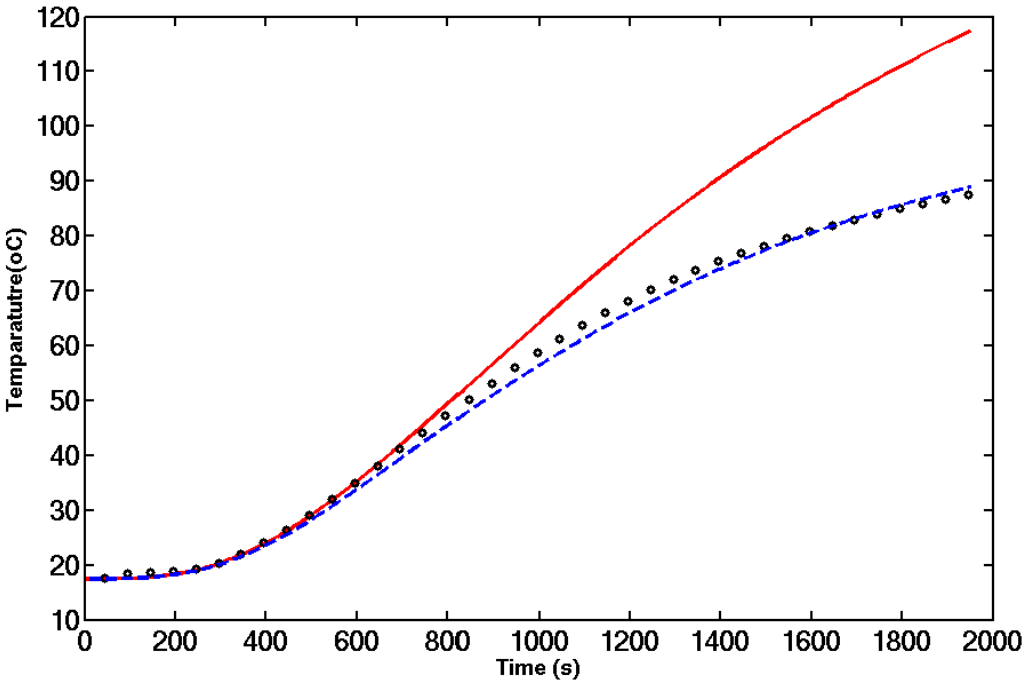

Figure 7-5 Centre temperature (cylindrical meat pieces) (-) pure conduction model, (--) the current model (conduction +convection + evaporation) (o) measured data

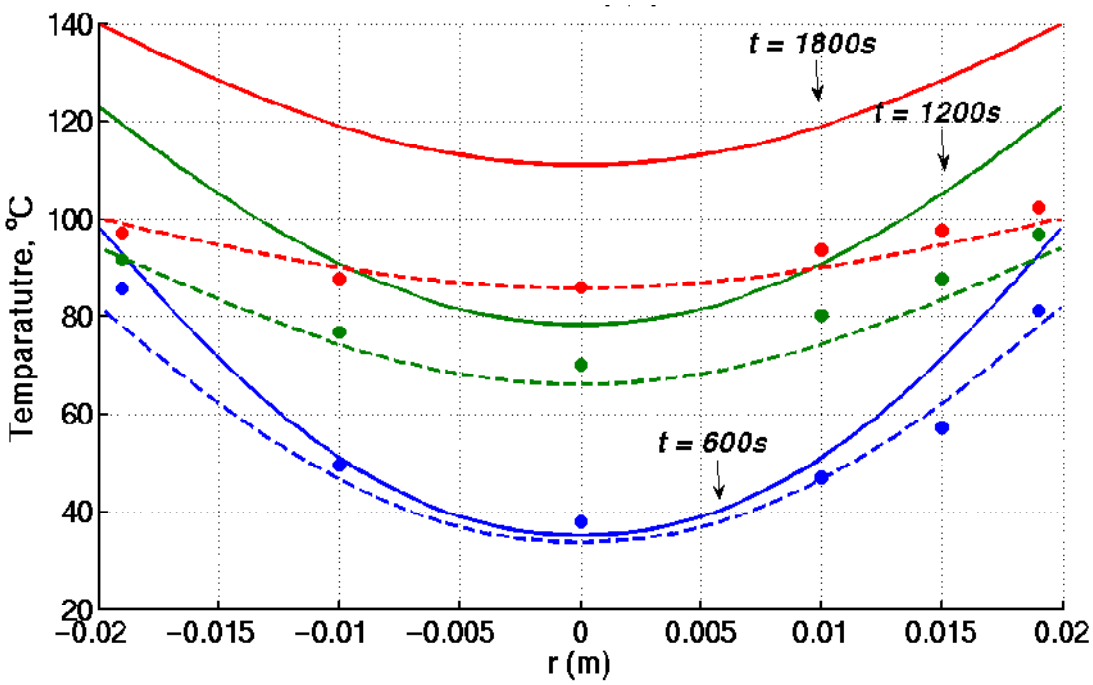

Figure 7-6 Cross sectional temperature profile of cylindrical meat, (-) pure conduction model, (--) the current model (conduction +convection + evaporation) (o) measured data

7.4 Summary

In this chapter, a mathematical model of coupled heat and mass transfer of a contact baking process was validated. The developed model gives a good understanding of the contact baking process, by predicting the temperature and water content profile within the product. A good agreement between the measured and the predicted temperature profile was obtained at positions A, B, and C, which allows us to conclude that the developed model of heat and mass transfer is suitable for describing the contact baking process. Similarly, a mathematical model of coupled heat and mass transfer of a roasting of meat in convection was also validated.

8 Uncertainty and sensitivity analysis

8.1 Introduction

The purpose of a mathematical heat and mass transfer model in a food production process is to describe the physical processes as accurately as possible for the given food production process. As discussed in the previous chapters, setting up the equations of the model, defining the model assumptions, analyzing the model and its simulation output and, finally, comparing this simulation output with experimental data usually result in a much deeper understanding of the process and the main phenomena determining its output dynamics. Baking and roasting operations are usually rather challenging to model due to their complexity, since those operations often involve heat and mass transfer simultaneously with many complex physical-chemical processes (chapter 1 and 3).

The modelling of heat and mass transfer during food processing involves uncertainty in the values of input parameters (e.g., heat and mass transfer coefficients, evaporation rate parameters, thermo-physical properties, initial and boundary conditions) which leads to uncertainty in the model predictions. The uncertainty on parameter values – required for the numerical solution of a mechanistic model, and for example related to material properties and transport coefficients – can be attributed to the fact that the parameters are often not available or come with a large inherent uncertainty. Specifically for solid food products, the values of parameters reported in the literature are not consistent, which is due to the inherent complexity and variability of a food matrix. A good example to illustrate this is the extensive study on thermo-physical properties of bakery products (Baik, et al., 2001, Rask, 1989).

The uncertainty in the values of parameters is a great challenge in many branches of the food industry, and results in difficulties when using models for predictions as well as problems in correctly setting the process parameters (Wong, et al., 2006). One way to cope with this challenge is to take into account the uncertainty in the input parameters, and to evaluate their impact on the predictions. This is precisely what will be discussed in this chapter. An uncertainty analysis is used to map input uncertainty to output uncertainty, while a sensitivity analysis is

applied to decompose input uncertainty, i.e. to identify the parameters that are most influential on the model output (Saltelli, et al., 2008). In this chapter, we will apply the uncertainty analysis and global sensitivity analysis to the heat and mass transfer model of a contact baking process. We use the Monte Carlo procedure for propagating uncertainty in the input parameters to uncertainty in the model predictions. We will apply a global sensitivity analysis method which is based on Monte Carlo simulations followed by linear regression on the Monte-Carlo simulation output. This method is also known as the standardized regression coefficients (SRC) method (Saltelli, et al., 2008).

8.2 Contact baking process

8.2.1 Model equations

The contact baking process involves heat and mass transfer (liquid water and water vapour), where the state variables in the model are temperature, liquid water concentration (X_l), and water vapour concentration (X_V).The coupled heat and mass transfer of the contact baking process is described with a system consisting of partial differential equations (PDEs) and constitutive equations (chapter 4). The numerical simulation of the coupled heat and mass transfer model is used in the prediction of the state variables as a function of time at different positions in the pancake batter (paper III and IV). In the coupled heat and mass transfer model of a contact baking process, the values of heat and mass transfer coefficients, phase change parameters, boundary condition parameters and thermo-physical properties (e.g. thermal conductivity) are uncertain (section 8.2.3).

8.2.2 Model output variables

The four positions (A, B, C, and D) within the product (pancake batter) were considered as the target of interest for the state variables (temperature, T, liquid water concentration, X_l, and water vapour concentration, X_v). Thirteen model output variables were considered: (1) the prediction of the three state variables (T, X_l, and X_v) for each of the four positions in the pancake batter gives 12 output variables, and (2) an additional output variable is the average water content of the pancake batter. All the output variables are represented by the vector Y, where Y = [T_A, T_B, T_C, T_D, X_{ave}, $X_{l,A}$, X_{lB}, X_{lc}, X_{lD}, Xv_A, Xv_B, Xv_C, Xv_D].

8.2.3 Input parameters

The model input parameters were classified as: (1) parameters with fixed values (parameters in Table 7-1 without parameters in Table 8-1), and (2) parameters with uncertain values (paper IV), where in the latter case, the variation in the input parameter values is taken into account in the uncertainty analysis (Table 8-1). The input parameters with uncertain values are parameters related to: (1) the boundary conditions (T_{set}, T_{air}, h_{top}, h_{bot}, k_v, k_l); (2) the initial conditions (T_o *and* X_{lo}); (3) the transfer coefficient (k, D_l, D_v,); and (4) the phase change parameters (k_{evp}, T_{evp}, H_{evp}). All the uncertain input parameters (14 parameters) are represented by the vector θ, where $\theta = [k_{evp}\ T_{set},\ T_{air},\ h_{top},\ h_{bot},\ k_v,\ k_l,\ T_o,\ X_{lo},\ T_{evp},\ k,\ D_l,\ D_v,\ H_{evp}]$. The main objective is to quantify the uncertainty in the model predictions (Y) due to the uncertainty of these parameters (θ), and to identify and rank the parameters based on their relative impact.

8.3 Monte Carlo method

The Monte Carlo analysis is a probabilistically based sampling procedure used to map uncertainty from the model input to the model output (Helton and Davis, 2003). The mapping provides a basis for the evaluation of the uncertainty in the model output. Although, a variety of techniques exist for the uncertainty analysis (Cacuci, et al., 2005, Saltelli, et al., 2008), the Monte Carlo technique was chosen because it provides the most effective approach for the propagation and analysis of the uncertainty for various reasons (Helton and Davis, 2003). The method is generally accepted as computationally-effective and reliable (Sin, et al., 2009). The Monte Carlo technique for uncertainty analysis is a step-wise procedure (Sin, et al., 2009): (1) determination of the uncertain input, (2) sampling the uncertain input (3) model evaluations (FEM simulations); and (4) representation of output uncertainty.

***Step 1* (*uncertainty in the input parameters*)**: The first step is the most crucial step in the Monte Carlo procedure (Cacuci, et al., 2005). A nominal value of each parameter was derived from the scientific literature (Table 7-1, chapter 7). The uncertainty range of an input parameter was determined on the basis of literature data, experimental data and expert assumptions (see for detail in paper IV). The range of parameter values are summarized in Table 8-1. The wider range indicates the parameter with more uncertainty, whereas the narrower range indicates the

parameter with less uncertainty. It was furthermore assumed that each model parameter has a uniform distribution within the specified range.

Table 8-1 Uncertainty ranges for the input parameters

Parameters	unit	minimum[21]	maximum[22]
D_v^{**}	$m^2 \cdot s^{-1}$	$6.8 \cdot 10^{-7}$	$9.2 \cdot 10^{-7}$
D_l^{***}	$m^2 \cdot s^{-1}$	$7 \cdot 10^{-10}$	$1.3 \cdot 10^{-9}$
T_{air}^{*}	K	308	319
T_{set}^{*}	K	425	433
h_{top}^{**}	$W \cdot m^{-2} \cdot K^{-1}$	6.8	9.2
h_{bot}^{**}	$W \cdot m^{-2} \cdot K^{-1}$	306	414
k_v^{**}	$m \cdot s^{-1}$	$8 \cdot 10^{-5}$	$1 \cdot 10^{-4}$
k_l	$m \cdot s^{-1}$	1.10^{-11}	$1 \cdot 10^{-10}$
k_{evp}^{**}	s^{-1}	$0.97 \cdot 10^{-4}$	$1.38 \cdot 10^{-4}$
k**	$W \cdot m^{-1} \cdot K^{-1}$	0.55	0.7
T_{evp}	K	371	375
H_{evp}^{**}	$J \cdot kg^{-1}$	$2.07 \cdot 10^{6}$	$2.5 \cdot 10^{6}$
X_{lo}^{*}	kg of water / kg of solid	1.24	1.26
To^{*}	K	291	295

The superscript: (*): obtained from measurement, (**): ±15% of the nominal value, and (***): ±30 % of the nominal value

Step 2* (*sampling*):* The Latin Hypercube Sampling (LHS) was used for probabilistic sampling of the input parameter space (Helton and Davis, 2003, Sin, et al., 2009). In total, 1000 samples were selected from the input parameter space, where each sample, θ_i, contains one value for each input parameter Eq. (8.1): $\theta_i = [\theta_{1i}, \theta_{2i}, \theta_{3i}, ...\theta_{Mi}]$ for $i = 1,2,3,....,N$ (8.1)

[21] $\theta_{\min} = (1 - \%Variation)\theta_{mean}$

[22] $\theta_{\max} = (1 + \%Variation)\theta_{mean}$

i.e.

$$\begin{bmatrix} \theta_1 \\ . \\ . \\ \theta_i \\ . \\ . \\ \theta_N \end{bmatrix} = \begin{bmatrix} \theta_{11}, \theta_{21}, \theta_{31}, ... \theta_{M1} \\ . \\ . \\ \theta_{1i}, \theta_{2i}, \theta_{3i}, ... \theta_{Mi} \\ . \\ . \\ \theta_{1N}, \theta_{2N}, \theta_{3N}, ... \theta_{MN} \end{bmatrix}$$

where M is the total number of input parameters and N is the total number of Latin-hypercube samples (e.g., 1000), and θ_{1i}, *and* θ_{2i}, are the samples for the first and the second input parameters, respectively.

Step 3 (model evaluations): The sampled input matrix, θ_{NxM} was propagated by performing N Finite Element simulations, i.e. one simulation (a row of input matrices) for each parameter combination sampled in step 2 , (N = 1000). For each simulation, the governing model equations of heat and mass transfer (heat, liquid water and water vapour), consisting of a system of partial differential equations (PDE) combined with constitutive equations, were solved using the *Finite Element Method*. The simulations resulted in a three dimensional matrix Y_{GxKxN} that contains G time instant (10 seconds interval between the 0 and 1200 s) predictions of K output variables (13) and N Latin hypercube samples (1000 samples). This step is the most computational intensive part in the entire uncertainty and sensitivity analysis (Cacuci, et al., 2005).

Step 4 (representation of output uncertainty): The simulation results obtained in step 3 were processed. The mean, the 10th and 90th percentile of the distributions were constructed using the raw data obtained from the Monte Carlo simulations (e.g., the shaded area in the Figure 8-1 is the temperature profile at position A obtained after N = 1000 simulations). For each output variable, and for every time point where model output is generated, the output uncertainty was represented by the mean and the 10th and the 90th percentile of the output distribution (Figure 8-1).

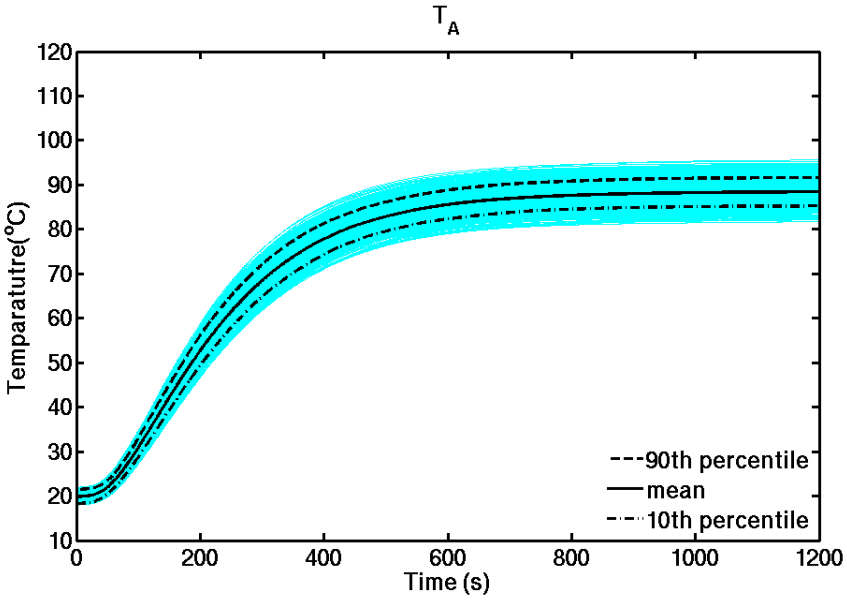

Figure 8-1 Uncertainty in the model prediction for the temperature at position A (the shaded area is Monte Carlo simulations, N = 1000 and the lines (-, -.-, and ---) are mean, 10th and 90th percentile, respectively)

8.4 Uncertainty in the model prediction

Figure 8-2 and Figure 8-3 illustrate the mean, the 10th and 90th percentile of the temperature profiles and the water concentrations (liquid and vapour) profile, respectively. The larger the spread (band) of the model predictions is the larger the uncertainty in the model output. Consequently, a narrow spread of the output corresponds to a small uncertainty. Generally, the uncertainty of the model output varies with time (growing trend). Initially (in the heating zone, for time < 200 s, chapter 4), the spread is small for most of the model output, while in the evaporation period, the band becomes larger for most model output (Y).

The temperature profiles at the positions A, B, C, and D (Figure 8-2) have similar uncertainty trends, while the uncertainty on the prediction of the water content (both for liquid water and water vapour, Figure 8-3) varies for different positions in the pancake batter. The uncertainty range in the prediction of the liquid water concentration is larger at position D (X_{lD}) compared to position A (X_{lA}) (Figure 8-3, top-right and top-left). Moreover, at position A, the prediction of the water vapour concentration, X_v is relatively less uncertain compared to the prediction at position D (Figure 8-3, bottom-left and with the bottom-right). For example, the uncertainty

range or the band width of X_{vD} is 1.5 and 1.23 times the band width of X_{vA} at t = 300 s and t =1000s, respectively. The water vapour concentration, X_v has the largest uncertainty in the transition zone between the heating phase and the evaporation phase (t = 200 to 400 s).

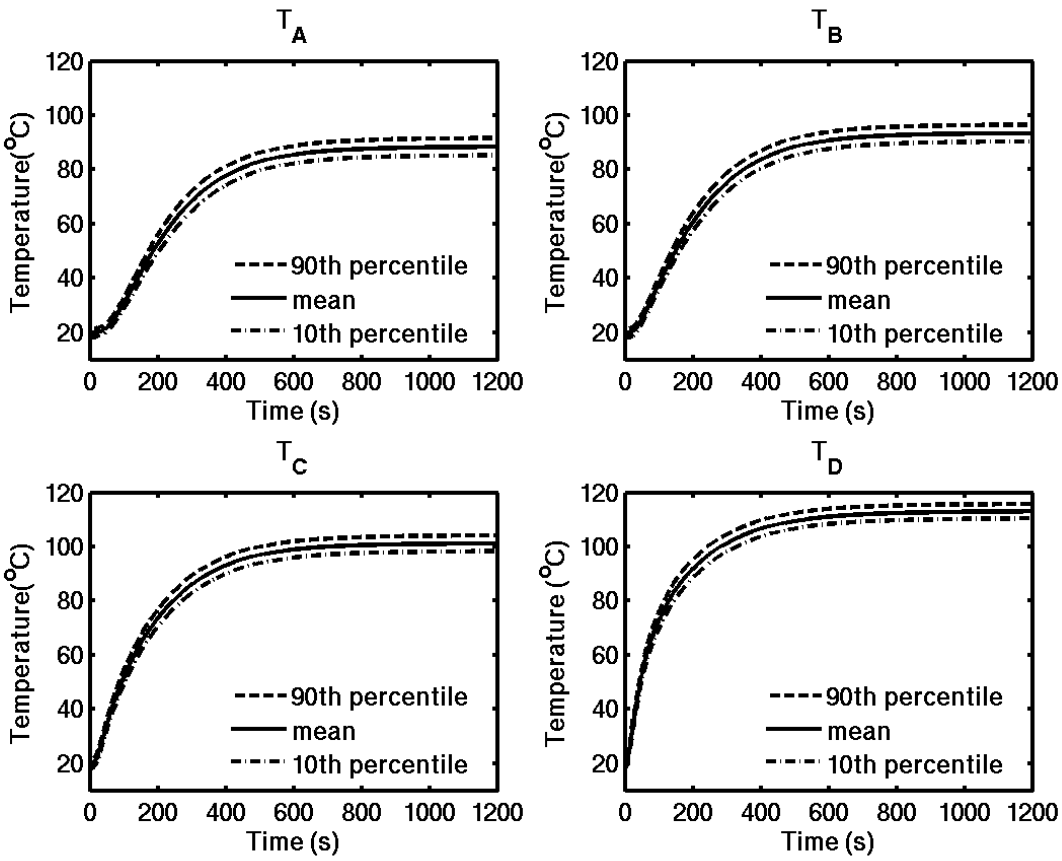

Figure 8-2 Representation of uncertainty of the temperature profile predictions using the mean, the 10th and 90th percentile at position A, B, C, and D, (T_A, T_B, T_C and T_D, respectively).

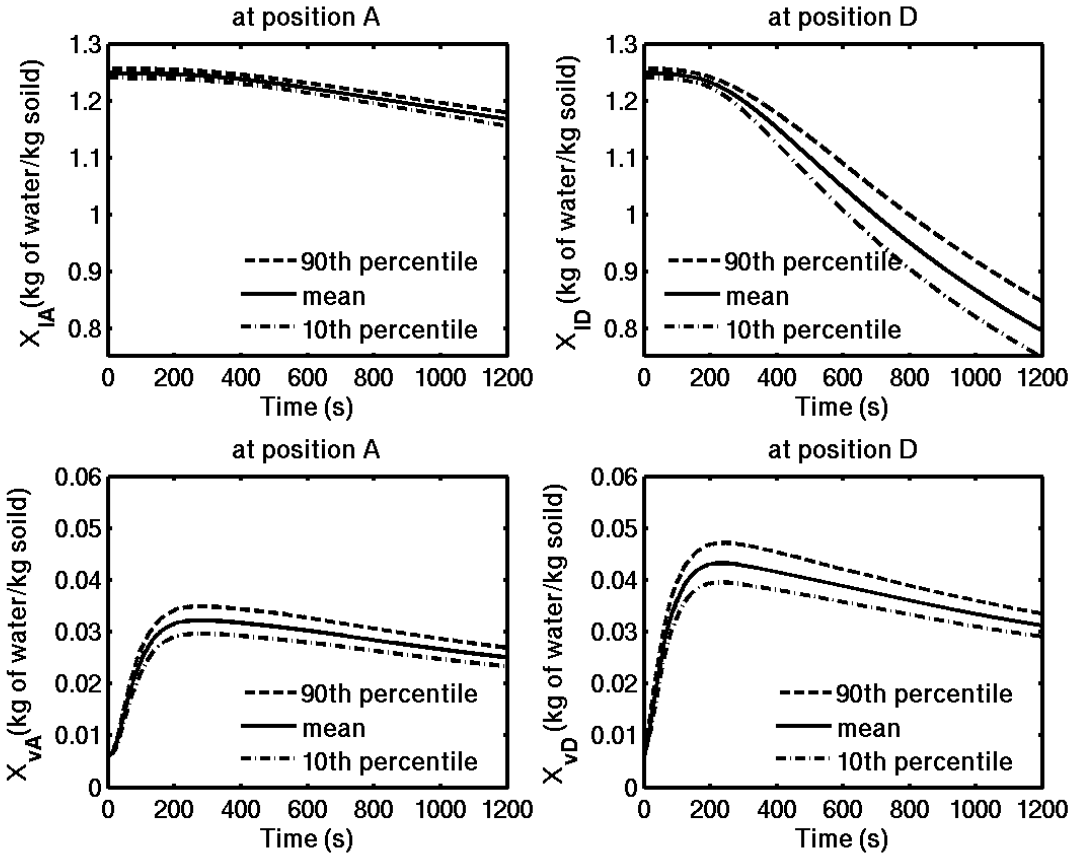

Figure 8-3 Representation of uncertainty of the water concentration (kg of water/kg of solid) profile predictions using the mean, the 10th and 90th percentile at positions A and D for liquid water ($X_{l,A}$ and $X_{l,D}$) and water vapour ($X_{v,A}$ and $X_{v,D}$)

8.5 Sensitivity analysis

In section 8.4, the uncertainties of the input parameters were propagated to output uncertainty. The next task was to identify the parameters with large impact (or the main source of the uncertainty) from those with less impact on the model predictions. The Monte Carlo simulations and the least square method were used in the sensitivity analysis (Helton and Davis, 2003, Sin, et al., 2009). The standardized regression coefficients (SRC) were obtained by constructing linear regression models on the model output obtained from the Monte Carlo simulations (section 8.3). For each model output in Y, a linear regression model was constructed using Eq. (8.2), which is

the standardized mean-centred sigma-scaling (Sin, et al., 2009). The standardized mean-centred sigma-scaling is the scaling of the linear regression equation[23] by the output and the parameters using their corresponding mean and standard deviations (Cariboni, et al., 2007). The scaling gives a dimensionless form of regression equation (as Eq.8.2).

$$\frac{sY_{im} - \mu_{sym}}{\sigma_{sym}} = \sum_{j=1}^{M} \beta_{im} \frac{\theta_{ij} - \mu_{\theta j}}{\sigma_{\theta j}} + \varepsilon_{im} \qquad \text{for } i = 1,2,3,....,N \text{ and for } m = 1,2,3,....., K \qquad (8.2)$$

Where: Y is the vector with output variables, θ is the vector with input parameters, m is the index of the output vector, i is the index of the Monte Carlo simulations (samples), j is the index of the parameter vector θ, e_{im} is the error of the linear regression model, β_{im} is the SRC and M is the total number of the parameters (*M = 14, section 8.2.2*). For each model output (Y), the corresponding SRCs were obtained using the linear least square method. The β_{im} were computed for each input parameters and output combination, its magnitudes relate to how strong the input parameters contribute to the predictions (Y).

Scalar output is required for the calculation of SRCs. The SRCs can be evaluated at different time instant during the baking process. Here, the focus was on the time t = 1000 s, i.e. towards the end of the baking process. For most of the model output (Y), the uncertainty analysis results (section 8.3, Figure 8-2) confirmed that the larger uncertainty was observed towards the end of the baking.

The coefficient of determination (R^2) was computed for each model output (Y). The original model of coupled heat and mass transfer is non-linear, and the R^2 is used to evaluate the degree of linearization for each Y. The method can be used, if the R^2 is above the recommended value of 0.7 (Cariboni, et al., 2007).

The obtained SRCs and R^2 for each model output at *t = 1000 s* is illustrated in Table 8-2 (see for detail in paper IV). The R^2 values were found to be above 0.99 for all variables in Y, 13 model output variables. This means that the linearized model expressed by Eq. (8.2) is able to explain

[23] $sY_{im} = b_{ok} + \sum_{j=1}^{M} b_{jm}\theta_{ij} + \varepsilon_{im}$ for $i = 1,2,3,....,N$ and for $m = 1,2,3,....., K$

most of the variance in the model output, and this confirms that the SRC values can be used to evaluate the relative importance of input parameters (θ) on the model output (Y). The absolute value of the SRCs' in Table 8-2 indicates the impact of each parameter, while the sign indicates either a positive or a negative correlation between the output (Y) and the input parameter (θ). For example, the temperature at position A decreases as the evaporation rate constant (k_{evp}) increases (i.e., the correlation between k_{evp} and T_D is negative, since SRC = -0.62, Table 3). This is reasonable, because increasing the evaporation rate increases the heat of evaporation, and therefore decreases the sensible heat.

8.6 Parameter ranking

A summary of the parameter ranking for each model output (Y) is presented in Table 8-2, and Figure 8-4 and Figure 8-5 for three state variables: temperature, liquid water concentration and water vapour concentration, respectively.

Temperature: The product temperature at the four positions (A, B, C, and D) is very sensitive to the evaporation rate constant k_{evp}, which ranks the highest in the list provided in Table 8-2. The correlation between the k_{evp} and the product temperature is negative (e.g., at D, the SRC = -0.62, Table 8-2), and the product temperature at all positions decreases as k_{evp} increases.

Table 8-2 Sensitivity analysis: SRCs and parameter ranking for temperature (only the 6 top among 14 parameters)

	T_A		T_B		T_C		T_D	
rank	**parameter**	***SRC***	**parameter**	***SRC***	**parameter**	***SRC***	**parameter**	***SRC***
1	$\boldsymbol{k_{evp}}$	**-0.619**	$\boldsymbol{k_{evp}}$	**-0.623**	$\boldsymbol{k_{evp}}$	**-0.607**	$\boldsymbol{k_{evp}}$	**-0.540**
2	$\boldsymbol{k}$	**0.541**	$\boldsymbol{k}$	**0.499**	$\boldsymbol{k}$	**0.430**	$\boldsymbol{T_{set}}$	**0.496**
3	H_{evp}	-0.310	H_{evp}	-0.337	H_{evp}	-0.369	H_{evp}	-0.393
4	T_{evp}	0.308	T_{evp}	0.314	T_{set}	0.343	h_{bot}	0.302
5	T_{set}	0.226	T_{set}	0.266	T_{evp}	0.315	T_{evp}	0.300
6	h_{bot}	0.153	h_{bot}	0.175	h_{bot}	0.216	k	0.295
	R^2	0.998	R^2	0.998	R^2	0.998	R^2	0.998

The thermal conductivity parameter, *k* is the second most sensitive parameter in the prediction of the product temperature (Table 8-2), except at position D. The product temperature (at all positions, T_A, T_B, T_C, and T_D) is increasing with increasing k (e.g., at position D, SRC = 0.54, Table 8-2). The larger *k* value allows more heat flux to transfer through the product compared to smaller *k* values. The temperature at position D, T_D is more sensitive to the temperature set point, T_{set}, compared to k. The temperature set point (T_{set}) has a strong impact on T_D, because the position D is closer to the bottom surface.

The bottom boundary condition parameters, T_{set} and h_{bot}, and the evaporation parameters H_{evp} and T_{evp} have a moderate impact on the product temperature prediction, while the rest of the parameters, including all the top boundary condition parameters (e.g., T_{air}, h_{top}) relatively have no impact on the uncertainty in the product temperature prediction. Thus, it can be concluded that the uncertainty in the prediction of the product temperature, (section 8.4, Figure 8-1, top-left) is mostly due to the six highest-ranking parameters (k_{evp}, k, T_{set}, H_{evp}, T_{evp}, h_{bot} *and* T_{set}).

Liquid water concentration (X_l): The ranking of the parameter impact on the liquid water concentration is illustrated in Figure 8-4 for the four positions within the pancake batter. At position D, the prediction of liquid water concentration has a larger uncertainty (section 3.3) compared to the other remaining positions (A, B, and C). The large uncertainty on the prediction of the liquid water concentration at position D is mainly due to uncertainty in the value of the liquid diffusion coefficient, D_l; D_l has the largest impact among all the parameters (θ) (Table 3, and Figure 8-4 top-left). The liquid water concentration at position D, $X_{l,D}$ decreases as D_l increases (detailed in Paper IV). This is because, at the bottom surface (z = 0), the liquid water evaporates vigorously, and as the result of that the liquid water concentration is reduced rapidly. The liquid water diffuses from position D (z = 1.6 mm) where the concentration is higher, to the bottom surface (z = 0) where the concentration is much lower. This means that the diffusion coefficient of the water is the limiting factor and the mechanism for the liquid water transport inside the product is strongly diffusion dependent, particularly in that region (close to the bottom surface).

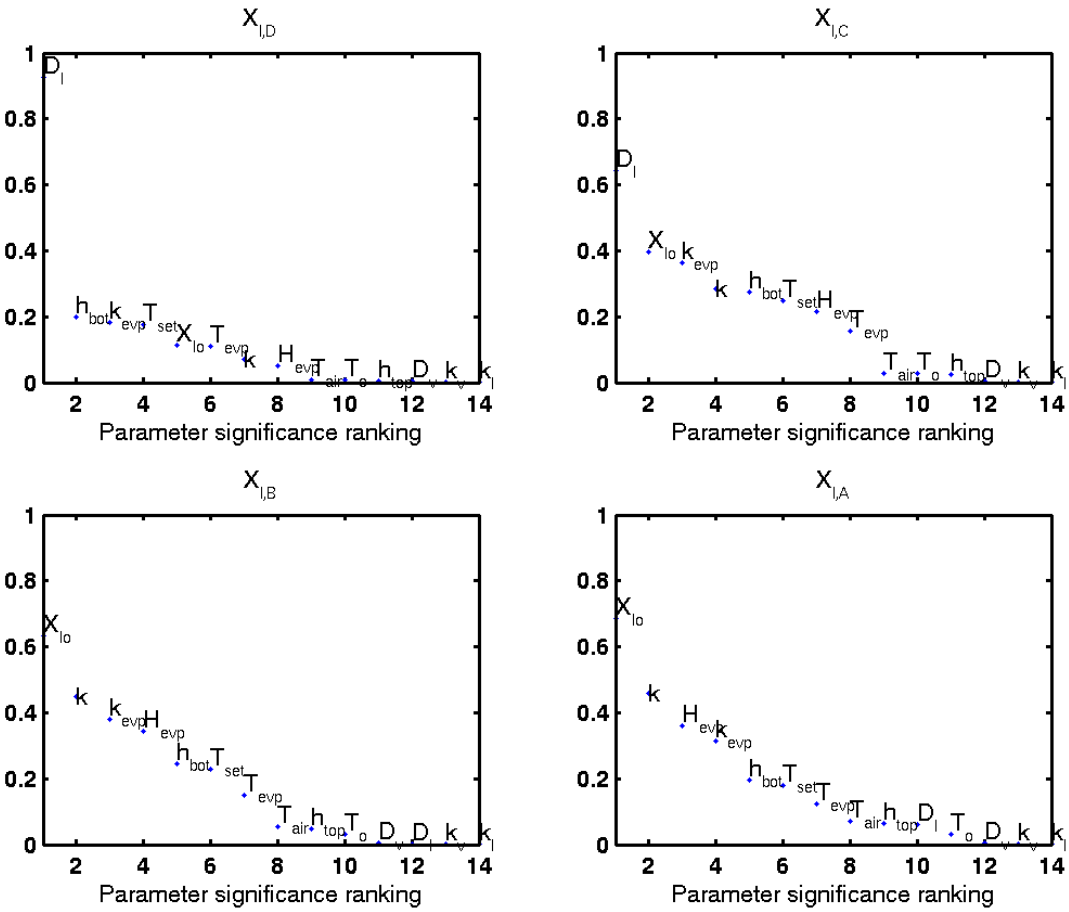

Figure 8-4 Relative importance of input parameters for X_{lD}, X_{lC}, X_{lD} and X_{lA}

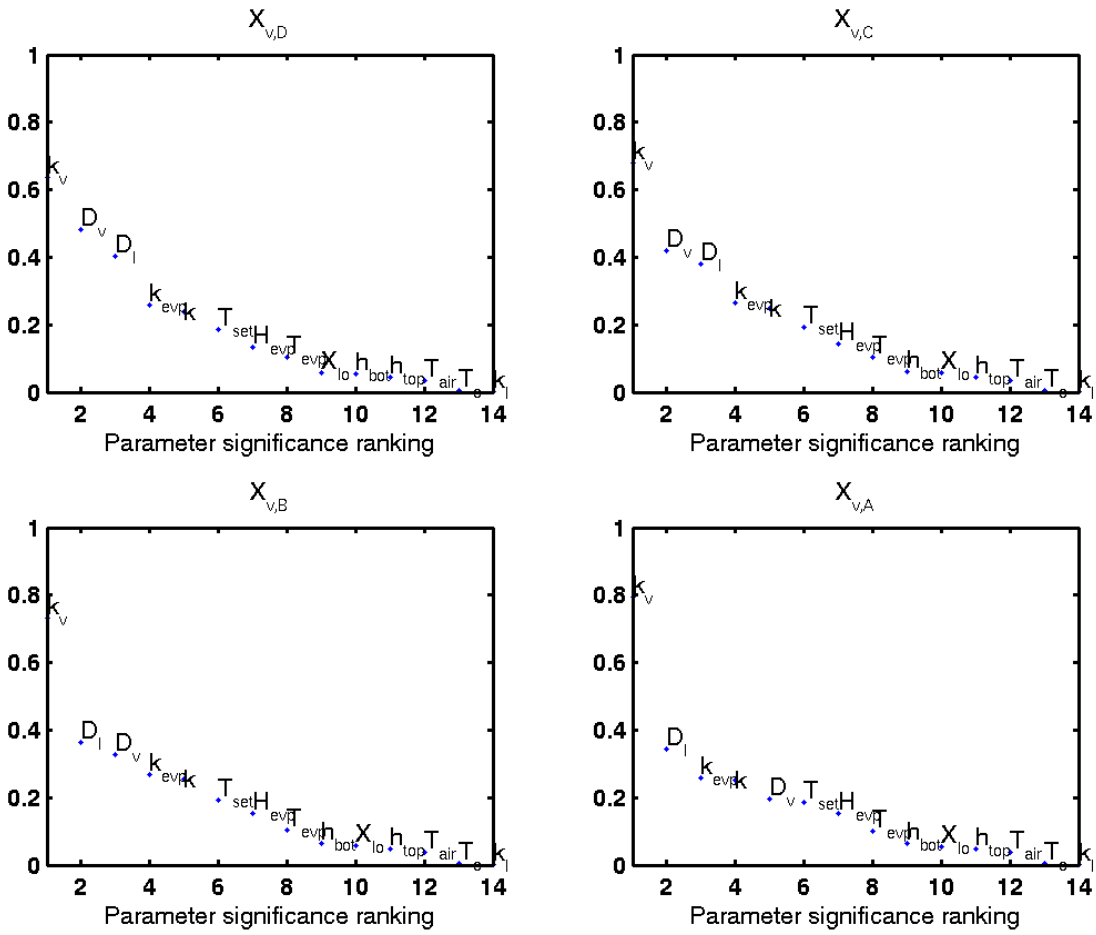

Figure 8-5 Relative impact of parameter on prediction for Xv_D, Xv_C, Xv_D and Xv_A

In similarly way, an uncertainty and sensitivity analysis was applied for the roasting of meat in the convection oven and the obtained results are attached in the Appendix A.1.

8.7 Conclusion

The uncertainty analysis and the global sensitivity analysis were applied to the coupled heat and mass transfer model of the contact baking process. The method was implemented in the framework *COMSOL-MATLAB® version 3.5.* The impact of the uncertain input parameters was mapped to the model output. The results demonstrated that the extent of uncertainty of the model predictions varies with time, and varies among the different model output. The global sensitivity analysis results with the SRC method provided a ranking of the parameters, from influential to non-influential. This ranking is different for the different state variables (T, X_l, and X_v). Moreover, there were differences in the rank of input parameters within the same state variable depending on the position in the pancake batter. Overall, some of the parameters (k_l, T_{air}, h_{top}) have no impact on all the state variables. On the other hand, some of the input parameters have a strong impact: k and k_{evp} on the temperature predictions and D_l on the prediction of the liquid water concentration at the bottom layer of the product.

In this chapter, for the coupled heat and mass transfer model during the contact baking process: (1) using the uncertainty analysis we were able to determine, how the temperature and water content trends change as a result of uncertainty in the value of the parameters; and (2) using the sensitivity result, we were also able to identify the relative impact of uncertain parameters on model predictions and their rank according to their impact.

In the temperature prediction, the thermal conductivity parameter k, and the evaporation rate constant k_{evp} are the most important parameters. This implies that, in order to reduce the uncertainty in the temperature prediction, the parameters should be estimated with high precision. On the other hand, the parameters ranking at the bottom of the list in the ranking have no effect, and will not change the predictions, as long as their value is kept within the acceptable range. The method gives a good indication on where to focus for obtaining a better fit. Summarizing, an uncertainty and sensitivity analysis is an essential step to discover potential deficiencies in a model formulation that help to explain and correct the lack of fit. It also provides guidance for model reduction and parameterization.

9 Conclusion and general perspective

9.1 Conclusion

Coupled heat and mass transfer is governing many solid food processes such as baking and frying. During baking and frying, the food undergoes several changes in microstructure and other physical properties of the food matrix. Modelling of heat and mass transfer during baking and frying is a significant scientific challenge, because the heat and water transport inside the food is coupled in a complex way, which for some food systems such as roasting of meat, it is not fully understood. A quantitative description of the heat and mass transfer during the solid food processing, in the form of mathematical equations, implementation of the solution techniques, and the value of the input parameters involves uncertainty. Setting up the equations of the model, defining the model assumptions, analyzing the model and its simulation output and, finally, comparing this simulation output with experimental data usually result in a much deeper understanding of the process and the main phenomena determining its output dynamics. Motivated by these facts, robust modelling approach with four main stages was proposed and an attempt was made to develop mechanistic mathematical models of heat and mass transfer during baking and roasting processes.

In this work, mechanistic mathematical models of coupled heat and mass transfer during processing of solid foods were developed on the basis of the robust modelling approach proposed. The mechanistic models of coupled heat and mass transfer were developed for two representative cases: a contact baking process and roasting of meat in convection oven. In both cases, the governing model equations of heat and mass transfer are based on the conservation of heat and mass. The parameters and mechanisms of heat and mass transfer were identified on the basis of theory and experiments. For example in the case of roasting of meat in the convection oven, the mechanism of the water transport was tested by measuring the local water content. A large increase in the water content was not observed in the centre of the meat as it was predicted by other studies elsewhere (Van der Sman, 2007). Nevertheless, the pressure driven transport induced by the meat shrinkage is the main mechanism for water transport. The permeability, the

water holding capacity and elastic modulus – their changes during roasting have an important role for water transport mechanisms.

Physical-based models of heat and mass transfer (3D without and 2D with moving boundary) were developed for roasting of meat in a convection oven. The developed model incorporates the effect of the shrinkage, water holding capacity and evaporation during the meat roasting. The models were implemented and solved in COMSOL Multiphyics® version 3.5. The temperature and water content distributions as function of position and time were predicted. Using the FEM simulations of the model provided better insight into the process and process mechanisms. Such a model can be helpful in understanding the physics of meat roasting, and can be used to improve the prediction of temperature and moisture loss.

In a similar way, in the case of the contact baking process, heat transfer with multiphase water transport (liquid and vapour) and local evaporation were modelled. The unknown parameters in the model were obtained by the parameter estimation method. The solution method and its algorithms were implemented in the COMSOL-Matlab® software. The developed model gives a good understanding of the contact baking process, by predicting the temperature and water content profiles within the product. The model was validated with the experimental data and a reasonable agreement between the measured and the predicted temperature profiles was obtained. The developed model of heat and mass transfer is suitable for describing the contact baking process (except for close to bottom surface). The experiments also showed that the temperature set point has a significant effect on the product, and more specifically on the obtained temperature profiles and the mass loss.

The novelty of the current approach is its capability to incorporate the parameter uncertainty. The uncertainty analysis and global sensitivity analysis were applied to the coupled heat and mass transfer model of solid food processes – it was illustrated using the model of the contact baking process. The impact of uncertain input parameters was mapped to the model output using the Monte Carlo method. The methods and the model equations were implemented in the COMSOL-MATLAB® *version 3.5.* Using the uncertainty analysis we were able to determine, how the model prediction (e.g., temperature and water content trends) changes as a result of

uncertainty in the value of the parameters; and using the sensitivity result, we were also able to identify the relative impact of uncertain parameters on model predictions and their rank according to their impact.

From the uncertainty analysis, the extent of uncertainty of the model predictions varies with time, and varies among the different model output (see chapter 8). The global sensitivity analysis results with the SRC method provided a ranking of the parameters, from influential to non-influential. For example, for the contact baking of pancake batter, the ranking is different for the different state variables (T, X_l, and X_v), further, the ranking to some extent depends on the position in the pancake batter. There are some differences in the ranking of parameters within the same state variable at different positions. Some of the parameters for example k_l, T_{air}, h_{top} have no impact on all the state variables. On the other hand, some of the input parameters have a strong impact: k and k_{evp} on the temperature predictions and D_l on the prediction of the liquid water concentration at the bottom layer of the product. The parameters ranking at the bottom of the list in the ranking have no effect, and will not change the predictions, as long as their value is kept within the acceptable range. The method gives a good indication on where to focus for obtaining a better fit and to further refine the model. It also provides guidance for model reformulation and reduction.

Generally, the developed mathematical models of heat and mass transfer provide better insights about the processes. The proposed robust modelling approach was found to be a useful tool in the model building that help to cope up with different challenges in modelling of heat and mass transfer during processing of solid foods. Therefore, the established modelling approach can be used as reference for modelling other solid food systems.

9.2 Perspective

There is a great benefit of numerical simulations in the food industry: for better understanding the process mechanisms, to ensure food quality and safety, for designing, optimizing, and controlling the food process more precisely. The developed mathematical model provides a better insight into the process. The developed process model can be integrated with other quality and safety models.

The developed model of heat and mass transfer is a useful tool in developing an improved process, where it can be used in the optimization of the process (roasting process or contact baking process) by performing 'in silico' experiments, for example to study the effect of different process parameters. Moreover, the developed process model can in principle be integrated with other quality attribute models as well, in order to perform further optimization of the concerned processes. For example, browning reactions take place in the product during baking, where temperature and water content are two important factors responsible for the change of colour (Zanoni et al., 1995) due to such browning reactions. To study such phenomena the kinetics of the browning reactions can easily be integrated with the heat and mass transfer model presented here.

The obtained results, for example the ranking of the parameters, can be used in different ways. First of all, parameters that do not seem to have any influence on any of the model output might point towards parts of the model that could be omitted or at least reduced in complexity. The influential parameters, on the contrary, are helpful in further model refining, and point towards those parameters that must be measured more precisely or estimated from experimental data in order to better capture the fundamental behavior of the heat and mass transfer during the baking process. Thus, the global sensitivity analysis plays a key role in mapping the impact of input parameters on the model predictions in a systematic way. Note also that in order to reduce the amount of uncertainty in the model predictions, the parameters on the top list in the ranking should be estimated or measured with a higher precision compared to parameters on the bottom of the list. This is one of great advantages both in cost and time – for example if one wants to do only a selected experiment set-up i.e., for only few among several input parameters.

There is a general interest in the food industry to know, how the variations or change in the input parameters affect the final product quality. In that case, the result of an uncertainty and global sensitivity analysis plays an important role for the food industry's efforts to maintain the product quality consistent. The developed method can also easily be adapted to other food processes that involve: (1) many input parameters with uncertain values and (2) the variability of the input parameters (e.g. the variability in the product properties).

The relationship between the microstructure changes of a food product and the heat and mass transfer process needs further research, because if more quantitative relationships of the microstructure and heat and mass transfer are available, more understanding will be obtained. The change of microstructure such as pore formation influences for example the permeability and diffusion coefficient of food materials. There are quite limited data on the porosity of the concerned solid foods (meat, baked product) – particularly, its time and spatial variation during the processing is unavailable. Microscopic images of the product can be taken, and using the image analysis techniques the detailed information i.e., about the porosity and its distribution within the product can be obtained. This information can be used to obtain the permeability of the food material (meat). In the years ahead, more efforts will be needed to relate this structural and other changes during processing, which would help us to better predict the changing heat and mass transfer and make modelling more realistic. Further, the models established here serves as a reference against which simpler, more practical-oriented models can also be tested. Therefore, this will be future work.

References

Adeler-Nissen J. (2002). The Continuous Wok: A New Unit Operation in Industrial Food Processes. *Journal of Food Process Engineering*, 25(5), 435-453.

Adler-Nissen J. (2007). Continuous Wok-frying of Vegetables: Process Parameters Influencing Scale up and Product Quality. *Journal of Food Engineering*, 83(1), 54-60.

Aguilera J.M. (2005). Why Food Microstructure? *Journal of Food Engineering*, 67(1-2), 3-11.

Anahid M., Khoei A.R. (2010). Modeling of Moving Boundaries in Large Plasticity Deformations via an Enriched Arbitrary Lagrangian-Eulerian FE Method. *Scientia Iranica Transaction A-Civil Engineering*, 17(2), 141-160.

Anderson B.A., Singh R.P. (2006). Effective Heat Transfer Coefficient Measurement during Air Impingement Thawing using an Inverse Method. *International Journal of Refrigeration*, 29(2), 281-293.

Ahrne L., Andersson C., Floberg P., Rosen J., & Lingnert H. (2007). Effect of Crust Temperature and Water Content on Acrylamide Formation during Baking of White Bread: Steam and Falling Temperature Baking. *LWT - Food Science and Technology*, 40(10), 1708-1715.

Arvidsson M., Gremyr I. (2008). Principles of Robust Design Methodology. *Quality and Reliability Engineering International*, 24(1), 23-35.

Ashokkumar, S., and Adler-Nissen., (2011) Evaluating the Non-Stick Properties of Different Surface Materials for Contact Frying. *Journal of Food Engineering* (re-submitted version under review)

Baik O.D., Marcotte M., Sablani S.S., & Castaigne F. (2001). Thermal and Physical Properties of Bakery Products. *Critical reviews in food science and nutrition*, 41(5), 321-352.

Barriere B., Leibler L. (2003). Kinetics of Solvent Absorption and Permeation Through a Highly Swellable Slastomeric Network. *Journal of Polymer Science Part B-Polymer Physics*, 41(2), 166-182.

Bendall J.R., Restall D.J. (1983). The Cooking of Single Myofibres, Small Myofibre Bundles and Muscle Strips from beef M. psoas and M. sternomandibularis Muscles at Varying Heating rates and Temperatures. *Meat Science*, 8(2), 93-117.

Bengtsson N.E., Jakobsson B., & Dagerskog M. (1976). Cooking of Beef by Oven Roasting - Study of Heat and Mass-Transfer. *Journal of Food Science*, 41(5), 1047-1053.

Benson D.J. (1992). Computational methods in Lagrangian and Eulerian hydrocodes. *Computer Methods in Applied Mechanics and Engineering*, 99(2-3), 235-394.

Bird R.B., Sterwart W.E., & Lightfoot E.N. (Eds.) (2001). *Transport phenomena.* (2nd edn.). John Wiley and Sons,Inc, New York.

Brodkey R.S., Hershey H.C. (1988). *Transport phenomena ; a unified approach.* (). McGraw-Hill, New York.

References

Cacuci D.G., Ionescu-Bujor M., & Corporation E. (2005). *Sensitivity and Uncertainty Analysis*. CRC Press, London.

Campolongo F., Saltelli A. (1997). Sensitivity Analysis of an Environmental Model an Application of Different Analysis Methods. *Reliability Engineering & System Safety*, 57(1), 49-69.

Cariboni J., Gatelli D., Liska R., & Saltelli A. (2007). The Role of Sensitivity Analysis in Ecological Modelling. *Ecological Modelling*, 203(1-2), 167-182.

Carvalho M.G., Martins N. (1992). Mathematical Modelling of Heat and Mass Transfer in a Forced Convection Baking oven. *AICHE Symposium Series*, 88(288), 205-211.

Cengel Y.A. (2007). *Heat and mass transfer ; A practical approach.* McGraw-Hill Education, London.

Chang H.C., Carpenter J.A., & Toledo R.T. (1998). Modeling Heat Transfer during Oven Roasting of Unstuffed turkeys. *Journal of Food Science*, 63(2), 257-261.

Chen H., Marks B.P., & Murphy R.Y. (1999a). Modeling Coupled Heat and Mass Transfer for Convection Cooking of Chicken Patties. *Journal of Food Engineering*, 42(3), 139-146.

Chen H., Marks B.P., & Murphy R.Y. (1999b). Modeling Coupled Heat and Mass Transfer for Convection Cooking of Chicken Patties. *Journal of Food Engineering*, 42(3), 139-146.

Cheng-Jin Du, Da-Wen Sun. (2005). Correlating Shrinkage with Yield, Water Content and Texture of Pork ham by Computer Vision. *Journal of Food Process Engineering*, 28(3), 219-232.

Datta A.K. (2007a). Porous Media Approaches to Studying Simultaneous Heat and Mass Transfer in Food processes. I: Problem Formulations. *Journal of Food Engineering*, 80(1), 80.

Datta A.K. (2007b). Porous Media Approaches to Studying Simultaneous Heat and Mass Transfer in Food Processes. II: Property Data and Representative Results. *Journal of Food Engineering*, 80(1), 96-110.

Datta A.K. (2006). Hydraulic Permeability of Food Tissues. *International Journal of Food Properties*, 9(4), 767-780.

Datta A.K. (2008). Status of Physics-Based Models in the Design of Food Products, Processes, and Equipment. *Comprehensive Reviews in Food Science and Food Safety*, 7(1), 121-129.

Davey L.M., Pham Q.T. (1997). Predicting the Dynamic Product Heat Load and Weight Loss during Beef Chilling using a Multi-region Finite Difference Approach. *International Journal of Refrigeration*, 20(7), 470-482.

Dimov I., Georgieva R. Monte Carlo Algorithms for Evaluating Sobol' Sensitivity Indices. *Mathematics and Computers in Simulation*, In Press, Corrected Proof.

Dincer I. (1996). Modelling for Heat and Mass Transfer Parameters in Deep-frying of Products. *Heat and Mass Transfer*, 32(1-2), 109-113.

Dincer I., Hussain M.M., Sahin A.Z., & Yilbas B.S. (2002). Development of a New Moisture Transfer (Bi–Re) Correlation for Food Drying Applications. *International Journal of Heat and Mass Transfer*, 45(8), 1749-1755.

References

Donea J., Huerta A., Ponthot J., & Rodríguez-Ferran A. (2004). Arbitrary Lagrangian-Eulerian Methods. *Encyclopedia of Computational Mechanics*. John Wiley & Sons, Ltd.
Eichler S., Ramon O., Cohen Y., & Mizrahi S. (2002). Swelling and Contraction Driven Mass transfer Processes during Osmotic Dehydration of Uncharged Hydrogels. *International Journal of Food Science and Technology*, 37(3), 245-253.

Ellwein L.M., Tran H.T., Zapata C., Novak V., & Olufsen M.S. (2008). Sensitivity Analysis and Model Assessment: Mathematical Models for Arterial Blood Flow and Blood Pressure. *Cardiovascular Engineering*, 8(2), 94-108.

Erdogdu F., Balaban M.O., & Chau K.V. (1998). Modeling of Heat Conduction in Elliptical Cross Section: I. Development and Testing of the Model. *Journal of Food Engineering*, 38(2), 223-239.

Erdogdu F., Sarkar A., & Singh R.P. (2005). Mathematical modeling of Air-impingement Cooling of Finite Slab Shaped Objects and Effect of Spatial Variation of Heat Transfer Coefficient. *Journal of Food Engineering*, 71(3), 287-294.

Erdoğdu F., Turhan M. (2006). Analysis of Dimensional Ratios of Regular Geometries for Infinite Geometry Assumptions in Conduction Heat Transfer Problems. *Journal of Food Engineering*, 77(4), 818-824.

Farid M.M., Chen X.D. (1998). The Analysis of Heat and Mass Transfer during Frying of Food using a Moving Boundary Solution Procedure. *Heat and Mass Transfer*, 34(1), 69-77.

Farkas B.E., Singh R.P., & Rumsey T.R. (1996). Modeling Heat and Mass Transfer in Immersion Frying. I, Model Development. *Journal of Food Engineering*, 29(2), 211-226.

Fasina O.O., Fleming H.P. (2001). Heat Transfer Characteristics of Cucumbers during Blanching. *Journal of Food Engineering*, 47(3), 203-210.

Floury J., Le Bail A., & Pham Q.T. (2008). A Three-dimensional Numerical Simulation of the Osmotic Dehydration of Mango and Effect of Freezing on the Mass Transfer Rates. *Journal of Food Engineering*, 85(1), 1-11.

Fowler A.J., Bejan A. (1991). The Effect of Shrinkage on the Cooking of Meat. *International Journal of Heat and Fluid Flow*, 12(4), 375-383.

Frey H.C., Patil S.R. (2002). Identification and Review of Sensitivity Analysis Methods. *Risk Analysis*, 22(3), 553-578.

Gebhart B. (1993). *Heat conduction and mass diffusion.* McGraw-Hill, New York,N.Y.

Ghazala S., Ramaswamy H.S., Smith J.P., & Simpson M.V. (1995). Thermal Process Simulations for Sous vide Processing of Fish and Meat Foods. *Food Research International*, 28(2), 117-122.

Godsalve E.W., Davis E.A., Gordon J., & Davis H.T. (1977). Water Loss Rates and Temperature Profiles of Dry Cooked Bovine Muscle. *Journal of Food Science*, 42(4), 1038-1045.

Gupta T.R. (2001). Individual Heat Transfer Modes during Contact Baking of Indian Unleavened Flat Bread (chapati) in a Continuous Oven. *Journal of Food Engineering*, 47(4), 313-319.

References

Halder A., Dhall A., & Datta A.K. (2007a). An Improved, Easily Implementable, Porous Media Based Model for Deep-Fat Frying: Part I: Model Development and Input Parameters. *Food and Bioproducts Processing*, 85(3), 209-219.

Halder A., Dhall A., & Datta A.K. (2007b). An Improved, Easily Implementable, Porous Media Based Model for Deep-Fat Frying: Part II: Results, Validation and Sensitivity Analysis. *Food and Bioproducts Processing*, 85(3), 220-230.

Halder A., Dhall A., & Datta A.K. (2011). Modeling Transport in Porous Media With Phase Change: Applications to Food Processing. *Journal of Heat Transfer-Transactions of the Asme*, 133(3), 031010.

Hangos K.M., Cameron I.T. (2001). *Process Modelling and Model Analysis.* (, pp. 1-543). Academic Press.

Helton J.C., Davis F.J. (2003). Latin Hypercube Sampling and the Propagation of Uncertainty in Analyses of Complex Systems. *Reliability Engineering & System Safety*, 81(1), 23-69.

Hirt C.W., Amsden A.A., & Cook J.L. (1974). An arbitrary Lagrangian-Eulerian Computing Method for all Flow Speeds. *Journal of Computational Physics*, 14(3), 227-253.

Hirt C.W., Amsden A.A., & Cook J.L. (1997). An Arbitrary Lagrangian–Eulerian Computing Method for All Flow Speeds, *Journal of Computational Physics*, 135(2), 203-216.

Hossain M.M., Cleland D.J., & Cleland A.C. (1992). Prediction of Freezing and Thawing Times for Foods of Regular Multi-dimensional Shape by using an Analytically Derived Geometric Factor. *International Journal of Refrigeration*, 15(4), 227-234.

Hostetler R.L., Landmann W.A. (1968). Photomicrographic Studies of Dynamic Changes in Muscle Fiber Fragments. 1. Effect of Various Heat Treatments on Length, Width and Birefringence. *Journal of Food Science*, 33(5), 468-470.

Huang E., Mittal G.S. (1995). Meatball Cooking - Modeling and Simulation. *Journal of Food Engineering*, 24(1), 87-100.

Huang H., Lin P., & Zhou W. (2007). Moisture Transport and Diffusive Instability During Bread Baking. *SIAM Journal on Applied Mathematics*, 68(1), 222-238.

Huff-Lonergan E., Lonergan S.M. (2005). Mechanisms of Water-holding Capacity of Meat: The Role of Postmortem Biochemical and Structural Changes. *Meat Science*, 71(1), 194-204.

Ikediala J.N., Correia L.R., Fenton G.A., & Ben-Abdallah N. (1996). Finite element Modeling of Heat Transfer in Meat Matties during Single-sided Pan-frying. *Journal of Food Science*, 61(4), 796-802.

Ilhan D., Ashwini K. (2006). Fluid Flow and Its Modeling Using Computational Fluid Dynamics. In Anonymous *Handbook of Food and Bioprocess Modeling Techniques.* (, pp. 41-83). CRC Press.

Incropera F.P., De Witt D.P. (Eds.) (1985). *Fundamentals of Heat and Mass Transfer*. John Wiley and Sons Inc., New York.

Jefferson D.R., Lacey A.A., & Sadd P.A. (2006). Understanding Crust Formation during Baking. *Journal of Food Engineering*, 75(4), 515-521.

References

Jefferson D.R., Lacey A.A., & Sadd P.A. (2007). Crust Density in Bread Baking: Mathematical Modelling and Numerical Solutions. *Applied Mathematical Modelling*, 31(2), 209-225.

Jensen B.B.B., Lennox M., Granby K., & Adler-Nissen J. (2008). Robust Modelling of Heat-induced Reactions in an Industrial Food Production Process Exemplified by Acrylamide Generation in Breakfast Cereals. *Food and Bioproducts Processing*, 86(3), 154-162.

Kaasschieter E.F., Frijns A.J.H. (2003). Squeezing a Sponge: A Three-dimensional Solution in Poroelasticity. *Computational Geosciences*, 7(1), 49-59.

Kassama L.S., Ngadi M.O. (2005). Pore Structure Characterization of Deep-fat-fried Chicken Meat. *Journal of Food Engineering*, 66(3), 369-375.

Katekawa M.E., Silva M.A. (2006). A Review of Drying Models Including Shrinkage Effects. *Drying Technology*, 24(1), 5-20.

Khoei A.R., Anahid M., & Shahim K. (2008). An Extended Arbitrary Lagrangian–Eulerian Finite Element Method for Large Deformation of Solid Mechanics. *Finite Elements in Analysis and Design*, 44(6-7), 401-416.

Kołczak T., Krzysztoforski K., & Palka K. (2007). The Effect of Post-mortem Ageing and Heating on Water Retention in Bovine Muscles. *Meat Science*, 75(4), 655-660.

Kondjoyan A., Rouaud O., McCann M.S., Havet M., Foster A., Swain M., & Daudin J.D. (2006). Modelling coupled Heat–water Transfers during a Decontamination Treatment of the Surface of Solid Food Products by a Jet of Hot Air. I. Sensitivity Analysis of the Model and First validations of Product Surface Temperature under Constant air Temperature Conditions. *Journal of Food Engineering*, 76(1), 53-62.

Kovacsne Oroszvari B., Bayod E., Sjöholm I., & Tornberg E. (2006). The Mechanisms Controlling Heat and Mass Transfer on Frying of Beefburgers. III. Mass transfer evolution during frying. *Journal of Food Engineering*, 76(2), 169-178.

Kovácsné Oroszvári B., Sofia Rocha C., Sjöholm I., & Tornberg E. (2006). Permeability and Mass transfer as a Function of the Cooking Temperature during the Frying of Beefburgers. *Journal of Food Engineering*, 74(1), 1-12.

Lee K.H., &Taylor T.A. (1996). Modeling of Bread Baking with Simultaneous Heat and Mass Transfer and Structural Changes. *United States of America, Institute of Food Technologists [1996 Annual Meeting]*, 20.

Martienssen W., Warlimont H. (2005). *Springer Handbook of Condensed Matter and Materials data.* (, pp. 1-1119). Springer, Heidelberg.

Maroulis Z.B., Krokida M.K., & Rahman M.S. (2002). A Structural Generic Model to Predict the Effective Thermal Conductivity of Fruits and Vegetables during Drying. *Journal of Food Engineering*, 52(1), 47-52.

Martins R.C., Lopes V., Vicente A.A., & Teixeira J.A. (2008). Numerical Solutions. *Optimization in Food Engineering.*CRC Press.

McDonald K., Sun D. (2001b). The Formation of Pores and Their Effects in a Cooked Beef Product on the Efficiency of Vacuum Cooling. *Journal of Food Engineering*, 47(3), 175-183.

Mendoza F., Aguilera J.M. (2004). Application of Image Analysis for Classification of Ripening Bananas. *Journal of Food Science*, 69(9), E471-E477.

Mizrahi S., Eichler S., & Ramon O. (2001). Osmotic Dehydration Phenomena in Gel Systems. *Journal of Food Engineering*, 49(2-3), 87-96.

Moens D., Vandepitte D. (2005). A survey of Non-probabilistic Uncertainty Treatment in Finite Element Analysis. *Computer Methods in Applied Mechanics and Engineering*, 194(12-16), 1527-1555.

Mohamed I.O. (2010). Development of a Simple and Robust Inverse Method for Determination of Thermal Diffusivity of Solid Foods. *Journal of Food Engineering*, 101(1), 1-7.

Mondal A., Datta A.K. (2008). Bread baking – A review. *Journal of Food Engineering*, 86(4), 465-474.

Ngadi M.O., Watts K.C., & Correia L.R. (1997a). Finite Element Method Modelling of Moisture Transfer in Chicken Drum during Deep-fat Frying. *Journal of Food Engineering*, 32(1), 11-20.

Ngadi M.O., Watts K.C., & Correia L.R. (1997b). Finite Element Method Modelling of Moisture Transfer in Chicken Drum during Deep-fat Frying. *Journal of Food Engineering*, 32(1), 11-20.

Ni H., Datta A.K. (1999). Moisture, Oil and Energy Transport During Deep-Fat Frying of Food Materials. *Food and Bioproducts Processing*, 77(3), 194-204.

Nicolai B.M., DeBaerdemaeker J. (1996). Sensitivity Analysis with Respect to the Surface Heat Transfer Coefficient as Applied to Thermal Process Calculations. *Journal of Food Engineering*, 28(1), 21-33.

Nitin N., Karwe M.V. (2001). Heat Transfer Coefficient for Cookie Shaped Objects in a Hot Air Jet Impingement Oven. *Journal of Food Process Engineering*, 24(1), 51-69.

Offer G., Cousins T. (1992). The Mechanism of Drip Production: Formation of Two Compartments of Extracellular Space in Muscle Post Mortem. *Journal of the science of food and agriculture*, 58(1), 107-116.

Omlin M., Reichert P. (1999). A Comparison of Techniques for the Estimation of Model Prediction uncertainty. *Ecological Modelling*, 115(1), 45-59.

Ou D., Mittal G.S. (2006). Double-sided Pan-frying of Unfrozen/Frozen Hamburgers for Microbial Safety using Modelling and Simulation. *Food Research International*, 39(2), 133-144.

Pan Z., Singh R.P., & Rumsey T.R. (2000). Predictive Modeling of Contact-heating Process for Cooking a Hamburger Patty. *Journal of Food Engineering*, 46(1), 9-19.

Pan Z., Singh R.P. (2002). Heating Surface Temperature and Contact-Heat Transfer Coefficient of A Clam-Shell Grill. *Lebensmittel-Wissenschaft und-Technologie*, 35(4), 348-354.

Peters B., Schroder E., Bruch C., & Nussbaumer T. (2002). Measurements and Particle Resolved Modelling of Heat-up and Drying of a Packed Bed. *Biomass & Bioenergy*, 23(4), 291-306.

References

Puri V.M., Anantheswaran R.C. (1993). The Finite-element Method in Food Processing: A Review. *Journal of Food Engineering*, 19(3), 247-274.

Purlis E. (2010). Browning Development in Bakery Products – A review. *Journal of Food Engineering*, 99(3), 239-249.

Purlis E., Salvadori V.O. (2009). Bread Baking as a Moving Boundary Problem. Part 1: Mathematical Modelling. *Journal of Food Engineering*, 91(3), 428-433.

Rao M.A., Rizvi S.H., & Datta A.K. (Eds.) (2005). *Engineering Properties of Foods.* (Third Edition edn., pp. 738). Talyor and Francis.

Rask C. (1989). Thermal Properties of Dough and Bakery Products: A Review of Published Data. *Journal of Food Engineering*, 9(3), 167-193.

Ratto M., Young P.C., Romanowicz R., Pappenberger F., Saltelli A., & Pagano A. (2007). Uncertainty, Sensitivity Analysis and the Role of Data Based Mechanistic Modeling in Hydrology. *Hydrology and Earth System Sciences*, 11(4), 1249-1266.

Ressing H., Ressing M., & Durance T. (2007). Modeling the Mechanisms of Dough Puffing during Vacuum Microwave Drying using the Finite Element Method. *Journal of Food Engineering*, 82(4), 498-508.

Saisana M., Saltelli A., & Tarantola S. (2005). Uncertainty and Sensitivity Analysis Techniques as Tools for the Quality Assessment of Composite Indicators. *Journal of the Royal Statistical Society Series A-Statistics in Society*, 168, 307-323.

Sakin M., Kaymak-Ertekin F., & Ilicali C. (2007). Simultaneous Heat and Mass Transfer Simulation Applied to Convective Oven Cup Cake Baking. *Journal of Food Engineering*, 83(3), 463-474.

Sakin M., Kaymak-Ertekin F., & Ilicali C. (2009). Convection and Radiation Combined Surface Heat Transfer Coefficient in Baking Ovens. *Journal of Food Engineering*, 94(3-4), 344-349.

Saltelli A., Ratto M., Tarantola S., & Campolongo F. (2005). Sensitivity Analysis for Chemical Models. *Chemical reviews*, 105(7), 2811-2827.

Saltelli A., Scott M. (1997). The Role of Sensitivity Analysis in the Corroboration of Models and its Link to Model Structural and Parametric Uncertainty. *Reliability Engineering & System Safety*, 57(1), 1-4.

Saltelli A., Tarantola S., & Campolongo F. (2000). Sensitivity Analysis as an Ingredient of Modeling. *Statistical Science*, 15(4), 377-395.

Saltelli A., Ratto M., Andres T., Campolongo F., Cariboni J., Gatelli D., Saisana M., & Tarantola S. (2008). *Global Sensitivity Analysis: The primer.* (pp. 292). John Wiley & Sons, Ltd, West Sussex, England.

Sandeep K., Soojin J., & Joseph I. (2008). Introduction to Modeling and Numerical Simulation. *Food Processing Operations Modeling.* (, pp. 1-11). CRC Press.

Schmalko M.E., Morawicki R.O., & Ramallo L.A. (1997). Simultaneous Determination of Specific Heat Capacity and Thermal Conductivity using the Finite-difference Method. *Journal of Food Engineering*, 31(4), 531-540.

References

Shilton N., Mallikarjunan P., & Sheridan P. (2002). Modeling of Heat Transfer and Evaporative Mass Losses during the Cooking of Beef Patties using Far-infrared Radiation. *Journal of Food Engineering*, 55(3), 217-222.

Sin G., Gernaey K.V., & Lantz A.E. (2009). Good Modeling Practice for PAT Applications: Propagation of Input Uncertainty and Sensitivity Analysis. *Biotechnology progress*, 25(4), 1043-1053.

Singh N., Akins R.G., & Erickson L.E. (1984). Modelling Heat and Mass Transfer during the Oven Roasting of Meat. *Journal of Food Process Engineering*, 7(3), 205-220.

Skjöldebrand C., Hallstroem B. (1980). Convection Oven Frying. Heat and Mass Transport in the Product. *Journal of Food Science*, 45(5), 1347-1353.

Srikiatden J., Roberts J.S. (2007). Moisture Transfer in Solid Food Materials: A Review of Mechanisms, Models, and Measurements. *International Journal of Food Properties*, 10(4), 739-777.

Sumnu S.G., Sahin S. (2008). Food Engineering Aspects of Baking Sweet Goods. .

Taciroglu E., Acharya A., Namazifard A., & Parsons I.D. (2009). Arbitrary Lagrangian–Eulerian Methods for Analysis of Regressing Solid Domains and Interface Tracking. *Computers & Structures*, 87(5-6), 355-367.

Talla A., Puiggali J., Jomaa W., & Jannot Y. (2004). Shrinkage and Density Evolution during Drying of Tropical Fruits: Application to banana. *Journal of Food Engineering*, 64(1), 103-109.

Therdthai N., Zhou W. (2003). Recent Advances in the Studies of Bread Baking Process and their Impacts on the Bread Baking Technology. *Food Science and Technology Research*(3), 219-2269.

Thorvaldsson K., Janestad H. (1999a). A Model for Simultaneous Heat, Water and Vapour Diffusion. *Journal of Food Engineering*, 40(3), 167-172.

Thorvaldsson K., Janestad H. (1999b). A Model for Simultaneous Heat, Water and Vapour Diffusion. *Journal of Food Engineering*, 40(3), 167-172.

Thorvaldsson K., Skjöldebrand C. (1996). Water Transport in Meat during Reheating. *Journal of Food Engineering*, 29(1), 13-21.

Tijskens E., De Baerdemaeker J. (2004). Mathematical Modelling of Syneresis of Cheese Curd. *Mathematics and Computers in Simulation*, 65(1-2), 165-175.

Tornberg E. (2005). Effects of Heat on Meat Proteins – Implications on Structure and Quality of Meat Products. *Meat Science*, 70(3), 493-508.

Trujillo F.J., Wiangkaew C., & Pham Q.T. (2007). Drying Modeling and Water Diffusivity in Beef Meat. *Journal of Food Engineering*, 78(1), 74-85.

Van der Sman R.G.M. (2007). Soft Condensed Matter Perspective on Moisture Transport in Cooking Meat. *AICHE Journal*, 53(11), 2986-2995.

Wang L., Singh R.P. (2004). Finite Element Modeling and Sensitivity Analysis of Double-sided Contact-Heating of Initially Frozen Hamburger Patty. *Transactions of the ASAE*, 47(1), 147-157.

References

Wang L., Sun D. (2002). Modelling Three Conventional Cooling Processes of Cooked Meat by Finite Element Method. *International Journal of Refrigeration*, 25(1), 100-110.

Wang L., Sun D. (2003). Recent Developments in Numerical Modelling of Heating and Cooling Processes in the Food industry—a Review. *Trends in Food Science & Technology*, 14(10), 408-423.

Wichchukit S., Zorrilla S.E., & Singh R.P. (2001). Contact Heat Transfer Coefficient during Double-sided Cooking of Hamburger Patties. *Journal of Food Processing and Preservation*, 25(3), 207-221.

Wong S.Y., Zhou W., & Hua J. (2006). Robustness Analysis of a CFD Model to the Uncertainties in its Physical Properties for a Bread Baking Process. *Journal of Food Engineering*, 77(4), 784-791.

Wu S., Li H., Chen J.P., & Lam K.Y. (2004). Modeling Investigation of Hydrogel Volume Transition. *Macromolecular Theory and Simulations*, 13(1), 13.

Wählby U., Skjöldebrand C. (2001). NIR-measurements of Moisture Changes in Foods. *Journal of Food Engineering*, 47(4), 303-312.

Yamsaengsung R., Moreira R.G. (2002). Modeling the Transport Phenomena and Structural Changes during Deep Fat Frying: Part I: Model Development. *Journal of Food Engineering*, 53(1), 1-10.

Yang H., Sakai N., & Watanabe M. (2001). Drying Model with Non-isotropic Shrinkage Deformation Undergoing Simultaneous Heat and Mass Transfer. *Drying Technology*, 19(7), 1441-1460.

Zanoni B., Peri C., & Bruno D. (1995a). Modelling of Browning Kinetics of Bread Crust during Baking. *Lebensmittel-Wissenschaft und -Technologie*, 28(6), 604-609.

Zanoni B., Peri C., & Gianotti R. (1995b). Determination of the Thermal Diffusivity of Bread as a Function of Porosity. *Journal of Food Engineering*, 26(4), 497-510.

Zhang J., Datta A.K. (2006). Mathematical Modeling of Bread Baking Process. *Journal of Food Engineering*, 75(1), 78-89.

Appendix

Appendix A

A.1 Illustration of uncertainty and sensitivity results of model heat and mass transfer during the meat roasting in convection oven

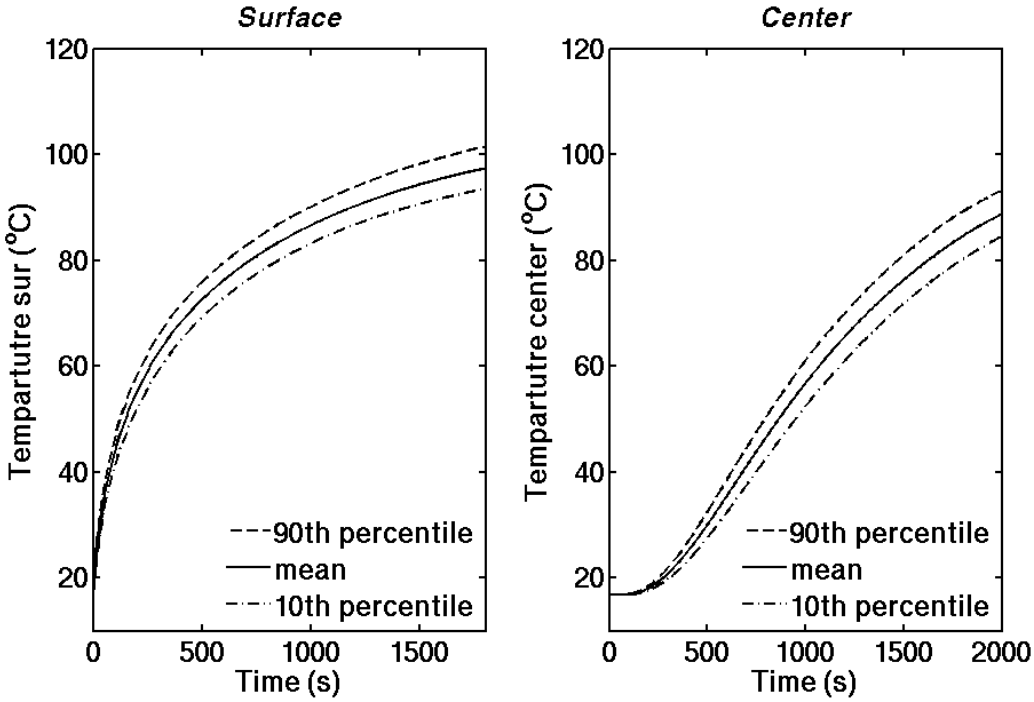

Figure A.1 Uncertainty of the temperature predictions (due to input parameters uncertainty) for surface and centre, respectively

Table A.1 Sensitivity analysis: parameter ranking for temperature at centre, T_{cen} and temperature at centre, at T_{sur} at t = 1500 s during the

T_{cen}		T_{sur}	
parameter	*SRC*	*parameter*	*SRC*
k_m	**0.728**	**a**	**-0.847**
a	**-0.458**	**h_t**	**0.392**
h_t	**0.423**	**T_{evp}**	**0.289**
T_{evp}	0.158	T_{oven}	0.118
T_{oven}	0.111	k_m	0.126
C_o	-0.061	C_o	-0.028
g	-0.071	g	-0.022
D	-0.015	D	-0.008
R^2	*0.97*	R	*0.98*

For better prediction of output variables (e.g. T_{cen}), those parameters ranked highest – i.e. most influential on a specific model output- should be estimated /measured with as high a precision as possible. Ranking depends on the output variable of interest. Ranking is different for centre temperature and temperature near the surface

- The impact of k_m is very large on the T_{cen}
- Larger values of k_m: more heat is transferred to the centre of the product - i.e. the faster centre T rises, and *vice versa*
- h_t and a influence the T_{cen}, both related to energy available at the surface
- When a value increases more energy is used for evap., i.e., less for heating , therefore T_{cen} decreases
- When the value of the h_t is increased more energy is available, i.e. T_{cen} increases with it.

A.2 The image of meat at different time during roasting process

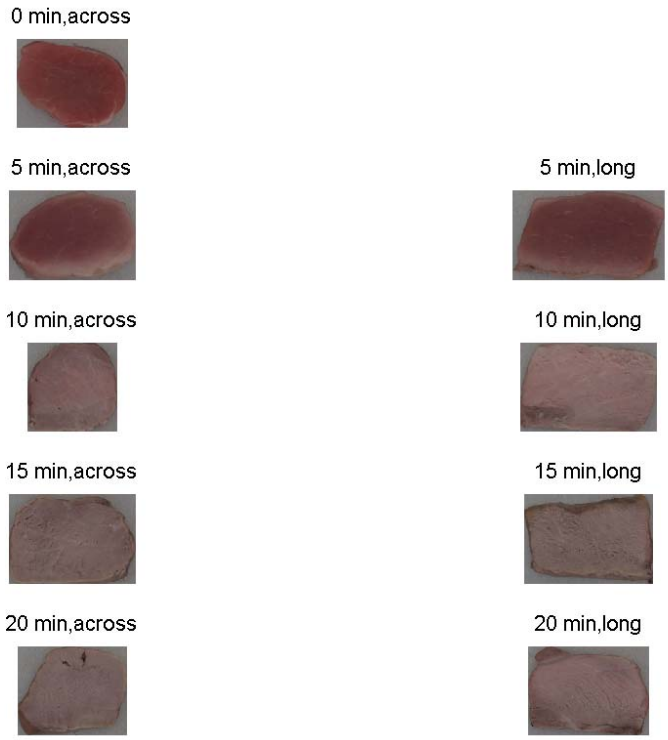

Figure A.2 Image of the meat during the roasting: left column, across = when the meat cut across the fiber direction and long = when the meat cut parallel to the fiber direction

A.3 Illustration of average water content

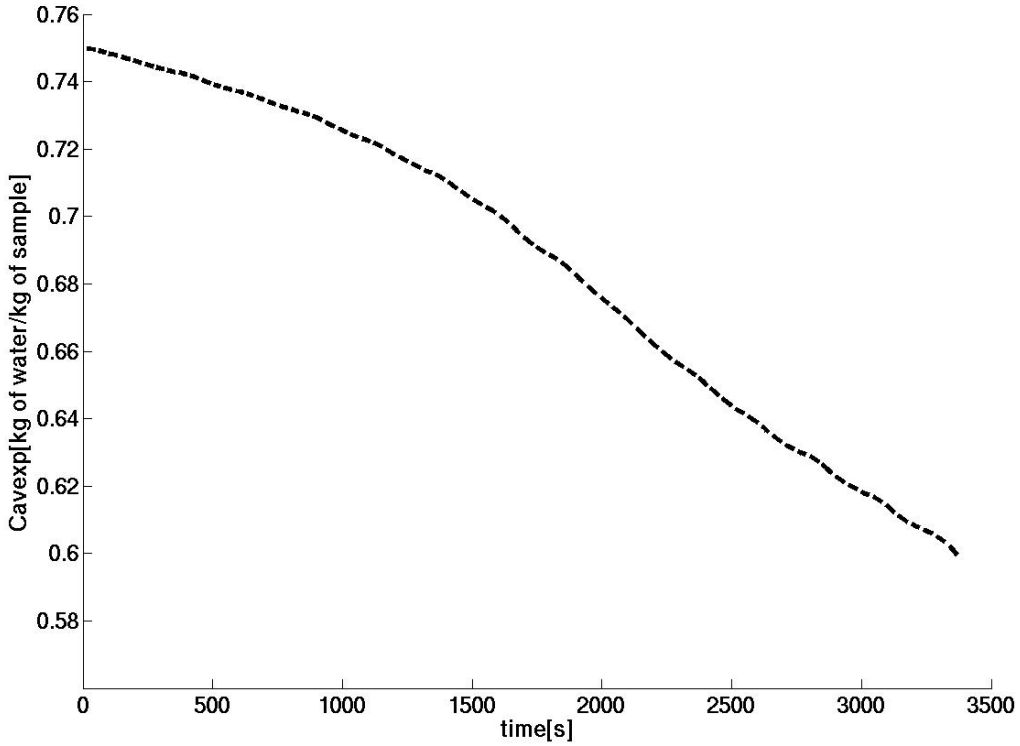

Figure A.3 Illustration of average water content of the meat obtained from mass loss as function of time during the roasting process

Appendix B:

B.1. calculation of mass fraction (from measured mass loss)

m_w = mass water, m_d = mass of solid, y_{wo} = initial mass of water (kg of water/kg of sample)

m_o = initial mass, m = mass at any time, X is the mass fraction (kg of water/ kg of dry solid)

$$\Delta m_w = \Delta m$$

$$m_{wo} - m_w = m_o - m \quad => m_w = m_{wo} - (m_o - m)$$

$$y_{wo} = m_{wo}/m_o$$

Appendix

$$m_w = (y_{wo} - 1)m_o + m$$

$$X = m_{w/md}$$

$$m_d = (1 - y_{wo})mo$$

$$X = \frac{(y_{wo} - 1)m_o + m}{(1 - y_{wo})mo} = \frac{m}{(1 - y_{wo})mo} - 1$$

[Mass fraction (kg of water/ kg of dry solid) as function of time]

$$X(t) = \frac{m(t)}{(1 - y_{wo})mo} - 1$$

Converting from dry basis to wet basis:

$$C = y_w = \frac{X}{X+1}$$

B.2 the simulated average water content profile was computed using the volume integral as:

$$X_{\text{av}}(t) = \frac{\int XdV}{\int dV}$$

For cylnedrical object, with R and L, Xav can be given:

$$X_{\text{av}}(t) = \frac{\int_0^L \int_0^R X(r,z,t).2\pi r.dr.dz}{\int_0^L \int_0^R 2\pi r.dr.dz} = \frac{2}{R^2 L} \int_0^L \int_0^R X(r,z,t).r.dr.dz$$

where X_{av} is the average moisture content (kg of water/kg of solid); $L = z_5$ and R_d are the height (thickness) and the total radius of the dough (m), respectively; z and r represent distance from centre, in the height and radial directions, respectively.

B.3 Updating the composition of each component during the processing:

$$y_p = \frac{y_{po}}{y_{po} + y_{co} + y_{fo}}\left(1 - y_{wo}\right) \tag{B.3.1}$$

$$y_f = \frac{y_{fo}}{y_{po} + y_{co} + y_{fo}}\left(1 - y_{wo}\right) \tag{B.3.2}$$

$$y_c = \frac{y_{co}}{y_{po} + y_{co} + y_{fo}}\left(1 - y_{wo}\right) \tag{B.3.2}$$

$$y = \sum y_i = 1$$

w, pr, c, and f are water, protein, carbohydrate and fat, respectively and subscript o is initial state and without o is the state at certain time during the processing.

B.4. The heat transfer coefficient correlations for natural convection (Cengel, 2007):

$$Nu = \frac{hL_c}{k}$$

$$Ra = GrPr = \frac{g\beta(T_s - T_{air})L_c^3}{v^2}$$

$$\beta = 1/T$$

For upper surface of hot plate ($L_c = A_s/p$):

$$for\ Ra = 10^4 - 10^7 \qquad Nu = 0.54Ra^{1/4}$$

$$for\ Ra = 10^7 - 10^{11} \qquad Nu = 0.54Ra^{1/3}$$

The properties of the air are taken at film temperature.

Paper I

PS4.04 Mechanism of water transport in meat during the roasting process 96.00

Aberham Hailu Feyissa (1) abhfe@food.dtu.dk, J Adler-Nissen (1), KV Gernaey (2)
(1)National Food Institute, Food Production Engineering, Technical University of Denmark, Lyngby, Denmark
(2)Department of Chemical and Biochemical Engineering, Technical University of Denmark, Lyngby, Denmark

***Abstract*— Mass and heat transfer play an important role in the roasting of meat. It is essential that the mechanisms are well understood for controlling and optimising the roasting process. This paper focuses on the mechanism of water transport during roasting of meat in a convection oven. A theoretical assessment was made from literature data on change in structure, water holding capacity and shrinkage. A current hypothesis of water transport predicts a rise of the water content at the center; this was tested by measuring the spatial distribution of the local moisture content. For different periods of roasting shrinkage of meat samples was measured in 3 dimensions and mass loss was measured. Several shrinking phenomena could be distinguished, which have different effects on water transport. For low fat meat, the quantity of dissolved solids lost (DSL) with water during roasting was found to be very small and can be neglected.**

A.H. Feyissa and J. Adler-Nissen are with the National Food Institute, Food Production Engineering, Technical University of Denmark, Søltofts Plads, 2800, Kgs. Lyngby, DK (e-mail: abhfe@food.dtu.dk; jadn@food.dtu.dk).

K.V. Gernaey is with the Department of Chemical and Biochemical Engineering, Technical University of Denmark, Building 229, 2800, Kgs. Lyngby, DK (e-mail: kvg@kt.dtu.dk).

Corresponding author: abhfe@food.dtu.dk Tel.+4545252636

Key words: Mass transfer, Mechanism of water transport, Roasting process, Shrinkage

I. INTRODUCTION

Roasting in a convection oven is a common way of frying whole meat in households, in professional kitchens and in the ready-meal industry. Setting the process parameters to obtain a culinary optimal result of the roasting process is, however, mostly done on an empirical basis, i.e. based on the judgment, experience and skills of the cook or the operator. Roasting is considered an art, and the aphorism of the founder of gastronomy, Brillat-Savarin (1826) still holds true: “A cook may be taught, but a man who can roast, is born with the faculty” "[1]” This situation, which is not confined to oven roasting of meat but is common to many food processes, makes it difficult to scale up the oven roasting process and to predict the result of transferring the process to new equipment or to apply automatic process control. Scaling up would be facilitated if a more quantitative understanding of the meat frying process was available [2].

Modelling studies of meat frying processes have hitherto largely been concerned with contact frying of meat patties or deep-fat frying of (battered) meat products, reflecting the wide-spread industrial interest in these types of products [3-5]. There are some earlier modelling studies of the oven roasting process, which all emphasize the crucial effect on the energy transfer from water evaporating from the meat [6-8]. As shown already in the now classical study by Skjöldebrand and Hallström (1980), the transport of water inside the meat is coupled to the heat transfer in a complex and yet not fully understood way. Most of the existing models are based on Fickian diffusion of the water [5, 9]. However, the shrinking of the meat due to heat denaturation means that water transport inside the meat is also driven by pressure gradients [10-11]. No study has yet, however, considered all significant aspects of the mechanism of water transport, as discussed below. It is the aim of this paper to test different hypotheses of water transport and investigate the mechanisms which govern the transformation of raw meat into a palatable steak by the convective transfer of heat from the circulating hot air in a convection oven.

II. MECHANISM OF WATER TRANSPORT DURING THE ROASTING PROCESS

Several researchers have formulated different hypotheses to model mass transfer during roasting, mostly from the perspective of diffusion [5, 9] while disagreements are often seen with regard to other types of water transport mechanisms [10, 12]. Diffusion based models do not adequately describe the moisture transport phenomena during meat cooking [10, 12], because the effects of water binding capacity and shrinkage phenomena are not considered. These are, however, main driving mechanisms for the exudation of water during the cooking or roasting of meat, as is argued in the following: Roasting of meat causes the

muscle protein to denature, resulting in a decrease in water holding capacity and leading to shrinkage of the protein network. Shrinkage of protein in meat occurs at different temperatures. Shrinkage transverse to the fibre axis occurs mainly at 40–60°C and it widens the gap between the fibres and their surrounding endomysium [13]. Connective tissue network and muscle fibres cooperatively shrink longitudinally at 60–70°C [13]. This shrinkage exerts a pressure on the aqueous solution in the extracellular void, and the liquid will flow because the meat tissue has become porous with the transverse shrinkage. Outside the field of meat science, such physics occur during syneresis of curd [14] and polymer gels [15] and models are based on poroelastic theory. A similar approach was also applied in meat science for first time by Van der Sman to study water transport during meat cooking [16]. Van der Sman, however, predicted a quite large rise in the moisture content at the centre of whole meat, which is in disagreement with the observations of Wahlby and Skjöldebrand [12]. Although Skjöldebrand and Thorvaldsson in their earlier [10] study on pre-cooked meat observed a slight rise in water content at the center of the sample, they did not observe any rise in water content in their later study on the roasting of *raw* whole meat [12]. The reasons for the disagreement between theory and observation are: 1) raw and pre-cooked meat are different in their microstructure and composition and behaviour during heating; 2) misinterpretation of the results of previous work and 3) lack of sufficient data on local water content for verification. Item 1) will be expounded on below.

The dynamic change of the microstructure of meat during the heating process plays a great role in water transport. This is often neglected, however, and this leads to ambiguity in the description and modelling of the water transport, as discussed above. The structure of pre-cooked meat is quite different from that of the raw meat. The pre-cooked meat has relatively large pore spaces from the beginning because of the pre-cooking, which gives the pre-cooked meat a low resistance to water transport. This allows the local water content to rise at the centre if there is a temperature gradient towards the centre. On the contrary, in the case of raw meat, the structure is intact at the start of the cooking process, and water transport is hindered towards the centre, despite the temperature and pressure gradients. During the roasting of the raw meat dramatic changes in the microstructure are induced. Spatial variation in temperature creates spatial difference in permeability and elastic modulus, where parts of the meat sample closer to the surface have larger permeability and elastic modulus than the parts closer to the centre. There is therefore a much larger resistance to water flux towards the centre than towards the surface of the meat piece. Since water moves in the direction of least resistance, the water will preferentially flow towards the surface against the temperature gradient and form exudate. It is therefore predicted that migration of water towards the centre is insignificant, in contrast to what Van der Sman predicted [16]. This prediction needs experimental verification, and this verification is the major purpose of this paper.

III. MATERIALS AND METHODS

A. Sample Preparation

Pork meat (*Longissimus-dorsi*) was bought from the local butchery. It was kept in a plastic bag and stored at 5°C before sample preparation to avoid moisture loss. For all experiments, the fat layer of the meat was removed before the samples were prepared for the required shape (see below, section C).

B. Oven setting

A professional oven, Rational Combi-steamer ccc, with an oven space of 0.83x0.645x0.495 m^3 was used for the roasting process. Dry hot air is circulated inside the oven by a fan, which reverses its direction of rotation every 1-2 min to ensure a more uniform heat transfer from the hot air to the product. The temperature of the hot air is controlled by the oven thermostat and was found to be stable by ± 3°C. The oven was set to dry air (no humidification), 50% of the maximum fan speed and an oven temperature of 175°C. The meat samples are placed in the oven on a stainless steel baking tray.

C. Measurements

1) Local moisture content

Rectangular block samples of pork of an approximate size of *54×40×40 mm^3* were prepared by hand cutting. The meat samples were roasted in the convection oven for a specified period of time of 8, 11, 15, 20, 25, 30 and 35 min respectively. Each sample was instantaneously taken from the convection oven and immersed in liquid nitrogen for approximate 30 s to stop water migration by freezing. The samples were placed in a freezer for 2-4 hours. Then the sample was sliced with a meat slicer and a knife into small sub-samples of approximately 4×4×4 mm^3. The moisture content of each local sample was determined using oven drying at 105°C for 24 hours [17].

2) Overall shrinkage

Meat samples were prepared as rectangular blocks of the same dimensions as in 1). For all the samples, the length (*L*) direction was assigned along the fibre orientation (in the x-direction), and width (*W*) and height (*H*) were assigned across the fibre orientation (in the y and z direction, respectively). Samples were measured using a digital vernier caliper both before and after roasting. Initial dimensions ('L_o', 'W_o' and 'H_o') and mass (M_o) of each sample were measured. The convection oven was heated to 175°C and samples were placed in the oven and heated for a specified time. At time t, the sample was instantly taken from the oven and its dimensions (*L, W and H*) and mass (*M*) were measured. Then, the sample was placed back in the oven. This procedure was repeated at all specified times.

3) DSL during roasting

16 meat samples were roasted (under the same condition as above) and their initial (M_o) and final mass were measured. A sample was taken from the oven and the dry matter lost with the exudate left on the tray was collected after the water had been evaporated in the oven. The solid residual was removed from the tray with a knife and its mass was determined. These procedures were repeated for all samples.

IV. RESULTS AND DISCUSSION

A. Local moisture content

The local water content of the meat was determined at different positions and time as shown in Table 1. A local water content rise towards the center (16-20) was not observed: This result agrees well with the work of Skjöldebrand in (2001) [12]. Generally, the local water content decreases with an increase in distance from the centre and decreases with increasing roasting time (with few exceptions). The local water content at position (0-4) decreases steadily for the initial stage up to t = 20 min (to 0.646 kg of water/kg of sample). Then at t = 25 min it increases (to 0.705 kg of water/kg of sample) and then later on it decreases again. The increased water content near the surface at t = 25 min, is probably due to the large outward water flux directing water from the center of the piece of meat to the surface. A rapid drop in water binding capacity and a large pressure gradient at the center, and larger permeability in the outer part (0-4) than in the inside part (16-20) causes the water to move faster towards the surface. When the internal water flux is larger than the transport flux of water away from the surface, water is accumulated near the surface (0-4), and consequently the local water content rises. Later on the internal flux decreases and the local water content continues to drop for the remaining time of the roasting experiment.

In later work not reported here, we have occasionally observed a slight moisture rise (up to 0.03 kg water/kg of sample) near the centre after 15 and 20 min of roasting in the convection oven. Still, that level of increase of the moisture content is far below Van der Sman's prediction (0.1 kg of water/kg of sample, 10% rise) [16]: The rise of the local water content is not necessarily observed at the center of the meat piece; the local rise can be anywhere within the sample, depending on the magnitude of pressure gradients and the permeability of the medium. Our hypothesis is that the onset of heat denaturation and shrinking may give rise to occasional crevices in the meat because the shrinking causes uneven stresses in the meat piece. This will be investigated in future work and does not distract from the overall conclusion that the water transport towards the centre is negligible because of the low permeability of the raw meat.

Table 1 Local water content (kg of H_2O per kg of sample)

Time(in min)	Position(mm) from surface to center				
	(0-4) *Surface*	(4-8)	(8-12)	(12-16)	(16-20) *center*
0	0.746	0.752	0.748	0.745	0.720
8	0.720	0.730	0.740	0.730	0.740
11	0.701	0.716	0.727	0.737	0.745
15	0.690	0.720	0.730	0.730	0.740
20	0.646	0.727	0.744	0.741	0.736
25	0.705	0.706	0.727	0.732	0.736
30	0.693	0.712	0.719	0.716	0.734
35	0.659	0.618	0.665	0.667	0.681

Position is distance from surface in mm, 0 and 20 are surface and center respectively·

B. Shrinkage

Fig 1 a and b show that relative dimensions (L/Lo, W/Wo and H/Ho) and relative mass (M/Mo) as function of time for two samples, taken out of 5 samples showing extreme shrinkage phenomena. Meat samples shrink in the length and width direction: with larger shrinkage in the length direction. The rate of shrinkage is large from t=900 to t= 2100 s, Fig 1a and from t=500 to t=2900 s, Fig 1b and the corresponding mass loss rate is also large in the same range, relative mass decrease from 90 to 70% and 90 to 69%, respectively. This verifies that shrinkage is the basis for larger water loss which agrees with the hypothesis of Godsalve [10]. However, later on, after 2700 s (Fig 1a) the rate of shrinkage is considerably reduced, a change

of 4% in the length and 2% in the width from t = 2700 to t = 4500 s. The most probable reason for such reduction shrinkage rate is that the elastic modulus of the meat increases drastically when the meat is heated above 65°C [13].

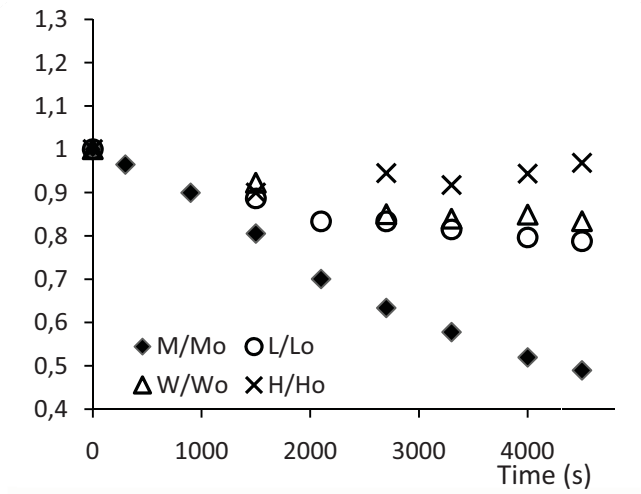

a)

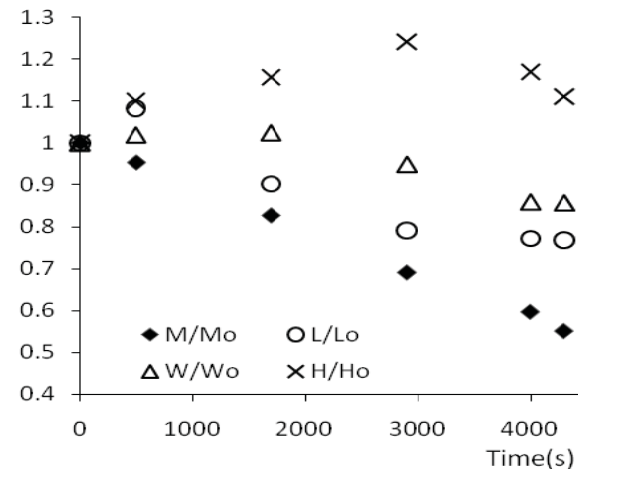

b)

Figure 1 Shrinkage and mass loss as function of time: a) meat sample shrinking in 3 directions; b) meat sample shrinking in x and y-direction and expanding in the z direction (height). M is mass (g), L, W and H are length width and height (mm), respectively. Subscript 'o' refers to initial state

Another interesting observation was that mass loss is larger if the sample is shrinking in all directions (Fig. 1a) compared to a situation where it is expanding in one of its directions (Fig 1b). This can be explained by the fact that the stress is larger when the meat shrinks in all directions than when it expands in one of its directions. Larger stress causes a greater squeezing pressure, which means more water is squeezed to the surface (larger mass loss). The exact cause for the differences in shrinking behaviour between meat samples is not identified, but must be related to the fact that the biological variation between the same muscles but from different animals is considerable.

C. *Dry matter loss with water as drip*

Meat with low fat content was used for our study to avoid complication from fat transport. To test the validity of this assumption, the percentage of DSL was estimated as 1.33±0.18% of the total weight loss. Thus, it is quite a small fraction of the total loss (1.33 g per 100 g of total loss) and it substantiates the hypothesis of mass transfer based on water transport alone.

V. CONCLUSION

A mechanism for water transport during roasting of meat is proposed and partially substantiated by experimental data. Spatial distribution of the local moisture content in meat was studied, and a large rise of the water content was not observed in the center of the meat. Our hypothesis of water transport is that shrinkage plays a great role in water transport mechanisms that cause large water losses during meat roasting. Different shrinkage phenomena can result in substantial differences in mass loss: shrinkage in all directions leads to greater mass loss than if the meat piece expands in one of its directions.

The novelty of the present work lies in the emerging mechanistic understanding of water transport in meat during roasting. This understanding is corroborated by measurements of spatial local moisture content and overall shrinkage. The dynamic change of permeability plays a crucial role in the water transport mechanism and its effect needs to be considered in the future modelling of heat and mass transfer during meat roasting processes.

ACKNOWLEDGEMENT

The Author would like to thank DTU for a Ph.D. grant under the aegis of Food-DTU.

REFERENCES

[1] Anthelme Brillat-Savarin (1755-1826). (2007). The physiology of taste. eBooks@Adelaide.

[2] Singh, R. P. & Vijayan J.(1998). Predictive modeling in food process design. Food Science and Technology International, 4(5):303-310.

[3] Dincer, I. (1996). Modelling for heat and mass transfer parameters in deep-frying of products. Heat Mass Transfer, 32(1-2):109-113.

[4] Pan, Z., Singh R.P., & Rumsey, T.R. (2000). Predictive modeling of contact-heating process for cooking a hamburger patty. Journal of Food Engineering, 10/1;46(1):9-19.

[5] Ngadi, M.O., Watts, K.C., & Correia, L.R. (1997). Finite element method modelling of moisture transfer in chicken drum during deep-fat frying. Journal of Food Engineering, 4;32(1):11-20.

[6] Skjoeldebrand, C., & Hallström, B. (1980). Convection oven frying. Heat and mass transport in the product. Journal of Food Science,45(5):1347-1353.

[7] Singh, N., Akins, R.G., & Erickson, L.E. (1984). Modeling heat and mass transfer during the oven roasting of meat. Journal Food of Process Engineering, 7(3):205-2207.

[8] Chang, H.C., & Carpenter, J.A., Toledo, R.T. (1998). Modeling heat transfer during oven roasting of unstuffed turkeys. Journal of Food of Science, 63(2):257-261.

[9] Huang, E., & Mittal, G.S. (1995). Meatball Cooking - Modeling and Simulation. Journal of Food Engineering, 24(1):87-100.

[10] Godsalve, E.W., Davis, E.A., Gordon, J., & Davis, H.T. (1977). Water loss rates and temperature profiles of dry cooked bovine muscle. Journal of Food Science, 42(4):1038-1045.

[11] Thorvaldsson, K., & Skjöldebrand, C.(1996). Water transport in meat during reheating. Journal of Food Engineering, 7;29(1):13-21.

[12] Wählby, U., & Skjöldebrand, C. (2001). NIR-measurements of moisture changes in foods. Journal of Food Engineering, 3;47(4):303-312.

[13] Tornberg, E. (2005). Effects of heat on meat proteins – Implications on structure and quality of meat products. Meat Science,7;70(3):493-508.

[14] Tijskens, E., & De Baerdemaeker, J., (2004) Mathematical modelling of syneresis of cheese curd. Mathematics and Computers in Simulation,65(1-2):165-175.

[15] Barriere, B., & Leibler, L. (2003). Kinetics of solvent absorption and permeation through a highly swellable elastomeric network. Journal of Polymer Science Part B-Polymer Physics 15;41(2):166-182.

[16] Van der Sman, R.G.M. (2007). Moisture transport during cooking of meat: An analysis based on Flory–Rehner theory. Meat Science,76(4):730-738.

[17] Nielsen, S. S. (ed.). (1994). Introduction to Chemical Analysis of Foods, Jones and Bartlett, Boston, pp. 94-100.

Paper II

Model of Heat and Mass Transfer with Moving Boundary during Roasting of Meat in Convection-Oven

A.H. Feyissa*[1, 2], J. Adler-Nissen[1] and K.V. Gernaey[2]
[1] National Food Institute, Food production Engineering, Technical University of Denmark
[2] Department of Chemical and Biochemical Engineering, Technical University of Denmark
*Corresponding author: Søltofts Plads, 2800, Kgs. Lyngby, DK (e-mail: abhfe@food.dtu.dk)

Abstract: A 2D mathematical model of coupled heat and mass transfer describing oven roasting of meat was formulated from first principles. The current formulation of model equations incorporates the effect of shrinkage phenomena and water holding capacity. The model equations are based on conservation of mass and energy. The pressure driven transport of water in meat is expressed using Darcy's equation. The arbitrary Lagrangian–Eulerian (ALE) method was implemented to capture the moving boundary (product-air interface) during the roasting process. The model equations were solved using the Finite Element Method (Multiphysics® version 3.5). The state variables (temperature and water content) were predicted. The effect shrinkage on both predictions was evaluated.

Keywords: Coupled heat and mass transfer; Evaporation; Moving boundary; Multiphyics; Shrinkage.

1. Introduction

Roasting in a convection oven is a common way of frying whole meat in households, in professional kitchens and in the ready-meal industry. Mass and heat transfer play an important role in the roasting process. It is essential that their interaction and mechanisms are well understood to allow for better control and optimisation of the roasting process. The effect of shrinkage on meat roasting is often neglected due to the complexity of the process [1]-[4]. However, it is necessary to incorporate such effects into a heat and mass transfer model of meat roasting, because shrinkage is considerable (7-19 % on a area basis [5], and 11-20.3 % on diameter basis [6]) and plays a key role in the water transport during the roasting process) [7].

Several researchers have formulated different hypotheses to model mass transfer during roasting, mostly from the perspective of diffusion [1]-[3] while disagreements are often seen with regard to other types of water transport mechanisms [8]-[10]. Purely diffusion based models do not adequately describe the moisture transport phenomena during meat cooking because the effects of water binding capacity and shrinkage phenomena are not considered. These are, however, main driving mechanisms for the exudation of water during the cooking or roasting of meat, and some of the early studies on this topic agree with this fact [5],[8]-[10]. Roasting of meat causes the muscle protein to denature, resulting in a decrease in water holding capacity and leading to shrinkage of the protein network. Shrinkage of the network ultimately induces a pressure gradient inside meat muscle. The excess pressure induces a transport of water inside the meat [11], and in the end leads to water loss from the meat.

Most of the published work on the modelling of mass and heat transfer during meat roasting does not at all consider shrinkage, and thus the governing model equations were typically solved using a fixed boundary, where the evaporation interface and the material boundary remain the same for the entire roasting period [1]-[3],[11]. Usually, the reason for making such assumptions is that model equations become considerably simpler and thus easier to solve. However, the model based on such fixed boundary assumptions may not be valid for meat that is heated above the denaturation temperature, where the meat shrinks considerably, loses water and changes its dimensions. When temperatures exceed the denaturation temperature, shrinkage phenomena should therefore be taken into account in the heat and mass transfer model, in order to successfully describe heat and water transport inside the meat product. Therefore the objective of this work is to develop a model of

heat and mass transfer by taking into account the shrinkage effect (moving boundary and pressure driven transport) and ultimately to describe and predict heat and mass transfer processes for meat roasting in a convection oven.

Nomenclature

C	Moisture content (wet basis) (kg /kg)	*Greek letters*	
C_{eq}	Water holding capacity at equilibrium (kg /kg)	β	Shrinkage coefficient
c_p	Specific heat (J/(kg.°C)	ρ	Density (kg/m^3)
D	Diffusion coefficient (m^2/s)	μ_w	Viscosity (kg/(m.s))
E	Elastic modulus(N/m^2)	∇	Gradient(1/m)
f	Fraction of energy used for evaporation (J/kg)		
H	Latent heat of vaporization (J/kg)	*Subscripts*	
h	Heat transfer coefficient (W/(m^2 °C)	*av*	Average
K	Permeability (m^2)	*eq*	Equilibrium
k	Thermal conductivity (W/(m. °C))	*c*	Carbohydrate
m	Mass (kg)	*d*	Solid
P	Pressure (Pa)	*evp*	*evaporation*
q	Heat flux (W/m^2	*f*	Fat
T	Temperature (°C)	*i*	Component
t	Time (s)	*m*	Meat
$T\sigma$	Sigmoidal temperature(°C)	*p*	Protein
R	Radius (m)	*w*	Water
y_i	Mass fraction of component *i* *(kg/kg)*	*0*	Initial value
Z	Length (m)	*oven*	Oven
V	Volume (m^3)	*s*	Surface
v	Interface velocity (m/s)	*r*	Radial direction
u	velocity of water (m/s)	z	Length direction

2. Mathematical Model of Heat and Mass Transfer

2.1 Process Descriptions and Problem Formulation

The product (meat) is heated in a convection oven by circulating hot air at 175°C. Heat is supplied to the product surface by convective heat transfer. The heat is transferred from the surface the product to the center of the product mainly by conduction. Meanwhile, moisture is transported within the product via convection and diffusion processes, and moves from the inside of the product to its surface. With increase in temperature, muscle protein denatures, leading to a decrease in its water holding capacity and shrinkage of the protein network. The shrinkage of network ultimately induces a pressure gradient inside the meat muscle and excess water is expelled to the surface by convection phenomena. Simultaneously, liquid water is evaporated at the product surface and diffuses to the surrounding fluid (hot air). As the meat sample shrinks the interface or the surface at which water is evaporated changes with time. The most important mechanisms occurring during the convection oven roasting process are described in Fig.1, as shown below.

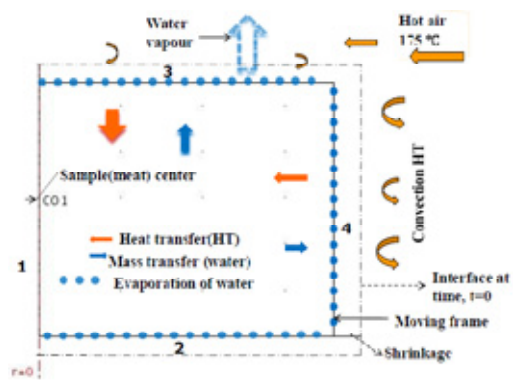

Figure 1: A schematic representation of coupled heat and mass transfer accompanied by shrinkage and evaporation processes

2.2 Assumptions:

In this study the following basic assumptions are made to formulate the governing coupled mass and heat transfer equations for a cylindrical body of meat:

a) Fat transport is negligible (lean meat is considered having less than 2% fat)
b) The crust is thin (this is observed when inspecting a cut through the cooked meat) and does not hinder transport of water to the surface. Evaporation therefore takes place at the surface (moving interface)
c) No internal heat generation and no chemical reaction.
d) Dissolved matter lost with water can be

neglected in the material and energy balance [7].

e) The process can be represented two dimensions, due to symmetry of the cylindrical body that is modelled.

f) The initial distributions of water content and temperature are uniform.

2.3 Governing equations

Using conservation of energy, the heat transfer within meat is assumed to be given by (1)

$$\rho_m c_{p_m} \frac{\partial T}{\partial t} + \nabla(-k_m \nabla T) + \rho_w c_{p_w} u_w \nabla T = 0 \quad (1)$$

From the conservation of mass, the governing equation for water transport within the product is given by (2)

$$\frac{\partial C}{\partial t} + \nabla(C u_w) = \nabla D \nabla C \quad (2)$$

The relationship between the velocity and pressure gradient (that drives the moisture transport) inside the meat can be expressed using Darcy's law of porous media :

$$u_w = \frac{-K}{\mu_w} \nabla P \quad (3)$$

The pressure (swelling pressure) is proportional to the excess moisture concentration within the meat [11]-[10] and the expression for swelling pressure P is given as

$$P = E\left(C - Ceq(T)\right) \quad (4)$$

The expression for the water holding capacity is given by an empirical, sigmoid relation [11], [13]

$$C_{eq(T)} = 0.745 - \frac{0.345}{(1 + 30\exp(-0.25(T - T\sigma)))} \quad (5)$$

The expression for velocity can be re-written using Eq. (3-5)

$$u_w = \frac{-KE}{\mu_w} \nabla\left(C - C_{eq}\right) \quad (6)$$

2.4 Boundary Conditions

2.4.1 Heat Transfer Boundary Condition

For product subjected to convection roasting (boundary 2, 3 and 4, see Fig.1), the governing heat transfer equation (1) is solved using

$$-n.\left(k_m \nabla T + u_w c_{pw} \rho_w T\right) = h\left(T_{oven} - T_s\right) - q_{evp} \quad (7)$$

For the sample center line, boundary 1 (see Fig.1), axial symmetry boundary is applied:

$$-n.\left(k_m \nabla T + u_w c_{pw} \rho_w T\right)\Big|_{r=0} = 0 \ ; \ t > 0 \quad (8)$$

Where the term on the left-hand side of equation (7) refers to heat transferred by conduction and convection from the outer surface to the inside of the meat sample, the first term on the right-hand side is heat penetrating from the oven (hot air) to the product by means of convection, and the second term on the right-hand side denotes heat dissipation for evaporation of the water at the interface. The initial condition has the following form (9):

$$T(r, z) = T_0 = \text{const} \quad \text{at} \quad t = 0 \quad (9)$$

2.4.2 Mass Transfer Boundary Condition

For product subjected to convection roasting (boundary 2, 3 and 4), the governing mass transfer equation (2) is solved using (10)

$$n..\left(-D\nabla C + u_w C\right) = \frac{q_{evp}}{H_{evp}\rho}\left(C - C_{eq}\right) \quad (10)$$

For boundary 1(at r = 0), the axial symmetry boundary condition applies:

$$n.\left(-D\nabla C + u_w C\right)\Big|_{r=0} = 0 \ ; \ t > 0 \quad (11)$$

The initial condition has the following form (12):

$$C(r, z) = C_0 = \text{const} \quad \text{at} \quad t = 0 \quad (12)$$

2.4 Shrinkage

The methods used to consider material shrinkage differ greatly throughout the literature [14]. It is often considered that the change of dimensions (shrinkage) is proportional to the volume of liquid water removed [14]. For meat cooking, Sun and Du found a good correlation between the shrinkage (volume based dimensions change) and cooking loss, (a higher shrinkage leads to more cooking loss, and vice versa) [15]. The action of roasting causes denaturation of meat proteins, which allows for dehydration and shrinkage of the meat, and the simultaneous formation of air filled pores [6]. By assuming that the relationship between volume of water removed and shrinkage holds for roasting of

meat, with an additional consideration for the effect of pore formation, the following theoretical expressions are formulated.

The volume of a cylindrical meat sample at any given time is expressed in terms of the initial volume (V_o) and volume of water lost ($V_{w,l}$) as

$$V = V_0 - \beta V_{w,l} \tag{13}$$

The coefficient β is used to describe the effect of pore formation during roasting process. For shrinkage, the value of β varies between 0 and 1. If β is 1, there is no pore formation (i.e. the volume of water removed is equal to the volume deformation) and if β = 0, then there is no shrinkage (i.e the volume water lost is entirely replaced by air and no deformation occurs). The fraction (1-β) is the fraction of the volume of water removed from the meat during roasting that is replaced by pore space (filled with air). For minced meat, this value is roughly estimated (for a mass loss of 15%, the corresponding pore formation is 3%) to be around 0.2, and in that case β = 0.8 [6].

For isotropic shrinkage [16], Eq. (13) can be re-written as:

$$V = V_0\left(1-\frac{\beta V_{w,l}}{V_0}\right) = \pi R_0^2\left(1-\frac{\beta V_{w,l}}{V_0}\right)^{2/3} Z_0\left(1-\frac{\beta V_{w,l}}{V_0}\right)^{1/3} = \pi R^2.Z \tag{14}$$

From (14) the expressions for Z and R are given as:

$$Z = Z_0\left(1-\frac{\beta V_{w,l}}{V_0}\right)^{1/3} \tag{15}$$

$$R = R_0\left(1-\frac{\beta V_{w,l}}{V_0}\right)^{1/3} \tag{16}$$

Differentiating (15) and (16) with respect to time, the interface velocity components can be obtained as:

$$v_z = \frac{dZ}{dt} = -\frac{Z_0\beta}{3V_0}\left(1-\frac{\beta V_{w,l}}{V_0}\right)^{-2/3}\frac{d}{dt}\left(V_{w,l}\right) \tag{17}$$

$$v_r = \frac{dR}{dt} = -\frac{R_0\beta}{3V_0}\left(1-\frac{\beta V_{w,l}}{V_0}\right)^{-2/3}\frac{d}{dt}\left(V_{w,l}\right) \tag{18}$$

$V_{w,l}$ can be expressed as function of water content as in Eq. (19) :

$$V_{w,l} = \frac{m_d\left(X_0 - X\right)}{\rho_w} = \frac{\rho_0 V_0\left(1-C_0\right)}{\rho_w}\left(\frac{C_0}{1-C_0} - \frac{C_{av}}{1-C_{av}}\right) \tag{19}$$

and the rate change of $V_{w,l}$ is given by (20) :

$$\frac{dV_{w,l}}{dt} = -\frac{\rho_0 V_0\left(1-C_0\right)}{\rho_w}\left(\frac{1}{1-C_{av}}\right)^2\frac{dC_{av}}{dt} \tag{20}$$

at the sample center (boundary r = 0)

$$v_r = 0 \tag{21}$$

3. Numerical Method

The above model equations (system of partial differential equations) describing coupled heat and mass transfer in convection roasting of meat were solved using the finite element software, COMSOL Multiphyics®version3.5. A 2D cylindrical geometry of dimensions (radius of 20 mm and length of 54 mm) was built in COMSOL for numerical simulations. The coupled partial differential equations for heat and mass transfer along with the boundary condition were solved using the *Chemical Engineering module* (transient heat transfer and transient mass transfer) and the *moving mesh module (ALE)*. The incorporation of ALE gives the ability to track the position of the product-air interface. The input parameter values and the algebraic expressions in the model are given in table 1.

4. Result and Discussion

4.1 Temperature and water content distributions

In the meat roasting process, temperature and water content distributions are important factors which determine the quality of the product. The water content distribution is influenced by the temperature distribution. Fig 2a and 2b show simulated spatial temperature and moisture distribution, respectively, for 2D cylindrical meat sample at different times of roasting process (*t* = 0, 500, 1000, 1500, 2000, 2500, 3000, and 3500 s). Generally, inside the meat sample, the temperature increases with increase in time, whereas water content and dimensions are decrease with increase in time. From that the figure, a change of dimensions - a moving boundary - can be noticed.

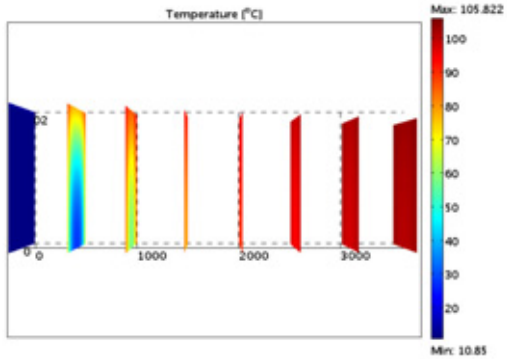

a)

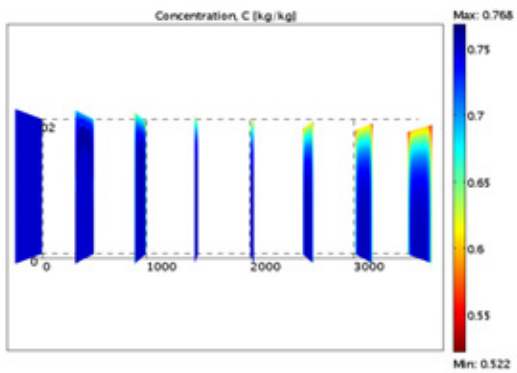

b)

Figure 2. a) Temperature distribution, and b) water content distribution at (*t* = 0, 500, 1000, 1500, 2500, 2000, 3000, and 3500 s)

Fig. 2a, illustrates the progress of the temperature distribution during meat roasting in a convection oven. Initially, there is a sharp increase in surface temperature because of the large temperature difference between hot air (175°C) and the meat (13°C). At *t* = 500 s, the surface of the meat is at a much higher temperature than the inside part of the meat sample, and a large temperature gradient is developed in the region close to the surface,(see Fig. 2a and Fig. 3). When the roasting process proceeds, this large temperature gradient shifts gradually from near the surface to inside of the product. Moreover, its magnitude decreases as a function of time, as the heat energy is slowly penetrating into the centre of the product, thereby raising its temperature (Fig. 3). In the final period of this roasting experiment, at time *t* = 3000 s, the temperature of the meat is almost uniform.

Fig. 2b, illustrates the progress of the water content distribution within the meat product during the roasting process. The water content distribution changes from being uniform (= initial condition) to a non-uniform profile. The increase in temperature (to the denaturation temperature zone) causes the meat to reduce its water holding capacity and induces shrinkage. The reduction of the water holding capacity and the shrinkage of the meat protein network cause the meat to exudate water to the surface, which is lost by evaporation at the surface. As a result, the water content gradient is developed within the meat, as shown by iso-concentration lines at t = 500 s (Fig. 4). A large water concentration gradient is observed near the surface and the gradient gradually shifts towards the interior of the product (Fig. 2b). The water transport depends upon the material properties (permeability and elastic modulus), the diffusivity coefficient and the pressure gradient.

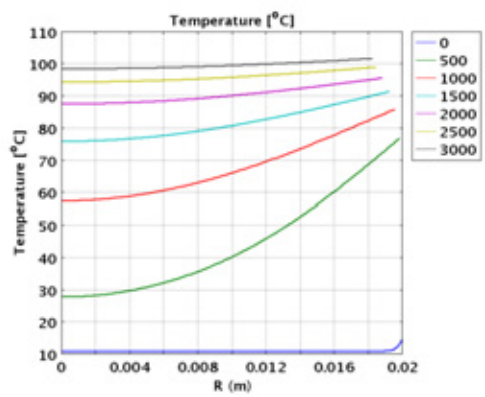

Figure 3 Temperature profile across cylindrical sample (Z = 0)

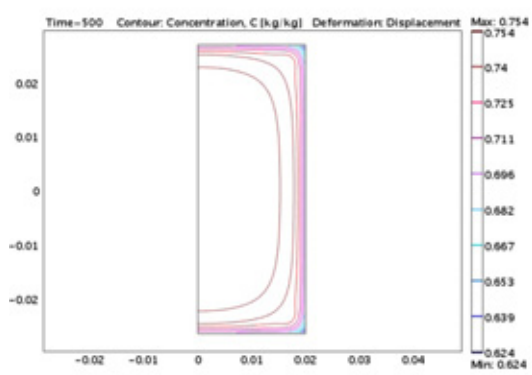

Figure 4 .Iso-concentration, C (kg/kg) at t = 500 s

4.2 **Effect of Moving Boundary**

The temperature profiles with moving boundary (MB) and fixed boundary (FB) are compared in Fig. 5a and 5b. From Fig. 5a, the center and the surface temperature values predicted by both methods coincide well at the beginning of the process (t = 0 to t = 1000 s). But later one, (t > 1000 s), the two predictions start deviating from each other. The FB predicts lower center temperature than MB. However, the FB predicts higher water content than MB (Fig 5b).

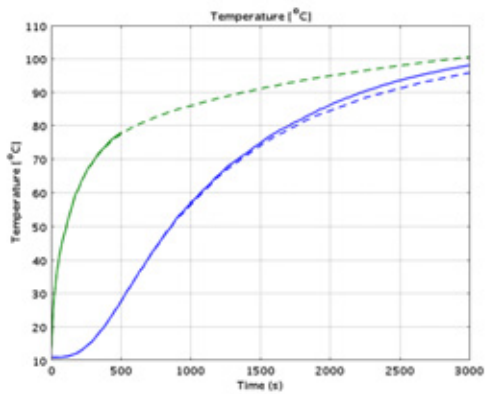

Figure 5a Temperature profile –MB -- FB (blue) center (0, 0) (green) surface (R = 0.02, Z = 0)

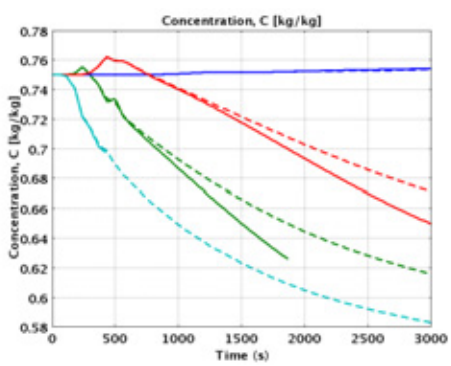

Figure 5b Water content profile – (MB), -- (FB), blue is center (0, 0), red is at (0.017, 0), green is at (0.019, 0), and is surface (0.02, 0).

4.3 Relative Change of Dimension

Fig. 6 shows the plot of the relative dimension change, R/R_o, in the r-direction. In the first part of the roasting process (until t = 300 s), there is no shrinkage. The product (meat) starts shrinking slowly from t = 300 s to 500 s. In the second period (between t = 500 s to t = 2000 s), the relative change of dimension is large (steep profile). In this zone, a major part of the meat is in the denaturation zone (where a reduction of water holding capacity and shrinkage of protein network take place). In the third period, (after t = 2000 s), the relative change of deformations (shrinkage rate) is reduced. After t = 3500 s, the rate of change of the relative dimension has clearly diminished. The probable reasons for such situation are; 1) the mechanical properties of the meat have changed (e.g. elastic modulus increase) and 2) reduction of the water content near the surface, which make the product more rigid and less susceptible to deformations.

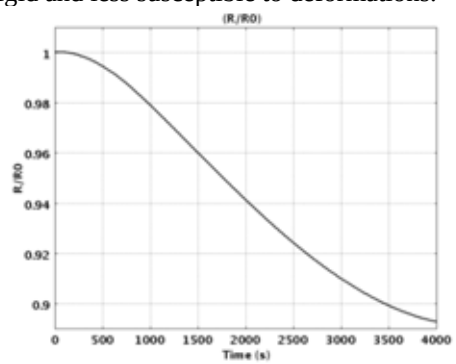

Figure 6 Relative length of cylinder as function of time (R/R0)

5. Conclusions

A first-principles-based model of heat and mass transfer with moving boundary is developed for a convection meat roasting process. The model equations were solved using COMSOL Multiphyics®version3.5. Temperature and water content distributions as function of position and time were predicted. Using the model better insight of the process mechanisms is obtained, which would otherwise not be possible. The novelty of the developed model is its capability to incorporate the effect of the shrinkage and water holding capacity. Such model can be helpful in understanding the physics of meat roasting, and can be used to improve prediction of temperature and moisture loss.

6. References

[1] Huang, E. and Mittal, G.S., Meatball Cooking - Modeling and Simulation, *J. Food Eng.*, **24**: 87-100, 1995.

[2] Ngadi, M.O., Watts, K.C. and Correia, L.R., Finite element method modelling of moisture transfer in chicken drum during deep-fat frying, *J. Food Eng.*, **32**: 11-20, 1997.

[3] Chen, H., Marks, B.P. and Murphy, R.Y., Modeling coupled heat and mass transfer for convection cooking of chicken patties, *J. Food Eng.*, **42**: 139-146, 1999.

[4] Skjoeldebrand, C., and Hallström, B., Convection oven frying Heat and mass transport in the product, *J. Food Sci*. **45** :1347-1353, 1980.

[5] Tornberg, E. , Effects of heat on meat proteins – Implications on structure and quality of meat products, *Meat Sci*.**,70**: 493-508, 2005.

[7] Feyissa, A.H., Adler-Nissen, J., and. Gernaey, K.V., Mechanism of water transport in meat during the roasting process, *Icomst Conference*, 11-15, Copenhagen, 2009.

[6] Oroszvari, B.K., Bayod, B.E., Sjoholm, I. and Tornberg, E. The mechanisms controlling heat and mass transfer of the frying of beef burgers. III. Mass transfer evolution during frying, *J. Food Eng.*, **76**: 169-178.

[8] Godsalve, E.W. Davis, E.A. , Gordon, J. ,and Davis, H.T., Water loss rates and temperature profiles of dry cooked bovine muscle, *J. Food Sci.*, **42**: 1038-1045, 1977.

[9] Thorvaldsson, K. , and Skjöldebrand, C., Water transport in meat during reheating, *J. Food Eng.*, **29**: 13-21, 1996.

[10] Wählby, U., and Skjöldebrand, C. , NIR-measurements of moisture changes in foods, *J. Food Eng.*, **47**: 303-312, 2001.

[11] Van der Sman, R.G.M., Moisture transport during cooking of meat: An analysis based on Flory–Rehner theory, *Meat Sci.*, **76**: 730-738, 2007.

[12] Barriere, B., and Leibler, L., Kinetics of solvent absorption and permeation through a highly swellable elastomeric network, *J. Polymer Sci. Part B-Polymer Physics*, **41**:166-182, 2003.

[13] Bengtsson N.E., Jakobsson B., and Dagerskog M., Cooking of Beef by Oven Roasting - Stuy of Heat and Mass-Transfer, J. Food Sci., 41: 1047-1053, 1976.

[14] Katekawa, M.E. and Silva, M.A..A review of drying models including shrinkage effects , *Drying Technol.* , **24**: 5-20, 2006.

[15] Sun D.-W. and DU C.-J., Correlating shrinkage with yield, water content and texture of the pork ham by computer vision, *Journal Food Process Engineering*, **28** :219-232, 2005.

[16] Pham, Q.T., Trujilo, F.J., and Wiangkaew, C., Drying modeling and water diffusivity in beef meat, *J. Food Eng.*, **78:** 74-85, 2007.

[17] Rao, M.A., Syed, S.H.R, and Datta, A.K., Engineering properties of foods, 3rd ed. Talyor and Francis.

[18] Datta, A.K., Hydraulic permeability of food tissues., *Int. J. Food.*, **9:**767-780, 2006

[19] Hodgman, C.D., Handbook of chemistry and physics, *The chemical rubber publishing Co.*, Cleveland, Ohio, 2257.

7. Acknowledgement

The Author would like to thank DTU for a Ph.D. grant under the aegis of Food-DTU.

8. Appendix

Table 1: **Parameters values, thermophysical properties and other expression.**

	Value or expression	*Reference*
y_p	0.2 kg/kg	*[5]*
y_c	0.02 kg/kg	*Initial*
y_f	0.03 kg/kg	*mass*
y_w	0.75 kg/kg	*fraction*
ρ_f	920 kg/m^3	*[17]*
ρ_p	1320 kg/m^3	*[17]*

ρ_c	1600 kg/m^3	*[17]*
ρ_w	1000 kg/m^3	*[17]*
k_m	0.47 W/(m. ^{o}C)	*[17]*
$c_{p,w}$	4170 J/(kg· ^{o}C	*[17]*
H_{evap}	2.3 10^6 J/kg	
h	33.4 (W/(m$^{2.}$ ^{o}C)	*Measured*
K	10^{-17}-10^{-19} (raw meat) 10^{-17}m^2	*[18]*
T_{0ven}	175 °C	*Set*
T_0	13 °C	*Set*
C_0	0.75 kg /kg	*[5][7]*
β	0.8	[6]
$D = 2.23e\text{-}5\exp(-3382.212/T)$		*[16]*
$-\log \mu_w = 0.0072\ T + 2.8658$		*Using data [19]*
$\rho_m = \dfrac{1}{\sum \dfrac{y_i}{\rho_i}}$		*[17]*
$c_{pm} = (1.6y_c + 2y_p + 2y_f + 4.2y_w).10^3$		*[17]*
$E_{(T)} = E_o + \dfrac{E_{mx}}{(1+\exp(-E_n(T-E_D))}$ For whole meat, E_0=*12 kpa*, E_{mx}=83 kpa at T=80 ^{o}C; E_n=0.3, and E_D=60		*Using data [5]*
$q_{evp} = fh(T_{oven} - T_s)$		

Paper III

Feyissa A.H., Gernaey K.V., Ashokkumar S., & Adler-Nissen J., (2011). Coupled Heat and Mass Transfer during a Contact Baking Process, *Journal of Food Engineering,* doi:10.1016/j.jfoodeng.2011.05.014 *(in press, Accepted Manuscript, published online)*

ARTICLE IN PRESS

Journal of Food Engineering xxx (2011) xxx–xxx

Contents lists available at ScienceDirect

Journal of Food Engineering

journal homepage: www.elsevier.com/locate/jfoodeng

Modelling of coupled heat and mass transfer during a contact baking process

A.H. Feyissa [a,*], K.V. Gernaey [b], S. Ashokkumar [a], J. Adler-Nissen [a]

[a] Food Production Engineering, National Food Institute, DTU, Denmark
[b] Center for Process Engineering and Technology, Department of Chemical and Biochemical Engineering, DTU, Denmark

ARTICLE INFO

Article history:
Received 1 November 2010
Received in revised form 9 May 2011
Accepted 11 May 2011
Available online xxxx

Keywords:
Contact baking process
Evaporation
Finite Element Method
Heat and mass transfer
Modelling

ABSTRACT

A mathematical model of coupled heat and mass transfer of a contact baking process is developed. In the current model formulation, a local evaporation of water is described with a reaction–diffusion approach, where a simultaneous diffusion and evaporation of water takes place. The resulting coupled model equations (unsteady state heat transfer, liquid water and water vapour) were solved using the Finite Element Method (*COMSOL Multi-physics® version 3.5*). During the baking process, local temperatures and overall moisture loss were measured continuously. The model – predicting temperature, liquid water content in the product and water in the vapour phase – was calibrated and partially validated using data obtained during baking of a representative food model (a pancake batter) under controlled conditions on a specially designed experimental rig. The unknown parameters in the model equations were estimated using the standard least squares method by comparing the measured with the predicted temperature profile. Good agreement was achieved between model predictions and the experimental values.

© 2011 Elsevier Ltd. All rights reserved.

1. Introduction

Contact baking is a widely applied process used in for example baking of crisp bread, tortillas, pizzas, chapatti, pancakes, pita breads etc. Being a traditional process, optimization and process control to obtain the desired final product quality is still largely based on experience and good craftsmanship rather than on predictive, engineering calculations. A transition from this traditional empirical approach towards methods that rely on calculations based on predictive models requires a deeper mechanistic understanding of the contact baking process and a knowledge of the physics involved, particularly heat and mass transfer. During the baking process heat and mass transfer occur simultaneously and induce many complex physical–chemical processes such as evaporation of water, crust formation, browning reactions, denaturation of proteins, and gelatinization of starch, (Lee et al., 1996; Mondal and Datta, 2008; Sablani et al., 1998; Therdthai and Zhou, 2003). In the literature, there are only a few publications on the modelling of contact baking (Gupta, 2001; Pyle, 2005) and the related contact frying process (Pan et al., 2000; Pan and Singh, 2002; Wichchukit et al., 2001), as compared to baking in a convection oven. Pyle (2005) studied the baking of crumpet (a product made of diluted batter). Pyle (2005) did not obtain a good agreement between the measured and the simulated temperature profile. In this paper, we have chosen a mechanistic model as the framework to represent available knowledge on heat and mass transfer in the contact baking process.

A mechanistic mathematical model of heat and mass transfer should take into account the main phenomena explaining the physical behaviour of the product during the contact baking process. In the present work, we will therefore develop a model for one-sided contact baking, where we have chosen a thick pancake as a representative food model. One-sided contact baking is a very common type of contact baking. In one-sided contact baking, heat is transferred to the product – placed on a specially designed heating rig for the experiments reported in this manuscript – by conduction from a hot surface. During the contact baking process, multi-phase water transport (liquid water and water vapour) and phase change (evaporation) occur; these processes are coupled and interact with each other during the baking process. The objective of this work is to present a detailed mechanistic mathematical model of the coupled heat and water transport during the contact baking process, and to validate that model with experiments.

2. Model of mass and heat transfer

2.1. Descriptions of the process and model formulations

Contact baking is a thermal process, where the product is heated at high temperature (140–300 °C) by contact with a hot surface. In the present work, the product (pancake batter) is heated on a horizontal heating rig, where heat is transferred by conduction through several layers of materials. These layers of materials include: (1) the heating rig (see Section 3.2), (2) thermal conduct-

* Corresponding author. Address: Søltofts Plads, Building 227, 2800 Kgs, Lyngby, DK, Denmark. Tel.: +45 45252636.
E-mail address: abhfe@food.dtu.dk (A.H. Feyissa).

0260-8774/$ - see front matter © 2011 Elsevier Ltd. All rights reserved.
doi:10.1016/j.jfoodeng.2011.05.014

Please cite this article in press as: Feyissa, A.H., et al. Modelling of coupled heat and mass transfer during a contact baking process. Journal of Food Engineering (2011), doi:10.1016/j.jfoodeng.2011.05.014

Nomenclature

c_{pp} and c_{pAl}, specific heat capacity (J/(kg K) of product (batter), and aluminium, respectively
D_l and D_v liquid and vapour diffusion coefficient (m^2/s), respectively
E_a activation energy (kJ/mol)
h_{bot} overall heat transfer coefficients at bottom boundary (baking disc–frying rig interface)
H_{evp} latent heat of evaporation (J/kg)
h_{top} heat transfer coefficients at top surface at air–product interface (W/(m^2 K))
k_{evp} evaporation rate constant at the evaporation temperature (1/s)
k_l and k_v liquid and vapour mass transfer coefficient (m/s), respectively
k_p, k_{Al} and k_{air} thermal conductivity (W/(m K)) of product, aluminium, and air, respectively
M_w the molecular weight of water (kg/mol)
R_{evp} rate of evaporation (kg/(kg s))
R_g the gas constant (J/K mol)
T temperature (K)
t time (s)
T_{air} surrounding air temperature (K)
T_{evp} evaporation temperature (K)
T_{set} heating rig temperature set point (K)
X_l and X_v liquid and vapour water content (kg of water/kg dry solid), respectively
y_i the mass fraction of each component (water, protein, carbohydrate and fat) (kg/kg of sample)
z the position in the z direction (m)
ρ_p, ρ_s, ρ_{Al} and ρ_{air} density (kg/m^3) of product (bulk), solid, aluminium, and air, respectively
ε porosity, dimensionless

Subscripts
air air
Al aluminium
l and v liquid and vapour, respectively
p product (pancake batter)
exp experimental
SD standard deviation

ing paste, and (3) bottom surface of the baking disc, which is made of aluminium (Al), as shown in Fig. 1a. For the remaining part of this paper, the term 'heating rig' will be used when referring to the rig and the thermal conducting paste together (domain 1 and 2, in Fig. 1a) and the problem can be represented in the simplified form as Fig. 1b. The heat transfer causes a rapid raise of the temperature within the pancake batter, which induces water migration by diffusion and evaporation. Heat and mass transfer interact via evaporation (Huang et al., 2007). The most important phenomena influencing key process variables are temperature, concentration of liquid water and concentration of water vapour within the pancake batter.

The following assumptions were made when developing the model: (a) heat is transferred within the pancake batter by conduction in the beginning (later, evaporation and partial condensation also contribute to heat transfer, see item c and e); this is reasonable, because the pancake batter is rather viscous and its thickness is relatively low (no natural convection); (b) heat is lost from the product to the surrounding air via convection: rough calculations indicate that the radiation can be neglected because the surface temperature of the product is below 100 °C, (the measured temperature at position A, 6.4 mm from the bottom, only 1.6 mm from the top surface is well below 100 °C); (c) the liquid water is transferred by diffusion within the pancake batter and simultaneously local evaporation takes place; (d) liquid water and water vapour transport through the product are considered separately as multi-phase water transport; (e) the water vapour is generated within the pancake batter, then it migrates to the top surface (water–air interface, at $z = 0.008$ m, Fig. 1b) and subsequently diffuses to the external environment (air); and the energy transport with the vapour can be neglected, the latter is justified by a crude total energy balance (see, Section 4.1); (f) a transient one dimensional model (only heat and mass transfer in the z direction) is considered. This assumption is valid, because the diameter ($2R = 90$ mm) of the pancake batter is very large compared to the height (8 mm), and the effect of heat flux from the sides (in x and y directions) is small compared to the effect of heat flux from the bottom.

2.2. Governing model equations

2.2.1. Heat transfer

Heat transfer within the pancake is treated as a problem of transient heat conduction with phase change that includes evaporation

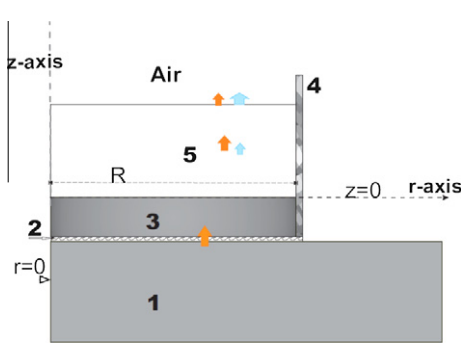

Fig. 1. a Part of the heating rig used for studying the contact baking process; domain 1 is the rig (aluminum block), domain 2 is the thermal conducting paste (copper paste), domain 3 is the aluminum plate (bottom part of the baking disc), domain 4 is the wall of the baking disc (stainless steel), and domain 5 is the product (pancake batter).

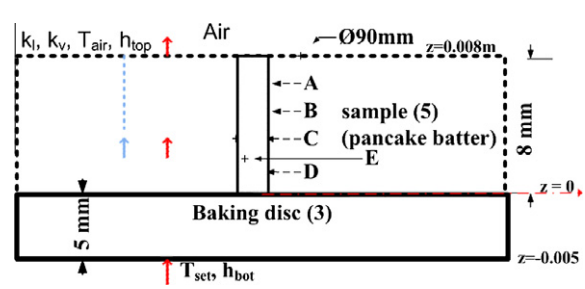

Fig. 1b. Simplified schematic representation for studying the contact baking process showing: the pancake batter, baking disc and temperature sensor position within pancake batter ($A = 6.4$ mm, $B = 4.8$ mm, $C = 3.2$ mm, and $D = 1.6$ mm from bottom surface, E = the sensor holder). The position of the boundary conditions are: $z = -0.005$ m (baking disc and heating rig interface), $z = 0$ m (baking disc–pancake interface) and $z = 0.008$ m (the top surface of the pancake batter or pancake–air interface).

Please cite this article in press as: Feyissa, A.H., et al. Modelling of coupled heat and mass transfer during a contact baking process. Journal of Food Engineering (2011), doi:10.1016/j.jfoodeng.2011.05.014

of water. Using the conservation of energy, the governing equation for the heat conduction with phase changes within the pancake batter is given by Eq. (1). A similar formulation was also used by Huang et al. (2007) to model the bread baking process:

$$\rho_p c_{p,p} \frac{\partial T}{\partial t} = \frac{\partial}{\partial z}(k_p \frac{\partial T}{\partial z}) - \rho_s R_{evp} H_{evp} \tag{1}$$

where T is the temperature (K), t is time (s), k_p is the thermal conductivity of the product (W/(m K)), $c_{p,p}$ is the specific heat capacity of the product (J/(kg K)), ρ_p and ρ_s are the density of the product and of the dry solid (kg/m^3), respectively, H_{evp} is the latent heat of evaporation (J/kg), and R_{evp} is the rate of evaporation (kg of water/(kg of solid·s)), (see Section 2.3.1). The above formulation, Eq. (1), incorporates the local evaporation of water (the second term on the right-hand side), and it represents the heat dissipated by evaporating the water.

Heat transfer through the bottom surface of the baking disc (Fig. 1b) is given by:

$$\rho_{Al} c_{p,Al} \frac{\partial T}{\partial t} = k_{Al} \frac{\partial^2 T}{\partial^2 z} \tag{2}$$

where ρ_{Al}, $c_{p,Al}$ and k_{Al} are the density, specific heat capacity, and thermal conductivity of the aluminium, respectively.

The following boundary conditions apply for heat transfer:

The heat flux from the heating rig to the baking disc (at $z = -0.005$ m):

$$-k_{Al} \frac{\partial T}{\partial z}\bigg|_{z=-0.005} = h_{bot}(T_{set} - T) \tag{3}$$

where T_{set} is the frying rig's temperature set point (K), and h_{bot} is the contact heat transfer coefficient at the bottom boundary (at the heating rig–baking disc interface). h_{bot} was estimated together with other parameter by fitting the measured temperature and simulated temperature profile (see Section 4.3).

At the bottom surface of the pancake batter ($z = 0$, pancake batter–baking disc interface), the heat transfer by conduction from baking disk is equal to the heat transfer by conduction to the pancake batter plus heat of evaporation which is given by Eq. (4):

$$\underbrace{-k_{Al} \frac{\partial T}{\partial z}\bigg|_{z=0}}_{\text{baking disk}} = \underbrace{(-k_p \frac{\partial T}{\partial z}\bigg|_{z=0})}_{\text{pan cake}} + q_{evp}\big|_{z=0} \tag{4}$$

where the first term and the second term in Eq. (4) is the heat flux (heat transfer by conduction) at $z = 0$, from baking disc and to pancake batter, respectively.

At the top surface of the pancake batter ($z = 0.008$ m, pancake–air interface), conductive heat flux is equal to the convective heat transfer and heat of the evaporation which is given (Eq. (5)):

$$-k_p \frac{\partial T}{\partial z}\bigg|_{z=0.008} = q_{evp}\big|_{z=0.008} + h_{top}(T - T_{air}) \tag{5}$$

where T_{air} is the surrounding air temperature (K), and h_{top} is the heat transfer coefficient at the top surface, i.e. at the air–product interface (W/(m^2 K)).

The value of h_{top} is 8 W/m^2, which was estimated using dimensionless correlations for natural convection and the properties of the air above the product (Cengel, 2007).

2.2.2. Mass transfer

2.2.2.1. Liquid water transport. The governing liquid water transport within the pancake batter (Fig. 1b) is given by Eq. (6) (Huang et al., 2007):

$$\frac{\partial X_l}{\partial t} = D_l \frac{\partial^2 X_l}{\partial^2 z} - R_{evp} \tag{6}$$

2.2.4.2. Water vapour transport. The governing equation for water vapour transport within the pancake batter is given by Eq. (7), (Huang et al., 2007):

$$\frac{\partial X_v}{\partial t} = D_v \frac{\partial^2 X_v}{\partial^2 z} + R_{evp} \tag{7}$$

where X_l, and X_v are liquid and vapour water content on a dry basis (kg of water/kg of solid), respectively; D_l and D_v, are the liquid and vapour diffusion coefficient (m^2/s), respectively; and t is time (s). The sign of the source term, R_{evp}, is negative in Eq. (6) and is positive in Eq. (7), i.e. liquid water disappears, while water vapour is generated during the baking process. When, R_{evp} is zero, there is no local evaporation.

In the baking disc (domain 3), there is no mass transfer.

The following boundary conditions apply for mass transfer:

At the bottom surface of the pancake batter ($z = 0$), the rate of liquid water removal from the pancake batter, the rate of water vapour generation and the rate of evaporation are equal, Eq. (8).

$$-D_l \frac{\partial X_l}{\partial z}\bigg|_{z=0} = D_v \frac{\partial X_v}{\partial z}\bigg|_{z=0} = -\frac{q_{evp}}{H_{evp}\rho_s}\bigg|_{z=0} \tag{8}$$

At the top surface ($z = 0.008$ m): the boundary conditions for liquid water and vapour are given by Eqs. (9) and (10), respectively:

$$-D_l \frac{\partial X_l}{\partial z}\bigg|_{z=0.008} = k_l(X_l - X_{l,air}) \tag{9}$$

$$-D_v \frac{\partial X_v}{\partial z}\bigg|_{z=0.008} = k_v(X_v - X_{v,air}) \tag{10}$$

where k_l and k_v are the liquid and vapour mass transfer coefficient (m/s), respectively.

2.3. Constitutive equations

2.3.1. Evaporation rate

A phase change from liquid water to water vapour is considered as a heterogeneous reaction with first order kinetics (Peters et al., 2002), where the evaporation rate is based on the Arrhenius equation. The basic Arrhenius equation for the rate of evaporation incorporates varying water content and temperature dependence. However, the limitation to the basic Arrhenius type equation when used for the evaporation rate is that it induces evaporation of water at low temperature in the model (temperature far below the evaporation temperature), which is not the case in practice. Here a modified rate equation has been adopted by considering the fact that the evaporation takes place around the evaporation temperature. The modified rate equation which mathematically takes the same form as the Clausius–Clapeyron equation, for the evaporation rate near the evaporation temperature, T_{evp}, is given by:

$$R_{evp} = k_{evp} X_l \underbrace{\exp(-\frac{E_a}{R_g}(\frac{1}{T} - \frac{1}{T_{evp}}))}_{f_{phase}} \tag{11}$$

where k_{evp} is the evaporation rate constant at the evaporation temperature (1/s), R_g is the gas constant (J/(K·mol)), E_a is the activation energy (J/mol). Evaporation of water utilizes evaporation enthalpy, and then $E_a = H_{evp} M_w$ and M_w is the molecular weight of the water (kg/mol), T_{evp} is the evaporation temperature (K) (reference temperature), and f_{phase} is a function that describes the phase change coefficient.

Eq. (11) can describe the evaporation rate, because (1) at lower temperatures (far below T_{evp}), the value of f_{phase} is close to 0, and thus the rate of evaporation is close to zero. On the contrary, when T is close to T_{evp}, the value of f_{phase} is close to 1, and the rate is close

Please cite this article in press as: Feyissa, A.H., et al. Modelling of coupled heat and mass transfer during a contact baking process. Journal of Food Engineering (2011), doi:10.1016/j.jfoodeng.2011.05.014

to the rate at T_{evp}, (2) when Eq. (11) is combined with the above governing model Eqs. (1), (6), and (7), the resulting set of equations describes the heat and mass transfer during the contact baking process for the entire heating period (heating and evaporation phase), without any discontinuity. Thus it eliminates numerical problems as well. In this study, the value of the parameter k_{evp} (rate constant of evaporation) is estimated together with the other unknown parameters by comparing the numerical results of the current model with measured experimental data as described in Section 3.4.

2.4. Thermo-physical properties

Thermo-physical properties are given in Table 1 (appendix A).

3. Materials and methods

3.1. Sample preparations

Pancake batter was prepared by mixing 50 g egg white, 30 g egg yolk, 150 g of milk, 125 g of wheat flour and 20 g of sugar. For every baking experiment, 50 g of pancake batter was used to make a pancake with an approximate thickness of 8 mm.

The initial composition of the pancake was estimated from the composition of the ingredients, and was found to be 56.1% water, 6.9% protein, 33.8% carbohydrate and 3.2% fat (%w/w, mass basis). For cross-validation, a dry matter analysis was made to determine the initial water content in the pancake batter. The water content (%w/w) of the pancake batter was measured by drying for 24 h at 105 °C (Nielsen 1994) and found to be (55.6 ± 0.2)%, (mean ± SD). The small difference (0.5%) between the calculated and the measured water content may be due to a slight evaporation loss during the mixing of the ingredients.

3.2. Baking and experimental setup

3.2.1. Heating rig

The heating rig was constructed with a 300 × 300 × 25 mm aluminium slab cast of the alloy AA-6082 (AlMgSi1). The aluminium slab was placed on a thermostated hot-plate of 300 × 300 mm (KR433-U12, Svend Nielsen A/S, DK) which has a maximum capacity of 3 KW. A PT100, class B temperature sensing resistor in a flexible stainless steel sheath (IEC60751, Labfacility, UK) is inserted into a hole which is drilled into the centre of the aluminium slab. The sides and bottom of the heating rig are insulated with Fiberfrax Duraboard MD, 50 mm (Unifrax, UK). The heating rig temperature set point was controlled within +/− 1 °C with a proportional-integral-derivative controller (PID controller) for temperature set points in the range of 100–300 °C. The entire heating rig is placed on a balance (Signum 1, Sartorius, VWR, DK). The balance has a maximum capacity of 35 kg and an accuracy of 0.1 g. The balance is connected to a computer to allow continuous monitoring of the mass. The mass data is recorded every second by the program Sartoconnect (version 3.5).

3.2.2. Baking disk and position of sensors

A circular baking disc with a diameter of 90 mm and a thickness of 5 mm was used for the pancake baking experiments. The experimental set up is shown in Section 2.1 (Fig. 1a). The baking disc is made of 5754-aluminum (domain 3, Fig 1a). A removable stainless steel ring (domain 4, Fig. 1a) was made to fit to the aluminium disc during baking experiments. The higher thermal expansion of aluminium as compared to stainless steel results in expansion of the aluminium plate during heating such that it fits tightly to the stainless steel ring when the plate is heated.

To fix the temperature sensors at a given position within the pancake batter, a temperature sensor holder (E) was constructed at the centre of the baking disc, as shown in Fig. 1b. Four holes were made through the sensor-holder (E), which is made of Teflon. In each hole, temperature sensors (T-type thermocouples) were placed at four different positions (A = 6.4 mm, B = 4.8 mm, C = 3.2 mm and D = 1.6 mm, measured as the distance from the bottom surface), as illustrated in Fig. 1b. The weight of the baking disc within the above setup (baking disc and temperature sensor holder and four sensors) was measured separately. Then, approximately 50 g of pancake batter was taken from the pre-prepared pancake batter (see Section 3.1) and gently added into the baking disc. The initial weight was then recorded. The pancake batter sample with sensors and baking disc were finally placed on the heating rig and the pancake batter sample was baked for 20 min. This procedure was repeated for all the samples, each time performing all the measurements (weight loss and temperature measurements).

3.3. Data collection/measurement

All the temperature sensors (T-type thermocouples) were connected to the computer with data logger (Tc-08 Pico Technology, Cambridgeshire, UK) where the temperature is recorded every second. At the same time, mass loss due to evaporation was monitored continuously by recording the weight every second, using the set up described in Section 3.2.

3.4. Effect of heating rig temperature

The temperature and mass measurements were performed at three different temperature set points (160, 200 and 240 °C) (see Section 3.2). The measurements were repeated four times for each temperature set point. Average temperature and water content profiles – where the latter was obtained from mass loss data – were computed for each temperature set point.

3.5. Model solution, calibration and validation

The model equations were solved in COMSOL using the Finite Element Method. The set up in COMSOL consists of two domains: the product (domain 5, in Fig. 1a) and the baking disc (domain 3, in Fig. 1a). The governing equations of heat and mass transfer with their constitutive equations and initial values were set for each domain. The generated mesh was refined (e.g., at the boundaries where there is high gradient) to improve the accuracy of the numerical results. The impact of mesh quality on the convergence and coherence of the results were checked by performing a series of simulations with increasingly finer mesh until the change in mesh density no longer had an impact on the solution. The initial values were obtained from the measurements; the values of the input parameters used in the model are given in appendix B (Table 2). The model was calibrated and validated using the available experimental data (measured temperature, see Section 3.3a) obtained during the baking of the model food. The temperature measured at position A was used for parameter estimation while the remaining temperature measurements were used for model validation. The unknown parameters in the model were estimated using the least squares method by comparing the simulated and experimental temperature profiles. The resulting solution of the parameter estimation problem is a set of model parameters which minimizes the value of the objective function. The objective function is the sum of the squared differences between the simulated temperature (T_A) and the measured temperature profile ($T_{A,exp}$). The measured and simulated temperature values were taken at 10 s sampling intervals. For the minimization of the objective function, the

Please cite this article in press as: Feyissa, A.H., et al. Modelling of coupled heat and mass transfer during a contact baking process. Journal of Food Engineering (2011), doi:10.1016/j.jfoodeng.2011.05.014

Trust-Region Methods numerical algorithm (within the Matlab® environment), suited for nonlinear estimation problems, was used. The model solution, calibration and validation were implemented in the *COMSOL-Matlab® version 3.5* interface environment.

4. Results and discussion

4.1. Experimental temperature profile

The measured temperature profiles at different positions within the pancake batter (positions *A*, *B*, *C* and *D*, respectively) for the three temperature set points are plotted in Fig. 2a. Generally, two major distinct periods can be distinguished in the temperature profiles: the heating period (sensible heat dominant zone, $t < 350$) and the evaporation period (latent heat dominant zone, $t > 350$) (for $T_{set} = 160$ °C, see Fig. 2b). In the heating period (preheating), most of the supplied heat energy (from the heating rig) is used to rise the temperature of the product (pancake batter). The heating period is short compared to the evaporation period, particularly for the position in the product that is closest to the bottom surface (e.g. at position D, about 200 s, Fig. 2a top-left).

During the evaporation period, where the temperature curves only rise slowly, nearly all of the supplied heat to the product is used for evaporating the water. In the evaporation period, with a temperature set point of 160 °C, the temperature at position C is more or less stable around the boiling point of water (attains $T = 100$ °C at $t = 600$ s), while towards the end of the baking process, there is a slight temperature rise ($t = 1200$ s, $T = 103$ °C). For the same temperature set point of 160 °C, however, the temperatures at the positions *A* and *B* remain below 100 °C for the entire period of baking. Also, they remain almost constant (*approximately at* $T_A = 89$ °C and $T_B = 95$ °C, respectively) for most of the heating time. The length of the period in which this constant temperature level is observed, is getting shorter as temperature sensor position moves from the top to the bottom surface.

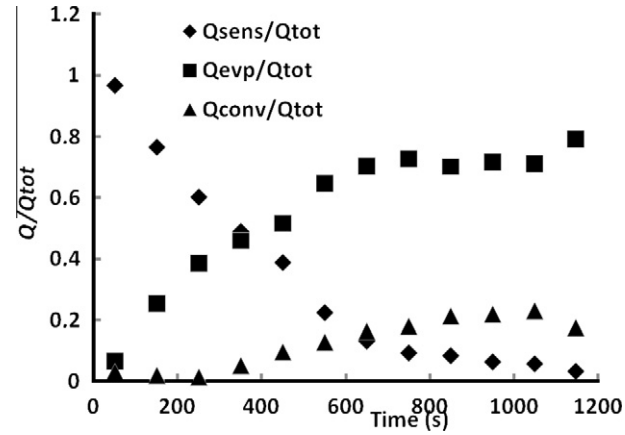

Fig. 2b. The extent heat used for evaporation, sensible heat and heat lose by convection to environment: (diamond = fraction of sensible heat consumed), (square = fraction of latent heat – heat used for evaporation of water), and (triangle = the fraction of heat loss to environment by convection. Notice, the latent heat was obtained from measured mass loss and the heat of evaporation; sensible heat was calculated at average product temperature using the measured temperature.

The heat transport with the vapour was neglected in the model. This assumption can be justified by a crude total energy balance (with $T_{set} = 160$ °C in the period from $t = 600$–1200 s) as follows: (i) the heat of evaporation (Q_{evp}) based on the measured mass loss ($= 14.2 \times 10^{-4}$ kg) and latent heat (= 2300 kJ/kg) is estimated to be around 4.1 kJ), (ii) the heat loss by convection to surrounding air, $Q_{conv,loss}$ is 1.56 kJ, which was obtained from ($h_{top} = 8$ w/(m^2 K), area, $A = 63.59 \times 10^{-4}$ m^2, $dT = (86–35)$ °C = 31 °C, $dt = 1200–600 = 600$ s), (iii) thus, the total heat loss by convection and evaporation, Q_{total} is 5.66 kJ. The total heat transferred between position *A* and *C*, for the same period ($t = 600$–1200 s), is Q_{total}. The average temperature gradient between point *A* and *C*, ($T_C - T_A$) for the same

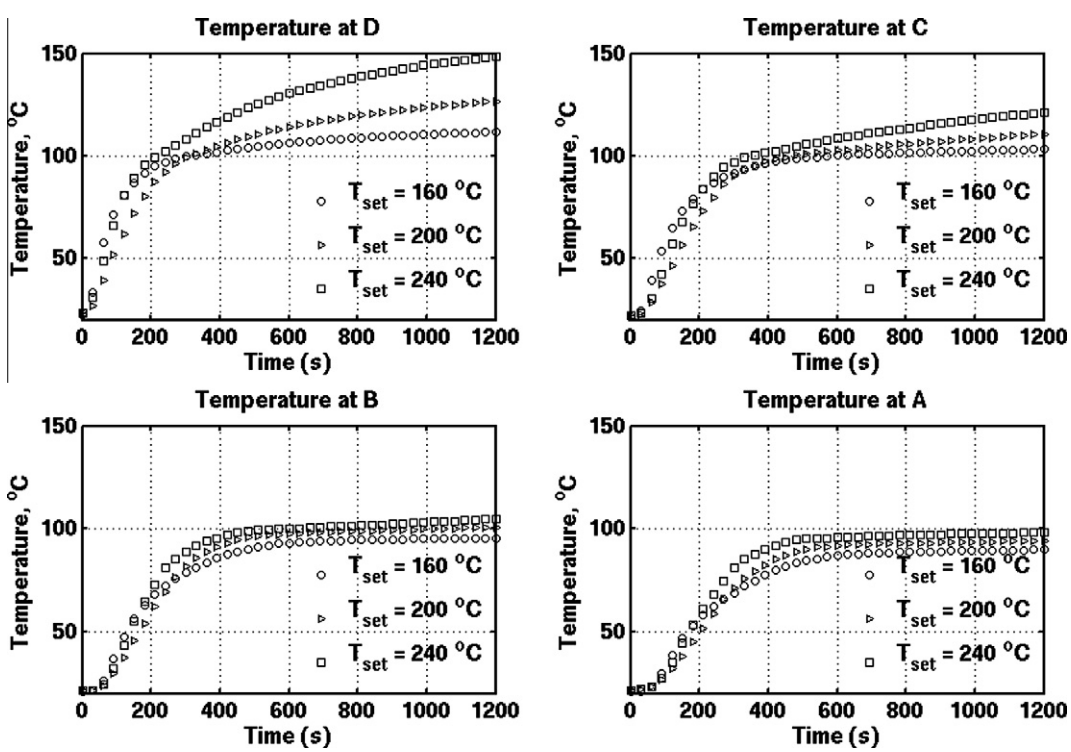

Fig. 2a. Temperature profile at different positions (position *A*, *B*, *C* and *D*) with temperature set point of 160 °C, 200 °C, and 240 °C. The data are only shown with a sampling interval of 30 s, for clarity.

Please cite this article in press as: Feyissa, A.H., et al. Modelling of coupled heat and mass transfer during a contact baking process. Journal of Food Engineering (2011), doi:10.1016/j.jfoodeng.2011.05.014

period is roughly 13 °C, which was obtained from measured data (T_{set} = 160 °C, position *A* and *C*, Fig. 2a). The apparent thermal conductivity (between the position *A* and *C*) is 0.36 w/(m K), which is obtained from: Q_{total} = 5.66 kJ, $(T_C - T_A)$ = 13 °C, $dz = z_A - z_C$ = 3.2 mm, $A = 63.59 \times 10^{-4}$ m^2 and dt = 600s). The value of apparent thermal conductivity is equivalent to the thermal conductivity of pancake batter calculated from its composition. This implies that the heat transport by other mechanisms (including the heat transfer with vapour) is insignificant.

At position D, in the evaporation period, an early rise of the temperature above 100 °C was observed. The early rise in temperature above the boiling point of water is explained by the drying-out effect at the bottom surface due to vigorous evaporation. This means that, as the liquid water content diminishes near the bottom surface: (1) an insulating layer is formed at the bottom surface, which reduces the thermal conductivity, and in turn the thermal diffusivity; and (2) less and less energy is consumed by evaporation at the bottom surface layer, compared to earlier times where the concentration of water was higher. This effect is more pronounced with higher temperature set points, especially at position D (Fig. 2a).

4.2. Effect of temperature set point

In the heating period, the temperature profiles with the three temperature set points follow each other and there is only a slight difference in temperature profile between each temperature set point (Fig. 2a). However, in the evaporation period, the three temperature set points have resulted in different product temperature profiles. This is particularly the case at position D (Fig. 2a, top-left). The increase of the temperature set point leads to a higher evaporation rate, and as a consequence a faster drying out, which in turn induces a temperature rise. Towards the end of the baking process (t = 1200 s), the product temperature at position D attains a temperature of 112, 127 and 148 °C, with temperature set points of 160, 200 and 240 °C, respectively. The temperature profile of the product closer to the bottom surface is very sensitive to the temperature set point, while this sensitivity decreases as the position of the temperature sensor is further away from the bottom surface (Fig. 2a, compare at four positions, *D*–*A*). The effect of the temperature set point on the product temperature profile at position *A* is quite small compared to the effects observed at position *D*. Besides, the spatial variation of temperature (temperature gradient) in the pancake batter is relatively smaller with lower temperature set point compared to higher temperature set points. This implies that the quality of the end product related to temperature, is more uniform when baked at a lower temperature set point compared to a higher temperature set point.

Fig. 3 shows the corresponding average water content of the product when baked at the three temperature set points (160, 200, and 240 °C). The average water content of the product decreases as a function of time. In the early stages of the experiment (t < 200 s), the rate of decrease is relatively low, and visually there is no difference between the three average water content profiles. The turning point for the rate of decrease is around t = 200 s, when the bottom region of the product has reached the evaporation temperature (Fig. 2a, at position D). After that time, t = 200 s, the average water content of the product decreases rapidly, and the rate is different for the three temperature set points (Fig. 3). The rate of evaporation, and thus the rate of weight loss, increases with increasing temperature set point. The latter is convincingly illustrated by the average slopes of the water content profiles: (−1.4, −2.3 and −3.8)·10^{-4} kg/kg/s, for a temperature set point of 160, 200, and 240 °C, respectively. This also agrees with the result obtained elsewhere during the baking of crumpet (Pyle, 2005). Pyle (2005) reported that the rate of evaporation during the baking of crumpet at 270 °C is about twice that of at 220 °C.

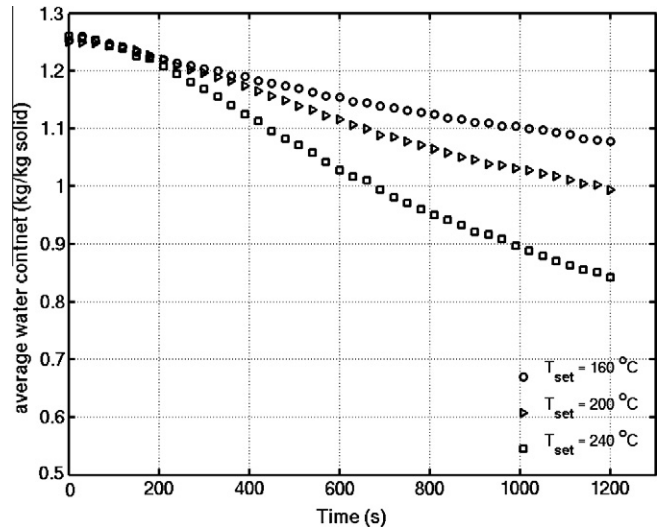

Fig. 3. Average water content (kg of water/kg of solid) during baking of the pancake batter at three different temperature set points (160, 200, and 240 °C, respectively). The data are only shown with a sampling interval of 30 s, for clarity.

4.3. Model calibration and validation

4.3.1. Model calibration

The model equations of heat and mass transfer developed in Section 2 were solved and the unknown parameters of the model were estimated. The parameters (k_{evp} and h_{bot}) were estimated by fitting the simulated temperature profile to the data available for position *A* (T_{set} = 160 °C). The estimation results, presented as nominal value ± confidence interval of the parameter, are: k_{evp} = (11.4 ± 0.2)·10^{-5} and h_{bot} = 360.7 ± 12.8. The model fit is shown in Fig. 4.

4.3.2. Model validation

The model was validated by comparing the simulated and measured temperature profiles at the three other positions (B, C, and D), using the parameters estimated on the basis of the data collected at position *A*. Results of that validation are presented in Fig. 5 (T_{set} = 160 °C), and show a good agreement between simulated and measured temperature profiles at positions B and C. At

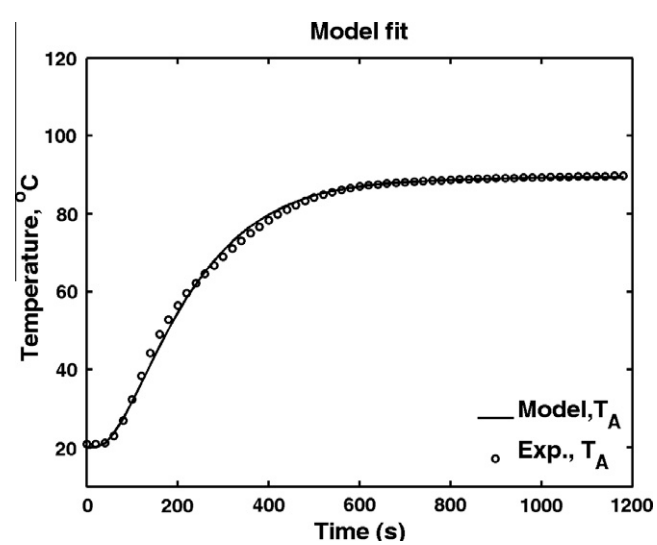

Fig. 4. Model fit: comparison between measured (o) and simulated (-) temperature profile at position *A* (*Tset* = 160 °C).

Please cite this article in press as: Feyissa, A.H., et al. Modelling of coupled heat and mass transfer during a contact baking process. Journal of Food Engineering (2011), doi:10.1016/j.jfoodeng.2011.05.014

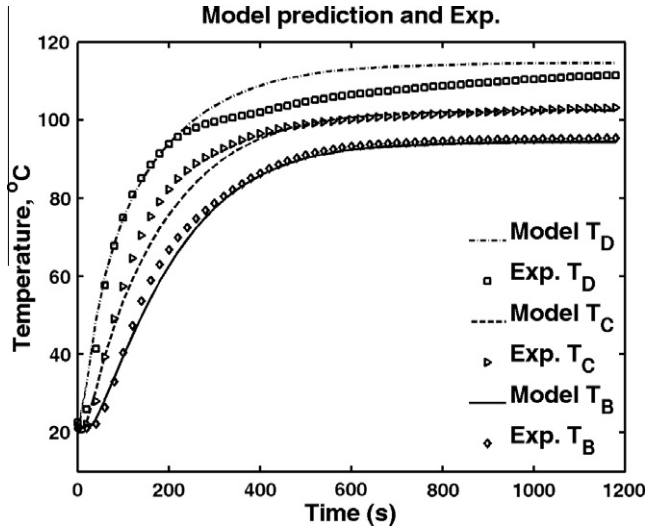

Fig. 5. Model validations: Simulated and measured temperature profiles compared at different positions (*B*, *C* and *D*) for a temperature set point of 160 °C.

position D, the simulated and measured temperature profile show a good agreement for the heating period, but there is a clear deviation between the simulated and measured temperature profile in the evaporation period (Fig. 5, at position D). This deviation is probable due to: (1) the burning and crust formation at the bottom surface, which is not well-described in the model; (2) uncertainty on the sensor position: the sensor at position D is less stable compared to the temperature sensors at other positions. The measured temperature at position D, from around $t = 200$ s, has large variation, this is probable due to the sensor position (D) might move slightly upward as a result of vigorous water vapour generation which can create upward pressure.

Moreover, the model was validated by comparing the simulated and measured temperature profile at other temperature set points (200 and 240 °C) at position *A* (Fig. 6) and B (Fig. 7). The simulated results in Figs. 6 and 7 were obtained on the basis of the model for the three temperature set points with all the same settings (as above, obtained in the model calibration, $T_{set} = 160$ °C), except that the thermal conductivity for the set points 200 and 240 °C is reduced by 10% compared to the value at the set point of 160 °C.

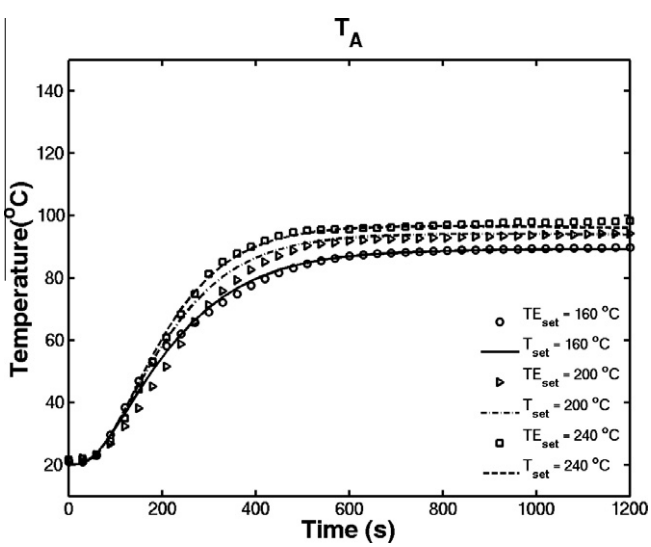

Fig. 6. Comparison of simulated and measured temperature profiles at position *A* with different temperature set point (160, 200, and 240 °C). The data are only shown with a sampling interval of 30 s, for clarity.

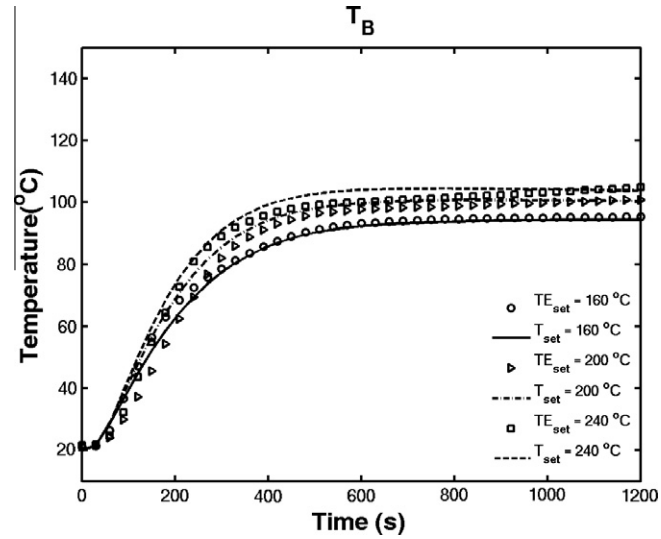

Fig. 7. Comparison of simulated and measured temperature profiles at position B with different temperature set point (160, 200, and 240 °C). The data are only shown with a sampling interval of 30 s, for clarity.

The reduced value of the thermal conductivity for higher temperature set points is motivated by the increased insulation effect at the bottom surface. This insulation effect, due to drying out and crust formation, is compensated in the model by reducing the thermal conductivity value. The higher temperature set point creates more crust and burned surface at the bottom surface of the product, and more insulating layer compared to the lower temperature set point.

5. Conclusion and perspectives

In this work, a mathematical model of coupled heat and mass transfer of a contact baking process was developed, taking into account multiphase water transport and local evaporation. The developed model gives a good understanding of the contact baking process, by predicting the temperature and water content profile within the product. A good agreement between the measured and the predicted temperature profile was obtained at positions *A*, B, and C, which allows us to conclude that the developed model of heat and mass transfer is suitable for describing the contact baking process. Moreover, the experiments also showed that the temperature set point has a significant effect on the product, and more specifically on the obtained temperature profiles and the mass loss.

The developed model of heat and mass transfer is a useful tool in developing an improved process, where it can be used in the optimization of the contact baking process by performing 'in silico' experiments, for example to study the effect of different process parameters on the baking process. Moreover, the developed process model can in principle be integrated with other quality attribute models as well, in order to perform further optimization of the contact baking process. For example, browning reactions take place in the product during baking, where temperature and water content are two important factors responsible for the change of colour (Zanoni et al., 1995; Purlis, 2010) due to such browning reactions. To study such phenomena the kinetics of the browning reactions could be integrated with the heat and mass transfer model presented here.

Acknowledgement

Aberham Hailu Feyissa would like to thank DTU for a Ph.D. grant under the aegis of Food-DTU.

Appendix A

Table 1
Thermo-physical properties (Rao et al., 2005).

Density:	$\rho = \frac{1-\varepsilon}{\sum_i \frac{y_i}{\rho_i}}$	(A.1)
y_i is the mass fraction of each component (water, protein, carbohydrate and fat), kg/kg of sample and ε is the porosity of the product.		
Specific heat capacity of product:	$c_p = \sum c_{pi} y_i$	(A.2)
	$c_{pi} = c_0 + c_1 T - c_2 T^2$	
where c_0, c_1 and c_2 are coefficients for the heat capacity of the components		
Thermal conductivity (function of moisture content):	$k_p = k y_w + \varepsilon k_{air}$	(A.3)
Conversion between the X(kg of water/kg solid) and y_w (kg of water/kg of sample):	$y_w = X/1 + X$	(A.4)

Appendix B

Table 2
Input parameter values.

Parameter	Value	Parameter	Value	Parameter	Value
$y_{p,o}$[b]	0.07 kg/kg	ρ_f[d]	920 kg/m^3	D_v[e]	8×10^{-7} m^2/s
$y_{c,o}$[b]	0.33 kg/kg	ρ_p[d]	1320 kg/m^3	D_l[g]	1×10^{-9} m^2/s
$y_{f,o}$[b]	0.03 kg/kg	ρ_c[d]	1600 kg/m^3	k[d]	0.65 W/(m·K)
X_{lo}[a]	1.25 kg/kg	ρ_w[d]	1000 kg/m^3	$X_{l,air}$[c]	0 kg/kg
T_o[a]	293.15 K	ρ_s[b]	1467 kg/m^3	k_{air}[d]	0.023 W/(m K)
z_5[a]	0.008 m	ρ_{Al}[f]	2660 kg/m^3	k_l[e]	2.3×10^{-11} m/s
z_3[a]	0.005 m	c_{pAl}[f]	960 J/(kg.K)	T_{set}[c]	433.15 K (160 °C)
R_g	8.314 J/(K mol)	k_{Al}[f]	150 W/(m·K)	T_{air}[a]	308.15 K (35 °C)
M_w	0.018 kg/mole	$X_{v,air}$	0.0062 kg/kg	T_{evp}[c]	373.15 K
H_{evp}	2.3×10^{-6} J/kg	k_v[e]	$9.6 \cdot 10^{-5}$ m/s	h_{top}[b]	8 W/(m^2 s)

Superscripts: a, measured; b, calculated or estimated; c, set (assumed); d, (Rao et al., 2005); e, obtained from (Thorvaldsson and Janestad, 1999); f, Obtained from (Martienssen and Warlimont, 2005); g, (Toledo,1991). Subscripts: p, protein; c, carbohydrate; f, fat; w, water.

References

Cengel, Y.A., 2007. Heat and Mass Transfer. A Practical Approach. McGraw-Hill Education, London.
Gupta, T.R., 2001. Individual heat transfer modes during contact baking of Indian unleavened flat bread (chapati) in a continuous oven. Journal of Food Engineering 47 (4), 313–319.
Huang, H., Lin, P., Zhou, W., 2007. Moisture transport and diffusive instability during bread baking. SIAM Journal of Applied Mathematics 68 (1), 222–238.
Lee K.H., & Taylor T.A. (1996). Modeling of bread baking with simultaneous heat and mass transfer and structural changes. United States of America, Institute of Food Technologists [1996 Annual Meeting], 20.
Martienssen, W., Warlimont, H. (Eds.), 2005. Springer handbook of condensed matter and materials data. Springer, Heidelberg, pp. 1–1119.
Mondal, A., Datta, A.K., 2008. Bread baking – A review. Journal of Food Engineering 86 (4), 465–474.
Nielsen, S.S. (Ed.), 1994. Introduction to Chemical Analysis of Foods. Jones and Bartlett, Boston, pp. 96–100.
Pan, Z., Singh, R.P., 2002. Heating Surface Temperature and contact-heat transfer coefficient of a clam-shell grill. Lebensmittel-Wissenschaft und -Technologie 35 (4), 348–354.
Pan, Z., Singh, R.P., Rumsey, T.R., 2000. Predictive modeling of contact-heating process for cooking a hamburger patty. Journal of Food Engineering 46 (1), 9–19.
Peters, B., Schroder, E., Bruch, C., Nussbaumer, T., 2002. Measurements and particle resolved modelling of heat-up and drying of a packed bed. Biomass and Bioenergy 23 (4), 291–306.
Purlis, E., 2010. Browning development in bakery products – A review. Journal of Food Engineering 99 (3), 239–249.
Pyle, D.L., 2005. Crumpet structures: experimental and modelling studies. Food and Bioproducts Processing 83 (2), 81–88.
Rao M.A., Rizvi, S.H., & Datta A.K. (Eds.), 2005. Engineering properties of foods, third ed. Taylor and Francis, pp. 738.
Sablani, S.S., Marcotte, M., Baik, O.D., Castaigne, F., 1998. Modeling of simultaneous heat and water transport in the baking process. Lebensmittel-Wissenschaft und -Technologie 31 (3), 201–209.
Therdthai, N., Zhou, W., 2003. Recent advances in the studies of bread baking process and their impacts on the bread baking technology. Food Science and Technology Research (3), 219–2269.
Thorvaldsson, K., Janestad, H., 1999. A model for simultaneous heat, water and vapour diffusion. Journal of Food Engineering 40 (3), 167–172.
Toledo, R.T., 1991. Fundamentals of Food Process Engineering. VNR, New York.
Wichchukit, S., Zorrilla, S.E., Singh, R.P., 2001. Contact heat transfer coefficient during double-sided cooking of hamburger patties. Journal of Food Processing and Preservation 25 (3), 207–221.
Zanoni, B., Peri, C., Bruno, D., 1995. Modelling of browning kinetics of bread crust during baking. Lebensmittel-Wissenschaft und -Technologie 28 (6), 604–609.

Please cite this article in press as: Feyissa, A.H., et al. Modelling of coupled heat and mass transfer during a contact baking process. Journal of Food Engineering (2011), doi:10.1016/j.jfoodeng.2011.05.014

Paper IV

Uncertainty and Sensitivity Analysis: Mathematical Model of Coupled Heat and Mass Transfer for a Contact Baking Process

A.H. Feyissa[1,*], K.V. Gernaey[2], J. Adler-Nissen[1]
[1] Food Production Engineering, National Food Institute, *DTU*
[2] Center for Process Engineering and Technology, Department of Chemical and Biochemical Engineering, *DTU*
*Corresponding author: Søltofts Plads, 2800, Kgs. Lyngby, DK (e-mail: abhfe@food.dtu.dk)

Abstract- Similar to other processes, the modelling of heat and mass transfer during food processing involves uncertainty in the values of input parameters (heat and mass transfer coefficients, evaporation rate parameters, thermo-physical properties, initial and boundary conditions) which leads to uncertainty in the model predictions. The aim of the current paper is to address this uncertainty challenge in the modelling of food production processes using a combination of uncertainty and sensitivity analysis, where the uncertainty analysis and global sensitivity analysis were applied to a heat and mass transfer model of a contact baking process. The Monte Carlo procedure was applied for propagating uncertainty in the input parameters to uncertainty in the model predictions. Monte Carlo simulations and the least squares method were used in the sensitivity analysis: for each model output, a linear regression model was constructed and the standardized regression coefficients (SRCs) and R^2 were computed. The effect of input parameters on model predictions was calculated, and the relative impact of the parameters was ranked. Results of the uncertainty and sensitivity analysis can be used to prioritize future experimental efforts.

Key words: Food process, Modelling, COMSOL-MATLAB, Heat and mass transfer, Uncertainty and Sensitivity analysis, Monte Carlo method, Finite Element Method

1. Introduction

The purpose of a mathematical model of the heat and mass transfer in a food production process is to describe the physical processes as accurately as possible for the given food production process. Specifically for operations such as baking and roasting, a model of heat and mass transfer can play an important role in analyzing the process. Indeed, setting up the equations of the model, defining the model assumptions, analyzing the model and

its simulation output and, finally, comparing that simulation output with experimental data usually results in a much deeper understanding of the process and the main phenomena determining its output dynamics. Baking and roasting operations are usually rather challenging to model due to their complexity, since those operations often involve heat and mass transfer simultaneously with many complex physical-chemical processes such as evaporation of water, crust formation, browning reactions, denaturation of proteins, and gelatinization of starch (Lee et al., 1996; Mondal and Datta, 2008; Sablani et al., 1998; Therdthai and Zhou, 2003). The uncertainty in the modelling of heat and mass transfer in such systems is mainly associated with: (1) model assumptions (assumptions made on the physics for simplification), and (2) the values of the parameters.

The first type of uncertainty – also called structural uncertainty – relates to the model assumptions and thus also to the model structure. Such uncertainties can to some extent be reduced by developing the model from first principles. Indeed, by considering the crucial physical phenomena, the physical reality is translated into a detailed mathematical model. However, in many cases only the main physical phenomena are incorporated in the model, in order to simplify the structure of the resulting model according to a number of model assumptions, thus resulting in a mismatch between predicted (model) dynamics and real process dynamics. The second type of uncertainty, the uncertainty on parameter values – required for the numerical solution of a mechanistic model, and for example related to material properties and transport coefficients – can be attributed to the fact that the parameters are often not available or come with a large inherent uncertainty since the phenomena taking place are poorly understood. Specifically for food products, the values of parameters reported in the literature are not consistent, which is due to the inherent complexity and variability of a food matrix. A good example to illustrate this is the extensive study on thermo-physical properties of bakery products (Baik et al., 2001~~,~~; Rask, 1989). The uncertainty in the values of parameters is a great challenge in many branches of the food industry, and results in difficulties when using models for predictions as well as problems in correctly setting the process parameters (Wong et al., 2006). One way to cope with this challenge is to take into account the uncertainty in the

input parameters, and to evaluate their impacts on the predictions. This is precisely what will be illustrated in this manuscript.

Uncertainty and sensitivity analysis have been used in many different disciplines for the evaluation of models. Some examples of applications are: quality assessment of composite indicators (Saisana et al., 2005), environmental models (Campolongo and Saltelli, 1997), ecological models (Cariboni et al., 2007), a blood flow and blood pressure model (Ellwein et al., 2008), a hydrology model (Ratto et al., 2007), chemical models (Saltelli et al., 2005), a fermentation model (Sin et al., 2009) and food risk models (Frey and Patil, 2002). Uncertainty analysis is used to map input uncertainty to output uncertainty, while sensitivity analysis is applied to decompose input uncertainty, i.e. to identify the parameters that are most influential on the model outputs.

Two general methods of sensitivity analysis are used in the literature (Dimov and Georgieva, 2011), namely the local and global methods. In the local sensitivity analysis method, also called one factor at a time method, small variations of inputs around a given value are introduced one at a time, and the resulting change of the value of the output is quantified. The local sensitivity analysis is used frequently, due to its relatively low computational burden. Global sensitivity analysis methods take into account all the variation in the values of the input on the prediction of the output variables. In other words, global methods will cover the whole parameter space. In this manuscript, we will apply a global sensitivity analysis method which is based on Monte Carlo simulations followed by linear regression on the Monte-Carlo simulation output. This method is also known as standardized regression coefficients (SRC) method (Saltelli et al., 2008).

The objective of the present work is thus to quantify the uncertainty in model predictions for a model describing coupled heat and mass transfer (CHMT) during a contact baking process, and to identify and rank the parameters based on their relative impact. The manuscript provides a description of the methodology, the model implementations, and the uncertainty and sensitivity analysis results. For the latter, special consideration was given to answering the following questions: (1) how does the model prediction (model outputs) change with respect to the change in the values of the parameters?; (2) which specific parameters need to be measured or estimated accurately in order to achieve better

predictions? That means that we will present results on the relative impact of parameters, their ranking, and how those results can be used to refine the model for further research, in order to better capture the fundamental behavior of the product as a consequence of heat and mass transfer during a contact baking process.

Nomenclature	
c_{pp}, and c_{pAl},	Specific heat capacity ($J \cdot kg^{-1} \cdot K^{-1}$) of product, and aluminium, respectively
D_l and D_v	Liquid and vapour diffusion coefficient ($m^2 \cdot s^{-1}$),respectively
E_a	Activation energy ($kJ \cdot mol^{-1}$)
h_{bot}	Overall heat transfer coefficient at the bottom boundary of the baking disc (rig)
H_{evp}	Latent heat of evaporation ($J \cdot kg^{-1}$)
h_{top}	Heat transfer coefficients at the top surface (at air-product interface) ($W \cdot m^{-2} \cdot K^{-1}$)
k_{evp}	Evaporation rate constant at the evaporation temperature (s^{-1})
k_l and k_v	Liquid and vapour mass transfer coefficient ($m \cdot s^{-1}$), respectively
k_p, k_{Al}, and k_{air}	Thermal conductivity ($W \cdot m^{-1} \cdot K^{-1}$) of product, aluminium, and air, respectively
M_w	The molecular weight of water ($kg \cdot mol^{-1}$)
R_{evp}	Evaporation rate ($kg \cdot kg^{-1} \cdot s^{-1}$)
R_g	The gas constant ($J \cdot K^{-1} \cdot mol^{-1}$)
T	Temperature (K)
t	Time (s)
T_{air}	Surrounding air temperature (K)
T_{evp}	Evaporation temperature (K)
T_{set}	Temperature set point (K)
X_l and X_v	Liquid and vapour water content (kg of water$\cdot$kg^{-1} of solid), respectively
Y	Output variable [*TA, TB,…], vector*

y_i	The mass fraction of each component (water, protein, carbohydrate and fat)
z	The variation along the z direction
ρ_p, ρ_{Al} and ρ_{air}	Density ($kg \cdot m^{-3}$) of product, aluminium, and air, respectively
e_{im}	Error of regression model
β	Normalized regression coefficient
ε	Porosity
θ	Uncertain input parameters [k_{evp} k_v k D_v …], vector
Subscripts	
air	Air
Al	Aluminium
i	Index of Monte Carlo simulations (a vector)
j	Index of parameter vector
l and v	Liquid and vapour
m	Index of output vector
p	Product (pancake batter)

2 Methodology

2.1 Model of contact baking process (case study)

In this manuscript, the contact baking process is considered as a system of interest, where a pancake batter is used as suitable model food. The contact baking process involves heat and mass transfer (liquid water and water vapour), where the state variables in the model are temperature, liquid water concentration (X_l), and water vapour concentration (X_V). The coupled heat and mass transfer (*CHMT*) of the contact baking process is described with a system consisting of partial differential equations (PDEs) and constitutive equations, (Feyissa et al., 2011) and the model equations are briefly summarized in the Table 1.

Table 1-Model equations of *CHMT* during the contact baking process

Heat transfer:

GE:

$$\begin{cases} \rho_p c_{p,p} \dfrac{\partial T}{\partial t} = \dfrac{\partial}{\partial z}\left(k_p \dfrac{\partial T}{\partial z}\right) - \rho_s H_{evp} R_{evp} & (1) \\ \rho_{Al} c_{p,Al} \dfrac{\partial T}{\partial t} = k_{Al} \dfrac{\partial^2 T}{\partial^2 z} & (2) \end{cases}$$

BC:

$$\begin{cases} -k_{Al} \left.\dfrac{\partial T}{\partial z}\right|_{z=-0.005} = h_{bot}\left(T_{set} - T\right) \\ \underbrace{-k_{Al} \left.\dfrac{\partial T}{\partial z}\right|_{z=0}}_{baking\ disk} = \underbrace{\left(-k_p \left.\dfrac{\partial T}{\partial z}\right|_{z=0}\right)}_{pan\ cake} + q_{evp}\Big|_{z=0} \\ -k_p \left.\dfrac{\partial T}{\partial z}\right|_{z=0.008} = h_{top}\left(T - T_{air}\right) \end{cases}$$

Mass transfer:

GE:

$$\begin{cases} L \rightarrow \dfrac{\partial X_l}{\partial t} = D_l \dfrac{\partial^2 X_l}{\partial^2 z} - R_{evp} & (3) \\ V \rightarrow \dfrac{\partial X_v}{\partial t} = D_v \dfrac{\partial^2 X_v}{\partial^2 z} + R_{evp} & (4) \end{cases}$$

BC:

$$\begin{cases} -D_l \left.\dfrac{\partial X_l}{\partial z}\right|_{z=0} = D_v \left.\dfrac{\partial X_v}{\partial z}\right|_{z=0} = -\left.\dfrac{q_{evp}}{H_{evp}\rho_s}\right|_{z=0} \\ -D_l \left.\dfrac{\partial X_l}{\partial z}\right|_{z=0.008} = k_l\left(X_l - X_{l.air}\right) \\ -D_v \left.\dfrac{\partial X_v}{\partial z}\right|_{z=0.008} = k_v\left(X_v - X_{v,air}\right) \end{cases}$$

Constitutive equations:

$$R_{evp} = k_{evp} X_l \underbrace{\exp\left(-\frac{E_a}{R_g}\left(\frac{1}{T} - \frac{1}{T_{evp}}\right)\right)}_{f_{phase}}$$

TPP:

$$\begin{cases} \rho = \dfrac{1-\varepsilon}{\sum_i \dfrac{y_i}{\rho_i}} \\ c_p = \sum c_{p_i} y_i \ , \quad c_{p_i} = c_o + c_1 T - c_2 T^2 \\ k_p = k.y_w + \left(1 - y_w\right) k_{air} \ , \ y_w = X/1+X \end{cases}$$

GE: Governing equation, BC: boundary condition, L: liquid water, V: water vapour, TPP: *thermo-physical properties* of pancake batter. The domains (i.e., pancake and baking disc) and boundaries are illustrated in Fig. 1.

Equation (1) and Eq. (2) describe the heat transfer inside the pancake and inside the baking disk, respectively. Eq. (3) and Eq. (4) describe the mass transfer within the pancake, for liquid water and water vapour, respectively. The numerical simulation of the *CHMT* model is used in the prediction of the state variables as a function of time at

different positions in the pancake batter. In the CHMT model of a contact baking process, values of heat and mass transfer coefficients, phase change parameters, boundary condition parameters and thermo-physical properties (e.g. thermal conductivity) are uncertain (see 2.3).

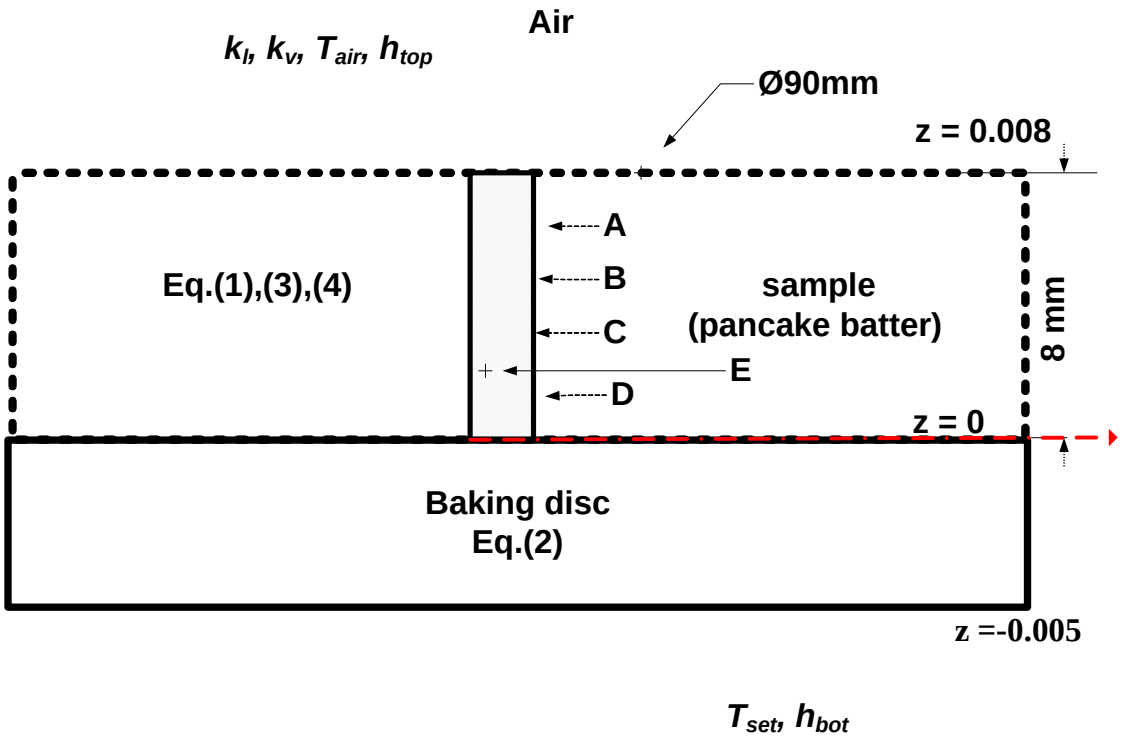

Figure 1 Simplified schematic representation for the contact baking process illustrating: (1) measurement positions within the pancake batter (A = 6.4 mm, B = 4.8 mm, C = 3.2 mm, and D = 1.6 mm from bottom surface and E = the sensor holder) and (2) the domains and the position of the boundary conditions. z =-0.005 is the baking disc and heating rig interface, z =0 is the baking disc-pancake interface and z =0.008 is the top surface of the pancake batter or pancake-air interface.

2.2 Model output variables

Four positions (A, B, C, and D) within the product were considered (Fig. 1) as the target of interest for the state variables (T, X_l, and X_v). The four positions are: A is 6.4 mm from the bottom surface (i.e. closest to the top surface); B and C are 4.8 mm and 3.2 mm from

the bottom surface, respectively (in the middle region); and D is 1.6 mm from the bottom surface (the measurement point closest to the bottom surface). Thirteen model output variables were considered: (1) the prediction of the three state variables (T, X_l, and X_v) for each of the four positions in the pancake batter gives 12 output variables, and (2) an additional output variable is the average water content of the pancake batter (X_{ave}). All the output variables are represented by the vector Y, where Y = [T_A, T_B, T_C, T_D, X_{ave}, X_{lA}, X_{lB}, X_{lc}, X_{lD}, X_{vA}, X_{vB}, X_{vC} , X_{vD}]. The output variables in Y will be used in the uncertainty and sensitivity analysis, as will be illustrated further on in the manuscript.

2.3 Model input parameters

The model input parameters were classified as: (1) parameters with fixed value, and (2) parameters with uncertain value, (Appendix A), where in the latter case, variation in the input parameter values is taken into account in the uncertainty analysis. The input parameters with uncertain values are parameters related to: (1) the boundary conditions (T_{set}, T_{air}, h_{top}, h_{bot}, k_v, k_l); (2) the initial conditions (T_o *and* X_{lo}); (3) the transfer coefficients (k, D_l, D_v,); and (4) the phase change parameters (k_{evp} , T_{evp}, H_{evp}). All the uncertain input parameters (14 parameters in total) are represented by the vector θ, where θ = [k_{evp}, T_{set} , T_{air}, h_{top}, h_{bot}, k_v, k_l, T_o, X_{lo} , T_{evp} , k, D_l, D_v , H_{evp}].

2.4 Parameter estimation

The unknown parameters in the model were estimated by fitting the simulated temperature profiles to the measured ones, as illustrated in Fig. 2. The classical least squares method was used for the solution of the parameter estimation problem. For the experimental data studied here, the objective function corresponds to the sum of the squared differences between the measured and simulated values of temperature at position A only. Temperature profiles at positions B, C and D were used for model validation. For minimization of such a function, the Trust-Region Reflective Method numerical algorithm was used.

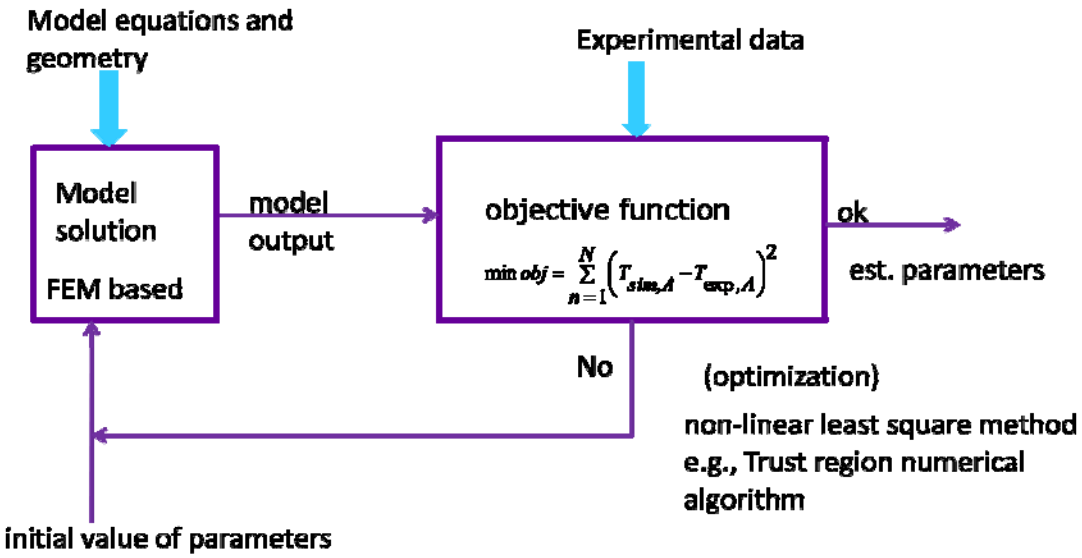

Figure 2 Schematic representation of the operation of the parameter estimation routine

2.5 Uncertainty analysis

A variety of techniques exist for the uncertainty analysis. Here, the Monte Carlo technique was chosen because it provides the most effective approach for the propagation and analysis of uncertainty for various reasons (Helton and Davis, 2003). The method is generally accepted as computationally-effective and reliable (Sin et al., 2009). Monte Carlo analysis is a probabilistically based sampling procedure used to map uncertainty from the model inputs to the model outputs (Helton and Davis, 2003). The mapping provides a basis for the evaluation of the uncertainty in the model outputs.

The Monte Carlo technique for uncertainty analysis is a step-wise procedure:

Step 1 (uncertainty in the input parameters): This first step is the most crucial step in the Monte Carlo procedure: the uncertainty range of the uncertain input parameters needs to be determined. In most cases, and this was also the case here, the so-called expert review procedure is used: uncertainty ranges of each input parameter are determined on the basis of literature data, experimental data and expert assumptions (see Table 2). Notice that the wider range means that the parameter is more uncertain, whereas a more narrow range means that the parameter is less uncertain. The nominal value of each parameter was derived from the scientific literature (***and **) and from measurements (*). For

measured parameters, the uncertainty range was taken from the measurement (the paramteters marked with *). For the remaining parameters, on the basis of the literature and expert knowledge, a variation of 15% of a variation of 30% (most uncertain parameters) around the nominal value (Table 2) was assumed. It was furthermore assumed that each model parameter has a uniform distribution within the specified range.

Table 2 Uncertainty ranges for the input parameters

Parameters	unit	minimum	maximum
D_v^{**}	$m^2 \cdot s^{-1}$	$6.8 \cdot 10^{-7}$	$9.2 \cdot 10^{-7}$
D_l^{***}	$m^2 \cdot s^{-1}$	$7 \cdot 10^{-10}$	$1.3 \cdot 10^{-9}$
T_{air}^{*}	K	308	319
T_{set}^{*}	K	425	433
h_{top}^{**}	$W \cdot m^{-2} \cdot K^{-1}$	6.8	9.2
h_{bot}^{**}	$W \cdot m^{-2} \cdot K^{-1}$	306	414
k_v^{**}	$m \cdot s^{-1}$	$8 \cdot 10^{-5}$	$1 \cdot 10^{-4}$
k_l	$m \cdot s^{-1}$	1.10^{-11}	$1 \cdot 10^{-10}$
k_{evp}^{**}	s^{-1}	$0.974 \cdot 10^{-4}$	$1.38 \cdot 10^{-4}$
k**	$W \cdot m^{-1} \cdot K^{-1}$	0.55	0.7
T_{evp}	K	371	375
H_{evp}^{**}	$J \cdot kg^{-1}$	$2.07 \cdot 10^{6}$	$2.5 \cdot 10^{6}$
X_{lo}^{*}	kg of water / kg of solid	1.24	1.26
To^{*}	K	291	295

The superscript: *: obtained from measurement, **: ±15% of the nominal value, and ***: ±30 % of the nominal value

Step 2 (Sampling): Latin Hypercube Sampling (LHS) was used for sampling the input parameter values from the parameter space (Helton and Davis, 2003).The sampling of the parameters was performed in the same way as reported in Sin et al. (2009). The value of each parameter was sampled from the corresponding interval (Table 2). In total, 1000 samples were selected from the input parameter space, where each sample, θ_i, contains one value for each input parameter Eq. (5):

$$\theta_i = [\theta_{1i}, \theta_{2i}, \theta_{3i}, ... \theta_{Mi}] \quad \text{for } i = 1,2,3,....,N \qquad (5)$$

i.e.

$$\begin{bmatrix} \theta_1 \\ . \\ . \\ \theta_i \\ . \\ . \\ \theta_N \end{bmatrix} = \begin{bmatrix} \theta_{11}, \theta_{21}, \theta_{31}, ... \theta_{M1} \\ . \\ . \\ \theta_{1i}, \theta_{2i}, \theta_{3i}, ... \theta_{Mi} \\ . \\ . \\ \theta_{1N}, \theta_{2N}, \theta_{3N}, ... \theta_{MN} \end{bmatrix}$$

where M is the total number of input parameters (in this case, M = 14) and N is the total number of Latin-hypercube samples (e.g., 1000), and θ_{1i}, *and* θ_{2i}, are the samples for the first and the second input parameter, respectively. As a result of applying Latin hypercube sampling, a θ_{NxM} matrix was obtained.

Step 3 (Simulation): The sampled input matrix, θ_{NxM} was propagated by performing N Finite Element simulations, i.e. one simulation (a row of the input matrix) for each parameter combination sampled in step 2, (N = 1000). The first row in the matrix generated the first simulation and the second row generated the second simulation, and so on, up to a number N of simulations. For each simulation, the governing model equations of heat and mass transfer (heat, liquid water and water vapour), consisting of a system of partial differential equations (PDE) combined with constitutive equations, were solved using the *Finite Element Method*. The simulations resulted in a three dimensional matrix Y_{GxKxN} that contains G time instants (10 seconds interval between 0 and 1200 s), predictions of K output variables (13) and N Latin hypercube samples (1000 samples). This step is the most computational intensive part in the entire uncertainty and sensitivity analysis.

Step 4 (Result analysis): The simulation results obtained in step 3 are processed. For each output variable, and for every time point where model output is generated, the output uncertainty was represented by the mean, the 10th and the 90th percentile of the output distribution.

2.6 Sensitivity analysis

For the sensitivity analysis both the scatter plot and the standardized regression coefficients method (SRC) were used.

Scatter plot: Scatter plots of Monte Carlo simulation outputs were presented in graphs and the sensitivity of the model output to the parameters was evaluated visually (Saltelli et al., 2008).

Standardized regression coefficients: The standardized regression coefficients (SRC) were obtained by constructing linear regression models on the model output obtained from the Monte Carlo simulations. The detailed description of the method can be obtained in (Helton and Davis, 2003, Sin, et al., 2009). For each model output in Y, a linear regression model was constructed using Eq. (6), which is the standardized mean-centered sigma-scaling (Sin et al., 2009):

$$\frac{sY_{im} - \mu_{sym}}{\sigma_{sym}} = \sum_{j=1}^{M} \beta_{im} \frac{\theta_{ij} - \mu_{\theta j}}{\sigma_{\theta j}} + \varepsilon_{im} \qquad (6)$$

Where: Y is the vector with output variables (see *section,* 2.2), θ is the vector with input parameters (*section,* 2.3), m is the index of the output vector, i is the index of the Monte Carlo simulations (samples), j is the index of the parameter vector θ, e_{im} is the error of the linear regression model, β_{im} is the standardized regression coefficient (SRC) and M is the total number of parameters ($M = 14$, *see section 2.3*). The β_{im} were computed for each input parameters and output combination. The coefficient of determination, R^2 was computed for each model output (Y). The values of R^2 indicated the degree of linearization, and if R^2 is above the recommended value of 0.7 (Cariboni, et al., 2007), then the SRC method can be applied. The ranking of the parameters for each output was obtained by comparing the relative absolute values of the SRC (see section 3.3).

2.7 Model implementation and solution

The solution of the model equations (Table 1) and the uncertainty and sensitivity analysis were performed in a *COMSOL-MATLAB* environment.

3. Results and discussion

3.1 Temperature profile

The measured temperature profiles at different positions within the pancake batter (positions A, B, C and D, respectively) for the temperature set point of 160 ^{o}C are plotted in Fig. 3. Generally, two major distinct periods can be distinguished in the temperature profiles: the heating period (sensible heat dominant zone) and the evaporation period (latent heat dominant zone), illustrated in Fig. 3 (Feyissa et al., 2011). In the heating period (preheating), most of the supplied heat energy (from the heating rig) is used to rise the temperature of the product (pancake batter). The heating period is short compared to the evaporation period, particularly for the position in the product that is closest to the bottom surface (e.g. at position D, about 200 s, Fig. 3. During the evaporation period, where the temperature curves only rise slowly, nearly all of the supplied heat to the product is used for evaporating the water.

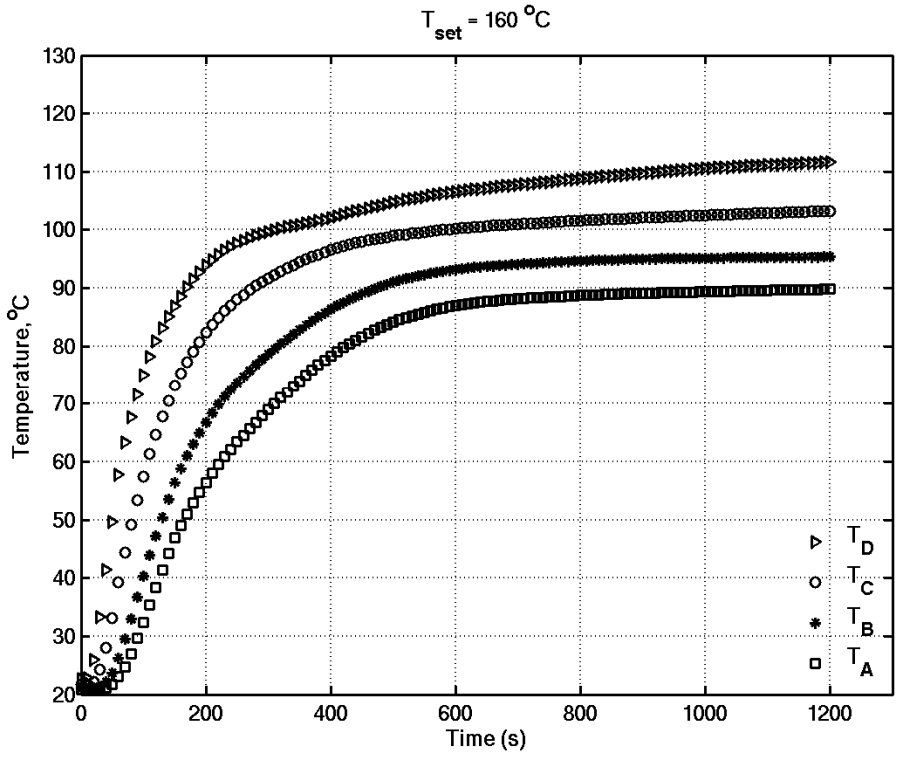

Figure 3 Temperature profile at different positions (position A, B, C and D) with temperature set point of 160 ^{o}C. The data are shown with a sampling interval of 10 seconds.

3.2 Uncertainty in model predictions

The mean, 10th and 90th percentile of the distributions were constructed using the raw data obtained from Monte Carlo simulations, and are reported in Fig. 4 and Fig. 5. The larger the spread (band) of the model predictions is at a certain point in time, the larger is the uncertainty in the model outputs. Consequently, a narrow spread of the output corresponds to a small uncertainty. Generally, the uncertainty of the model outputs varies with time (growing trend). Initially (in the heating zone, for time < 200 s), the spread is small for most of the model outputs, while in the evaporation period, the band becomes larger for most model outputs (Y).

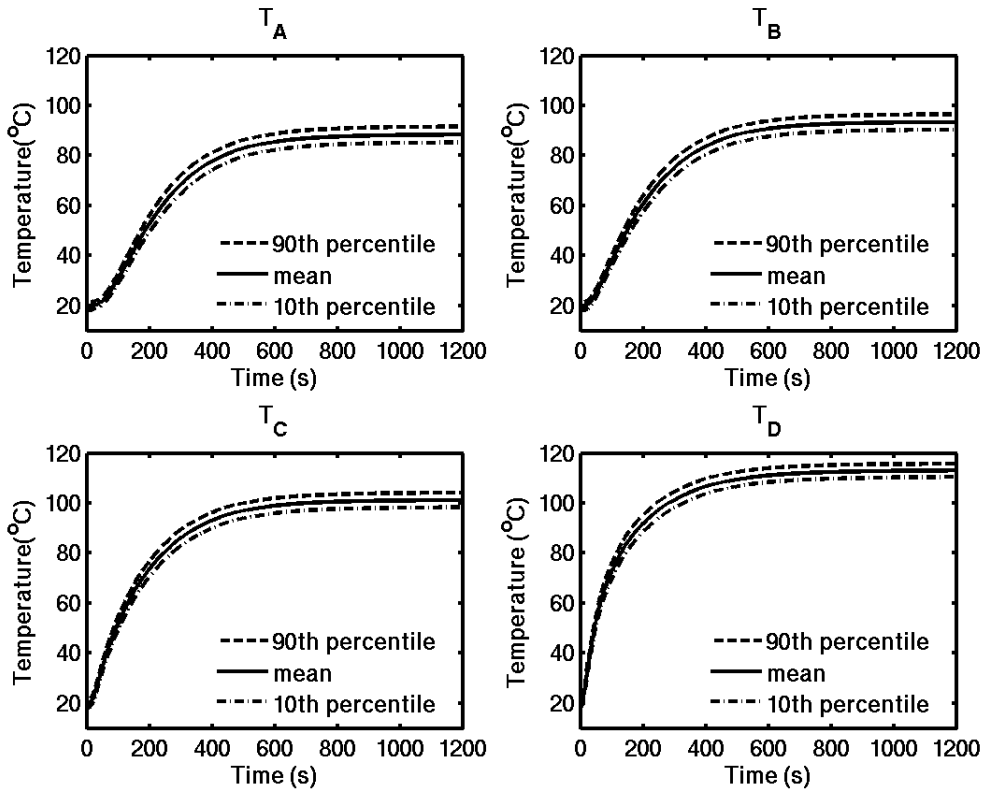

Figure 4 Representation of uncertainty of the temperature profile predictions using mean, 10th and 90th percentile at position A, B, C, and D, (T_A, T_B, T_C and T_D, respectively).

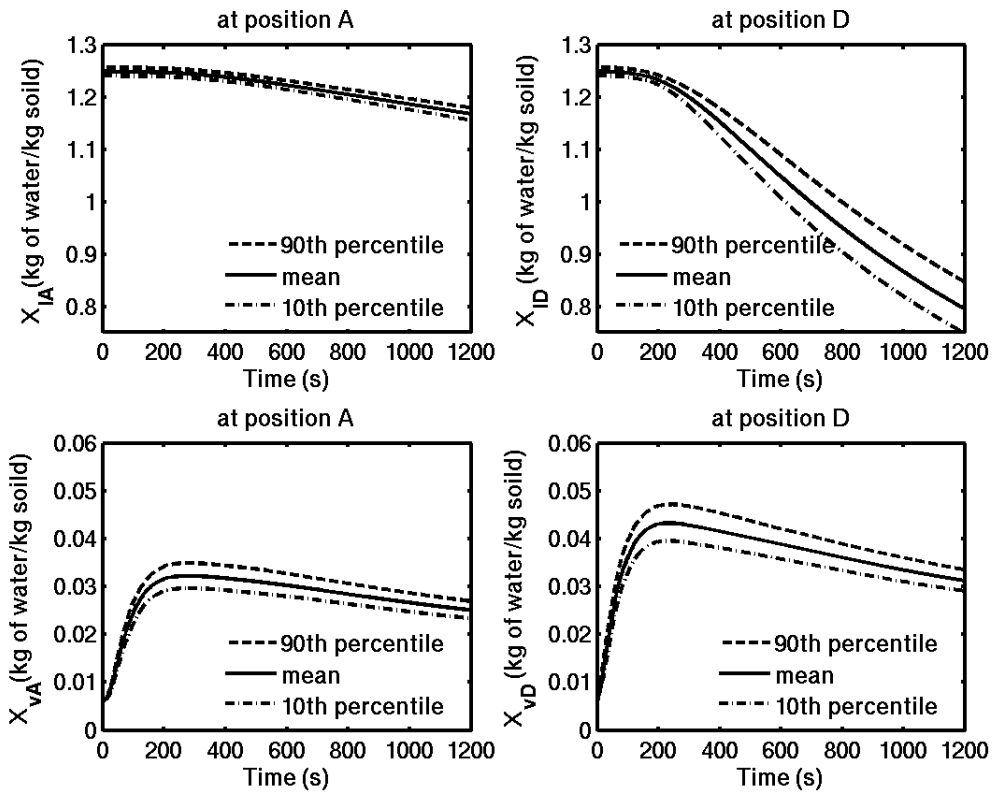

Figure 5 Representation of uncertainty of the water concentration (kg of water/kg of solid) profile predictions using mean, 10th and 90th percentile at positions A and D for liquid water (X_{lA} and X_{lD}) and water vapour (X_{vA} and X_{vD})

It can be observed from Fig. 4 that the temperature profile at positions A, B, C, and D has similar uncertainty trends, while the uncertainty on the prediction of the water content (both for liquid water and water vapour) varies for different positions in the pancake batter. The uncertainty range in the prediction of the liquid water concentration is larger at position D (X_{lD}) compared to the position A (X_{lA}) (Fig. 5, top-right and top-left). Moreover, at position A, the prediction of the water vapour concentration, X_v is relatively less uncertain compared to the prediction at position D (Fig. 5, compare bottom-left with bottom-right). For example, the band width of X_{vD} is 1.5 and 1.23 (for t = 300 s and t =1000s, respectively) times the band width of X_{vA}. The water vapour concentration, X_v has the largest uncertainty in the transition zone between the heating phase and the evaporation phase (t = 200 to 400 s).

3.3 Scatter plot: Monte Carlo method for sensitivity analysis

For illustration purposes, only one point of the output (X_{lD}) is shown here with a few representative scatter plots. Fig. 6 illustrates the scatter plot of the liquid water concentration at position D (X_{lD}) *with* respect to nine of the input parameters. From Fig. 6, it is clear that the liquid water concentration at position, X_{lD} is strongly correlated with the liquid water diffusion coefficient, D_l. The remaining parameters seem to have less impact on the uncertainty in the predictions of the X_{lD} (for details, see also section 3.4). Presenting and comparing the sensitivity analysis results using scatter plots is challenging for a large number of parameters and output combinations. Indeed, for the analysis reported here there is a total of 182 scatter plots (14 parameters on 13 outputs, one scatter plot for each parameter-output combination). The standardized regression coefficient method (SRCs) therefore forms a better option for global sensitivity analysis since the parameter ranking is obtained readily (see section 2.3).

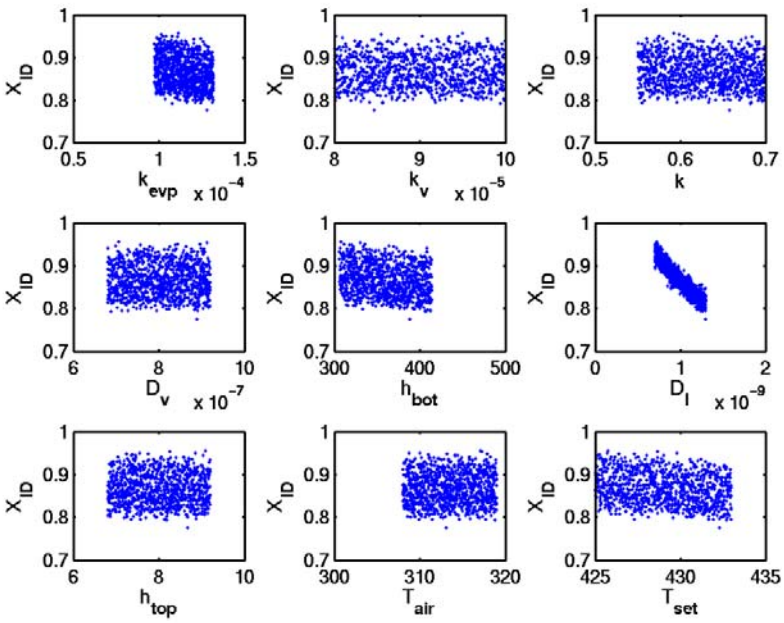

Figure 6 Scatter plot for liquid water concentration at position D (X_{lD}) evaluated at t = 1000 s. Only scatter plots for nine of the input parameters are presented here, for clarity.

3.4. Sensitivity analysis using standardized regression coefficients

For each model output (Y_i), a linear regression model was constructed, (see section 2.3) and the corresponding regression coefficients (SRCs) were obtained using the linear least squares method (using the standardized mean-centered sigma-scaling). Scalar outputs are required for the calculation of SRCs. For example, the SRCs can be evaluated at different time instants during the baking process. Here, it was chosen to calculate the SRCs at time t = 1000 s (i.e. towards the end of the baking process). This choice was motivated because the baking time is more important in the determination of the final product quality. Moreover, the uncertainty analysis results (section 3.2, Fig. 5 and Fig. 6) demonstrated for most of the model outputs (Y) that the larger uncertainty was observed towards the end of the baking. The obtained SRCs and coefficient of determination, R^2 for each model output at *t = 1000 s* are summarized in Table 3.

The original model of CHMT is non-linear, and the R^2 is used to evaluate the degree of linearization for each Y. The R^2 values were found to be above 0.99 for all variables in Y (13 output variables), Table 3. The linearized model expressed by Eq. (6) is able to explain most of the variance in the model outputs, and this confirms that the SRC values can be used to evaluate the relative importance of input parameters (θ) on the model outputs (Y). The absolute value of the SRCs' in Table 3 indicates the impact of each parameter, while the sign indicates either a positive or a negative correlation between the input parameter (θ) and the output (Y).

Table 3 Standardized regression coefficient (SRCs) and R^2 results

Y	T_D	T_C	T_B	T_A	X_{av}	X_{lD}	X_{lC}	X_{lB}	X_{lA}	X_{vD}	X_{vC}	X_{vB}	X_{vA}
R^2	0.998	0.998	0.998	0.998	0.997	0.995	0.994	0.997	0.998	0.995	0.995	0.995	0.995
				SRCs									
θ	T_D	T_C	T_B	T_A	X_{av}	X_{lD}	X_{lC}	X_{lB}	X_{lA}	X_{vD}	X_{vC}	X_{vB}	X_{vA}
k_{evp}	**-0.540**	**-0.607**	**-0.623**	**-0.619**	**-0.296**	**-0.183**	**-0.362**	**-0.379**	-0.314	**0.259**	**0.266**	**0.267**	**0.259**
k_v	0.000	0.000	0.000	0.001	-0.095	0.001	0.002	0.002	0.002	**-0.637**	**-0.679**	**-0.733**	**-0.793**
k	**0.295**	**0.430**	**0.499**	**0.541**	**-0.236**	**-0.072**	**-0.286**	**-0.449**	**-0.458**	**0.238**	**0.249**	**0.256**	**0.253**
D_v	0.001	0.001	0.001	0.001	-0.049	0.003	-0.006	-0.005	-0.004	**-0.481**	**-0.420**	**-0.328**	-0.196
h_{bot}	**0.302**	**0.216**	0.175	0.153	**-0.295**	**-0.198**	**-0.276**	**-0.245**	-0.195	0.055	0.061	0.064	0.063

D_l	-0.103	-0.104	-0.086	-0.075	**-0.683**	**-0.925**	**-0.642**	0.003	0.060	**0.402**	**0.381**	**0.364**	**0.343**
h_{top}	-0.045	-0.064	-0.089	-0.123	0.023	0.006	0.023	0.048	0.065	-0.043	-0.045	-0.047	-0.048
T_{air}	0.039	0.056	0.076	0.104	-0.028	-0.008	-0.029	-0.054	-0.070	0.034	0.036	0.037	0.038
T_{set}	**0.496**	**0.343**	**0.266**	**0.226**	**-0.265**	-0.176	**-0.249**	**-0.229**	-0.179	0.187	0.192	0.193	0.187
H_{evp}	**-0.393**	**-0.369**	**-0.337**	**-0.310**	0.167	0.052	0.216	0.345	**0.359**	-0.132	-0.144	-0.153	-0.154
T_{evp}	**0.300**	**0.315**	**0.314**	**0.308**	0.170	0.110	0.156	0.150	0.124	-0.102	-0.105	-0.104	-0.101
T_o	0.002	0.002	0.002	0.002	-0.022	-0.007	-0.027	-0.033	-0.030	-0.006	-0.006	-0.005	-0.005
X_{lo}	-0.022	-0.020	-0.019	-0.018	0.398	0.112	0.397	0.634	0.686	0.059	0.058	0.057	0.056
k_l	-0.002	-0.001	-0.001	0.000	0.001	0.001	-0.001	0.000	0.001	0.000	0.000	0.000	0.000

For example, the temperature at position A decreases as the evaporation rate constant (k_{evp}) increases (SRC = -0.62, Table 3). This is reasonable, because increasing the evaporation rate increases the heat of evaporation, and therefore decreases the sensible heat. The thermal conductivity parameter, k, is positively correlated with the temperature (at all positions, T_A, T_B, T_C, and T_D), Table 3. The temperature at position A, T_A increases as *k* increases (SRC = 0.54). This is reasonable because the larger *k* value allows more heat flux to transfer through the product compared to smaller *k* values.

3.5 Parameter ranking

A summary of the parameter ranking for each model output (at t =1000s) is presented in Fig. 7, Fig. 8, and Fig. 9 for three state variables: temperature, liquid water concentration and water vapour concentration, respectively.

Product temperature: The product temperature at all the positions (A, B, C, and D) is very sensitive to the evaporation rate constant k_{evp}, which ranks highest in the list provided in Fig. 7. The product temperature at all positions decreases as k_{evp} increases (Table 3). This is reasonable, because increasing the evaporation rate increases the heat of evaporation, and therefore decreases the sensible heat. Moreover, the evaporation of water is the dominant process (at t =1000s) during the baking process (section 3.1).

The thermal conductivity parameter, *k* is the second most sensitive parameter in the prediction of product temperature (Fig. 8), except at the position D. The temperature at the position D, T_D is more sensitive to the temperature set point, T_{set}, compared to *k*. The

temperature set point (T_{set}) has a strong impact on T_D, because, the position D is closer to the bottom surface.

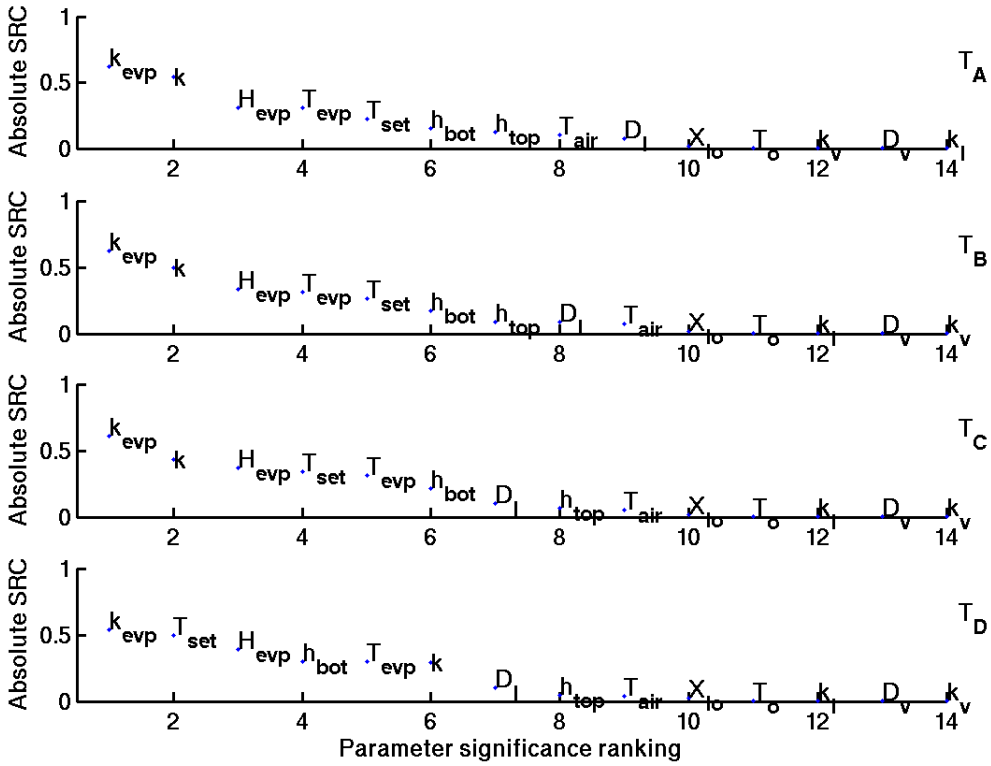

Figure 7 Relative importance of parameters for T_A, T_B, T_C and T_D

The bottom boundary condition parameters, T_{set} and h_{bot}, and the evaporation parameters H_{evp} and T_{evp} have a moderate impact on the product temperature prediction, while the rest of the parameters, including all the top boundary condition parameters (e.g. T_{air}, h_{top}) relatively have no impact on the uncertainty in the product temperature prediction. Thus, it can be concluded that the uncertainty in the prediction of the product temperature, (section 3.2, see Fig. 5, top-left) is mostly due to the six highest-ranking parameters (k_{evp}, k, T_{set}, H_{evp}, T_{evp}, *and* h_{bot}).

Liquid water concentration (X_l): The ranking of the parameter impact on the liquid water concentration is illustrated in Fig. 8 for the four positions within the pancake batter. At position D, the prediction of liquid water concentration has a larger uncertainty (see section 3.3) compared to the other remaining positions (A, B, and C). The large

uncertainty on the prediction of the liquid water concentration at position D is mainly due to uncertainty in the value of the liquid diffusion coefficient, D_l; D_l has the largest impact among all the parameters (θ) (Table 3, and Fig. 8 top-left). The liquid water concentration at position D, X_{lD} decreases as D_l increases (Fig. 6). This is because, at the bottom surface (z = 0), the liquid water evaporates vigorously, and as the result of that the liquid water concentration is reduced rapidly. The liquid water diffuses from position D (z = 1.6 mm) where the concentration is higher to the bottom surface (z = 0) where the concentration is much lower. This means that the diffusion coefficient of the water is the limiting factor and the mechanism for the liquid water transport inside the product is strongly diffusion dependent, particularly in that region (close to the bottom surface).

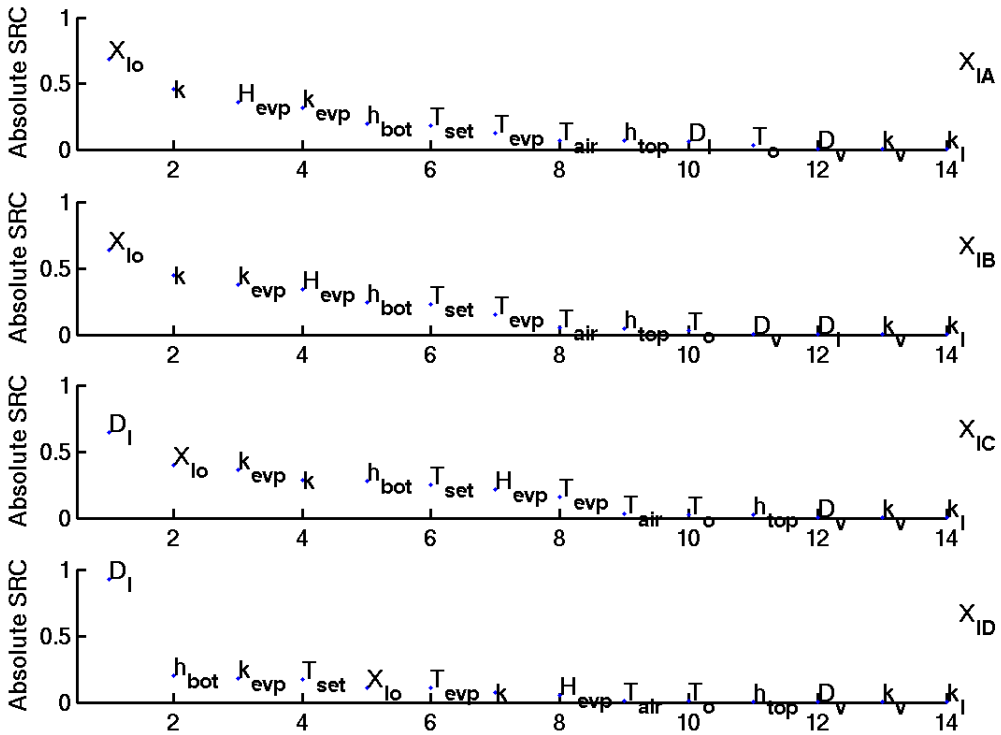

Figure 8 Relative importance of input parameters for X_{lA}, X_{lB}, X_{lC} and X_{lD}

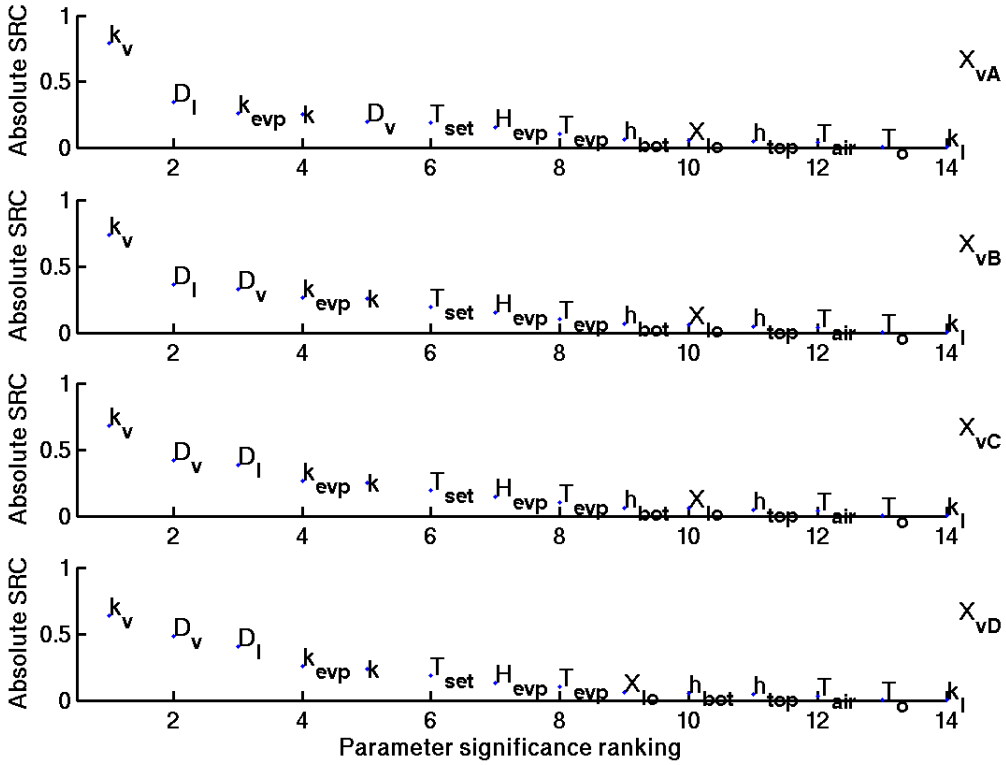

Figure 9 Relative impact of parameter on prediction for X_{vA}, X_{vB}, X_{vC} and X_{vD}

5. Conclusion and perspectives

The uncertainty analysis and the global sensitivity analysis were applied to the coupled heat and mass transfer model of the contact baking process. The method was implemented in the framework *COMSOL-MATLAB® version 3.5*. The impact of the uncertain input parameters was mapped to the model output. The results demonstrated that the extent of uncertainty of the model predictions varies with time, and varies among the different model outputs. The global sensitivity analysis results with the SRC method provided a ranking of the parameters, from influential to non-influential. This ranking is different for the different state variables (T, X_l, and X_v). Moreover, there can also be differences of the ranking within the same state variable depending on the position in the pancake batter. Overall, some of the parameters (k_l, T_{air}, h_{top}) have little or no impact on all the state variables of the model. On the other hand, some of the input parameters have

a strong impact: k and k_{evp} on the temperature predictions and D_l on the prediction of the liquid water concentration at the bottom layer of the product.

Here, for the coupled heat and mass transfer model during the contact baking process: (1) using the uncertainty analysis we were able to determine, how the temperature and water content trends change as a result of uncertainty in the value of the parameters; and (2) using the sensitivity result, we were also able to identify the relative impact of uncertain parameters on model predictions and their rank according to their impact.

The obtained results, for example the ranking of the parameters, can be used in different ways. First of all, parameters that do not seem to have any influence on any of the model output might point towards parts of the model that could be omitted or at least reduced in complexity. Indeed, why include an extra parameter if the parameter does not have any effect on the model output? The influential parameters, on the contrary, are helpful in further model refining, and point towards those parameters that must be measured more precisely or estimated from experimental data in order to better capture the fundamental behavior of the heat and mass transfer during the baking process. Thus, the global sensitivity analysis plays a key role in mapping the impact of input parameters on the model predictions in a systematic way. Note also that in order to reduce the amount of uncertainty in the model predictions, the most influential parameters (at the top of the list in the ranking) should be estimated with a higher precision compared to parameters at the bottom of the list.

In the temperature prediction, the thermal conductivity parameter k, and the evaporation rate constant k_{evp} are the most important parameters. This implies that, in order to reduce the uncertainty in the temperature prediction, those parameters should be estimated with high precision. On the other hand, the parameters ranking lowest have no effect, and will not change the predictions, as long as their value is kept within an acceptable range. The method gives a good indication on where to focus for obtaining a better fit. Summarizing, an uncertainty and sensitivity analysis is an essential step to discover potential deficiencies in model formulation that help to explain and correct the lack of fit. It also provides guidance for a model reduction and parameterization.

There is a general interest in the food industry to know, how the variations or change in the input parameters affect the final product quality. In that case, the result of an uncertainty and global sensitivity analysis plays an important role for the food industry's efforts to maintain the product quality consistent. The developed method can also easily be adapted to other food processes that involve: (1) many input parameters with uncertain values and (2) the variability of the input parameters (e.g. the variability in the product properties).

References

Baik O.D., Marcotte M., Sablani S.S., & Castaigne F. (2001). Thermal and physical properties of bakery products. *Critical reviews in food science and nutrition*, 41(5), 321-352.

Campolongo F., Saltelli A. (1997). Sensitivity analysis of an environmental model an application of different analysis methods. *Reliability Engineering & System Safety*, 57(1), 49-69.

Cariboni J., Gatelli D., Liska R., & Saltelli A. (2007). The role of sensitivity analysis in ecological modelling. *Ecological Modelling*, 203(1-2), 167-182.

Dimov I., Georgieva R. (2011) Monte Carlo algorithms for evaluating Sobol' sensitivity indices. *Mathematics and Computers in Simulation*, In Press, Corrected Proof.

Ellwein L.M., Tran H.T., Zapata C., Novak V., & Olufsen M.S. (2008). Sensitivity Analysis and Model Assessment: Mathematical Models for Arterial Blood Flow and Blood Pressure. *Cardiovascular Engineering*, 8(2), 94-108.

Frey H.C., Patil S.R. (2002). Identification and review of sensitivity analysis methods. *Risk Analysis*, 22(3), 553-578.

Feyissa A.H., Gernaey K.V., and Adler-Nissen. (2011). Modelling of Coupled Heat and Mass Transfer during a Contact Baking Process, *Journal of Food Engineering, (re-submitted version under review)*

Helton J.C., Davis F.J. (2003). Latin hypercube sampling and the propagation of uncertainty in analyses of complex systems. *Reliability Engineering & System Safety*, 81(1), 23-69.

Martienssen W., Warlimont H. (2005). *Springer handbook of condensed matter and materials data.* (, pp. 1-1119). Springer, Heidelberg.

Rao M.A., Rizvi S.H., & Datta A.K. (Eds.) (2005). *Engineering properties of foods.* (Third Edition edn., pp. 738). Taylor and Francis.

Rask C. (1989). Thermal properties of dough and bakery products: A review of published data. *Journal of Food Engineering*, 9(3), 167-193.

Ratto M., Young P.C., Romanowicz R., Pappenberger F., Saltelli A., & Pagano A. (2007). Uncertainty, sensitivity analysis and the role of data based mechanistic modeling in hydrology. *Hydrology and Earth System Sciences*, 11(4), 1249-1266.

Saisana M., Saltelli A., & Tarantola S. (2005). Uncertainty and sensitivity analysis techniques as tools for the quality assessment of composite indicators. *Journal of the Royal Statistical Society Series A-Statistics in Society*, 168, 307-323.

Saltelli A., Ratto M., Tarantola S., & Campolongo F. (2005). Sensitivity analysis for chemical models. *Chemical reviews*, 105(7), 2811-2827.

Saltelli A, Ratto M., Andres T, Campolongo F, Cariboni J, Gatelli D, Saisana M, Tarantola S. (2008) Global Sensitivity Analysis: The primer (2008) West Sussex, England, John Wiley & Sons.

Sin G., Gernaey K.V., & Lantz A.E. (2009). Good modeling practice for PAT applications: Propagation of input uncertainty and sensitivity analysis. *Biotechnology progress*, 25(4), 1043-1053.

Thorvaldsson K., Janestad H. (1999). A model for simultaneous heat, water and vapour diffusion. *Journal of Food Engineering*, 40(3), 167-172.

Wong S.Y., Zhou W., & Hua J. (2006). Robustness analysis of a CFD model to the uncertainties in its physical properties for a bread baking process. *Journal of Food Engineering*, 77(4), 784-791.

Appendix A: fixed parameters

Table 4 Input parameters with fixed values

parameter	value	parameter	value	parameter	value
$y_{p,o}$[b]	0.07 kg/kg	ρ_f[d]	920 kg/m^3	c_{pAl}[f]	960 J/(kg·K)
$y_{c,o}$[b]	0.33 kg/kg	ρ_p[d]	1320 kg/m^3	k_{Al}[f]	150 W/(m·K)
$y_{f,o}$[b]	0.03 kg/kg	ρ_c[d]	1600 kg/m^3	$X_{v,air}$	0.0062 kg/kg
z_5[a]	0.008 m	ρ_w[d]	1000 kg/m^3	$X_{l,air}$[c]	0 kg/kg
z_3[a]	0.005 m	ρ_s[b]	1467 kg/m^3	k_{air}[d]	0.023 W /(m·K)
R_g	8.314 J/(K·mol)	ρ_{Al}[f]	2660 kg/m^3	M_w	0.018 kg/mole

Superscripts: a: measured, b: calculated or estimated, *c: set (assumed),d:* (Rao et al., 2005), e: Obtained from Thorvaldsson and Janestad (1999), *f: Obtained from* (Martienssen and Warlimont, 2005)*,and g:* (Toledo,1991)

Subscripts: p: protein c: carbohydrate , f: fat,w: water

Paper V

3D Modelling of Coupled Mass and Heat Transfer of a Convection-Oven Roasting Process

A.H. Feyissa[1], J. Adler-Nissen[1] and K.V. Gernaey[2]

[1]National Food Institute, Food production Engineering, Technical University of Denmark
[2] Department of Chemical and Biochemical Engineering, Technical University of Denmark
Corresponding author: Søltofts Plads, 2800, Kgs. Lyngby, DK (e-mail: abhfe@food.dtu.dk)

***Abstract*—A 3D mathematical model of coupled heat and mass transfer describing oven roasting of meat is developed from first principles. The proposed mechanism for the mass transfer of water is new and based on a critical literature review of the effect of heat on meat. The model equations are based on a conservation of mass and energy, coupled through Darcy's equations of porous media, since the water flow is mainly pressure-driven. The developed model incorporates additional considerations of the effect of evaporation and water binding capacity that occur during the meat roasting process. The developed coupled partial differential equations are solved by using COMSOL Multiphysics®3.5 and state variables are predicted as functions of position and time. The proposed mechanism is partially validated by experiments in a convection oven where temperatures were measured online.**

***Keywords*—**3D coupled heat and mass transfer, COMSOL Multiphysics, convection roasting process, modeling porous media.

I. Introduction

Roasting in a convection oven is a common way of frying whole meat in households, in professional kitchens and in the ready-meal industry. The setting of the process parameters to obtain a culinary optimal result of the roasting process is, however, largely based on the experienced judgments and, skills of the cook or the operator. This makes it difficult to scale up the oven roasting process and to predict the result of transferring the process to new equipment or to apply automatic process control. A necessary step towards incorporating expert-operator knowledge into tools for scaling up and/or for automated process control, is a mathematical formalisation of the existing qualitative knowledge about the process – in other words a *process model* needs to be developed(Singh and Vijayan, 1998),(Allais, et al., 2007).

Modelling of meat frying processes is largely concerned with contact frying of meat patties or deep-fat frying of (battered) meat products, reflecting the wide-spread industrial interest in these types of products (Dincer, 1996, Ikediala, et al., 1996, Ou and Mittal, 2006, Pan, et al., 2000). There are some earlier modelling studies of the oven roasting process, which all emphasize the crucial effect on the energy transfer from water evaporating from the meat (Bengtsson, et al., 1976, Chang, et al., 1998, Singh, et al., 1984, Skjoldebrand and Hallstrom, 1980). As shown already in the now classical study by Skjöldebrand and Hallström (Skjoldebrand and Hallstrom, 1980), the transport of water inside the meat is also coupled to the heat transfer in a complex and yet not fully understood way.

Several researchers have formulated different hypotheses to model mass transfer during roasting, mostly from the perspective of diffusion (Chen, et al., 1999, Huang and Mittal, 1995, Ngadi, et al., 1997) while disagreements are often seen with regard to other types of water transport mechanisms (Godsalve, et al., 1977, Thorvaldsson and Skjöldebrand, 1996, Wählby and Skjöldebrand, 2001). Purely diffusion based models do not adequately describe the moisture transport phenomena during meat cooking because the effects of water binding capacity and shrinkage phenomena are not considered. These are, however, main driving mechanisms for the exudation of water during the cooking or roasting of meat, and some of early studies on this topic agree with this fact (Godsalve, et al., 1977, Tornberg, 2005, Wählby and Skjöldebrand, 2001).

Roasting of meat causes the muscle protein to denature, resulting in a decrease in water holding capacity and leading to shrinkage of the protein network. Shrinkage of the network ultimately induces a pressure gradient inside meat muscle. Outside the field of meat science, such physics occur during syneresis of curd (Barriere and Leibler, 2003) and polymer gels (Tijskens and De Baerdemaeker, 2004, Wu, et al., 2004) and models for such systems are based on a poroelastic theory. A similar approach was also applied in meat science for the first time by Van der Sman to study water transport during meat cooking (van der Sman, 2007). Van der Sman, however, predicted a quite large rise in the moisture content at the centre of whole meat, which is in disagreement with the observations of Wahlby and Skjöldebrand (Wählby and Skjöldebrand, 2001)

. Although Skjöldebrand and Thorvaldsson in their earlier (Thorvaldsson and Skjöldebrand, 1996) study on pre-cooked meat observed a slight rise in water content at the center of the sample, they did not observe any rise in water content in their later study on the roasting of *raw* whole meat (Wählby and Skjöldebrand, 2001).

The reason for the disagreement between theory and observation can be ascribed to differences in the microstructures of raw and pre-cooked samples. The dynamic change of the microstructure of meat during the heating process plays a great role in water transport. This is often neglected, however, and this leads to ambiguity in the description and modelling of the water transport. Our description of these changes, which are expounded in a forthcoming paper (Feyissa, et al., 2009) is as follows: The structure of raw meat is intact at the start of the cooking process, and water transport is hindered by low permeability. However, during the roasting of the raw meat, dramatic changes in the microstructure (such as pore formation, change of elastic modulus) are induced, which affect the water transport. Spatial variation in temperature creates spatial difference in permeability and elastic modulus, where parts of the meat sample closer to the surface have larger permeability and elastic modulus than the parts closer to the centre. There is therefore a much larger resistance to water flux towards the centre than towards the surface of the meat piece. Since water moves in the direction of least resistance, the water will preferentially flow towards the surface against the temperature gradient and form exudate. It is therefore crucial that the models consider these phenomena for better understanding and prediction of the roasting process. The objective of this paper is to develop a 3D model that by considering the effect of change in microstructure ultimately can describe and predict heat and mass transfer processes for meat roasting in a convection oven.

II. Modeling of Coupled Heat and Mass Transfer

A. Model formulation

The product (meat) is heated in a convection oven with hot air at 175°C. Heat is supplied from the hot air to the product surface by convection. The heat is then transferred from the surface to the center of the product. Meanwhile, moisture is transported within the product via convection and diffusion processes, with a net water transport from the inside of the product to the surface. With increase in temperature, muscle protein denatures and there is a decrease in water holding capacity parallel with the shrinkage of the protein network (Godsalve, et al., 1977). The shrinkage of the network ultimately induces a pressure gradient inside the meat muscle, and excess water is expelled to the surface. At the product surface the liquid water evaporates and is carried away with the hot circulating air. If the energy supplied from hot air is less than the energy needed for evaporation at the surface, moisture is lost from the product as drip. The most important mechanisms that occur during the convection oven roasting process are illustrated in Fig.1.

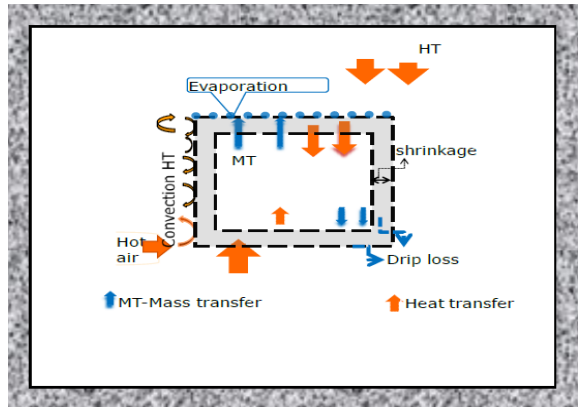

Fig. 1 Transport processes during convection roasting convection oven

In this study the following basic assumptions are made to formulate the governing coupled mass and heat transfer equations: a) fat transport is negligible (lean meat is considered having less than 2% fat), b) the crust is thin (this is observed when inspecting a cut through the cooked meat) and does not hinder transport of water to the surface. Evaporation therefore takes place at the surface, c) dissolved matter can be neglected in the material and energy balance (our forthcoming work, (Feyissa, et al., 2009) d) no internal heat generation, and e) no chemical reaction.

B. Governing Equations

1) Heat transfer

Using conservation of energy, the heat transfer within meat is assumed to be given by

$$\rho_m c_{p_m} \frac{\partial T}{\partial t} + \nabla(-k_m \nabla T) + \rho_w c_{p_w} u_w \nabla T = 0 \qquad (1)$$

where ρ_m and ρ_w are density of meat and fluid (water) (kg/m^3), respectively, k_m is the thermal conductivity of meat (W/(m·°C)), $c_{p,m}$ and c_{pw} are the heat capacities of meat and water (J/(kg·°C)), respectively, u_w is the fluid velocity (m/s), T is temperature (°C) and t is time (s).

2) Mass transfer

From the conservation of mass, the governing equation for water transport within the product is given by

$$\frac{\partial C}{\partial t} + \nabla(C u_w) = \nabla . D \nabla C \qquad (2)$$

where C is moisture concentration (kg of water/kg of sample), t is time(s), u_w is fluid (*water*) velocity (m/s) and D is the moisture diffusion coefficient (m^2/s).

3) Velocity of fluid within meat

The relationship between velocity and pressure gradient (that drives the moisture transport) inside the meat can be expressed using Darcy's law of porous media:

$$Q_w = \frac{-A K}{\mu_w} \nabla P \qquad (3)$$

where Q_w is the flow rate (discharge, m^3/s), K is the permeability of the medium(m^2), A is the flow area (m^2), and ∇P is the pressure gradient vector (pa/m), μ_w is the dynamic viscosity of the fluid (pa·s). Equation (3) can be rewritten in terms of velocity as

$$u_w = \frac{-K}{\mu_w}\nabla P \qquad (4)$$

where u_w is the velocity of the fluid (m/s). The swelling pressure is proportional to the excess moisture concentration within the meat (Barriere and Leibler, 2003, van der Sman, 2007) and the expression for swelling pressure P is given as

$$P = E\big(C - Ceq(T)\big) \qquad (5)$$

where, $Ceq(T)$ is the equilibrium water holding capacity as a function of temperature (T) and E is the modulus of elasticity (N/m^2). Substituting (5) for P into (4) gives the expression of velocity, u_w

$$u_w = -\frac{K\,E}{\mu_w}\nabla(C - Ceq(T)) \qquad (6)$$

The expression for the water holding capacity is given by an empirical relation (van der Sman, 2007)(Bengtsson, et al., 1976)

$$C_{eq(T)} = a_1 - \frac{a_2}{(1 + a_3\exp(-a_4(T - T\sigma)))} \qquad (7)$$

where T_σ =52 °C is the centre of a logistic curve (water holding capacity vs. Temperature), a_1= 0.745, a_3 = 0.345, a_3 = 30, a_4 = 0.25 (van der Sman, 2007)

a) Elastic modulus, E

The elastic modulus of meat changes during cooking and thus E is function temperature. However, there is no expression for $E(T)$ that can be readily incorporated in the model. A dramatic change of elastic modulus occurs between T = 50 and T = 80 °C (Tornberg, 2005). Based on the experimental observation a logistic with slight modification is proposed to describe the $E(T)$ functionality as shown in (8).

$$E_{(T)} = E_o + \frac{E_m}{(1 + \exp\big(-E_n\big(T - E_D\big)\big)} \qquad (8)$$

where E_o is the minimum value (at initial state, raw meat) of the elastic modulus, $E_0 = 12$ *kpa*, E_m is the maximum value, E_m=83 kpa at T=80 °C; E_n and E_D are the parameters of (8), which were obtained by fitting (8) the experimental data given in (Tornberg, 2005). For whole meat(Tornberg, 2005), E_n=0.3, and E_D=60 were obtained from the curve fitting.

b) Permeability of meat, K

Unfortunately, there are very limited data in literature for the permeability of whole meat, the permeability of raw meat was only reported by Datta as (10^{-17}-10^{-19} m^2)(Datta, 2006) .The intrinsic permeability of meat changes during roasting as a result of pore formation or collapse. During the cooking of a beef burger, a change of 100 fold in permeability was reported (Kovácsné Oroszvári, et al., 2006)
. However, this is comminuted meat and it is not likely that the increase will be as large as that in whole meat. However, we will show in this paper that even letting K remain constant at 10^{-17} m^2 will simulate important aspects of the observed distribution of moisture during cooking.

C. Thermo-physical proprieties

The density of meat and its heat capacity are estimated from the composition of the meat using (12) and (13), respectively (Rao, et al., 2005).

Density of meat:

$$\rho_m = \frac{1}{\sum \frac{y_i}{\rho_i}} \qquad (12)$$

(12)

Specific heat capacity of meat:

$$c_{pm} = (1.6y_c + 2y_p + 2y_f + 4.2y_w).10^3 \qquad (13)$$

where ρ_m, ρ_w, ρ_f, ρ_c, *and* ρ_p are the densities of meat, water, fat, carbohydrate and protein respectively, y_i is the mass fraction of each component i, (y_p is mass fraction of protein, y_f is mass fraction of fat, y_c is mass fraction of carbohydrate and y_w is mass fraction of water) and c_{pm} is the specific heat capacity of meat (J/(kg·°C)). A thermal conductivity for meat of 0.47 (W/($m^{2.}$°C)) was used (Rao, et al., 2005).

D. Boundary and Initial condition

The convective heat flux from the hot air to the product surface is given by (Bird, et al., 2001)

$$q = h(T_{oven} - T_s) \qquad (14)$$

Where q is the convective heat flux (W/m^2), h is the heat transfer coefficient (W/($m^{2.}$ °C)), T_{oven} is the oven temperature (°C) and T_s is the meat surface temperature (°C).

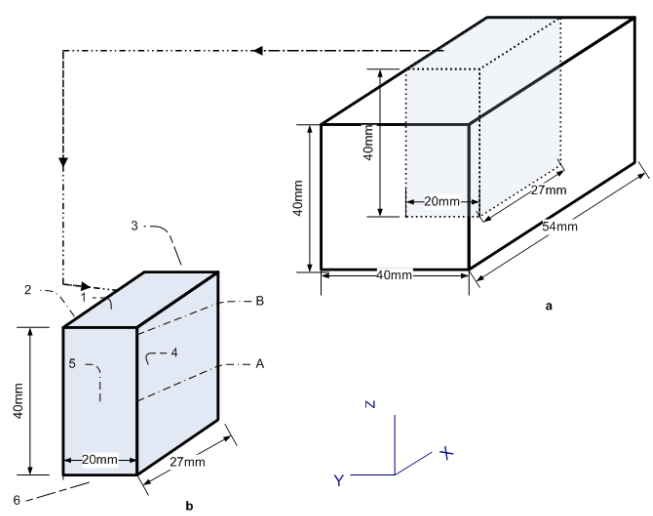

Fig.2 Schema of rectangular shaped meat sample showing a domain, boundaries (1-6) and dimensions. Point A and B are corresponding to the center (0, 0, 20mm) and a point close to the surface (0, 0, 38mm), respectively.

1) Heat Transfer Boundary Condition

Boundary 1, 2, 3, and 6 (Fig 2) are flux boundary conditions and are given by (15)

$$(1-f)h(T_{oven}-T_s) = -n.(k_m \nabla T + u_w c_{pw} \rho_w T) \qquad (15)$$

And where *f* is the fraction of energy that dissipates in the evaporating water at the surface. The value of *f* is between 0 and 1. The parameter *f* is interpreted as an empirical switching function that will determine the fraction of the supplied energy that is used for evaporation. At $T_s \geq 100^{\circ}C$ evaporation dominates, and *f* rapidly rises to a value closer to 1 than to 0. The concrete value of *f* will depend on the heat transfer conditions and mass loss, and must at this stage be estimated by trial and error. In future work we will aim at deriving a more theoretically based expression for *f*.

Boundary 4 and 5 are symmetry boundary conditions.

2) Mass Transfer Boundary Condition

Boundary 1, 2, and 3 are flux boundary conditions (16)

$$n.(-D\nabla C + u_w C) = f\ h \frac{(T_{oven}-T_s)}{H_{evp}\rho}(C - C_{eq}) \qquad (16)$$

Boundary 4 and 5 are symmetry boundary conditions. The mass flux for boundary 6 is zero, therefore there is no symmetry around the horizontal centre plane.

3) Initial condition

$T = T_0$ and $C = C_0$

E. Model solution

The governing mathematical model, describing coupled heat and mass transfer during the roasting process, was solved using the finite element method (FEM) with COMSOL Multiphyics®version3.5. A 3D rectangular geometry of dimensions (20mm x 20mm x 27mm, see Fig 2, corresponding to only one-fourth of the original dimensions of the sample) was built in COMSOL for numerical simulations. The generated mesh was refined at the boundaries to improve the accuracy of the numerical results. The coupled partial differential equations were solved and the state variables temperature and moisture concentration (water content) were predicted as a function of position and time.

Table 1 Model input parameters .

Quantity	*Symbol*	*Value*	*Reference*
Thermal conductivity of meat	k_m	0.4 W/(m. °C)	(Rao, et al., 2005)]
Specific heat of water	$c_{p,w}$	4170 J/(kg· °C	(Rao, et al., 2005)
Density of water	ρ_w	1000 kg/m^3	(Rao, et al., 2005)
Heat transfer coefficient	h	33.4 (W/(m$^{2.}$ °C)	*measured*
Oven temperature	T_0	175 °C	*set*
Protein composition	y_p	0.2 kg/kg	(Tornberg, 2005)
Carbohydrate composition	y_c	0.02 kg/kg	(Tornberg, 2005)
Fat composition	y_f	0.03 kg/kg	(Tornberg, 2005)
Water composition	y_w	0.75 kg/kg	(Tornberg, 2005)
Density of fat	ρ_f	920 kg/m^3	(Rao, et al., 2005)
Density of protein	ρ_p	1320 kg/m^3	(Rao, et al., 2005)
Density of carbohydrate	ρ_c	1600 kg/m^3	
Latent heat of vaporization of water	H_{evap}	2.3 10^6 J/kg	
Initial temperature	T_0	13 °C	*set*
Initial moisture concentration	C_0	0.75 (kg /kg)	*measured*
Diffusion coefficient	D	4 10^{-10} m^2/s	(Vestergaard, et al., 2005)
Viscosity of water	$\mu_{w\,(T)}$	*=-5* $-\log \mu_w = 0.0072T + 2.8658$ *log(2.41)-247.1/(T-140)*	*Using data* (Hodgman)

III. EXPERIMENTAL METHOD

A. Sample preparation and oven setting

Sample Preparation

Pork meat (*Longissimus-dorsi*) was bought from the local butchery. It was kept in a plastic bag and stored at 5°C, before sample preparation to avoid moisture loss. For all experiments, the fat layer of the meat was removed before samples were cut in the required shape (rectangular blocks).

Oven condition

A professional oven, Rational Combi-steamer ccc, with an oven space of 0.83 m x 0.645 m x 0.495 m was used for the roasting process. Dry hot air is circulated inside the oven by means of a fan, which reverses its direction of rotation every 1-2 min to ensure a more uniform heat transfer from the hot air to the product. Temperature of the hot air is controlled by the oven thermostat and was found to be stable around the set point with a standard deviation of ± 3°C. The oven was set to dry air (no humidification), 50% of maximum fan speed and oven temperature of 175°C. The meat samples are placed centrally on a stainless steel baking tray in the oven. Note that the oven is initially heated to 175°C before placing the sample. Temperature sensors were placed at different positions in the oven to measure air temperature. The samples were placed on the baking tray once the oven temperature reached the temperature set point. The preheating of the oven avoids non-stationary conditions at the beginning of the process and as such reduces uncertainty.

B. Measurement

1) Heat transfer coefficient

Rectangular and cylindrical aluminum (Al) blocks of a similar size as the food samples were constructed to determine the convective heat transfer coefficient. Temperature sensors were placed in the center of Al blocks through small holes.

The oven temperature was set to 175°C and the oven was heated until a constant temperature of 175°C was reached. At that point, the oven was opened quickly and the Al blocks with temperature sensors were placed in the oven. Temperature at the center of the Al blocks was measured as a function of time. The convective heat transfer coefficient was determined using the lumped heat transfer method (18). Since the Biot number for Al is very low (l_{Al}=0.02m, k_{Al}=168W/(m·K), h=33w/m^{2}K, the corresponding biot number is Bi=0.004, which is <<0.1). The heat transfer coefficient was determined both at 50% of the maximum fan speed and at full fan speed.

$$\ln\left(\frac{T_{oven}-T_{Al}}{T_{oven}-T_0}\right)=-bt \qquad (18)$$

$$b=\frac{hA_s}{V_{Al}\,\rho_{Al}\,c_{p,Al}}$$

Where T_{Al} and T_0 are the temperatures of the Al block at time t and at the start (t=0), respectively, A_s is the surface area of the Al block (m^2), $c_{p,Al}$, V_{Al} *and* ρ_{Al} are heat capacity (J/(kg·°C)) , volume (m^3) and density (kg/m^3) of Al, respectively.

2) Dynamic measurements

Local temperature measurement

Local temperatures were measured online using temperature sensors. Two sensors (thermocouples) were inserted into the sample and were placed at different positions within the meat: one at the center (point A) and one near the surface (point B), respectively (Fig 2). Once the temperature sensors were placed inside the meat sample, the meat was placed in the oven for roasting. Thermocouples were connected to the PC (computer) through a data logger (Pico). During roasting, temperature values were recorded with a 10 seconds sampling interval.

(20)

IV. Results and Discussion

A. 3D Prediction of State Variables (Temperature and Moisture Content)

Fig 3(a-f) shows the predicted temperature and moisture distribution within the meat sample at different times of roasting processess (after 600 s, 1500 s and 2400 s, respectively). The figure illustrates the progress of water transport and temperature profile during meat roasting in a convection oven. At t = 600 s, the surface temperature of the meat sample is at much higher temperature than the inside part (raw near centre) A large temperature gradient can be seen from Fig.3a, and it is also illustrated Fig 4a. At the same time, moisture gradient is created between inside part and outside part, Fig.3b. The meat is losing water, due to higher temperature that causes denaturation of meat protein on the surface, which leads to reduction in water binding capacity, whereas at the central part of meat sample, the water transport is not affected at this time of roasting since the temperature has not reached denauration temperature. However, the region between inside and outside, a larger gradient in water content profile can be seen from Fig.3b. This locally larger water content gradient is due to a large temperature gradient that causes reduction of water binding capacity and release excess water. When meat protein shrinks, excess water can move both in and out; thus simulation shows a slight rise in local moisture content (Fig.3b). However, this rise in water content is locally as shown in Fig.3b and the water cannot move towards the centre due to low elastic modulus and low permeability of still uncooked meat, despite the temperature and the excess moisture gradient.

At a later time, (t=1500 s), Fig. 3c, the temperature gradient is drastically reduced and finally at (t=2400 s), Fig.3e, the temperature distribution is almost uniform.

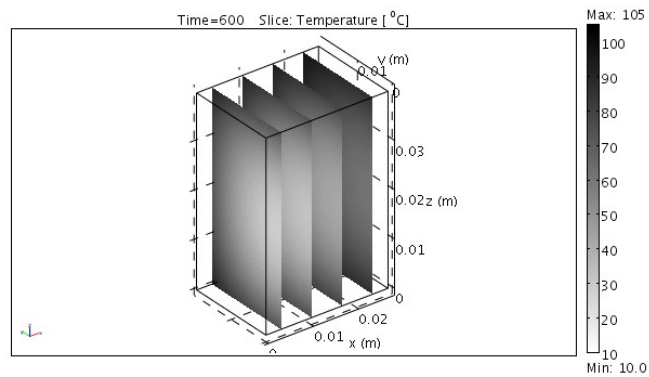

(a)

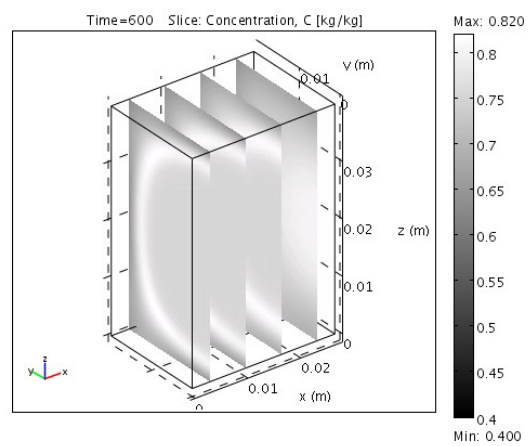

(b) C(x y, z, 600 s)

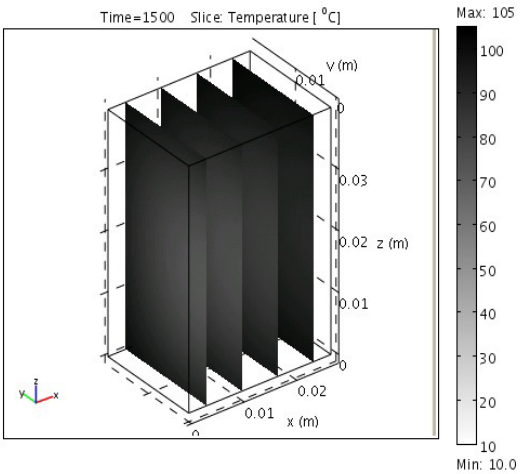

(c)

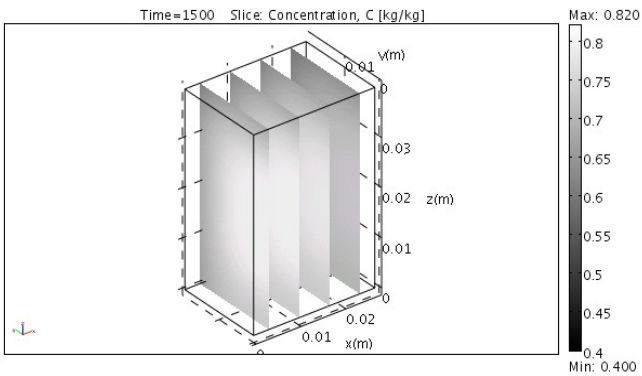

(d)

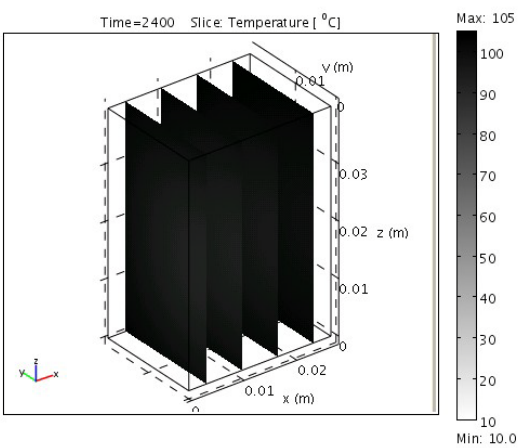

(e)

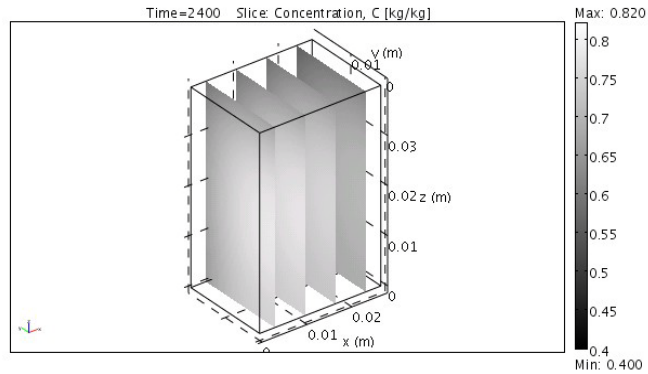

(f)

Fig. 3. 3D temperature and moisture distributions during the roasting process; a) temperature profile at t= 600s; b) moisture content profile at t = 600 s; c) temperature distribution at t = 1500 s; d) moisture content profile at 1500s; e) temperature profile at t = 2400s; f) moisture content profile at t = 2400s,

B. Temperature and moisture profile at a different time and position

To illustrate the effect of permeability, the model was simulated with two different values of *K*, ($K = 10^{-16}$ m^2 and $K = 10^{-17}$ m^2, corresponding to raw meat (Datta, 2006)and the moisture profile is plotted as Fig. 4b and 4c, respectively. The simulation indicated that there is a slight rise in water content at the centre with larger permeability ($K = 10^{-16}$ m^2), Fig. 4b; whereas with lower permeability which is a more realistic permeability for raw meat ($K = 10^{-17}$ m^2), Fig.4c, shows that there is no rise of water content at the centre. Further simulation which is not reported here, in which *K* is expressed as a function of temperature, using the arbitrary logistic function, shows that it gives a local rise in the moisture content in the zone where denatuartion takes place. The change the permeability *(K(T))* during roasting whole meat is not available yetThis will be investigated in future work and does not distract from the overall conclusion that the water transport towards the centre is negligible because of the low permeability of the raw meat from inside. And also the simulation with reasonable permeability of raw meat shows that there is no moisture rise at the center.

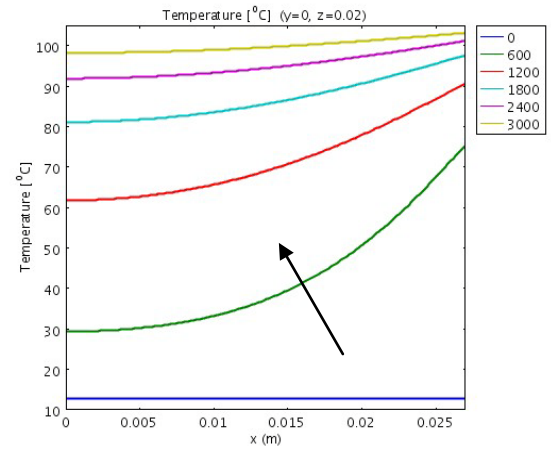

(a)

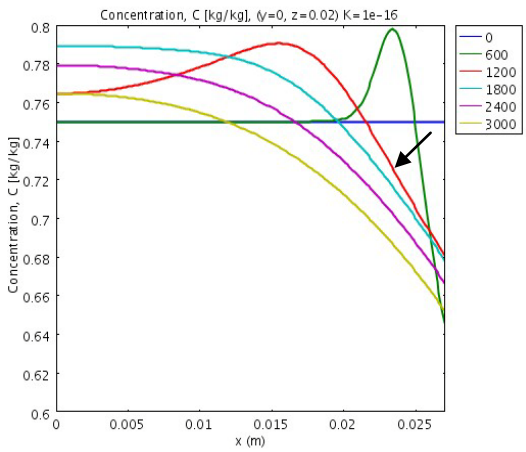

(b)

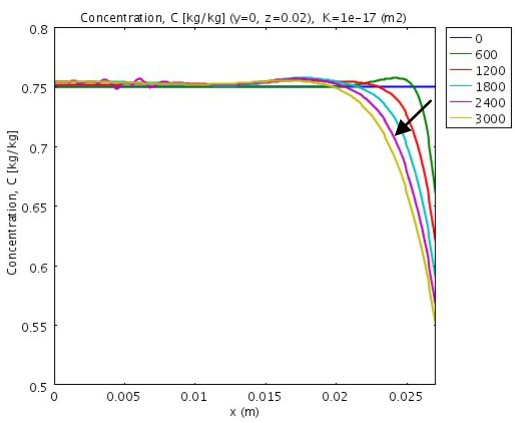

(c)

Fig. 4 Temperature and moisture profile during roasting (0, 600, 1000, 1500, 2400 and 3000 s) as a function of x a) temperature profile, (b) moisture content profile, (K=10^{-16} m^2**)** c) moisture content profile, **(**K=10^{-17} m^2**)**. The arrow in three figures shows the direction in which the curves change when time proceeds.

C. Model validation and verification

Fig 5 shows the comparison between the measured and predicted temperature profiles, respectively. The measured and simulated are compared at point A (centre) and B (near surface). Both curves show a similar trend, but with a slight offset between both curves. The deviation at the centre is probable due to the uncertainty in the thermal properties of the meat (eg constant thermal conductivity is used in simulation).

We assumed that at a later stage of roasting, evaporation is a dominant process and larger value of f is assumed (close 1 is used), which can be argued as the following: 1) the measured temperature has a slightly rise after t =1500 s and can not rise above 100^0C which indicate that most of the energy is consumed for evaporation Fig 5. 2) and 2) by performing a crude mass and energy balance. The latter will be expounded in the following. The average mass loss, between 1800 s and 2100 s, was calculated from the data reported in (Feyissa, et al., 2009) and found to be 2.27 10^{-4} kg/s (mass loss=0.0068 kg, dt = 300 *s)*. Assuming that if the latent evaporation of water, 2.3 10^6 J/s the effect used for evaporating water is 5200 W. The corresponding effect used for internal heating of meat sample, can be roughly calculated from measured centre temperature Fig.5. The temperature rise in the same range (t = 1800 s to t = 2100 s) is 5.52^{o}C, which gives a rise of 0.29 ^{o}C for every second. Assuming that the heat capacity of meat is 3500 J/(^{o}C.kg), the energy used for heating up meat samples is found to be 123 W. Then the fraction of total energy, f that is used for evaporating water at the surface, is around 0.81. This is the lower limit, since using a centre temperature and constant heat capacity, which actual overestimate energy for internal heating and underestimate energy used for evaporation. The use of a value of f close to one is a reasonable assumption. In future work, a theoretical based value of f will be derived. The effect of change in dimensions (shrinkage) of meat during roasting will also be incorporated into a model.

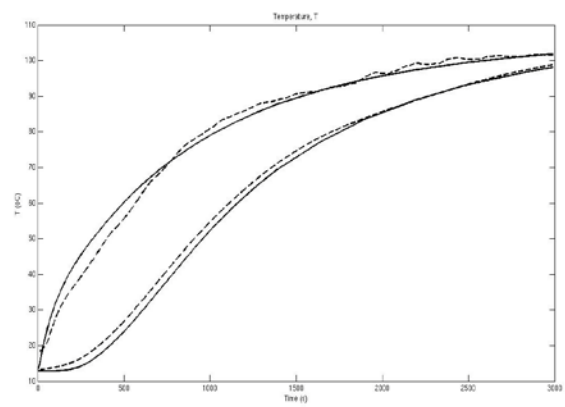

Fig.5 Measured and predicted temperature profile; (-) simulated (--) measured

V. Conclusion

The coupled mathematical model of heat and mass transfer during roasting of meat in a convection oven was developed from the first principles and was solved using COMSOL Multiphyics. Temperature and moisture distribution as a function of position and time are predicted with the model and based on simulation results, and better insight in process mechanisms can be obtained. The developed model is partially validated by experiments and a reasonable agreement between both was observed. The novelty of the developed model is its

capability to incorporate the effect of change in microstructure (permeability), water holding capacity and elastic modulus of the meat during roasting process. Such a model can be helpful in understanding the physics of meat during the roasting, and can be used to improve the prediction of temperature and moisture loss during roasting. Thus, the model can be a useful tool to support quality and excessive moisture loss. The water transport is very much related to the structural changes of the meat.

ACKNOWLEDGMENT

The Author would like to thank DTU for a Ph.D. grant under the aegis of Food-DTU.

References

Allais I., Perrot N., Curt C., & Trystram G. (2007). Modelling the operator know-how to control sensory quality in traditional processes. *Journal of Food Engineering*, 83(2), 156-166.

Barriere B., Leibler L. (2003). Kinetics of solvent absorption and permeation through a highly swellable elastomeric network. *Journal of Polymer Science Part B-Polymer Physics*, 41(2), 166-182.

Bengtsson N.E., Jakobsson B., & Dagerskog M. (1976). Cooking of Beef by Oven Roasting - Study of Heat and Mass-Transfer. *Journal of Food Science*, 41(5), 1047-1053.

Bird R.B., Sterwart W.E., & Lightfoot E.N. (Eds.) (2001). *Transport phenomena.* (2nd edn.). John Wiley and Sons,Inc, New York.

Chang H.C., Carpenter J.A., & Toledo R.T. (1998). Modeling heat transfer during oven roasting of unstuffed turkeys. *Journal of Food Science*, 63(2), 257-261.

Chen H., Marks B.P., & Murphy R.Y. (1999). Modeling coupled heat and mass transfer for convection cooking of chicken patties. *Journal of Food Engineering*, 42(3), 139-146.

Datta A.K. (2006). Hydraulic permeability of food tissues. *International Journal of Food Properties*, 9(4), 767-780.

Dincer I. (1996). Modelling for heat and mass transfer parameters in deep-frying of products. *Heat and Mass Transfer*, 32(1-2), 109-113.

Feyissa A.H., Adler-Nissen J., & Gernaey K.V. (2009). Mechanism of water transport in meat during the roasting process. In *55th International Congress of Meat Science and Technology, Meat - Muscle, Manufacturing and Meals*, .

Godsalve E.W., Davis E.A., Gordon J., & Davis H.T. (1977). Water loss rates and temperature profiles of dry cooked bovine muscle. *Journal of Food Science*, 42(4), 1038-1045.

Hodgman C.D. *Handbook of chemistry and physics.* (). The chemical rubber publishing Co., Cleveland, Ohio.

Huang E., Mittal G.S. (1995). Meatball Cooking - Modeling and Simulation. *Journal of Food Engineering*, 24(1), 87-100.

Ikediala J.N., Correia L.R., Fenton G.A., & Ben-Abdallah N. (1996). Finite element modeling of heat transfer in meat patties during single-sided pan-frying. *Journal of Food Science*, 61(4), 796-802.

Kovácsné Oroszvári B., Sofia Rocha C., Sjöholm I., & Tornberg E. (2006). Permeability and mass transfer as a function of the cooking temperature during the frying of beefburgers. *Journal of Food Engineering*, 74(1), 1-12.

Ngadi M.O., Watts K.C., & Correia L.R. (1997). Finite element method modelling of moisture transfer in chicken drum during deep-fat frying. *Journal of Food Engineering*, 32(1), 11-20.

Ou D., Mittal G.S. (2006). Double-sided pan-frying of unfrozen/frozen hamburgers for microbial safety using modelling and simulation. *Food Research International*, 39(2), 133-144.

Pan Z., Singh R.P., & Rumsey T.R. (2000). Predictive modeling of contact-heating process for cooking a hamburger patty. *Journal of Food Engineering*, 46(1), 9-19.

Rao M.A., syed S.H.R., & Datta A.K. (Eds.) (2005). *Engineering properties of foods.* (Third Edition edn., pp. 738). Talyor and Francis.

Singh N., Akins R.G., & Erickson L.E. (1984). MODELING HEAT AND MASS TRANSFER DURING THE OVEN ROASTING OF MEAT. *Journal of Food Process Engineering*, 7(3), 205-220.

Singh R.P., Vijayan J. (1998). Predictive modeling in food process design. *Food Science and Technology International*, 4(5), 303-310.

Skjoldebrand C., Hallstrom B. (1980). Convection oven frying heat and mass transport in the product. *Journal of Food Science*, 45(5), 1347-1353.

Thorvaldsson K., Skjöldebrand C. (1996). Water transport in meat during reheating. *Journal of Food Engineering*, 29(1), 13-21.

Tijskens E., De Baerdemaeker J. (2004). Mathematical modelling of syneresis of cheese curd. *Mathematics and Computers in Simulation*, 65(1-2), 165-175.

Tornberg E. (2005). Effects of heat on meat proteins – Implications on structure and quality of meat products. *Meat Science*, 70(3), 493-508.

van der Sman R.G.M. (2007). Moisture transport during cooking of meat: An analysis based on Flory–Rehner theory. *Meat Science*, 76(4), 730-738.

Vestergaard C., Risum J., & Adler-Nissen J. (2005). 23Na-MRI quantification of sodium and water mobility in pork during brine curing. *Meat Science*, 69(4), 663-672.

Wählby U., Skjöldebrand C. (2001). NIR-measurements of moisture changes in foods. *Journal of Food Engineering*, 47(4), 303-312.

Wu S., Li H., Chen J.P., & Lam K.Y. (2004). Modeling Investigation of Hydrogel Volume Transition. *Macromolecular Theory and Simulations*, 13(1), 13.

National Food Institute
Technical University of Denmark
Mørkhøj Bygade 19
DK - 2860 Søborg

Tel. 35 88 70 00
Fax 35 88 70 01

www.food.dtu.dk

ISBN: 978-87-92158-95-6